IRE
Transactions
on ANTENNAS and PROPAGATION

Volume AP-9 NOVEMBER, 1961 Number 6

Published Bimonthly

In This Issue

PUBLISHED BY THE
Professional Group on Antennas and Propagation

IRE TRANSACTIONS® PGAP IS A PUBLICATION DEVOTED TO EXPERIMENTAL AND THEORETICAL PAPERS ON RADIO ANTENNAS, ON GUIDED OR UNGUIDED PROPAGATION OF RADIO WAVES, AND ON ALLIED FIELDS OF RADIO PHYSICS SUCH AS RADIO ASTRONOMY

MANUSCRIPTS should be submitted to Sidney A. Bowhill, *Editor*, 222 Electrical Engineering, Pennsylvania State University, University Park, Pa. Manuscripts should be original typewritten copy, double-spaced, plus one carbon copy and two sets of copies of illustrations. Original illustrations will be called for if the paper is accepted. References should appear as footnotes and include author's name, title, journal, volume, initial and final page numbers, and date.

CONTRIBUTIONS, which should average 15 double-spaced typewritten pages in length, are subjected to review by the *Associate Editors* and their readers. Each paper must have a summary of less than 200 words.

COMMUNICATIONS should not exceed five double-spaced typewritten pages in length, together with not more than three illustrations. Accepted at the Editor's discretion, they appear in the first available issue.

NEWS ITEMS concerning PGAP members and group activities should be sent to the *News Editor*, R. C. Hansen, Aerospace Corp., Box 95085, Los Angeles 45, Calif.

ORIGINAL ILLUSTRATIONS should be submitted as follows: All line drawings (graphs, charts, block diagrams, cutaways, etc.) should be inked uniformly and ready for reproduction. If commercially printed grids are used in graph drawings, author should be sure printer's ink is of a color that will reproduce. Photographs should be glossy prints. Call-outs or labels should be marked on a registered tissue overlay, not on the illustration itself. No illustration should be larger than 8 x 10 inches. Lettering on illustrations must have height at least two per cent of the illustration width.

Copies can be purchased from **the INSTITUTE OF RADIO ENGINEERS, 1 East 79 St., New York 21, N.Y.** Individual copies of this issue, and all available back issues, except Vols. AP-5, No. 1; AP-6, No. 1; AP-7, Special Supplement, may be purchased at the following prices: IRE members (one copy) $2.25, libraries and colleges $3.25, all others $4.50. Yearly subscription rate: non-members $17.00; colleges and public libraries $10.00. IRE TRANSACTIONS ON ANTENNAS AND PROPAGATION. Printed in U.S.A. Printed by George Banta Co., Inc., Curtis Reed Plaza, Menasha, Wisconsin.

Second-class postage paid at MENASHA, WISCONSIN, and additional mailing offices under the act of August 24, 1912. Acceptance for mailing at a special rate of postage is provided for in the act of February 28, 1925, embodied in Paragraph 4, Section 412, P. L. & R., authorized October 26, 1927.

IRE Transactions on Antennas and Propagation

Volume AP-9 NOVEMBER, 1961 Number 6
Published Bimonthly

TABLE OF CONTENTS

CONTRIBUTIONS

COMMUNICATIONS

contributions

Scattering by a Periodically Apertured Conducting Screen*

R. B. KIEBURTZ†, MEMBER, IRE, AND A. ISHIMARU‡, MEMBER, IRE

Summary—**This paper presents a generalized variational method for calculation of equivalent-circuit parameters or scattering coefficients of any thin obstacle. The equivalent susceptance is obtained from an eigenvalue of a general-energy operator. The method is applied here to the scattering of a plane wave by a conducting screen containing a doubly-periodic array of square apertures.**

Previous variational formulations of analogous waveguide problems were largely restricted to cases in which only the dominant mode can propagate. In applying these methods to scattering problems, the ratio of aperture spacing to wavelength had to be restricted to less than unity at normal incidence so that no additional propagating modes were excited. The formulation presented here can be applied, however, for any number of propagating modes.

Numerical results are presented for scattering by a periodically apertured screen, giving scattering coefficients as a function of wave number of the incident wave. The distribution of energy into higher-order diffraction lobes is evaluated.

I. Introduction

THE introduction of variational techniques into electromagnetic theory by Schwinger[1] in 1945, provided a powerful new method for the evaluation of scattering by lossless obstacles in waveguides. Since that time the technique has been applied to the solution of many waveguide problems[2,3] and has been generalized by Levine and Schwinger[4,5] to the solution of certain diffraction problems.

It is the purpose of this paper to extend the variational method to enable evaluation of scattering of energy by a periodically-apertured screen into higher-order, off-center diffraction lobes. This evaluation has not been possible using previous variational formulations. It is shown here that the variational method arises from the properties of the eigenvalues of an energy operator, and that these eigenvalues are related to the equivalent admittance or impedance of a scattering obstacle.

The method is developed for scattering by obstacles in a waveguide, but it can be applied to any problem in which the waves can be characterized by an infinite set of discrete eigenfunctions analogous to the modes of a waveguide. For the problem of plane-wave excitation of an infinite, doubly-periodic structure, the period-

* Received by the PGAP, January 25, 1961; revised manuscript received, June 22, 1961. The research described in this paper was performed at the University of Washington, Seattle, under Contract No. AF19(604)-4098 with the Electronics Research Directorate, AF Cambridge Research Labs.

† Dept. of Elec. Engrg., New York University, New York, N. Y.
‡ Dept. of Elec. Engrg., University of Washington, Seattle, Wash.

[1] J. Schwinger, "Discontinuities in Waveguides," M.I.T. Rad. Lab., Cambridge, Mass., unpublished notes; 1945.

[2] N. Marcuvitz, "Waveguide Handbook," McGraw-Hill Book Co., Inc., New York, N. Y.; 1948.

[3] L. Lewin, "Advanced Theory of Waveguides," Iliffe, London, England; 1951.

[4] H. Levine and J. Schwinger, "On the theory of diffraction by an aperture in an infinite plane screen (I)," *Phys. Rev.*, vol. 74, pp. 958–974, October, 1948; (II), vol. 75, pp. 1423–1432; May, 1949.

[5] H. Levine and J. Schwinger, "On the theory of electromagnetic wave diffraction by an aperture in an infinite plane conducting screen," *Commun. Pure and Appl. Math.*, vol. 3, pp. 355–391; December, 1950.

rectangle of the periodic structure is analogous to the cross section of a waveguide.

To extend the variational method to evaluation of mode coupling by apertures in either a waveguide or a periodic screen, a new set of propagating modes is defined which are uncoupled by the aperture. These modes are composed of linear combinations of the propagating-plane wave or waveguide modes. Scattering coefficients can be evaluated then for the uncoupled modes, and from these, the scattering coefficients for the original set of modes can be obtained. This method is applied to obtain results for multimode scattering by a plane screen containing a periodic array of square apertures.

II. Generation of the Variational Principle from the Energy Operator

Consider an electromagnetic field having time dependence $e^{j\omega t}$ in a region of space V bounded by a surface S. Then from the Poynting theorem, the time-averaged energy entering the bounding surface is given by

$$4j\omega(W_H - W_E) + 2P = -\oint_S (\overline{E} \times \overline{H}^*) \cdot \overline{d\sigma}, \tag{1}$$

where $\overline{d\sigma}$ is directed along the outward normal to the surface, and the asterisk denotes complex conjugate. The imaginary part represents the net difference in the average energy stored in electric and magnetic fields. Now if the region V is taken to be the interior of a lossless waveguide containing a source, then the surface integral will be nonzero only over the waveguide cross section, and considering propagation in the positive z direction, (1) becomes

$$4j\omega(W_H - W_E) + 2P = -\iint_{\text{c.s.}} (\overline{E} \times \overline{H}^*)_z dxdy. \tag{2}$$

Now suppose there is a lossless obstacle, which may be conductor or dielectric, in the waveguide cross section at $z=0$ as in Fig. 1, and that the surface integral is evaluated at that point. The fields in the cross section will not now be the same as the field of the incident wave. They can, however, be expressed as an expansion in the wave functions of the orthonormal modes of the waveguide. Denoting the unknown fields at the obstacle by $\bar{e}$ and $\bar{h}$, these expansions are at any fixed value of z

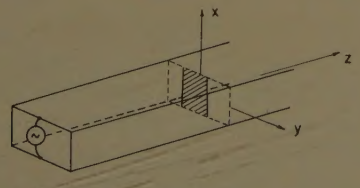

Fig. 1—Geometry of an obstacle in a waveguide or a period rectangle of a periodic screen.

$$\bar{e}(x, y, z) = \sum_{m,n} a_{mn} \bar{\Phi}_{mn}(x, y) f_{mn}(z)$$
$$\bar{h}(x, y, z) = \sum_{m,n} a_{mn} \bar{\Psi}_{mn}(x, y) g_{mn}(z). \tag{3}$$

The summations are over two independent indexes since the modal function $\phi_{mn}(x, y)$ are solutions of a two-dimensional wave equation in a closed region. Since the modal functions of a lossless waveguide are orthogonal over the guide cross section, it would be possible to evaluate the coefficients in terms of the fields $\bar{e}$ and $\bar{h}$ if they were known. Since the coefficient a_{mn} are the same in the electric and magnetic field expansions, it is sufficient to evaluate them in terms of the electric field alone:

$$a_{mn} = \iint_{\text{c.s.}} \bar{e}(x, y) \cdot \bar{\phi}_{mn}^*(x, y) dxdy. \tag{4}$$

The field functions $\bar{e}$ and $\bar{h}$ are eventually to be put into the surface integral (2), and since only the z component of $\bar{e} \times \bar{h}^*$ is to be taken, it is sufficient to consider only their two transverse components. This implies no loss of generality since it is well known that two scalar potential functions are sufficient to specify a vector electromagnetic field in an isotropic medium. From now on let $\bar{e}$, $\bar{h}$, $\bar{\phi}$, $\bar{\psi}$ denote only the transverse components. The transverse magnetic-field functions $\bar{\psi}_{mn}$ are now related to transverse electric-field functions $\bar{\phi}_{mn}$ by admittance coefficients Y_{mn} derived from the Maxwell curl equations.

Assuming the Y_{mn} have been found, the $\bar{\psi}_{mn}$ are given by

$$\bar{\psi}_{mn} = Y_{mn} \bar{a}_z \times \bar{\phi}_{mn}. \tag{5}$$

If the expressions (5) for $\bar{\psi}_{mn}$ and (4) for a_{mn} are substituted into the expansion (3) for $\bar{h}$, then substituting the expansion for $\bar{h}$ into (2), one arrives at the form of the energy integral which generates the variational principle:

$$4j\omega(W_H - W_E) + 2P \tag{6}$$
$$= -\iint_{\text{c.s.}} \iint_{\text{c.s.}'} \sum_{m,n} Y_{mn}^* [\bar{e}(x, y) \times (\bar{a}_z \times \bar{\phi}_{mn}^*(x, y)) \cdot (\bar{\phi}_{mn}(x', y') \cdot \bar{e}^*(x', y')] \cdot \bar{a}_z dx'dy'dxdy.$$

Before proceeding, however, it seems profitable to simplify the integral by use of a more elegant notation. First, the triple cross product can be expanded, simplifying the integrand of (6) to

$$\sum_{m,n} Y_{mn}^* \bar{e}(x, y) \cdot \bar{\phi}_{mn}^*(x, y) \bar{\phi}_{mn}(x', y') \cdot \bar{e}^*(x', y').$$

The notation may be simplified further by taking $\bar{\phi}_{mn}^*$ $\bar{\phi}_{mn}$ to be a dyad, or second-order tensor,

$$\overline{\overline{K}}_{mn}(x, y; x', y') = \bar{\phi}_{mn}^*(x, y) \bar{\phi}_{mn}(x', y') = \begin{bmatrix} \phi_{mnx}^* \phi_{mnx} & \phi_{mnx}^* \phi_{mny} \\ \phi_{mny}^* \phi_{mnx} & \phi_{mny}^* \phi_{mny} \end{bmatrix}. \tag{7}$$

From the matrix form of the tensor it can be seen that the tensor $\overline{\overline{K}}_{mn}$ is Hermitian, or self-adjoint. This important property will be used later. The tensor function

$$\overline{\overline{K}}(x, y; x', y') = \sum_{m,n} Y_{mn}^* \overline{\overline{K}}(x, y; x', y') \tag{8}$$

is then an example of the tensor Green's function defined by Levine and Schwinger.[4,5] With this notation, (6) simplifies to

$$4j\omega(W_H - W_E) + 2P = -\iint_{c.s.}\iint_{c.s.'} \bar{e}(x, y) \cdot \overline{\overline{K}}(x, y; x', y') \cdot e^*(x', y')dx'dy'dxdy. \quad (9)$$

Now the tensor Green's function $\overline{\overline{K}}$ will not be Hermitian because the Y_{mn} corresponding to propagating modes will be real while those corresponding to evanescent modes will be purely imaginary. This fact, however, allows one to write $\overline{\overline{K}}$ in terms of two Hermitian tensors,

$$\overline{\overline{K}} = \overline{\overline{K}}_1 - j\overline{\overline{K}}_2 \quad (10)$$

where $\overline{\overline{K}}_1$ contains all of the modal functions for which Y_{mn} is real and $\overline{\overline{K}}_2$ contains all of those for which Y_{mn} is imaginary. Since K_1 is Hermitian, the value of the operator in which it appears as the kernel must always be real and can therefore be associated with the power

$$2P = -\iint_{c.s.}\iint_{c.s.'} \bar{e}(x, y) \cdot \overline{\overline{K}}_1(x, y; x', y') dx'dy'dxdy. \quad (11)$$

Normalizing the stored energy term to the transmitted power, subtracting the power supplied by the source from both sides of the equation and dividing by j, (9) can be rewritten as

$$\frac{2\omega(W_H - W_E)}{-P}\iint_{c.s.}\iint_{c.s.'} \bar{e} \cdot \overline{\overline{K}}_1 \cdot \bar{e}^* d\sigma' d\sigma = \iint_{c.s.}\iint_{c.s.'} \bar{e} \cdot \overline{\overline{K}}_2 \cdot \bar{e}^* d\sigma' d\sigma. \quad (12)$$

This constitutes an integral operator equation in the unknown field $\bar{e}$ at the obstacle. The quantity $2\omega(W_E - W_E)/-P$ is an eigenvalue of the equation. This equation has an infinite spectrum of discrete eigenvalues and eigenfunctions $\bar{e}$. To insure that the eigenfunctions of (12) describe physically realizable electric field configurations, it is required that the vector functions $\bar{e}$ be continuous over the interior of the waveguide.

To find the eigenvalues of (12) one has only to divide both sides by the integral appearing on the left in order to obtain the variational form

$$\frac{2\omega(W_H - W_E)}{-P} = \frac{\iint_{c.s.}\iint_{c.s.'} \bar{e} \cdot \overline{\overline{K}}_2 \cdot \bar{e}^* d\sigma' d\sigma}{\iint_{c.s.}\iint_{c.s.'} \bar{e} \cdot \overline{\overline{K}}_1 \cdot \bar{e}^* d\sigma' d\sigma}. \quad (13)$$

Since the eigenvalues are stationary with respect to first variations in the functions $\bar{e}$ about their correct values, one does not have to solve the integral equations for the eigenfunctions in order to determine the eigenvalues. It is necessary only to assume a trial function $\bar{e}_t$ and substitute it into the variational expression (13) in order to obtain a close estimate on the value of the eigenvalue. This trial function is usually chosen such that it satisfies boundary conditions on the obstacle or agrees with the incident field. It will now be shown how the eigenvalues may be interpreted physically and how bounds on the eigenvalues may be obtained.

III. Equivalent Circuits for Thin Planar Obstacles

For the case of thin, planar obstacles, the surface over which the variational integral is to be evaluated is the cross section of the waveguide containing the obstacle. If the obstacle is a perfect conductor, the tangential electric field is zero on the obstacle and the surface integrals reduce the integrals only over the aperture in the plane. The fields of the evanescent modes are symmetrical about the plane of the obstacle; therefore, the energy stored in these fields is equally divided on both sides of the plane.

An equivalent circuit representation is useful also in the case of an infinite periodically apertured screen excited by a plane wave. A transmission line model can describe the scattering of plane-wave modes by such a screen equally as well as it describes scattering of modes by an obstacle in a waveguide. In the case of a periodic structure, the cross section over which the variational integrals are to be evaluated is the period-rectangle of the periodic structure.

If only one propagating mode is considered, the effect of the obstacle can be represented by a shunt admittance across a transmission line. The shunt admittance jB of a lossless obstacle is related to the ratio of stored energy divided by the transmitted power by

$$B = \frac{2\omega(W_H - W_E)}{-P_t}.$$

Since this is of the same form as the eigenvalues of the energy operator, these eigenvalues can be interpreted as equivalent susceptances of the obstacle. Since half the stored energy resides on each side of the obstacle, the variational expression (13) must be multiplied by 2 to obtain the total susceptance.

If the kernel $\overline{\overline{K}}_2$ of the integral equation is Hermitian, the eigenvalues obtained from (13) will all be real, corresponding to pure susceptances. The infinite spectrum of discrete eigenvalues occurs in the following way: the kernel $\overline{\overline{K}}_2$ is made up of an infinite sum of tensors each corresponding to a single one of the set of orthogonal modal functions. There will exist an eigenvalue B_0 with a corresponding eigenfunction $\bar{e}_0$ which is not orthogonal to any of the $\overline{\overline{K}}_{mn}$. This we may think of as the lowest-order eigenfunction corresponding to the physical solution. However, there will also exist eigenfunctions $\bar{e}_i$ which are orthogonal to one or more of the modal functions $\overline{\overline{K}}_{mn}$. These correspond to physical solutions only

when the incident field and the boundary conditions on the obstacle dictate their choice.

If all of the Y_{mn} are of the same sign, the kernel $\overline{\overline{K}}_2$ will be either positive or negative definite. For a definite kernel, the eigenvalues will be obtained as minimums of the absolute value of the variational integral.

Clearly then, there is an advantage to obtaining $\overline{\overline{K}}_2$ in a definite form. But any kernel K_2 can be split into a positive definite and a negative definite part.

$$\overline{\overline{K}}_2 = \overline{\overline{K}}_2^{+} + \overline{\overline{K}}_2^{-}. \tag{14}$$

This division corresponds to grouping together all of the $\overline{\overline{K}}_{mn}$ for TM modes and all of the $\overline{\overline{K}}_{mn}$ for TE modes. Since the two parts of the kernel are themselves Hermitian kernels, they too have stationary eigenvalues which are either all positive or all negative. These can be obtained by variational expressions:

$$B^{+} = \frac{2\iint_{\text{c.s.}}\iint_{\text{c.s.}'} \bar{e}\cdot\overline{\overline{K}}_2^{+}\cdot\bar{e}^{*}d\sigma' d\sigma}{\iint_{\text{c.s.}}\iint_{\text{c.s.}'} \bar{e}\cdot\overline{\overline{K}}_1\cdot\bar{e}^{*}d\sigma' d\sigma} \tag{15}$$

$$B^{-} = \frac{2\iint_{\text{c.s.}}\iint_{\text{c.s.}'} \bar{e}\cdot\overline{\overline{K}}_2^{-}\cdot\bar{e}^{*}d\sigma' d\sigma}{\iint_{\text{c.s.}}\iint_{\text{c.s.}'} \bar{e}\cdot\overline{\overline{K}}_1\cdot\bar{e}^{*}d\sigma' d\sigma}. \tag{16}$$

If the kernels $\overline{\overline{K}}_2^{+}$ and $\overline{\overline{K}}_2^{-}$ have any eigenfunctions in common, these also will be eigenfunctions of the combined kernel $\overline{\overline{K}}_2$. In general, however, they will not have common eigenfunctions and the eigenfunctions of $\overline{\overline{K}}_2$ will be different from those of $\overline{\overline{K}}_2^{+}$ and $\overline{\overline{K}}_2^{-}$. To obtain a variational estimate of the fundamental eigenvalue B_0 of $\overline{\overline{K}}_2$ then, the same trial function must be substituted into (15) and (16). The results of the variational calculations are then added:

$$B_0 = B_0^{+} + B_0^{-}. \tag{17}$$

If a variable parameter is incorporated in the trial function $\bar{e}_t$, it can be determined for specific cases whether the stationary value of B_0 corresponds to a maximum or a minimum of the algebraic sum (17). Thus, the parameter can be adjusted to give the best estimate of susceptance even in those cases in which the total susceptance is not a positive or negative definite quantity.

Eqs. (15)–(17) give a systematic variational method for accurately estimating the eigenvalue B_0 of any Hermitian kernel $\overline{\overline{K}}_2$, or equivalently, for evaluating the scattering coefficients or the equivalent susceptance of a lossless obstacle in a lossless waveguide. The value of B_0 is stationary and the eigenvalues of the kernels $\overline{\overline{K}}_2^{+}$ and $\overline{\overline{K}}_2^{-}$ provide bounds on the minimum absolute values of B^{+} and B^{-}.

IV. Stationary Property of the Eigenvalues

A proof of the stationary property of the variational integrals will not be presented here since several proofs have already been given by other authors.[1,3,4] Actually, the stationary property is a consequence of the characterization of the equivalent admittance as the eigenvalue of a Hermitian operator.[6] The eigenvalues of such an operator are all stationary with respect to first-order variations of the eigenfunctions about the correct values.

The variational form and the stationary property of the eigenvalues are consequences of the characterization of the equivalent circuit parameters as eigenvalues of a Hermitian operator. Therefore, the only fundamental limitation on the class of problems which may be treated by a variational method is that such a Hermitian operator exists. The kernel of the operator is formed by means of a sum of orthogonal modal functions. Thus, the requirement which must be satisfied is that the fields must be able to be expanded in terms of a set of discrete, orthogonal modal functions. This corresponds to a physical requirement that the waveguide, or the media in which the incident and transmitted waves propagate, be lossless and at least asymptotically uniform in the direction of propagation. It does not, however, require that the obstacle itself be lossless or that only one mode be able to propagate.

V. Multimode Scattering

It will now be shown how the variational method is to be applied to compute scattering coefficients if a finite number of modes propagate in the waveguide. The method can be used to evaluate the mode conversion produced by an obstacle in such a waveguide. Marcuvitz has obtained similar expressions for equivalent circuit parameters of obstacles in a multimode waveguide starting from a slightly different point of view.[7]

Possibly the most useful application of the method concerns itself not with waveguide propagation, but with diffraction of an incident field by an obstacle or an array of obstacles. Symmetries of the obstacle may make it possible to characterize the fields in terms of normal modes. In particular, for a periodic array of identical obstacles or apertures in a plane screen illuminated by a plane wave, the normal modes correspond to the spatial harmonics defined by the periodicity. The propagating modes are the incident and reflected plane waves and any spurious diffraction lobes which arise due to the periodic spacing.

If there exist a number of propagating modes, they are in general not orthogonal with respect to the bounda-

[6] P. R. Halmos, "Introduction to Hilbert Space," Chelsea Publishing Co., New York, N. Y., 2nd ed., p. 55; 1957.

[7] N. Marcuvitz, "Representation, Measurement, and Calculation of Equivalent Circuits for Waveguide Discontinuities with Application to Rectangular Slots," Polytechnic Institute of Brooklyn, Brooklyn, N. Y., Rept. No. PIB-137; 1949.

ries imposed by the obstacle. For instance, consider the obstacle to be a thin conducting iris, so that the tangential electric field is zero on the obstacle and finite only over the complementary aperture. Then the coupling between two propagating modes is proportional to

$$\iint_{\text{apert.}} \bar{\phi}_i \cdot \bar{\phi}_k^* d\sigma = b_{ik}. \tag{18}$$

However, in order to obtain variational expressions of the form and with definite Hermitian kernels, the tensor $\overline{\overline{K}}_1$ must contain the wave functions of all of the propagating modes. The difficulty is that the interpretation of

$$\iiiint_{\text{apert.}} \bar{e} \cdot \overline{\overline{K}}_1 \cdot \bar{e}^* d\sigma' d\sigma$$

as the transmitted power requires that the coupling between modes be known. The kernel $\overline{\overline{K}}_1$ must include the several wave functions in exactly the proportions in which they are coupled by the obstacle. Clearly there is no problem if the modes are uncoupled by the obstacle, for then all the power is carried by the same mode as the incident field, and only this wave function need be taken into $\overline{\overline{K}}_1$.

Then the solution is to define a new set of mode functions for the propagating modes which are not coupled by the obstacle. If there are N of the normal waveguide modes which can propagate, define a new set of N modes by

$$\bar{u}_i = \sum_{k=1}^{N} c_{ik} \bar{\phi}_k. \tag{19}$$

The coefficients are to be determined by imposing the conditions of orthogonality over the aperture and normalization over the waveguide cross section,

$$\iint_{\text{apert.}} \bar{u}_i \cdot \bar{u}_k^* d\sigma = \delta_{ik} d_{ik}, \qquad \iint_{\text{c.s.}} \bar{u}_i \cdot \bar{u}_i^* d\sigma = 1, \tag{20}$$

where δ_{ik} is the Kronecker delta, one if $i=k$ and zero otherwise. The number of propagating modes N is presumed to be finite, and the coefficients c_{ik} may be obtained by the Gram-Schmidt orthogonalization procedure.[8]

It is now possible to write variational expressions for the scattering coefficients of each of the uncoupled propagating-mode functions $\bar{u}_i$. The Hermitian tensor representing the transmitted power in the $\bar{u}_i$ mode will be

$$\overline{\overline{K}}_1 = Y_i^* \bar{u}_i^* \bar{u}_i, \tag{21}$$

where $Y_i^* \bar{u}_i^*$ means

$$Y_i^* \bar{u}_i^* = \sum_{k=1}^{N} c_{ik} Y_k^* \bar{\phi}_k^*, \tag{22}$$

and Y_k is the admittance coefficient of the normal $\bar{\phi}_k$ mode. Upon substituting an appropriate trial function into the variational expressions (15) and (16), one can obtain a stationary number B_i which characterizes the scattering of each of the modes $\bar{u}_i$ by the obstacle. Although with several modes propagating, the B_i no longer retain the significance of a simple equivalent shunt susceptance on a transmission line, it is possible to relate them in a simple manner to the voltage-scattering coefficient of the $\bar{u}_i$ mode,

$$r_i = \frac{-jB_i}{2 + jB_i}. \tag{23}$$

In order to evaluate the scattered fields in terms of the normal modes of the waveguide, it is first necessary to invert (19) obtaining the normal modes in terms of the $\bar{u}_i$.

$$\bar{\phi}_k = \sum_{i=1}^{N} (c^{-1})_{ki} \bar{u}_i. \tag{24}$$

This turns out to be very simple if the Gram-Schmidt process has been used, since the matrix of the coefficients c_{ik} which it provides is triangular. Assume now that only the $\bar{\phi}_1$ mode is incident, although this is not a necessary restriction. Then the total fields in the asymptotic region of the waveguide will be

$$\overline{E} = \bar{\phi}_1 e^{-j\beta_1 z} + \sum_{k=1}^{N} s_{1k} \bar{\phi}_k e^{j\beta_k z}. \tag{25}$$

The scattered field amplitudes can be written in terms of the r_i by substituting for the $\bar{\phi}_k$ from (24), giving

$$s_{1k} \bar{\phi}_k = \sum_{i=1}^{N} (c^{-1})_{ki} r_i \bar{u}_i. \tag{26}$$

The incident amplitudes of the $\bar{u}_i$ are related to the incident mode by (19) and the desired scattering coefficients can be evaluated:

$$s_{1k} = \sum_{i=1}^{N} (c^{-1})_{ki} c_{i1} r_i. \tag{27}$$

Finally, it might be pointed out that while the familiar variational expression for dominant mode susceptance,

$$Y = \frac{\sum_{m,n} Y_{mn} \iiiint_{\text{apert.}} \bar{e} \cdot \bar{\phi}_{mn}^* \bar{\phi}_{mn} \cdot \bar{e}^* d\sigma' d\sigma}{Y_{00} \iiiint_{\text{apert.}} \bar{e} \cdot \bar{\phi}_{00}^* \bar{\phi}_{00} \cdot \bar{e}^* d\sigma' d\sigma},$$

remains stationary in both real and imaginary parts even when several modes propagate in a waveguide, the simultaneous minimization of both real and imaginary

[8] P. Morse and H. Feshbach, "Methods of Theoretical Physics," McGraw-Hill Book Co., Inc., New York, N. Y., p. 928; 1958.

parts by variation of a parameter of the trial function may not be possible. Thus, the absolute value of the admittance may be approximated, but the relative magnitudes of the real and imaginary parts may be difficult to determine. The formulation given here obviates this difficulty, since the admittance of each of the uncoupled "incident" modes may be determined independently.

VI. The Tensor Green's Function for a Doubly-Periodic Array

The variational method developed in the last section will now be applied to the problem of the plane screen containing an infinite, periodic array of square apertures. Scattering coefficients of the screen can be evaluated by this method for each of the propagating plane-wave modes excited by the screen. Although the related two-dimensional problem of transmission through an infinite periodic array of slits in a screen has been treated by a variational method by Miles,[9] and the transmission cross section of a single rectangular aperture has been obtained by Lucke,[10] the angular distribution of energy was not evaluated.

Consider an array of square apertures spaced at equal intervals a in both the x and y directions. With uniform excitation the electric and magnetic fields must then satisfy the periodicity requirements imposed by Floquet's theorem. For simplicity, consider normally incident plane-wave excitation for which the phase shift between fields in adjacent apertures is zero. Then the field may be written as a Fourier series in two dimensions:

$$\bar{e}(x, y, z) = \sum_{m,n} \bar{a}_{mn} e^{j(2m\pi/a)x} \cdot e^{j(2n\pi/a)y} e^{-\gamma_{mn}}, \qquad (28)$$

where

$$\gamma_{mn} = \left[\left(\frac{2m\pi}{a}\right)^2 + \left(\frac{2n\pi}{a}\right)^2 - k^2\right]^{1/2}.$$

The terms of (28) for which γ_{mn} is imaginary correspond to propagating plane-wave modes for which the components of the propagation vector $\bar{k}$ are

$$k_x = \frac{2m\pi}{a} = k \sin\theta \cos\phi$$

$$k_y = \frac{2n\pi}{a} = k \sin\theta \sin\phi$$

$$k_z = \left[k^2 - \left(\frac{2m\pi}{a}\right)^2 - \left(\frac{2n\pi}{a}\right)^2\right]^{1/2} = k \cos\theta. \qquad (29)$$

The angle θ corresponds to the incidence angle between $\bar{k}$ and the normal to the plane of the screen; ϕ is the angle between the x axis and the projection of $\bar{k}$ on the x-y plane.

Terms of (28) for which γ_{mn} is real correspond to evanescent modes whose fields attenuate exponentially with distance from their sources. The electric or magnetic energy storage in these evanescent modes is that accounted for by the equivalent susceptance of the screen.

In accordance with waveguide terminology it is convenient to number the modes by the indexes m and n. It is also convenient to make the distinction between TE modes, which have no z component of electric field, and TM modes, which have no z component of magnetic field. For propagating modes, the TE modes are those with polarization of the electric field perpendicular to the plane of incidence defined by the normal to the screen and the propagation vector $\bar{k}$. Propagating TM modes are plane waves with polarization parallel to the plane of incidence. The normally incident exciting wave is a TEM wave, with neither E_z nor H_z.

One distinction between this problem and an analogous waveguide problem which must be noted is that to each γ_{mn} there correspond four modes (for m, n, both nonzero) since m and n may take on both positive and negative values. In the cases of propagating modes, these correspond to plane waves scattered at angles $\pm\theta$ and azimuthal angles $\pm\phi$.

The normalized transverse electric-field wave function for TE modes is found to be

$$\bar{\phi}_{mn\mathrm{TE}}(x, y) = \left(\frac{n}{\sqrt{m^2 + n^2}} \bar{a}_x - \frac{m}{\sqrt{m^2 + n^2}} \bar{a}_y\right) \frac{1}{a} e^{j(2m\pi/a)x} e^{j(2n\pi/a)y}, \qquad (30)$$

and the TE-mode admittance coefficients are

$$Y_{mn\mathrm{TE}} = -\frac{j\gamma_{mn}}{k\eta}. \qquad (31)$$

Similarly, for TM modes the normalized transverse electric-field wave functions are

$$\bar{\phi}_{mn\mathrm{TM}}(x, y) = \left(\frac{m}{\sqrt{m^2 + n^2}} \bar{a}_x + \frac{n}{\sqrt{m^2 + n^2}} \bar{a}_y\right) \frac{1}{a} \cdot e^{j(2m\pi/a)x} e^{j(2n\pi/a)y}, \qquad (32)$$

and the TM-mode admittance coefficients are

$$Y_{mn\mathrm{TM}} = \frac{jk}{\gamma_{mn}\eta}. \qquad (33)$$

These coefficients can now be used to construct the dyadic Green's functions $\overline{\overline{K}}_2^+$ and $\overline{\overline{K}}_2^+$. Using the definitions (7), (8), and (10), these are found to be

[9] J. W. Miles, "On the diffraction of an electromagnetic wave through a plane screen," *J. Appl. Phys.*, vol. 20, pp. 760–771; August, 1949.

[10] W. W. Lucke, "Transmission Through a Rectangular Aperture in a Conducting Screen," Stanford Research Inst., Stanford, Calif., Tech. Rept. No. 25; 1951.

$$\overline{\overline{K}}_2^{+} = \frac{k}{\eta} \sum_{\substack{m=-\infty \\ n=-\infty \\ m^2+n^2>\left(\frac{ka}{2\pi}\right)^2}}^{\infty} \frac{1}{\gamma_{mn} a^2} e^{j(2m\pi/a)(x-x')} e^{j(2n\pi/a)(y-y')} \begin{bmatrix} \frac{m^2}{m^2+n^2} & \frac{mn}{m^2+n^2} \\ \frac{mn}{m^2+n^2} & \frac{n^2}{m^2+n^2} \end{bmatrix} \tag{34}$$

$$\overline{\overline{K}}_2^{-} = \frac{1}{k\eta} \sum_{\substack{m=-\infty \\ n=-\infty \\ m^2+n^2>\left(\frac{ka}{2\pi}\right)^2}}^{\infty} \frac{-\gamma_{mn}}{a^2} e^{j(2m\pi/a)(x-x')} e^{j(2n\pi/a)(y-y')} \begin{bmatrix} \frac{n^2}{m^2+n^2} & \frac{-mn}{m^2+n^2} \\ \frac{-mn}{m^2+n^2} & \frac{m^2}{m^2+n^2} \end{bmatrix}. \tag{35}$$

To construct the dyadic function $\overline{\overline{K}}_1$, all of the modes with imaginary γ_{mn} must be included. In order to evaluate the scattering coefficients of these modes, however, a new set of propagating modes will be defined which are orthogonal over the aperture. These are evaluated in Section VIII.

VII. Choice of a Trial Function for the Aperture Distribution

The ability to choose an appropriate trial function for the aperture distribution has much to do with the success or failure of a calculation employing the variational method. Because of the stationary property, there exists no formal way in which the estimate of the trial function may be made to converge to the true aperture distribution.

Furthermore, a trial function which gives fairly accurate results at one wavelength may not be the best choice of trial function as the wavelength changes, since the true aperture field is not independent of wavelength. This dependence is most pronounced at wavelengths near a higher-mode cutoff as will be seen from the results. In spite of these difficulties, the great utility of the method is that it can be made to yield results for equivalent circuit parameters and scattering coefficients accurate enough to be extremely useful.

Now consider the geometry of Fig. 2 in which the normally incident plane wave is polarized in the y direction. In order to choose a trial function appropriate for square aperture of width d, consider the series of functions

$$e_y = \sum_{i,k} \alpha_{ik} \left\{1 - \left(\frac{2x}{d}\right)^2\right\}^{k-1/2} \left\{1 - \left(\frac{2y}{d}\right)^2\right\}^{i-1/2} \tag{36}$$

which satisfy the boundary conditions on E_y at the edge of the aperture for $i \geq 0$, $k \geq 1$. If the aperture susceptance is to be evaluated for a range of wavelengths of the order of magnitude of the aperture dimensions, the effect of the singularity of the component normal to the edge of the aperture will be very small. Thus, the term for which $i=0$ should be excluded as this function contains the singularity at the edge of the aperture. It should be pointed out also that although fields of finite energy may possess such singularities at knife edges, the Fourier

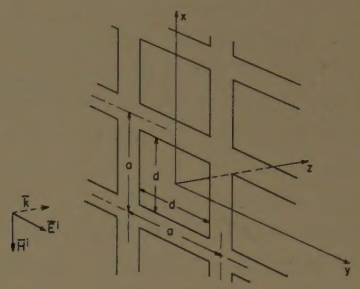

Fig. 2—Periodically-apertured plane screen.

series representation does not give the correct energy expressions in such cases, since a function of the form $\{1-(2y/d)^2\}^{-1/2}$ is not square integrable over the range of the aperture coordinates.

An appropriate trial function to choose would then be the leading term of the series above.

$$e_y = \left\{1 - \left(\frac{2x}{d}\right)^2\right\}^{1/2} \left\{1 - \left(\frac{2y}{d}\right)^2\right\}^{1/2}$$

$$e_x = 0. \tag{37}$$

With an incident wave polarized in the y direction, parallel to two of the edges of the aperture, the x component of the aperture electric field will be so small that it may be neglected. Upon substituting the trial function (37) and the Green's functions for TM and TE modes (34) and (35) into the variational expressions (15) and (16) and evaluating the integrals, the positive and negative definite parts of the susceptance for the lowest-order mode become

$$B^{+} = 4 \sum_{\substack{m=0 \\ n=0}}^{\infty} \epsilon_{mn} \frac{k}{\gamma_{mn}} \left\{ \frac{J_1\left(\frac{m\pi d}{a}\right)}{\frac{m\pi d}{2a}} \right\}^2 \left\{ \frac{J_1\left(\frac{n\pi d}{a}\right)}{\frac{n\pi d}{2a}} \right\}^2 \tag{38}$$

$$B^{-} = -4 \sum_{\substack{m=0 \\ n=0}}^{\infty} \epsilon_{mn} \frac{\gamma_{mn}}{k} \left\{ \frac{J_1\left(\frac{m\pi d}{a}\right)}{\frac{m\pi d}{2a}} \right\}^2 \left\{ \frac{J_1\left(\frac{n\pi d}{a}\right)}{\frac{n\pi d}{2a}} \right\}^2, \tag{39}$$

where

$$\epsilon_{mn} = \begin{cases} 1; & m \neq 0,\ n \neq 0,\ m \neq n \\ \frac{1}{2}; & m = 0 \text{ or } n = 0 \text{ or } m = n \\ 0; & m = n = 0. \end{cases}$$

The effect of other choices of trial function on the value of the equivalent susceptance and the relation between this value and the values of the component parts B^+ and B^- are discussed elsewhere.[11]

VIII. Evaluation of Multimode Scattering

Eqs. (38) and (39) may be used to evaluate the equivalent susceptance of the screen for wavelengths sufficiently long that only the normally incident plane wave is scattered. To calculate the scattering coefficients of higher modes, a new set of modal functions which are orthogonal over the aperture must be formed by the procedure described in Section V.

The variational expressions for the equivalent susceptance of the screen to each of the uncoupled modes then can be written. The expressions are similar to (38) and (39), except that the summations no longer begin with zero values of the indexes and are divided by finite sums representing the power carried by one of the uncoupled modes.

The susceptance expressions may be evaluated by taking a finite number of terms of the series and approximating the remainder by integrals. The transverse-field scattering coefficients s_{mn} are then calculated from the susceptances, using (23) and (27).

The amplitude of each scattered plane wave, represented by a plane-wave scattering coefficient t_{mn}, is related to the transverse-field scattering coefficient by

$$t_{\mathrm{TE}mn} = s_{mn} \cos \theta_{mn} = \frac{s_{mn}\gamma_{mn}}{k}$$

$$t_{\mathrm{TM}mn} = \frac{s_{mn}}{\cos \theta_{mn}} = \frac{s_{mn}k}{\gamma_{mn}}. \qquad (40)$$

For the incident mode, the transmission coefficient giving the amplitude of the incident wave transmitted through the screen is just

$$t_{00} = \left[1 - s_{00}^2 - 2\sum_{m,n} (t^2_{\mathrm{TE}mn} + t^2_{\mathrm{TM}mn})\right]^{1/2}. \qquad (41)$$

The transmission coefficients of the incident wave and the scattering coefficients of the higher-order modes are plotted as a function of ka in Fig. 3 for fixed ratio of aperture width to spacing $d/a = 0.7$.

Several interesting features are to be noted. First of all, it is seen that the transmission coefficient of the incident wave undergoes a discontinuity at values of ka

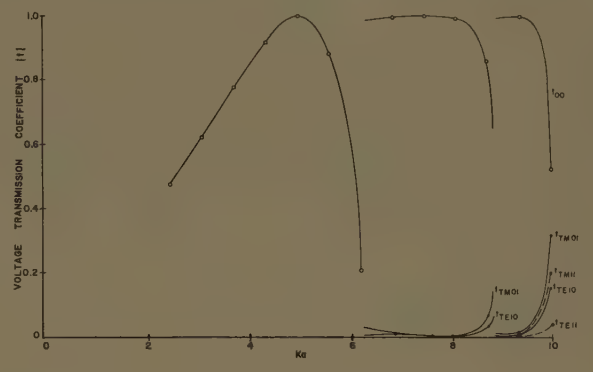

Fig. 3—Plane-wave voltage transmission and scattering coefficients of a plane conducting screen containing a periodic array of square apertures. The ratio of aperture width to spacing is $d/a = 0.7$.

corresponding to the cutoff of a higher-order plane-wave mode. This results from the fact that energy stored in the field of such a mode for k below the cutoff frequency contributes to the equivalent susceptance of the screen. Above the cutoff frequency the higher mode does not present a reactive component to the equivalent admittance, but a real component. Since the relation between stored energy and propagating energy in the fields changes at this point, it is to be expected that the transmission coefficient may also change.

Since the propagation constant goes to zero in changing from a real to an imaginary value at cutoff, the modal admittance coefficient of a cutoff TM mode approaches infinity. If the transverse electric-field amplitude of such a mode remains finite at the cutoff wavelength, the energy stored in this mode becomes infinite. Under such circumstances the equivalent susceptance of the obstacle will approach infinity and all of the energy will be reflected or scattered. It is interesting to note that this phenomenon has been observed experimentally with ruled diffraction gratings by Wood as early as 1902.[12]

However, the range of frequencies over which the large increase in reflected and scattered energy occurs is exaggerated by the variational calculation. The assumption of a trial function for the aperture distribution which is independent of frequency leads to a rather large error near a cutoff frequency, since the energy relations change rapidly in the vicinity of such a point.

[11] R. B. Kieburtz and A. Ishimaru, "The Variational Method for Evaluation of Scattering of Electromagnetic Waves by Obstacles," (II), "Scattering by a Periodically Apertured Conducting Screen," Dept. of Elec. Engrg., University of Washington, Seattle, Wash., Tech. Rept. No. 47; January, 1961.

[12] R. W. Wood, "On a remarkable case of uneven distribution of light in a diffraction grating spectrum," *Phil. Mag.*, vol. 4, pp. 396–402, September, 1902. "Diffractive gratings with controlled groove form with abnormal distribution of density." *Phil. Mag.*, vol. 23, pp. 310–317; February, 1912. "Anomalous diffractive gratings," *Phys. Rev.*, vol. 48, pp. 928–936; December, 1935.

Thus, the value of the variational expression for the susceptance becomes much more sensitive to the choice of a trial function. At such values of frequency an accurate estimate of the scattering is very difficult to achieve.

The sudden dip in transmission coefficient of the incident mode which occurs around $ka = 10.0$ is not due to proximity to a higher-mode cutoff. This is a different phenomenon which occurs when the directions of the off-center diffraction lobes coincide with a strong maximum of the radiation pattern of a single aperture. At this point, very little of the energy incident is reflected in the normal plane-wave mode in contrast with the singular points which occur at cutoff frequencies. Instead, most of the energy is scattered into off-center diffraction lobes which radiate from both sides of the screen.

The second point to notice from these calculations is the resonance phenomenon associated with the array of square apertures. This is not found in the two-dimensional problem of an infinite array of slits in a conducting screen; it occurs only with apertures of finite size. One interesting implication of the resonance of the periodic array is that at resonance, the incident wave is transmitted without coupling to any higher-order modes. This result is apparent from the formulation and does not depend on any assumption concerning the aperture distribution.

Although the effect of varying angle of incidence of the exciting wave has not been considered here, there is no fundamental reason why it cannot be. The problem is complicated considerably, however, so that calculations would become quite tedious. Since degeneracies are removed, more distinct terms appear in the series expressions for admittances, and more critical values of ka occur in a given range.

IX. Conclusions

The variational method for evaluation of scattering by periodic planar obstacles or by planar obstacles in waveguides has been formulated from consideration of the eigenvalues of an energy operator. It has been shown that a variational formulation should be possible for any problem in which the field functions can be expanded in a set of orthogonal modal functions.

Using this formulation, the variational method has been extended to enable evaluation of coupling of energy from a single incident mode into several propagating modes coupled by an obstacle. This has been applied to the specific problem of scattering of plane waves by a conducting screen containing a doubly-periodic array of square apertures.

Several interesting phenomena are predicted by the evaluation of scattering by an infinite periodic structure. One of these is the large discontinuity in scattering and transmission coefficients as functions of wave number k which occurs whenever a critical value of k is approached at the transition of a TM mode from an evanescent to a propagating state.

Another phenomenon predicted by the variational calculation is the occurrence of a resonance at a value of k somewhat below the cutoff of a higher mode. This resonance results in complete cancellation of the specular reflection of the incident wave by the conducting part of the screen, and is not to be confused with the aperture resonance which can occur as a maximum of the transmission cross section of a small aperture at a wavelength approximately equal to the aperture circumference. From the form of the variational expressions, it is seen that the coupling of energy into higher-order diffraction lobes should also go to zero at such resonant points, and the incident wave should be transmitted through the screen without being scattered.

A Reaction Theorem and Its Application to Antenna Impedance Calculations*

J. H. RICHMOND†, SENIOR MEMBER, IRE

Summary—**The reaction theorem is generalized to allow the fields of an antenna in one environment to be employed in calculations of mutual impedance in another environment.**

Several expressions for self-impedance and mutual impedance are presented. These are in the form of surface integrals or volume integrals of the field intensities or the current density. It is shown how the fields of an antenna in free space can be useful in calculating the impedance in the presence of scatterers.

Introduction

RECIPROCITY theorems are among the most useful tools in field and circuit problems, ranking with the superposition theorem and the equivalence theorems. It is convenient to classify the reciprocity theorems into three types: pure circuit, pure field, and mixed. The pure circuit form

$$V_{12}I_{11} = V_{21}I_{22} \tag{1}$$

developed by Rayleigh for networks of lumped elements was extended to antennas by Carson [1]. It applies to a pair of antennas only if each antenna has suitable terminals where voltage and current can be defined.

A theorem of the second type (pure field) involving electric- and magnetic-field intensities was derived by Lorentz [1] in the form of the surface integral

$$\int_{S_1} (\boldsymbol{E}_1 \times \boldsymbol{H}_2 - \boldsymbol{E}_2 \times \boldsymbol{H}_1) \cdot d\boldsymbol{s} = \int_{S_2} (\boldsymbol{E}_2 \times \boldsymbol{H}_1 - \boldsymbol{E}_1 \times \boldsymbol{H}_2) \cdot d\boldsymbol{s}, \tag{2}$$

where surface S_1 encloses antenna 1 and S_2 encloses antenna 2. (Subscripts indicate the source of the field. For example, $\boldsymbol{E}_1$ represents the electric-field intensity set up by antenna 1.) Carson [1] also presented a pure-field theorem in the form of a volume integral involving electric-current density and electric-field intensity,

$$\int_{V_1} \boldsymbol{J}_1 \cdot \boldsymbol{E}_2 dv = \int_{V_2} \boldsymbol{J}_2 \cdot \boldsymbol{E}_1 dv, \tag{3}$$

where volume V_1 includes antenna 1 and V_2 includes antenna 2. Since terminal currents and voltages are not involved, these pure-field theorems apply even when no suitable terminals exist.

Rumsey [2] has given the name "reaction" to the quantity represented by the integrals which appear in the reciprocity theorems of Lorentz and Carson and has proposed the symbol $\langle 1, 2 \rangle$ for the integrals on the left side in (2) and (3). In this terminology, the reciprocity theorems of Lorentz and Carson state that the reaction of antenna 1 on antenna 2 is equal to the reaction of antenna 2 on antenna 1.

Kouyoumjian [3] has developed an expression for the voltage or current induced in one antenna by another in terms of the reaction. This reaction theorem states the quantity on the left side in (1) is equal to the negative of the quantity on the left side in (2), that is

$$V_{12}I_{11} = -\langle 1, 2 \rangle. \tag{4}$$

This important relation was also pointed out by Rumsey [2]. It is valid under conditions more general than those required for reciprocity, as will be shown. However, if the conditions for reciprocity are satisfied, this reaction theorem (4) can be combined with any one of the "pure" reciprocity theorems given above to obtain a reciprocity theorem of the "mixed type." Circuit quantities (voltage and current) appear on one side of the equation, while field quantities appear on the other side.

In this paper a generalized form of the reaction theorem is presented, and equations are derived from it for the mutual impedance of two antennas. Expressions for self-impedance are derived by similar methods.

In most equations from physics all of the quantities involved in a given equation are understood to relate to a common situation. For example, Newton's second law relates the force acting on a body, the mass of the *same* body, and its acceleration, all at the *same* instant of time. On the other hand, each of the reciprocity and reaction theorems brings together quantities from different situations into a single equation. In the most familiar versions of these theorems the two situations differ only in that a battery and an ammeter have traded places in a network. In the generalized versions of these theorems developed herein some portions of the environment or network are considered to change when the source and observer trade places. Although this may seem confusing the mental effort is rewarded in the form of expressions which show how the fields of an antenna in one environment may be employed in calculations of impedance in another environment.

* Received by the PGAP, February 10, 1961; revised manuscript received, June 21, 1961. This research was sponsored by the Aeronautical Systems Div., AF Systems Command, Wright-Patterson AFB, under Contract AF33(616)-7614.

† Antenna Lab., Dept. of Elec. Engrg., The Ohio State Univ., Columbus.

Generalization of the Reaction Theorem

The concepts involved in the generalized reaction theorem can be introduced by means of the corresponding network theorem. Consider the two passive networks in Fig. 1. In antenna terminology, network 1 is transmitting and network 2 is receiving. The voltages V and V_{21} and the current I for this situation are defined in Fig. 1. Now let network 2 transmit with terminal current I_{22}' into a new impedance Z' as in Fig. 2. The voltage V' and currents I_{22}' and I' for this situation are defined in Fig. 2. The current generators I_{11} and I_{22}' are assumed to have the same frequency.

If the reciprocity theorem applies to network 2 (but not necessarily to network 1), it can easily be shown that

$$V_{21}I_{22}' = V'I - VI'. \tag{5}$$

Since V_{21} and I_{22}' are independent of Z', both sides of (5) must also be independent of Z'. This is true even though each of the two terms on the right side are dependent on Z' through V' and I'. As an example, suppose network 2 consists of three resistors as in Fig. 3, and let I be 2 amperes and I_{22}' 1 ampere. Then obviously V is 8 volts and V_{21} is 4 volts. The solutions for three values of Z' are tabulated below:

Z'	I'	V'	$V'I - VI'$
0Ω	$-1/2a$	$0v$	$0 + 4 = 4$
4	$-1/4$	1	$2 + 2 = 4$
∞	0	2	$4 + 0 = 4$.

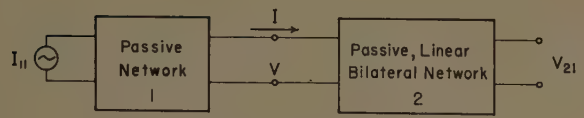

Fig. 1—First situation: Network 1 transmits, network 2 receives.

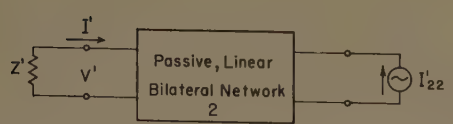

Fig. 2—Second situation: Network 2 transmits into a new impedance Z'.

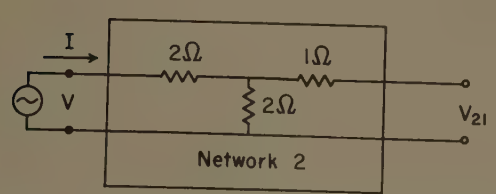

Fig. 3—An example to illustrate the network version of the reaction theorem.

In each case the quantity $V'I - VI'$ is equal to four, which is also the value of $V_{21}I_{22}'$ and the "reaction of network 1 on network 2."

This network theorem (5) is not widely used, partly because it is not well known. It is applicable to transmission-line problems and ladder networks. The quantity $V'I - VI'$ is independent not only of the impedance Z', but also of the point along the network or transmission line at which the theorem is applied.

This network theorem should pave the way to an understanding of the corresponding field theorem, which is presented next.

Consider the situation shown in Fig. 4 in which antenna 1 is transmitting, setting up the field ($\boldsymbol{E}_1$, $\boldsymbol{H}_1$) and inducing a voltage V_{21} at the open-circuited terminals of the receiving antenna (antenna 2). The environment "seen" by antenna 1 may be described by the complex permeability μ and permittivity ϵ, and it includes the structure of antenna 2 (with terminals open circuited). The medium need not be homogeneous.

In the usual reciprocity-theorem derivations, the roles of the two antennas are reversed at this point, and antenna 2 is considered to transmit while antenna 1 receives in the same environment (μ, ϵ) as before. On the contrary, consider the fields ($\boldsymbol{E}_2'$, $\boldsymbol{H}_2'$) of antenna 2 transmitting in a new environment (μ', ϵ') which does not necessarily include the structure of antenna 1. (However, let $\mu' = \mu$ and $\epsilon' = \epsilon$ within the regular surface S_2 enclosing antenna 2.) This situation is depicted in Fig. 5.

Now, as shown in Appendix I, these quantities are related as follows:[1]

$$V_{21}I_{22}' = -\int_{S_2} (\boldsymbol{E}_2' \times \boldsymbol{H}_1 - \boldsymbol{E}_1 \times \boldsymbol{H}_2') \cdot d\boldsymbol{s}. \tag{6}$$

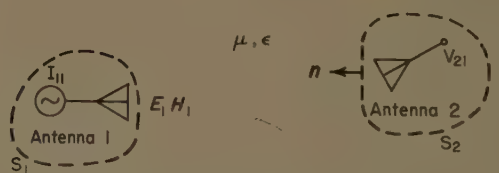

Fig. 4—First situation: Antenna 1 transmits, antenna 2 receives.

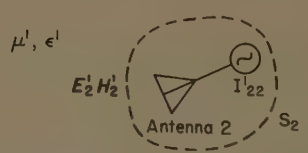

Fig. 5—Second situation: Antenna 2 transmits in a new environment.

[1] Eq. (6) and many of the other results presented in this paper are derived in J. H. Richmond, "On the Theory of Scattering by Dielectric and Metal Objects," Ohio State Univ. Res. Foundation, Columbus, Ohio, Antenna Lab. Rept. 786-3; April, 1958.

Eq. (6) is a generalization of the reaction theorem. The usual time dependence $e^{j\omega t}$ is understood. It is assumed that all media are linear, the permeability and permittivity are independent of time, and antenna 2 is constructed of isotropic media. (The other media are not necessarily isotropic.) It is assumed that the feed system of antenna 2 has a section of perfectly shielded waveguide or transmission line, and that only a single mode exists at some point on the feed. The antenna terminals are chosen at such a point, and I_{22}' represents the current there when antenna 2 transmits (Fig. 5).

The incremental area $d\mathbf{s}$ in (6) has a vector direction normal to the surface S_2 and away from antenna 2.

After using (6) to calculate the voltage V_{21} induced at the open-circuited terminals of antenna 2, Thevenin's theorem may be employed to determine the terminal voltage for any other load impedance.

Perhaps it should be emphasized here that the voltage V_{21} in (6) is the induced voltage in the original situation shown in Fig. 4, *not* in the new environment of Fig. 5. If a constant-current generator is employed when antenna 2 transmits, the current I_{22}' will be the same regardless of the environment in which antenna 2 transmits. Then the left-hand side of (6) is independent of the new environment, and so must also be the integral on the right hand, even though the integrand does depend on the new environment. (The difference integrates to zero.)

Thus, although the field $(\boldsymbol{E}_2', \boldsymbol{H}_2')$depends on the environment in which antenna 2 transmits, the integral in (6) is invariant with respect to changes in this environment. Therefore, the environment (μ', ϵ') may be chosen to represent any convenient situation such as

1) free space,
2) the same environment into which antenna 1 transmitted,
3) as perfectly conducting metal shell on S_2, or
4) an extension of the structure of antenna 2.

In the last case listed, where the environment is chosen to be an extension of the antenna structure, the generalized reaction theorem shows some similarity to the induction theorem of Schelkunoff [5].

The transmission formula of Friis [6] and the receiving antenna-sensitivity formula of Levis [7] can be derived from (6). These formulas apply only in the far-field case (where antennas 1 and 2 are far apart), whereas (6) does not have this restriction.

The analysis can readily be extended to the case where two or more modes can exist at the terminal surface of antenna 2. In this case, it is convenient to use the set of orthogonal modes of the waveguide or transmission line, letting V_{22n}' and I_{22n}' represent the voltage and current for mode n when antenna 2 transmits. If V_{21n} and I_{21n} denote the received voltage and current for mode n when antenna 1 transmits, it can be shown that the more general form of (6) is

$$\sum_n (V_{21n}I_{22n}' - I_{21n}V_{22n}') = -\int_{S_2} (\boldsymbol{E}_2' \times \boldsymbol{H}_1 - \boldsymbol{E}_1 \times \boldsymbol{H}_2') \cdot d\mathbf{s}. \quad (7)$$

Mutual Impedance of Two Antennas

The mutual impedance Z_{21} between antennas 1 and 2 in the environment (μ, ϵ) illustrated in Fig. 4 is

$$Z_{21} = V_{21}/I_{11} = \frac{-1}{I_{11}I_{22}'} \int_{S_2} (\boldsymbol{E}_2' \times \boldsymbol{H}_1 - \boldsymbol{E}_1 \times \boldsymbol{H}_2') \cdot d\mathbf{s}, \quad (8)$$

where I_{11} is the terminal current of antenna 1 when it transmits. Eq. (8) follows directly from the reaction theorem (6).

It will be recalled that $(\boldsymbol{E}_1, \boldsymbol{H}_1)$ represents the field of antenna 1 transmitting in the presence of antenna 2 with its terminals open circuited. With the aid of Thevenin's theorem it can be shown that a factor $(Z+Z_2)/(Z+Z_2')$ must be inserted in front of the integral in (8) in the more general case where $(\boldsymbol{E}_1, \boldsymbol{H}_1)$ represents the field with an impedance Z across the terminals of antenna 2. Here Z_2 and Z_2' represent the input impedance of antenna 2 in environment (μ, ϵ) and (μ', ϵ'), respectively.

If the conditions for reciprocity are satisfied, (8) yields the mutual impedance Z_{12}, as well as Z_{21}. To insure reciprocity, it will suffice if the two antennas are of finite dimensions and a finite distance apart, all media are linear and isotropic, and the medium is homogeneous outside an imaginary sphere of finite radius.

In some cases the fields of an extended antenna are known, whereas those of the corresponding truncated antenna are not. Examples include horns and biconical antennas. Eq. (8) permits the use of the known fields of an extended antenna in calculating the mutual impedance for a truncated antenna.

If a perfectly conducting metal shell is assumed on S_2 for environment (μ', ϵ'), the first term in the integral in (8) will vanish. Letting $\boldsymbol{J}_2 = -\boldsymbol{n} \times \boldsymbol{H}_2'$ represent the electric-current density induced on the shell by antenna 2, (8) reduces to

$$Z_{21} = \frac{1}{I_{11}I_{22}'} \int_{S_2} \boldsymbol{J}_2 \cdot \boldsymbol{E}_1 ds. \quad (9)$$

Eq. (9) is particularly convenient in mutual impedance calculations when one of the antennas consists of a waveguide or cavity perforated with holes or slots. Let the perfectly conducting surface S_2 coincide with the metal surface of the antenna plus the apertures formed by the holes. Then the integral in (9) vanishes except in the holes, since the tangential components of $\boldsymbol{E}_1$ vanish on the metal. Furthermore, the current $\boldsymbol{J}_2$ will in many cases be a simple known function, since it is

the current on the inside walls of the waveguide or cavity when the holes are covered with conductor.

The divergence theorem and Maxwell's equations can be employed to obtain another expression for mutual impedance from (8),

$$Z_{21} = \frac{-1}{I_{11}I_{22}'} \int_{V_2} (J_2 \cdot E_1 - K_2 \cdot H_1) dv, \tag{10}$$

where J_2 and K_2 are the densities of electric- and magnetic-source current, and V_2 is the volume within S_2. Since magnetic current does not exist in realizable sources, the term $K_2 \cdot H_1$ may be omitted.

For an aperture antenna such as a horn or paraboloid, it is convenient to choose S_2 to coincide with the outer surface of the antenna plus the aperture. Then the integrand in (8) vanishes everywhere on S_2, except on the aperture.

Although (8) is suitable for aperture antennas, it is difficult to apply to cylindrical-wire antennas. The difficulty arises from the fact that the integrand vanishes everywhere on the antenna surface, except where S_2 crosses the terminal gap. This problem also exists with the induced EMF formulas for self- and mutual impedance [4], [8]. The following expression, derived in Appendix II is more convenient for cylindrical wire antennas:

$$Z_{21} = \frac{-1}{I_{11}I_{22}} \int_{S_2} (E_2 \times H_1^i - E_1^i \times H_2) \cdot ds. \tag{11}$$

Eq. (11) is the same as (8), except that the environment (μ', ϵ') has been chosen to be the same as (μ, ϵ), and the field of antenna 1 has been replaced by its incident component.

Eq. (11) is convenient even when S_2 coincides with the perfectly conducting metal surfaces of a cylindrical-wire antenna. In this case the first term in the integral vanishes, with a possible exception where S_2 crosses the terminal gap. The second term, however, does not vanish because it involves the incident field rather than the total field. The surface current J_2 on the metal can be introduced in place of $n \times H_2$ to obtain the following result:

$$Z_{21} = \frac{1}{I_{11}I_{22}} \int_{S_2} J_2 \cdot E_1^i ds. \tag{12}$$

Self-Impedance

Consider an antenna transmitting in some environment (μ, ϵ), and let (E, H), V, I, and Z represent the field, the voltage, the current, and the impedance, respectively. Now let the antenna transmit in a new environment (μ', ϵ') with field (E', H'), voltage V' and impedance Z'. If the current I is adjusted to be the same in both cases, and if the "scattered voltage" V_s is defined by

$$V_s = V' - V, \tag{13}$$

then the impedances are related as follows:

$$Z' = Z + V_s/I. \tag{14}$$

Letting the two environments coincide ($\mu' = \mu$ and $\epsilon' = \epsilon$) within a surface S which encloses the antenna, a useful expression for the impedance is

$$Z' = Z + \frac{1}{I^2} \int_S (E' \times H - E \times H') \cdot ds. \tag{15}$$

The derivation will not be given here, since it is similar to that in Appendix I.

It is possible to let the environment (μ', ϵ') represent an extension of the antenna structure. In this way, (15) and some of the other impedance expressions in this section can be used to calculate the change in impedance associated with an increase or decrease in the length of an antenna. Furthermore, the impedance of a truncated antenna can thereby be related to the impedance of the corresponding complete antenna. This procedure would be particularly convenient for antennas of simple geometry (such as horns and spheroidal antennas) where the impedance and fields of the complete antenna are known.

If the antenna is a waveguide or cavity which is perforated with holes or slots, it will be convenient to let surface S be the metallic outer surface of the antenna plus the aperture surface of the holes. A perfectly conducting metal shell may enclose the antenna for environment (μ', ϵ'), in which case the first term in the integral in (15) will vanish. In terms of the current density $J' = -n \times H'$ induced on the inner surface of the shell, (15) can be written in the form

$$Z' = Z - \frac{1}{I^2} \int_S J' \cdot E ds. \tag{16}$$

It is sufficient to integrate over the holes, since the tangential components of E vanish elsewhere on S. In many cases, Z' and J' will be known quantities, namely, the impedance and current density of the cavity or waveguide with no holes. Eq. (16) allows these to be employed in the calculation of the impedance Z with holes.

Suppose the two environments coincide everywhere except within a finite region called the "scattering region" enclosed by surface S_s. Then an alternative expression for the impedance is

$$Z' = Z - \frac{1}{I^2} \int_{S_s} (E' \times H - E \times H') \cdot ds. \tag{17}$$

Eq. (17) can be derived from (15) by using the radiation conditions to show that the integral vanishes on an infinite sphere, using Maxwell's equations to show that $\nabla \cdot (E' \times H - E \times H')$ vanishes at each point outside S and S_s, and using the divergence theorem.

Antenna impedance can be expressed in terms of a volume integral by using (15), the divergence theorem, and Maxwell's equations. The result is

$$Z' = Z - \frac{1}{I^2}\int_V (\boldsymbol{J}\cdot\boldsymbol{E}^s - \boldsymbol{K}\cdot\boldsymbol{H}^s)dv, \tag{18}$$

where V represents the antenna region which is enclosed by surface S, $\boldsymbol{J}$ and $\boldsymbol{K}$ are the densities of electric and magnetic source current[2] and $(\boldsymbol{E}^s, \boldsymbol{H}^s)$ is the scattered field defined by

$$\boldsymbol{E}^s = \boldsymbol{E}' - \boldsymbol{E} \tag{19}$$

$$\boldsymbol{H}^s = \boldsymbol{H}' - \boldsymbol{H}. \tag{20}$$

Another expression can be obtained in a similar manner by starting with (17)

$$Z' = Z - \frac{j\omega}{I^2}\int_{V_s} [(\epsilon' - \epsilon)\boldsymbol{E}'\cdot\boldsymbol{E} - (\mu' - \mu)\boldsymbol{H}'\cdot\boldsymbol{H}]dv, \tag{21}$$

where V_s is the scattering region enclosed by surface S_s.

If environment (μ', ϵ') includes a perfectly conducting metallic body which fills the "scattering region," (17) reduces to

$$Z' = Z - \frac{1}{I^2}\int_{S_s} \boldsymbol{J}'\cdot\boldsymbol{E}ds, \tag{22}$$

where $\boldsymbol{J}'$ is the current density induced on the conducting surface. The conducting body in the scattering region can be arranged as an extension of a cylindrical wire as in Fig. 6. In this way, (22) expresses the change in impedance associated with a change in the length of such an antenna. The integral in (22) has the same form as that appearing in the induced EMF method, but the integrand does not vanish on the surface of integration.

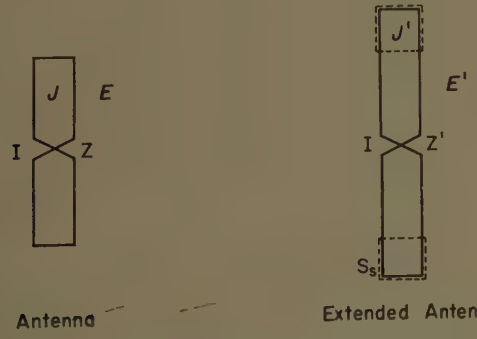

Fig. 6—Cylindrical wire antennas illustrating an application of (22).

Conclusion

The reaction theorem has been generalized to allow the fields of an antenna in one environment to be employed in calculations of mutual impedance in another environment. For example, the known fields of an infinitely long horn can be used in calculating the mutual impedance between a truncated horn and another antenna. As another example, this formulation permits the known current on the inside of a waveguide to be used in calculating the radiation from an antenna consisting of a waveguide with holes or slots.

In some cases it is advantageous to let the two environments be the same. If this is done one of the fields involved in the mutual impedance equation can be replaced by the incident field. This avoids the difficulty which arises in the induced EMF method, where the integral vanishes over perfectly conducting portions of the antenna.

Several expressions are presented for the self-impedance of an antenna. They permit the known fields and impedance of a "complete antenna" to be used in calculating the impedance of the corresponding truncated antenna.

Appendix I

A Generalized Reaction Theorem

Antenna 2 may be constructed partly of dielectric and partly of metal, as suggested in Fig. 7. Any conductivity in the dielectric portions will be accounted for by letting μ and ϵ be complex. Maxwell's equations for the fields within S_2, but excluding the "source region" shown in Fig. 7, are

$$\nabla \times \boldsymbol{E}_1 = -j\omega\mu\boldsymbol{H}_1, \tag{23}$$

$$\nabla \times \boldsymbol{H}_1 = j\omega\epsilon\boldsymbol{E}_1, \tag{24}$$

$$\nabla \times \boldsymbol{E}_2' = -j\omega\mu\boldsymbol{H}_2', \tag{25}$$

$$\nabla \times \boldsymbol{H}_2' = j\omega\epsilon\boldsymbol{E}_2'. \tag{26}$$

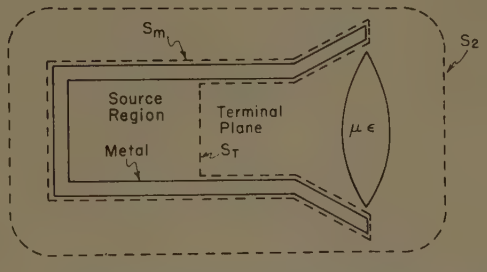

Fig. 7—A metal horn with a dielectric lens, illustrating the surfaces employed in the derivation.

From (23)–(26) and a vector identity, it can be shown that

$$\nabla\cdot(\boldsymbol{E}_1 \times \boldsymbol{H}_2' - \boldsymbol{E}_2' \times \boldsymbol{H}_1) = 0. \tag{27}$$

The reaction of antenna 1 on antenna 2 is

$$\langle 2, 1\rangle = \int_{S_2} (\boldsymbol{E}_2' \times \boldsymbol{H}_1 - \boldsymbol{E}_1 \times \boldsymbol{H}_2')\cdot d\boldsymbol{s}. \tag{28}$$

Eq. (28) is simply a definition of reaction; it differs slightly from the standard form in that the two fields which are involved in the integral are for different environments. The divergence theorem and (27) allow the

[2] It is assumed that the currents $\boldsymbol{J}$ and $\boldsymbol{K}$ are held constant when the environment is changed from (μ, ϵ) to (μ', ϵ').

surface of integration in (28) to be changed from S_2 to S_m+S_T (see Fig. 7). Furthermore, the integral on the metal surface S_m vanishes if it is assumed to be perfectly conducting, since $\boldsymbol{E}_1$ and $\boldsymbol{E}_2'$ are normal to this surface. This leaves only the integration over the terminal surface S_T.

Letting subscript "t" denote tangential-field components on the terminal plane, the voltage and current are defined as follows when antenna 2 transmits [9]:

$$\boldsymbol{E}_{2t}' = V_{22}'\boldsymbol{e} \tag{29}$$

and

$$\boldsymbol{H}_{2t}' = I_{22}'\boldsymbol{h}. \tag{30}$$

The vector-mode functions are related by

$$\boldsymbol{h} = \boldsymbol{n} \times \boldsymbol{e}, \tag{31}$$

and they are normalized by letting

$$\int_{S_T} \boldsymbol{e}\cdot\boldsymbol{e}\,ds = 1. \tag{32}$$

The voltage and current induced at antenna 2 when antenna 1 transmits are defined in a similar manner by

$$\boldsymbol{E}_{1t} = V_{21}\boldsymbol{e} \tag{33}$$

and

$$\boldsymbol{H}_{1t} = I_{21}\boldsymbol{h}. \tag{34}$$

Eqs. (29)–(34) can be used to reduce (28) to

$$\langle 2, 1\rangle = V_{22}'I_{21} - V_{21}I_{22}'. \tag{35}$$

The received current I_{21} is zero, since the terminals are assumed to be open circuited when receiving. Therefore, (35) becomes

$$V_{21}I_{22}' = -\langle 2, 1\rangle. \tag{36}$$

This leads directly to the "reaction theorem," (6).

Appendix II

Mutual Impedance in Terms of the Incident Field

Let the field $(\boldsymbol{E}_2, \boldsymbol{H}_2)$ be the field of antenna 2 when transmitting with current I_{22} in the environment (μ, ϵ), which includes the structure of antenna 1.[3] The field of antenna 1 in this same environment is resolved into incident and scattered components by means of the following equations:

$$\boldsymbol{E}_1 = \boldsymbol{E}_1{}^i + \boldsymbol{E}_1{}^s \tag{37}$$

[3] To be more specific, let $(\boldsymbol{E}_2, \boldsymbol{H}_2)$ be the field of antenna 2 in the presence of antenna 1, the generator across the terminals of antenna 1 being replaced by its internal impedance.

and

$$\boldsymbol{H}_1 = \boldsymbol{H}_1{}^i + \boldsymbol{H}_1{}^s. \tag{38}$$

To complete the definition of these fields, Maxwell's equations for the incident and scattered fields are given:

$$\left.\begin{aligned} \nabla \times \boldsymbol{H}_1{}^i &= j\omega\epsilon_0\boldsymbol{E}_1{}^i \\ \nabla \times \boldsymbol{E}_1{}^i &= -j\omega\mu_0\boldsymbol{H}_1{}^i \end{aligned}\right\} \text{ within } S_2 \tag{39, 40}$$

$$\left.\begin{aligned} \nabla \times \boldsymbol{H}_1{}^s &= j\omega\epsilon\boldsymbol{E}_1{}^s \\ \nabla \times \boldsymbol{E}_1{}^s &= -j\omega\mu\boldsymbol{H}_1{}^s \end{aligned}\right\} \text{ outside } S_2. \tag{41, 42}$$

Eq. (11) can be derived by starting with (8) and using (37) and (38) to split the integral into one involving the incident field and another involving the scattered field. The integral of $\boldsymbol{E}_2\times\boldsymbol{H}_1{}^s-\boldsymbol{E}_1{}^s\times\boldsymbol{H}_2$ on a sphere vanishes as the radius goes to infinity in view of the radiation conditions. (Antenna 2 is assumed to be of finite dimensions, and the medium outside a finite sphere is assumed to be free space.) The integral on the infinite sphere can be expressed via the divergence theorem as a volume integral of $\nabla\cdot(\boldsymbol{E}_2\times\boldsymbol{H}_1{}^s-\boldsymbol{E}_1{}^s\times\boldsymbol{H}_2)$. Maxwell's equations can be used to show that this integrand vanishes at each point outside S_2. It follows that the integral of $\boldsymbol{E}_2\times\boldsymbol{H}_1{}^s-\boldsymbol{E}_1{}^s\times\boldsymbol{H}_2$ on S_2 is zero, and (11) is established.

Acknowledgment

Discussions with Dr. R. G. Kouyoumjian of The Ohio State University have been most helpful and are gratefully acknowledged. Many of the ideas presented in this paper were stimulated by Prof. V. H. Rumsey through a course he presented in the 1950's at The Ohio State University.

References

[1] J. R. Carson, "Reciprocal theorems in radio communication," Proc. IRE, vol. 17, pp. 952–956; June, 1929.

[2] V. H. Rumsey, "Reaction concept in electromagnetic theory," *Phys. Rev.*, vol. 94, pp. 1483–1491; June 15, 1954.

[3] R. G. Kouyoumjian, "The Calculation of the Echo Areas of Perfectly Conducting Objects by the Variational Method," Antenna Lab., Ohio State Univ. Res. Foundation, Columbus, Rept. No. 444-13, pp. 29, 80–84; 1953.

[4] A. B. Bronwell and R. E. Beam, "Theory and Application of Microwaves," McGraw-Hill Book Co., Inc., New York, N. Y., pp. 424–434; 1947.

[5] S. A. Schelkunoff and H. Friis, "Antennas: Theory and Practice," John Wiley and Sons, Inc., New York, N. Y., p. 516; 1952.

[6] H. T. Friis, "A note on a simple transmission formula," Proc IRE, vol. 34, pp. 254–256; May, 1946.

[7] C. Levis, "Note on Receiving Antenna Sensitivity," Antenna Lab., Ohio State Univ. Res. Foundation, Columbus, Ohio, Rept. No. 486-29; 1954.

[8] P. S. Carter, "Circuit relations in radiating systems and applications to antenna problems," Proc. IRE, vol. 20, pp. 1004–1041; June, 1932.

[9] N. Marcuvitz, Ed., "Waveguide Handbook," McGraw-Hill Book Co., Inc., New York, N. Y., Sec. 1–2; 1951.

Single-Channel Direction Finding in a Multicomponent Field*

W. M. SHERRILL†, MEMBER, IRE, AND D. N. TRAVERS†, MEMBER, IRE

Summary—**On the basis of theoretical argument and experimental results, the capability of a single-channel spinning-loop direction finder to resolve the directional components of a multicomponent field of plane waves is demonstrated. Calculated bearing displays are compared with corresponding displays obtained by experiment for the cases of two and three components. Directional resolution of components of equal and differing frequencies is demonstrated, and methods of presenting the bearing display are discussed.**

Introduction

THE capability of loop antennas to resolve the directional components of a multicomponent field has been generally known among investigators for some time. Gabler and Waechtler[1] have reported that by means of crossed loops and a twin-channel receiver, the directions of two components of equal frequency may be resolved when the antenna properly samples the resultant field. Recently the authors have reported[2] the analogous capability of a spinning loop antenna and single channel receiver to resolve the directional components of a field of two components of equal frequency by means of the intersection of antenna patterns obtained at positions of different phase in the resultant field. In the discussion which follows, general component resolution properties of a single-channel spinning-loop direction finder in a multicomponent field will be demonstrated on the basis of analysis and experimental results.

Theory

Consider a multicomponent field of n components incident upon a single spinning loop antenna as shown in Fig. 1. Assume the components to be vertically polarized plane waves with differing azimuths, amplitudes, frequencies, and phase. Referring phase to the origin (O) of the coordinate system, the resultant field ($\mathcal{E}_T$) at any point P may be given by

$$\mathcal{E}_T = \sum_{k=1}^{n} \mathcal{E}_k e^{j(\omega_k t + \phi_k)}, \tag{1}$$

where $\mathcal{E}_k$ = the amplitude of the kth component and ω_k is its angular frequency . The phase of the kth component (ϕ_k) is given by

$$\phi_k = \beta_k \rho \cos(\tau - \delta_k) + \eta_k, \tag{2}$$

where $\beta_k = 2\pi/\lambda_k$, the free space phase constant of the kth wave, and

ρ = radial distance to the point P,
τ = polar angle of the point P,
δ_k = azimuth of the kth component,
η_k = an arbitrary phase constant associated with the kth component.

If a single spinning loop antenna of radius (r) much less than the shortest wavelength is placed at P, the total output voltage signal (V_T) of the antenna will be

$$V_T = \sum_{k=1}^{n} r[\beta_k h_{ek} \mathcal{E}_k \sin(\theta - \delta_k) e^{j(\omega_k t + \phi_k)}], \tag{3}$$

where

r = radius of the loop antenna $\ll \lambda_k$,
h_{ek} = effective height of the antenna corresponding to the kth component,
θ = angle of rotation of the loop antenna (see Fig. 1).

Let E_k be defined in the following way:

$$E_k = r\beta_k h_{ek} \mathcal{E}_k.$$

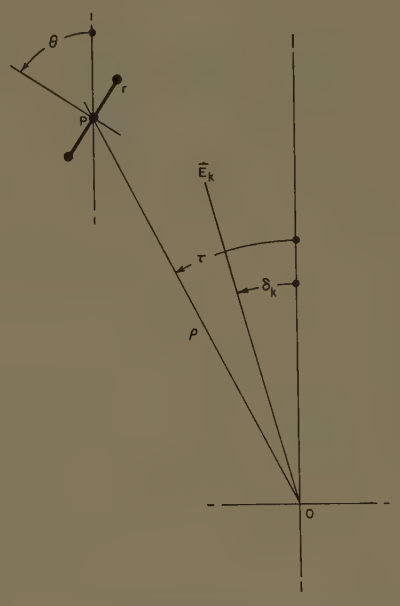

Fig. 1—Geometry of a single-channel direction finder in a multicomponent field.

* Received by the PGAP, March 4, 1961; revised manuscript received, July 14, 1961. This work was supported by the U. S. Navy, Bureau of Ships, Contract NObsr-85086.

† Southwest Research Inst., San Antonio, Tex.

[1] H. Gabler and M. Waechtler, "A new method of determining the components of radio bearings from coherent waves," *Elektrotech. Z.*, vol. 79A, pp. 385–388; June, 1958. Natl. Res. Council of Canada Tech. Translation No. 819.

[2] D. N. Travers and W. M. Sherrill, "Direction finding in a two-component field," IRE TRANS. ON ANTENNAS AND PROPAGATION, vol. AP-8, pp. 520–521; September, 1960.

Then the total output voltage signal of the antenna may be more simply written

$$V_T = \sum_{k=1}^{n} E_k \sin(\theta - \delta_k) e^{j(\omega_k t + \phi_k)}. \quad (4)$$

The frequency relations in the multicomponent field are such that the interference pattern of the components possesses a period of either finite or infinite duration. The highest common factor of the ω_k of (1) determines the common angular beat frequency ω_B of finite period. Thus

$$\omega_k = m_k \omega_B, \quad (5)$$

where

m_k = an integer.

For the cases where the ω_k possess no common factor or that the ω_k are equal, the beat period is infinite. However, in practice, multicomponent fields with the ω_k related by a common beat frequency or with the ω_k equal (hence zero beat frequency) are of greatest importance. The following discussion is limited to these two cases.

Substituting (5) into (4), it is seen that the antenna output voltage may be written

$$V_T = \sum_{k=1}^{n} E_k \sin(\theta - \delta_k) e^{j(m_k \omega_B t + \phi_k)}. \quad (6)$$

Assuming that the receiver has sufficient bandwidth to pass the range of ω_k, the voltage signal represented by (6) will determine the direction finder display. In general, for the single-channel receiver the bearing display signal is given by the detected antenna output voltage, that is, $|V_T|$. Therefore all the bearing information, as obtainable from the spinning simple loop, is contained in (6). It remains to be shown analytically under what conditions (6) yields bearing information, if any, and the accuracy of the bearing information obtained. One can then investigate the physical conditions necessary for the display of the bearing information shown analytically to be available.

The quantity V_T of (6), which is valid at a given point (ρ, τ) in the resultant field, may be thought of as a function of the variable (θ), the rotation angle of the antenna. Direction finder bearing indicators cover the range of observed bearing θ_{OB} between 0° and 360°. Thus, as θ increases, *i.e.*, as the antenna completes many revolutions, V_T may appear as a multivalued function of θ_{OB} at the bearing indicator, depending upon the time periodicity of the signal.

If the ω_k are unequal such that $\omega_B \neq 0$, then the beat period $T_B = 2\pi/\omega_B$ determines the time period of V_T. The antenna rotation angle may alternatively be written: $\theta = \Omega t$ where Ω = angular frequency of antenna rotation and t = time. Thus the relation of Ω to ω_B determines whether or not the bearing display is multivalued. If ω_B is some integral multiple of Ω or $\omega_B = \Omega$, then the display will be single valued. On the other hand, if $\omega_B \ll \Omega$ or $\omega_B \gg \Omega$ and Ω and ω_B are not integral multiples, the bearing display will appear multivalued because of the superposition of antenna signals corresponding to successive antenna rotations. This multivalued function may be periodic, however, depending on the beat frequency between ω_B and Ω. It may be further noted that if the ω_k are equal, *i.e.*, $\omega_B = 0$, V_T is a single valued function of θ_{OB} at a given point (ρ, τ) in the field, since the resultant field is time invariant.

A property of the antenna output V_T which is derivable from (6) and which will clearly appear at the bearing indicator is the curve of the maximum possible value of V_T as a function of θ_{OB}. Consideration of (6) shows that the maximum possible value of V_T for any value of θ_{OB} is given by

$$(V_T)_m = \sum_{k=1}^{n} E_k |\sin(\theta_{OB} - \delta_k)|. \quad (7)$$

The significance of (7) with regard to determining the true bearings (δ_k) of the field components is shown by the following analysis. Each component in (7) is represented by its own term; hence, it is possible to differentiate each term twice, producing infinite discontinuities in the second derivative at $\theta_{OB} = \delta_k, \delta_k + \pi$. This analysis shows that the contour $(V_T)_m$ plotted as a function of θ_{OB} has break points where $\theta_{OB} = \delta_k, \delta_k + \pi$. In Fig. 2, (7) is plotted as a function of θ_{OB} demonstrating the branched characteristic at $\theta_{OB} = \delta_k, \delta_k + \pi$.

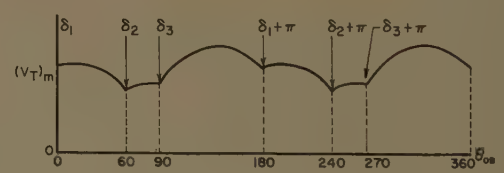

Fig. 2—The maximum antenna output signal $(V_T)_m$ vs bearing azimuth.

Since the bearing indicator of single-channel direction finders plots the detected antenna output signal $|V_T|$ vs θ_{OB}, the true bearings of the field components would be indicated in the display at the break points of the contour of $(V_T)_m$ with no inherent error as in Fig. 2. That the maximum possible value of V_T appears as a function of θ_{OB} in the bearing display may be predicted by consideration of the following two cases.

Case I: If $\omega_B \neq 0$, during the period T_B all possible phase relations between the components of the field are produced. Thus, for each value of θ in (6) the apparent phase conditions which produce addition of all the components

$$\left[\sum_n E_k |\sin(\theta - \delta_k)| \right]$$

are produced during a finite time of sampling by the antenna. For example, if V_T is a slowly varying function of the time, *i.e.*, $\omega_B \ll \Omega$, the contour $(V_T)_m$ will be produced at the bearing display. A time exposure of the display trace during the period T_B will disclose a multivalued function of θ_{OB}, the maximum envelope of which will contain the bearing information.

Case II: If $\omega_B = 0$ (all ω_k equal), (6) may be written

$$V_T = \left[\sum_{k=1}^{n} E_k \sin (\theta_{OB} - \delta_k) e^{j\phi_k} \right] e^{j\omega t}. \qquad (8)$$

Eq. (8) reduces to the form of (7) when the phase relations in the field are such that at a given θ all the terms of (8) add positively. At a given point in the field, V_T may reach $(V_T)_m$ over only a restricted region of θ. Thus, in order to find the directions of the unknown components, the antenna must be moved throughout the field, sampling the resultant field until the contour of $(V_T)_m$ vs θ_{OB} is obtained. Because of the assumption of incident plane waves, E_k, δ_k, and ω remain constant when the antenna is moved in the resultant field. Although an optimum sampling path exists so that it is not necessary to sample every point of the field, this path in an unknown field would be itself unknown and in general would be complicated.

Experimental Results

On the basis of the arguments above, experimental verification of the component resolution capability of a single-channel spinning-loop direction finder was undertaken. The experimental data reported below were obtained using a standard AN/SRD-7 spinning loop direction finder. The bearing indication of the AN/SRD-7 is obtained by means of an inverted polar plot of the loop antenna pattern (nulls at the periphery, maxima at the center of the CRO display). In order to obtain a rectilinear plot of the antenna pattern, the video detector output of the receiver was fed through an isolation stage to the vertical deflection plates of an oscilloscope. The oscilloscope sweep was externally synchronized with the antenna rotation. Thus, simultaneous polar and rectilinear plots of the bearing information were obtained.

The direction finder antenna and receiver with the extra display oscilloscope were placed in a screen room fitted with vertical radiators placed empirically in apparent thirty degree increments from 0° to 180° in azimuth with respect to the loop antenna.[3] A schematic diagram of the screen room equipment is shown in Fig. 3. The vertical azimuthal radiators were driven by variable frequency signal generators adjusted for relative amplitude as desired. Although located in the near field of the radiators, the antenna pattern of the small loop antenna in the near field is identical to that in the far field by virtue of the form of the field equations at the loop.

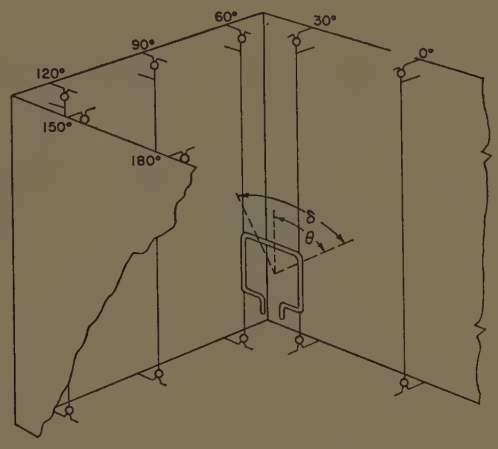

Fig. 3—Schematic diagram of screen room radiators for producing a multicomponent field.

The Two Component Field

An analytical treatment of the case of two components of equal frequency has been reported by these authors.[2] In summary it was found that as the antenna was moved in the resultant field, *i.e.*, as the relative phase of the two signals was varied through 2π radians, the antenna patterns intersect at four points, defining the bearing azimuths of the two components.

This property was verified experimentally by driving two vertical radiators in the screen room described above with a 2-Mc signal generator equipped with a phase shifting resolver capable of varying the relative phase of the two signals through 2π radians. A time exposure of the AN/SRD-7 bearing-indicator display of the antenna patterns as the phase was rotated through 360° is shown in Fig. 4(a). The bearings of the two radiators with respect to the antenna were 0° and 60°, respectively, and the amplitude ratio $(A) = E_2/E_1 = 0.86$. The antenna patterns intersect at four points in Fig. 4(a) which define two diametral lines, indicating the true bearings of the signals.

The general analysis indicates that the maximum envelope of V_T should contain break points at δ_k and $\delta_k + \pi$. The display voltage maximum envelope is plotted in inverted polar form in Fig. 4(b) for the case shown in Fig. 4(a): $\delta_1 = 0°$, $\delta_2 = 60°$, $E_1 = 1$, $E_2 = 0.86$. Examination of the interior maximum envelope obtained experimentally in Fig. 4(a) and that plotted in Fig. 4(b) show that the two contours are identical within practical limits.

On the basis of the general analysis, a pattern similar to that obtained with the ω_k equal should be obtained with unequal ω_k when $\omega_B \neq 0$. Experimental verification of this prediction was obtained with 0° and 60° azimuth radiators driven by two variable frequency signal generators at approximately 2 Mc. The amplitude ratio obtained was $(A) = 1.27$. The beat period between the two

[3] See also F. Haber, "Generation of standard fields in shielded enclosures," Proc. IRE, vol. 42, pp. 1693–1698; November, 1954.

$\delta_1 = 0$ $E_1 = 1$
$\delta_2 = 60°$ $E_2 = .86$
$\omega_1 = \omega_2$ $0 \leq (\phi_1 - \phi_2) \leq 2\pi$

(a)

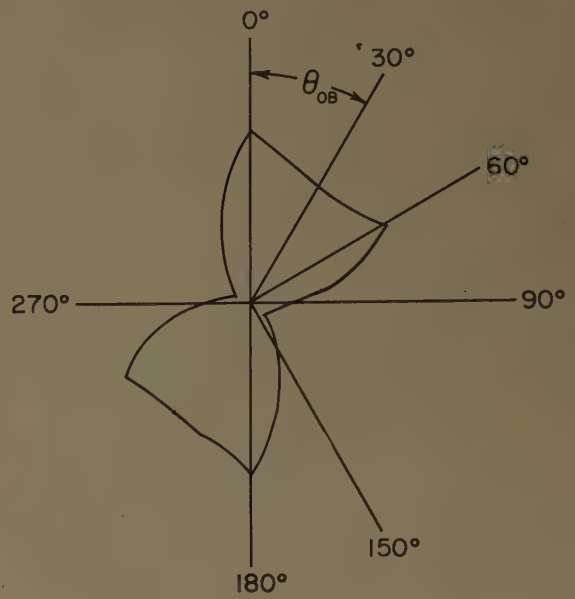

$|\sin\theta_{OB}| + .86\,|\sin(\theta_{OB} - 60°)|$
$\delta_1 = 0$ $E_1 = 1$
$\delta_2 = 60°$ $E_2 = .86$

(b)

$\delta_1 = 0$ $E_1 = 1$
$\delta_2 = 60°$ $E_2 = 1.27$
$\omega_1 \neq \omega_2$

(c)

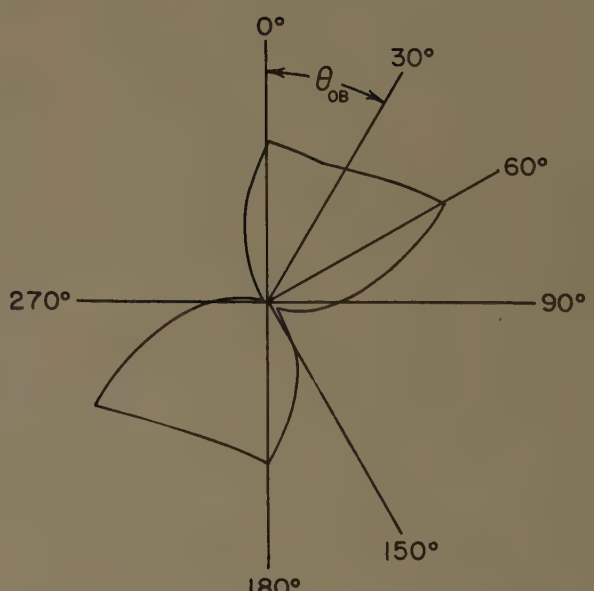

$|\sin\theta_{OB}| + 1.27\,|\sin(\theta_{OB} - 60°)|$
$\delta_1 = 0°$ $E_1 = 1$
$\delta_2 = 60°$ $E_2 = 1.27$

(d)

Fig. 4—(a) Single-channel direction finder display for the case of two components of equal frequency. (b) Predicted bearing display for the case of the two component field of Fig. 4(a). (c) Single-channel direction finder display for the case of two components of slightly different frequency. (d) Predicted bearing display for the case of the two component field of Fig. 4(c).

$\delta_1 = 0°$ $\delta_2 = 60°$ $\delta_3 = 150°$

$E_1 = 1$ $E_2 = 1$ $E_3 = 1$

$\omega_1 \neq \omega_2 \neq \omega_3$

(a)

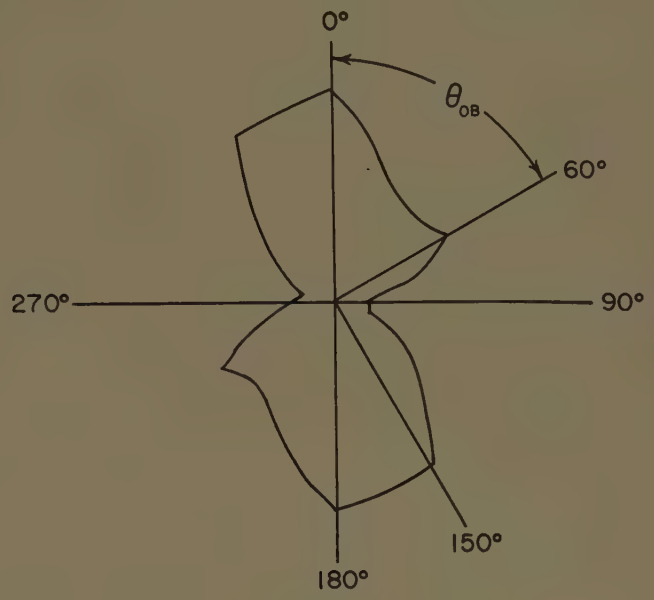

$|\sin(\theta_{OB}-0°)| + |\sin(\theta_{OB}-60°)| + |\sin(\theta_{OB}-150°)|$

$\delta_1 = 0°$ $\delta_2 = 60°$ $\delta_3 = 150°$

$E_1 = 1$ $E_2 = 1$ $E_3 = 1$

(b)

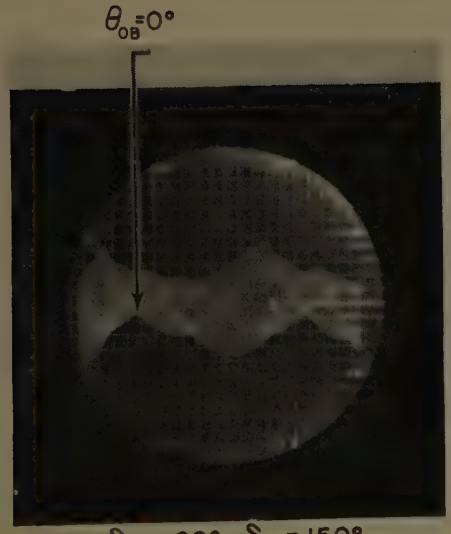

$\delta_1 = 0°$ $\delta_2 = 60°$ $\delta_3 = 150°$

$E_1 = 1$ $E_2 = 1$ $E_3 = 1$

$\omega_1 \neq \omega_2 \neq \omega_3$

(c)

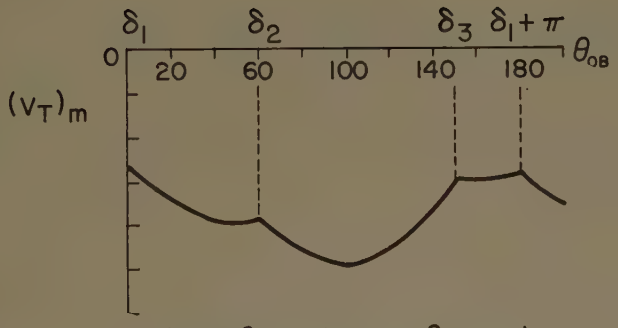

$|\sin(\theta_{OB}-0°)| + |\sin(\theta_{OB}-60°)| + |\sin(\theta_{OB}-150°)|$

$\delta_1 = 0°$ $\delta_2 = 60°$ $\delta_3 = 150°$

$E_1 = 1$ $E_2 = 1$ $E_3 = 1$

(d)

Fig. 5—(a) Single-channel direction finder display for the case of three components of slightly different frequency. (b) Predicted bearing display for the case of the three component field of Fig. 5(a). (c) Rectilinear single-channel direction finder display for the case of three components of slightly different frequency. (d) Predicted bearing display for the case of the three component field of Fig. 5(c).

generators was of the order of seconds. Fig. 4(c) shows a 10-second time exposure of the AN/SRD-7 bearing indicator.

The corresponding theoretical display voltage maximum envelope is plotted in inverted polar form in Fig. 4(d), where $\delta_1=0°$, $\delta_2=60°$, $E_1=1$, $E_2=1.27$. Comparison of Figs. 4(c) and 4(d) shows detailed similarity between the experimental and theoretical displays. Furthermore the predicted similarity between the displays of Fig. 4(a) and 4(c) is obtained. The relatively broad central portion of the experimental display of Fig. 4(c) occurs because of the distortion produced by reduction in receiver gain with respect to that in Fig. 4(a).

The Three Component Field

The three component field was investigated by driving three vertical radiators with signals of approximately equal amplitude and frequency at azimuths of 0°, 60°, and 150°, respectively. The frequencies of the signals were approximately 2 Mc with a beat period of the order of seconds. A ten-second time exposure photograph of the bearing indicator of the AN/SRD-7 is shown in Fig. 5(a). The inverted polar plot of the theoretical maximum envelope is shown in Fig. 5(b).

A rectilinear display of the video detected antenna voltage is shown in Fig. 5(c). The maximum signal voltage envelope is the lower contour in the figure. For further comparison of the theoretical and experimental maximum envelopes, the rectilinear plot of the maximum envelope is shown in Fig. 5(d).

Inspection of these displays indicates that break points in the maximum envelope occur at points corresponding to the true bearings of the signals. The experimental maximum envelopes are essentially identical to the corresponding theoretical envelopes.

Because of the lack of a signal generator with suitable relative phase controls, the three component field could not be investigated for the case of equal frequencies. However, the evidence presented above suggests that a bearing display similar to that of Fig. 5(a) or 5(c) would be obtained for the ω_k equal.

Bearing Indication

It has been shown in the foregoing sections that bearing information is obtained from the envelope of the maximum possible antenna output voltage. In the experiments described above, this envelope was obtained by photographing the display of the complete antenna output signal. However, only the maximum envelope contains the bearing information; thus a means of detecting only this envelope would be sufficient for bearing determination.

The essential requirement of such a detector is the capability to store the maximum voltage signal associated with each angular position (θ) of the antenna. This stored envelope waveform must then be plotted as a function of θ_{OB} for bearing determination. It is also seen that visual display of this waveform is not necessary for bearing indication. If the waveform were differentiated twice, voltage spikes would appear at the break points of the waveform. With suitable associated timing circuitry, these spikes could be made to operate a bearing readout device.

Conclusions

The investigation reported above has shown that a spinning simple-loop single-channel direction-finding system is capable, in principle, of resolving the directional components of a multicomponent field. Furthermore, component resolution may be achieved either with the ω_k different, equal, or with some equal, so long as a common beat frequency exists between the different frequency components and the antenna is moved in the field so as to sample all the phase relations which lead to $(V_T)_m$ for θ_{OB} between 0° and 360°. However, bearing determination depends upon detection of the maximum envelope of V_T. Thus, because of the frequency relations between ω_B and Ω, detection of the maximum envelope requires a memory device which stores the maximum received voltage signal corresponding to a given value of θ_{OB}. This stored waveform is then processed for its bearing information.

This direction finding technique requires a finite time (sometimes of the order of seconds) for the collection of the bearing information. Furthermore, as the number of components increases, the envelope $(V_T)_m$ becomes more uniform.

In order to make a flexible component resolution system capable of resolution under a broad range of operating conditions, a variable speed antenna drive is indicated. If the beat period of the resultant field equals the antenna rotation period, component resolution is not possible because the antenna cannot sample the maximum (V_T) at each value of θ_{OB}. Furthermore, for a given resultant field configuration, there may be an optimum antenna rotation speed, *i.e.*, sampling rate, which would obtain the bearing information in a minimum of time.

A simplification of the receiving system required for component resolution is indicated by the fact that $(V_T)_m=|(V_T)_m|$. Thus the need for a detector is eliminated. A simple component resolution direction finding system could consist of a crossed loop antenna and goniometer (or spinning loop) fed to a broad-band storage oscilloscope.

It should be noted that component resolution in a multicomponent field of components with equal or differing frequencies can be achieved either by means of a twin-channel crossed-loop direction finder or a single-channel spinning-loop direction finder as discussed above. Although different methods of display are used, the component resolution capability of both these direction finding systems is essentially equivalent. It is not within the scope of the present article, however, to compare the two systems with respect to their respective component resolution capabilities.

A Solution to the Frequency-Independent Antenna Problem*

B. R.-S. CHEO†, MEMBER, IRE, V. H. RUMSEY‡, FELLOW, IRE, AND W. J. WELCH‡, MEMBER, IRE

Summary—**A solution of Maxwell's equations is obtained for an antenna consisting of an infinite number of equally spaced wires in the form of coplanar equiangular spirals. Radiation amplitude patterns obtained from this solution agree closely with measurements on two-element spiral antennas. The phase pattern shows the approximate validity of a phase center at a distance behind the antenna which decreases with the tightness of the spiral. The current distribution clearly shows increased attenuation with increase in the tightness of the spiral, thus showing how the frequency-independent mode depends on the curvature. A remarkable feature of the solution is that the current consists of an inward traveling wave at infinity when the antenna is excited in that sense which produces an outward wave at the center.**

I. Introduction

IT has been found in recent years that there is a large class of antennas which are independent of frequency in essentially all their characteristics such as impedance, pattern, polarization and so on.[1–3] The equiangular spiral antenna is one of the basic types: that illustrated in Fig. 1 consists of two conductors cut out of a plane metal sheet. Let us consider how this antenna scales with the wavelength. The shape of the antenna is given by the formula (in polar coordinates r and ϕ)

$$r = e^{-a\phi} \qquad (a \text{ is a constant}). \tag{1}$$

Therefore,

$$\frac{r}{\lambda} = e^{-a(\phi-\phi_0)}, \tag{2}$$

where

$$\phi_0 = \frac{1}{a} \ln \lambda. \tag{3}$$

This shows that a change of wavelength λ is equivalent to turning the antenna through the angle ϕ_0, except for the scaling of the radius r_0 shown in Fig. 1. Now the remarkable property of these antennas is that, so long as the wavelength is shorter than about $2r_0$, the performance is independent of frequency, except for the rotation described in (2) and (3), and therefore it is the same as if r_0 were infinite. Evidently this means that the current distribution must decrease with distance from the input much more rapidly than it does for conventional antennas.

To bring out this point let us compare it with the biconical antenna, shown in Fig. 2. The field, represented by the vectors E and H, decreases as $1/r$ for large values of r, and therefore the surface current J (which equals tangential H) also decreases as $1/r$. The total current I is $2\pi r \sin \alpha J$, where α is the angle of the cone shown in Fig. 2. Thus I remains constant with increasing r. The peculiarity of frequency-independent antennas is then that the field at the surface of the antenna must decrease more rapidly than $1/r$, or alternatively, the total current must decrease fast enough, so that the infinite antenna can be truncated with practically no effect on the radiation pattern.

The theoretical problem posed by the equiangular spiral antenna is to solve Maxwell's equations subject to the vanishing of tangential E on the metal surface, the radiation condition at infinity and the input condition at $r=0$. For the two-element antenna of Fig. 1, this has so far proved intractable even for the infinite case.[4] We are therefore driven to consider some simpler problem which, while retaining the frequency-independent feature, is amenable to theoretical solution. The problem we shall consider in this paper is such a simplification. It can be described by taking an antenna with many elements, as in Fig. 3, the space between the ele-

Fig. 1.

Fig. 2.

Fig. 3.

* Received by the PGAP, May 3, 1961. This research was supported by the U. S. Army Signal Corps under Contract DA 36-039 SC-84923.

† Bell Telephone Labs.; formerly with the University of California, Berkeley, Calif.

‡ Elec. Engrg. Dept., University of California, Berkeley, Calif.

[1] V. H. Rumsey, "Frequency independent antennas," 1957 IRE National Convention Record, pt. 1, pp. 114–118.

[2] R. H. DuHamel and D. E. Isbell, "Logarithmically periodic antennas," 1957 National Convention Record, pt. 1, pp. 119–128.

[3] J. D. Dyson, "Equiangular spiral antennas," IRE Trans. on Antennas and Propagation, vol. AP-7, pp. 181–187; April, 1959.

[4] P. E. Mast, "A Theoretical Study of the Equiangular Spiral Antenna," Elec. Engrg. Res. Lab., University of Illinois, Urbana, Tech. Rept. No. 35; September, 1958.

ments being the same as the space occupied by an element, so that the antenna is "self-complementary" in the sense of Rumsey.[1] We now suppose that the number of elements is infinite, so that the antenna takes the form of a smooth anisotropic sheet which is perfectly conducting in the direction of the spiral lines and perfectly transparent in the perpendicular direction.

This is the kind of problem which can be solved[5] by putting $E=j\eta H$ on one side of the antenna and $E=-j\eta H$ on the other side, where E and H are complex vectors defined according to the $e^{j\omega t}$ time convention, and η is the intrinsic impedance of space. The boundary conditions at the surface are that tangential E be continuous, tangential H be discontinuous by the amount of the surface-current density, E parallel to the spirals be zero, and H parallel to the spirals be continuous. All of these conditions are met if we make E parallel to the wires vanish and tangential E continuous, with $E=j\eta H$ above the surface, and $E=-j\eta H$ below the surface.

The source of fields on this antenna is located at its center. Recognizing that the structure is essentially uniform in azimuth, we assume that the fields of the antenna will have the same dependence on the coordinate ϕ as the source. Thus, we shall take the ϕ variation of the field to be everywhere $e^{jn\phi}$, where n is an integer. This corresponds to the excitation arrangement shown in Fig. 3, in which each generator has the same magnitude as its neighbor and differs infinitesimally from its neighbor in phase. The case $n=1$ corresponds approximately to the excitation of the balanced two-arm antenna, shown in Fig. 1.

II. Formal Solution

Suppose that the antenna lies in the plane $z=0$ of the cylindrical coordinate system of Fig. 4. Let $E_1=j\eta H_1$ for $z>0$ and $E_2=-j\eta H_2$ for $z<0$. Then we have[5]

$$E_1 = -\beta\nabla\times(\hat{z}U_1)+\nabla\times\nabla\times(\hat{z}U_1), \tag{4}$$

$$E_2 = \beta\nabla\times(\hat{z}U_2)+\nabla\times\nabla\times(\hat{z}U_2). \tag{5}$$

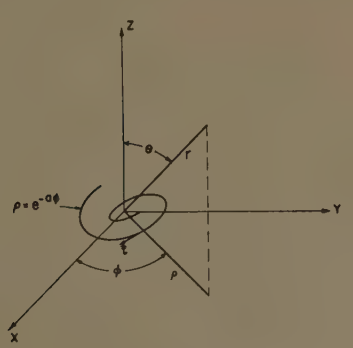

Fig. 4.

[5] V. H. Rumsey, "A New Way of Solving Maxwell's Equations," Electronics Res. Lab., University of California, Berkeley, Series No. 60, Issue No. 335; December 19, 1960. Also to be published in IRE Trans. on Antennas and Propagation.

The functions U_1 and U_2 satisfy the scalar wave equation

$$\nabla^2 U+\beta^2 U=0, \qquad \beta=\omega/c. \tag{6}$$

We can express a general solution of (6) which varies as $e^{jn\phi}$ by using the Hankel transform formula:

$$U_1 = e^{jn\phi}\int_0^\infty g_1(\lambda)J_n(\lambda\rho)e^{\pm jz\sqrt{\beta^2-\lambda^2}}\lambda d\lambda, \tag{7}$$

$$U_2 = e^{jn\phi}\int_0^\infty g_2(\lambda)J_n(\lambda\rho)e^{\pm jz\sqrt{\beta^2-\lambda^2}}\lambda d\lambda, \tag{8}$$

in which $g_1(\lambda)$ and $g_2(\lambda)$ are arbitrary functions. The Bessel function of the first kind, namely J_n, has been chosen in order that the field be regular at $\rho=0$ for $z\neq 0$. In order that the fields radiate away from the structure, the negative sign must be taken in the exponential factor in the integrand of (7), and the positive sign in the integrand of (8). Then the continuity of tangential electric field at $z=0$ is satisfied if we put $g_1(\lambda)=g_2(\lambda)=g(\lambda)$, as can be verified by direct substitution into (4) and (5). Then,

$$U_1 = e^{jn\phi}\int_0^\infty g(\lambda)J_n(\lambda\rho)e^{-jz\sqrt{\beta^2-\lambda^2}}\lambda d\lambda, \tag{9}$$

$$U_2 = e^{jn\phi}\int_0^\infty g(\lambda)J_n(\lambda\rho)e^{+jz\sqrt{\beta^2-\lambda^2}}\lambda d\lambda. \tag{10}$$

The remaining condition, $E_1\cdot\hat{t}=0$, $\hat{t}$ being tangential to the spiral wires, will determine $g(\lambda)$. From (1) we find $E_1\cdot\hat{t}=0$ implies that

$$aE_{1\rho}=E_{1\phi}. \tag{11}$$

Substitution into this equation from (4) leads to the following expression for the boundary condition:

$$a\left(\frac{\partial^2 U_1}{\partial z\partial\rho}-\frac{\beta}{\rho}\frac{\partial U_1}{\partial\phi}\right)=\frac{1}{\rho}\frac{\partial^2 U_1}{\partial\phi\partial z}+\beta\frac{\partial U_1}{\partial\rho}\bigg|_{z=0}. \tag{12}$$

Then, substituting (9) into (12), we find

$$\int_0^\infty g(\lambda)\left\{(jna\beta+n\sqrt{\beta^2-\lambda^2})\frac{\lambda J_n(\lambda\rho)}{\rho} + (ja\sqrt{\beta^2-\lambda^2}+\beta)\lambda^2 J_n'(\lambda\rho)\right\}d\lambda=0. \tag{13}$$

Then term containing the derivative of the Bessel function may be integrated by parts, so that (13) becomes

$$\int_0^\infty\left\{g(\lambda)(jna\beta+n\sqrt{\beta^2-\lambda^2})\lambda - \frac{d}{d\lambda}\left[g(\lambda)\lambda^2(ja\sqrt{\beta^2-\lambda^2}+\beta)\right]\right\}\frac{J_n(\lambda\rho)}{\rho}d\lambda + \frac{g(\lambda)[ja\sqrt{\beta^2-\lambda^2}+\beta]\lambda^2 J_n(\lambda\rho)}{\rho}\bigg|_0^\infty=0. \tag{14}$$

Suppose that $g(\lambda)[ja\sqrt{(\beta^2-\lambda^2)}+\beta]\lambda^2 J_n(\lambda\rho)$ vanishes for λ equal to zero or infinity. Then the boundary terms in (14) may be discarded. (We shall see later that this assumption is justified.) Applying the inverse Hankel transform to (14) with the boundary terms set equal to zero yields an ordinary differential equation for $g(\lambda)$:

$$(\beta\lambda + j\lambda a\sqrt{\beta^2-\lambda^2})g'(\lambda)$$

$$+\left[\beta(z-jna)-(n-2ja)\sqrt{\beta^2-\lambda^2}-\frac{ja\lambda^2}{\sqrt{\beta^2-\lambda^2}}\right]g(\lambda)=0. \quad (15)$$

For convenience let $\lambda=y\beta$ and $g(y\beta)=f(y)$. In terms of $f(y)$ the solution to (15) is

$$g(\lambda) = g(y\beta) = f(y) = k\left(\frac{1-\sqrt{1-y^2}}{1+\sqrt{1-y^2}}\right)^{n/2} \cdot y^{-2}(1+aj\sqrt{1-y^2})^{-1-j(n/a)}. \quad (16)$$

Notice that $f(y)$ is independent of β, exhibiting the frequency-independent nature of the solution explicitly.

For $n>0$, the behavior of $f(y)$ is such that the integral (9) exists, and the assumption that the boundary terms in (14) vanish is valid. For $n<0$, $f(y)$ becomes infinite at $y=0$ or $\lambda=0$ and (9) diverges. It turns out that we can obtain a solution for $n<0$ only if we begin with the assumption that $E_1=-j\eta H_1$ and $E_2=j\eta H_2$. There appears to be a simple explanation for this. With the radiation condition fixed, the choice of the plus or minus sign in the equation $E=\pm j\eta H$ determines the sense of polarization of the far field. At the same time, the sign of n specifies the polarization sense of the source. The interpretation of the situation described above is that the field must have the same sense of polarization as the source.

The complete expressions for U_1 are (taking $n>0$)

$$U_1=ke^{jn\phi}\int_0^\infty \left(\frac{1-\sqrt{1-y^2}}{1+\sqrt{1-y^2}}\right)^{n/2} \frac{(1+aj\sqrt{1-y^2})^{-1-j(n/a)}}{y} \cdot e^{-j\sqrt{1-y^2}\,\beta z}J_n(\beta\rho y)dy, \quad (17)$$

or, for $n<0$,

$$U_1=ke^{-jn\phi}\int_0^\infty \left(\frac{1-\sqrt{1-y^2}}{1+\sqrt{1-y^2}}\right)^{n/2} \frac{(1-ja\sqrt{1-y^2})^{-1+j(n/a)}}{y} \cdot e^{-j\sqrt{1-y^2}\,\beta z}J_n(\beta\rho y)dy, \quad (18)$$

where k is a constant which is to be adjusted according to the source strength. Notice that the integrand contains a branch point at $y=+1$ in the complex y plane. The branch cut must be taken in the fourth quadrant, and the path of integration must pass over the branch point in order that $(1-y^2)^{1/2}\to -j(y^2-1)^{1/2}$ for $y>1$. This completes the formal solution to the boundary-value problem.

III. Limiting Cases

In this section we shall evaluate the integral for several limiting cases to find the behavior of the field near the input terminals, the radiation pattern, and the behavior of the antenna current at large distances from the input terminals.

A. The Field Near the Input Terminals

The requirement that the behavior of the field approach the static field distribution near the input terminals was never actually employed in the derivation of the preceding section, and it must be verified that this condition is in fact satisfied by (17) and (18). Let us consider the behavior of the electric field as $\beta r\to 0$. According to (4) and (6),

$$E_1 = -\beta\nabla\times(\hat{z}U_1) + \nabla\times\nabla\times(\hat{z}U_1) = -\beta\nabla\times(\hat{z}U_1) + \nabla\left(\frac{\partial U_1}{\partial z}\right) + \beta^2\hat{z}U_1. \quad (19)$$

In the limit as $\beta r\to 0$, the second term of (19) dominates.

$$\lim_{\beta r\to 0} E_1 = \nabla\left(\frac{\partial U_1}{\partial z}\right). \quad (20)$$

This implies that as $\beta r\to 0$, $\partial U/\partial z$ must approach the static potential distribution, which is

$$V = r^{j(n/a)}e^{jn\phi}P_{j(n/a)}^{n}(\cos\theta) = (re^{-a\phi})^{j(n/a)}P_{j(n/a)}^{n}(\cos\theta) \quad (21)$$

The function V satisfies Laplace's equation and is constant along the wires: it is the standard form $r^m P_m{}^n(\cos\theta)e^{jn\phi}$ with $m=j(n/a)$.

From (17) we find that

$$\frac{\partial U_1}{\partial z}=ke^{jn\phi}\int_0^\infty \left(\frac{1-\sqrt{1-y^2}}{1+\sqrt{1-y^2}}\right)^{n/2} \frac{(1+aj\sqrt{1-y^2})^{-1-j(n/a)}}{y} \cdot(-j\sqrt{1-y^2})e^{-j\sqrt{1-y^2}\,\beta r\cos\theta}J_n(\beta ry\sin\theta)dy, \quad (22)$$

where we have put $z=r\cos\theta$ and $\rho=r\sin\theta$. For small values of βr, the Bessel function is small except where y is very large, because $J_n(x)\to x^n$ as $x\to 0$. Since the other part of the integrand is well behaved in the neighborhood of $y=0$, the entire integrand contributes very little, except where y is large, in this limit. Therefore, it is reasonable to approximate the part of the integrand other than the Bessel function by its behavior for large y and consider the resulting integral. Hence,

$$\lim_{\beta\rho->0}\frac{\partial U_1}{\partial z} = ke^{jn\phi}\int_0^\infty y^{-1-j(n/a)}e^{-\beta r\cos\theta y}J_n(\beta r\sin\theta y)dy = \frac{k\Gamma\left(n-j\frac{n}{a}\right)\Gamma\left(j\frac{n}{a}-n+1\right)}{\Gamma\left(j\frac{n}{a}+n+1\right)} \cdot e^{jn\phi}(\beta r)^{j(n/a)}P_{j(n/a)}{}^{n}(\cos\theta). \quad (23)$$

Apart from the constant multiplier, this agrees precisely with (21).

Furthermore, (23) shows that the magnitude of the current flowing into a sector of the antenna from the source is constant. Thus, if I_i is the current per unit angle at the input, $I_i=\rho J$, where J is the surface current density, and

$$J = 2(H_\rho + aH_\phi)/(1 + a^2)^{1/2} = (2/a)(1 + a^2)^{1/2}H_\phi.$$

According to (19) and (23),

$$H_\phi\big|_{\pi/2} \propto E_\phi\big|_{\theta=\pi/2} \propto \frac{1}{\rho} e^{jn\phi}(\beta\rho)^{j(n/a)}P_{j(n/a)}{}^n(0),$$

and ρ times this quantity has a constant magnitude.

B. Radiation Patterns

In order to investigate the radiation properties of the antenna, we need only consider the asymptotic behavior of the field at large distances from the structure. We shall see that the method of stationary phase readily lends itself to the asymptotic evaluation of (17) for large values of both ρ and z. However, before the integral can be approximated, the differentiations indicated in (5) for the electric field must first be performed. Of interest are the components of the electric field with respect to the spherical coordinate system (r, θ, ϕ) of Fig. 4. Because the distant field is circularly polarized,[5] we need only work out E_ϕ, a component which is common to both the cylindrical and spherical systems. Using (4), we find

$$E_\phi = k\beta^2 e^{jn\phi}\int_0^\infty f(y)\left\{\beta n\sqrt{1-y^2}\,\frac{J_n(\beta y\rho)}{\rho} + \beta^2 y\left[J_{n-1}(\beta\rho y) - \frac{n}{\beta\rho y}J_n(\beta\rho y)\right]\right\}e^{-j\sqrt{1-y^2}\,\beta z}y\,dy, \quad (24)$$

where $\rho=r\sin\theta$ and $z=r\cos\theta$. Except at $\theta=0$, both ρ and z are large when r is large. With ρ large, the leading term in the integrand of (24) is the term containing the factor $J_{n-1}(\beta\rho y)$. Furthermore, the Bessel function may be replaced by its asymptotic value for large argument.[6]

$$\lim_{x\to\infty} J_n(x) = \sqrt{\frac{2}{\pi x}}\left\{\frac{e^{j[x-(n+1/2)\pi/2]} + e^{-j[x-(n+1/2)\pi/2]}}{2}\right\}. \quad (25)$$

Using this in the integrand of (24) causes only a second-order error even in the neighborhood of $y=0$, because $f(y)$ tends to zero as y^{n-2} and therefore the integrand tends to zero as y^{2n-1}. Using these approximations and substituting r for $\rho/\sin\theta$ and $z/\cos\theta$, we obtain the following approximation for (24) for large r:

$$E_\phi \approx k\beta^4 e^{jn\phi}\int_0^\infty \frac{f(y)y^{3/2}}{\sqrt{\pi r\beta\sin\theta}} \cdot\left\{e^{-j\beta r[\cos\theta\sqrt{1-y^2}-y\sin\theta]-j(\pi/2)(n+1/2)} + e^{+j\beta r[\cos\theta\sqrt{1-y^2}+y\sin\theta]+j(\pi/2)(n+1/2)}\right\}dy. \quad (26)$$

This integral contains two terms of the following form: an exponential phase term with a large factor r, multiplied by a relatively slowly-varying function of the variable of integration. According to the principle of stationary phase, the main contribution to this integral comes from the neighborhood of the stationary points of the phase function. In general,[7]

$$\int_a^b g(t)e^{jxh(t)}dt \approx \left[\frac{2\pi}{x\,|\,h''(\tau)\,|}\right]^{1/2} g(\tau)e^{jxh(\tau)}e^{\pm j(\pi/4)}, \quad (27)$$

where x is the large parameter, $h'(\tau)=0$, and the plus or minus sign is to be taken according to whether the stationary point is a minimum or maximum. Only the second of the two terms in (26) has a real stationary point, and its value is $y=\sin\theta$. Applying formula (27), we find

$$E_\phi \approx k\beta^3 e^{jn\phi}\cos\theta f(\sin\theta)\,\frac{e^{-j\beta r}}{r}\,e^{jn(\pi/2)}. \quad (28)$$

Furthermore, from (16),

$$f(\sin\theta) = \frac{(1 + aj\cos\theta)^{-1-j(n/a)}\left(\tan\frac{\theta}{2}\right)^n}{\sin^2\theta}. \quad (29)$$

Finally, the far-zone electric field is

$$E_\phi \approx k\beta^3\,\frac{\cos\theta(1 + aj\cos\theta)^{-1-j(n/a)}\left(\tan\frac{\theta}{2}\right)^n}{\sin^2\theta} \cdot\frac{e^{j[n(\theta+\pi/2)-\beta r]}}{r}, \qquad n > 0. \quad (30)$$

If we express the field in terms of magnitude and phase

$$E_\phi \approx A(\theta)e^{-j\psi(\theta)}\,\frac{e^{j[n(\phi+(\pi/2))-\beta r]}}{r}, \quad (31)$$

we have

$$A(\theta) = \frac{\cos\theta\left(\tan\frac{\theta}{2}\right)^n e^{(n/a)\tan^{-1}(a\cos\theta)}}{\sin\theta\sqrt{1 + a^2\cos^2\theta}}, \quad (32)$$

and

$$\psi(\theta) = \frac{n}{2a}\ln\left|\,1 + a^2\cos^2\theta\right| + \tan^{-1}a\cos\theta. \quad (33)$$

[6] J. A. Stratton, "Electromagnetic Theory," McGraw-Hill Book Co., Inc., New York, N. Y., ch. 6, p. 359, (18); 1941.

[7] A. Erdelyi, "Asymptotic Expansions," Dover Publications, Inc., New York, N. Y., p. 51, 2.9(2); 1956.

For $e^{-jn\phi}$ excitation $A(\theta)$ is the same but the sign of $\psi(\theta)$ is reversed. The pattern $A(\theta)$ is plotted in Figs. 5 and 6 for various values of n and a. As is typical with frequency-independent antennas, there is no radiation along the surface of the structure. The patterns predicted by (33) agree remarkably well with measurements made by Dyson[3] on two-arm spiral antennas. According to (32), making a small decreases the beamwidth, but only up to a point. For the case $n=1$, the minimum beamwidth attainable is approximately 70°.

Before leaving the discussion of the radiation field, we shall consider the question of whether the antenna has a phase center. The total phase of the far field, apart from the ϕ dependence and some constants, is given by

$$\beta r + \psi(\theta). \tag{34}$$

Because of the complicated form of (33), (34) does not, in general, describe a circular phase front. However, when a is small, $\psi(\theta) \approx a \cos\theta$. In this case, the phase fronts are approximately circular, and, according to the diagram of Fig. 7, the antenna has a phase center located $a/2\pi$ wavelengths behind its center.

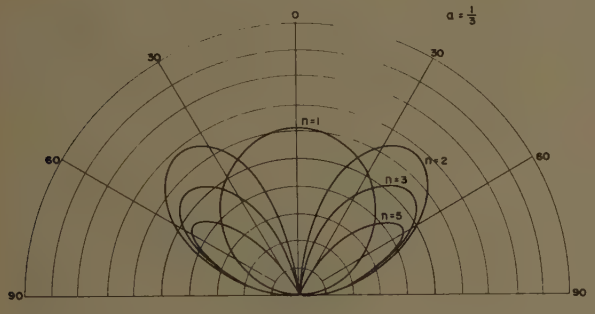

Fig. 5.

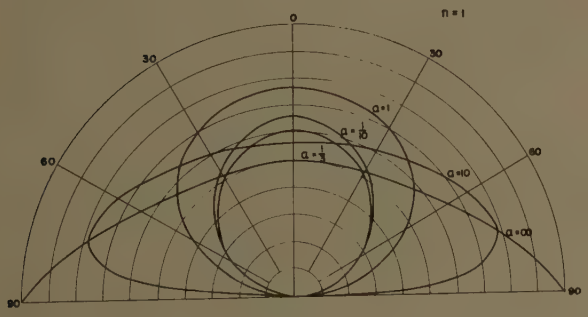

Fig. 6.

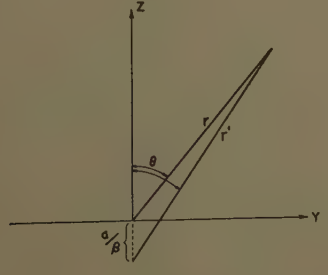

Fig. 7.

C. The Current Distribution

As we saw in Section I, the current distribution is one of the peculiar features of frequency-independent antennas. In the present case, it is obtainable from the field at the plane $z=0$. Since E is proportional to H and E_ϕ is proportional to E_ρ at $z=0$, the surface-current density is proportional to E_ϕ. The current density per unit of angle ϕ corresponds to the total antenna current I; it varies as ρE_ϕ. Unfortunately it has not been possible to work out the current for all values of ρ. However, fairly simple expressions have been obtained for small values of ρ and alternatively for large values of ρ. For small values of ρ we have already found that

$$I \approx e^{jn(\phi+(1/a)\ln\rho)},$$

which has constant amplitude and rapidly varying phase as a function of ρ. Note however that the phase is constant if we move along a spiral as it ought to be for the steady-current case.

Turning now to the case where ρ is large, according to (4) and (9) and (16), we find that

$$I \propto E_\phi = k\beta^3 e^{jn\phi} \int_0^\infty f(y) \left[n\sqrt{1-y^2}\, \frac{J_n(\beta y\rho)}{\rho} + \beta y J_n'(\beta y\rho) \right] y\,dy. \tag{35}$$

Upon integrating (35) by parts and substituting for $f(y)$ from (16), we obtain, with $n>0$,

$$I \propto e^{jn\phi} \int_0^\infty \left(\frac{1-\sqrt{1-y^2}}{1+\sqrt{1-y^2}}\right)^{n/2} \left(n + \frac{1}{\sqrt{1-y^2}}\right) \cdot (1 + aj\sqrt{1-y^2})^{-2-j(n/a)} J_n(\beta\rho y)\, y\,dy. \tag{36}$$

For $n<0$ the correct formula is the conjugate of (36), not the result of reversing the sign of n—see (18). We express the integral as the sum of two integrals over the intervals (0, 1) and (1, ∞), and treat the two parts separately. Consider first the integration over (0, 1):

$$I_1 = \int_0^1 \left(\frac{1-\sqrt{1-y^2}}{1+\sqrt{1-y^2}}\right)^{n/2} \left(n + \frac{1}{\sqrt{1-y^2}}\right) \cdot (1 + aj\sqrt{1-y^2})^{-2-j(n/a)} J_n(\beta\rho y)\, y\,dy. \tag{37}$$

The singularity at $y=1$ makes the major contribution to the integral. This is especially true for large $\beta\rho$, in which case the Bessel function oscillates very rapidly as a function of y and cancels all contributions to the integral, except from those regions where the rest of the integrand is also a rapidly varying function of y. We will expand the integrand, excepting the Bessel function, in ascending powers of $(1-y^2)^{1/2}$, beginning with $1/(1-y^2)^{1/2}$, and integrate term by term. Each term in

the resulting series will have successively less importance for large $\beta\rho$ because of the relative smoothness of the successive powers of $[(1-y^2)^{1/2}]^m$. We rewrite (37) slightly and then perform the expansion according to Maclaurin's formula:

$$I_1 = \int_0^1 \left\{ \frac{1}{y^n} \left(\frac{1-\sqrt{1-y^2}}{1+\sqrt{1-y^2}} \right)^{n/2} \left(n + \frac{1}{\sqrt{1-y^2}} \right) \cdot (1 + aj\sqrt{1-y^2})^{-2-j(n/a)} \right\} y^{n+1} J_n(\beta\rho y)\, dy$$

$$= \int_0^1 \sum_{m=-1}^{\infty} a_m (\sqrt{1-y^2})^m y^{n+1} J_n(\beta\rho y)\, dy. \quad (38)$$

Each term in the series may be integrated by means of Sonine's first formula.[8]

$$\int_0^{\pi/2} J_\mu(z \sin\theta) \sin^{\mu+1}\theta \cos^{\nu+1}\theta\, d\theta = \frac{z^{(\nu/2)+1}}{2^{(\nu/2)}\Gamma\left(\frac{\nu}{2}+1\right)} J_{\mu+(\nu/2)+1}(z). \quad (39)$$

Substituting $y = \sin\theta$ in (38) and using (39), we find

$$I_1 = \sum_{m=-1}^{\infty} \frac{a_m 2^{m/2}\Gamma\left(1+\frac{m}{2}\right)}{(\beta\rho)^{(m/2)+1}} J_{n+(m/2)+1}(\beta\rho). \quad (40)$$

Consider next the integration over $(1, \infty)$, which we write in the following form:

$$I_2 = \int_1^{\infty} \left\{ \left(\frac{1+j\sqrt{y^2-1}}{1-j\sqrt{y^2-1}} \right)^{n/2} (1+\sqrt{y^2-1})^{-2-j(n/a)} \cdot \left(n + \frac{j}{\sqrt{y^2-1}} \right) \right\} J_n(\beta\rho y)\, y\, dy. \quad (41)$$

Following the same reasoning as before, we expand the term in the braces of (41) in a series such that each term can be integrated and, furthermore, such that each term has successively less importance for large $\beta\rho$. In this case, the expansion is in powers of $(y^2-1)^{1/2}/y$.

$$I_2 = j \int_1^{\infty} \sum_{m=0}^{\infty} b_m \left(\frac{\sqrt{y^2-1}}{y} \right)^m \frac{J_n(\beta\rho y)\, dy}{\sqrt{y^2-1}\, y^{n-1}}. \quad (42)$$

There appears to be no single integral formula which can be applied to every term in (42), so that each term must be treated separately. In what follows, we shall work out only the first four terms of the series obtaining an asymptotic expansion in $\beta\rho$ up to terms which behave as $O(\beta\rho)^{-3}$. The first is

$$I_{20} = jb_0 \int_1^{\infty} \frac{J_n(\beta\rho y)\, dy}{\sqrt{y^2-1}\, y^{n-1}} = jb_0 \int_0^{\infty} \frac{J_n(\beta\rho\sqrt{1+\xi^2})\, d\xi}{(1+\xi^2)^{n/2}}, \quad (43)$$

where $y = (1+\xi^2)^{1/2}$. This may be evaluated by means of Sonine's second formula.[9]

$$\int_0^{\infty} \frac{J_\nu(a\sqrt{t^2+z^2})\, t^{2\mu+1}\, dt}{(t^2+z^2)^{\nu/2}} = \frac{2^\mu \Gamma(\mu+1)}{a^{\mu+1} z^{\nu-\mu-1}} J_{\nu-\mu-1}(az). \quad (44)$$

Let $z=1$, $\beta\rho = a$, and $\mu = -(\frac{1}{2})$. Then, applying (44) to (43) we obtain

$$I_{20} = \frac{jb_0\Gamma(\frac{1}{2})}{\sqrt{2\beta\rho}} J_{n-1/2}(\beta\rho). \quad (45)$$

The second term is

$$I_{21} = jb_1 \int_1^{\infty} \frac{J_n(\beta\rho y)\, dy}{y^n}. \quad (46)$$

An asymptotic expansion of this integral may be obtained by repeated integration by parts. In general,

$$-\int_1^{\infty} \frac{J_n(\beta\rho y)\, dy}{y^p} = \frac{1}{\beta\rho} J_{n+1}(\beta\rho) + \frac{p+n+1}{(\beta\rho)^2} J_{n+2}(\beta\rho) + O\left(\frac{1}{\beta\rho}\right)^3, \quad (47)$$

where $p > \frac{1}{2}$. In principle, one could carry out (47) to as many terms as desired. Thus, for the second term,

$$-I_{21} = jb_1 \left\{ \frac{J_{n+1}(\beta\rho)}{\beta\rho} + (2n+1) \frac{J_{n+2}(\beta\rho)}{(\beta\rho)^2} \right\} + O\left(\frac{1}{\beta\rho}\right)^3. \quad (48)$$

The third term is

$$I_{22} = jb_2 \int_1^{\infty} \frac{\sqrt{y^2-1}}{y} \frac{J_n(\beta\rho y)\, dy}{y^n}. \quad (49)$$

After one integration by parts we find

$$I_{22} = -jb_2 \left\{ \frac{1}{\beta\rho} \int_1^{\infty} \frac{J_{n+1}(\beta\rho y)\, dy}{y^n\sqrt{y^2-1}} - \frac{2n+2}{\beta\rho} \int_1^{\infty} \frac{J_{n+1}(\beta\rho y)\sqrt{y^2-1}\, dy}{y^{n+2}} \right\}. \quad (50)$$

[8] G. N. Watson, "A Treatise on the Theory of Bessel Functions," Cambridge University Press, Cambridge, Eng., 2nd ed., ch. 12, p. 373; 1952.

[9] *Ibid.*, ch. 13, p. 417.

The first term of (50) may be evaluated by means of Sonine's second formula (44). Repeated integration by parts shows that the second term of (50) is $O(\beta\rho)^{-3}$ and may be discarded. Thus,

$$I_{22} = \frac{-jb_2\Gamma(\frac{1}{2})}{\sqrt{2}(\beta\rho)^{3/2}} J_{n+(1/2)}(\beta\rho) + O\left(\frac{1}{\beta\rho}\right)^3. \tag{51}$$

The fourth term of the series is

$$I_{23} = jb_3 \int_1^\infty \left(\frac{y^2-1}{y^2}\right) \frac{J_n(\beta\rho y)dy}{y^n}$$

$$= jb_3 \int_1^\infty \frac{J_n(\beta\rho y)dy}{y^n} - jb_3 \int_1^\infty \frac{J_n(\beta\rho y)dy}{y^{n+2}}. \tag{52}$$

We may apply the result of (47) to the two terms in (52) to obtain

$$I_{23} = jb_3 \frac{2J_{n+2}(\beta\rho)}{(\beta\rho)^2} + O\left(\frac{1}{\beta\rho}\right)^3. \tag{53}$$

It is possible to show that the next term in (42) contributes only $O(\beta\rho)^{-3}$ to the series. Let the input current per unit angle be I_0. Then taking the first four terms of (40), adding them to (45), (48), (51), and (53), and adjusting the constant of proportionality to the input current, we find

Straight wires are represented by $a=\infty$, but our integral representation (17) fails in this case which therefore has to be considered separately. The solution is fairly simple and gives a distribution of $|I|$ which is constant with ρ^5, and a phase velocity equal to that of light, as illustrated on the graphs.

The phase characteristic is perhaps the most interesting feature of these results. For $n>0$ it consists of an inward slow wave when r is very small, changing to a fast wave as r increases, which becomes infinitely fast at the point where the phase is a maximum in Fig. 9. Passing beyond this point, we find a fast outward wave which slows down to the velocity of light when $r\to\infty$. For $n<0$ we find the same sequence of changes, except that the direction of the phase velocity is reversed everywhere. The extraordinary feature is that we now have an inward wave at infinity. At first sight this might appear to be physically inadmissible because certainly the power must flow outward at infinity. However, in this case we are not dealing with the ordinary radiation field, namely the field which varies as $1/r$, for this is zero on the antenna when $r=\infty$. Indeed, that such a reversal of the phase velocity is necessary with reversal of n can be quickly seen for small r by working from the requirement that the current along any individual wire must be constant in the quasi-static approximation. Also, when $r=\infty$, the curvature of the

$$I = I_0 \frac{a^a}{n} \left| \frac{\Gamma\left(j\frac{n}{a}+n+1\right)}{\Gamma\left(n-j\frac{n}{a}\right)\Gamma\left(j\frac{n}{a}-n+1\right)P_{j(n/a)}{}^n(0)} \right| e^{jn\phi} \left\{ \frac{e^{-j\beta\rho+jn(\pi/2)}}{\beta\rho}\left(j+\frac{n^2+j5an+6a^2}{2\beta\rho}\right) \right.$$

$$\left. - \sqrt{\frac{2}{\pi\beta\rho}} \frac{\left(\frac{n}{3}+3n^2-\frac{26a^2n}{3}-2ja-6jan-\frac{2jn^2a}{3}+8ja^3\right)\cos\left(\beta\rho-\frac{n\pi}{2}-\frac{\pi}{4}\right)}{(\beta\rho)^2} \right\} + O(\beta\rho)^{-3}. \tag{54}$$

For the case $n=1$, this expression reduces to

$$I = I_0 a\sqrt{1+a^2}\, e^{j\phi} \left\{ \frac{-e^{-j\beta\rho}}{\beta\rho}\left(1+\frac{5a-j-6ja^2}{2\beta\rho}\right) - \sqrt{\frac{2}{\pi\beta\rho}} \frac{(10-26a^2-26ja+24ja^3)\sin\left(\beta\rho-\frac{\pi}{4}\right)}{3(\beta\rho)^2} \right\}$$

$$+ O(\beta\rho)^{-3}. \tag{55}$$

In (54) and (55) the Bessel functions have been replaced by their asymptotic expansions.

The current distribution has also been worked out directly from the integral by using a digital computer for the cases $a=0.1$, 0.5 and 1.0 with $n=1$. The results are plotted in Figs. 8–11 (next page). The salient feature of these graphs is the marked increase in attenuation of the current with increase in the curvature of the spiral. spiral becomes negligible and the waves become essentially plane. By using the results of Rumsey,[5] it will be found that solutions for straight wires can be constructed in which the phase velocity is inward on the wires but outward some distance away. It is thus possible to see how the inward wave on the antenna is connected to the outward wave in the radiation field, and to the mode of excitation.

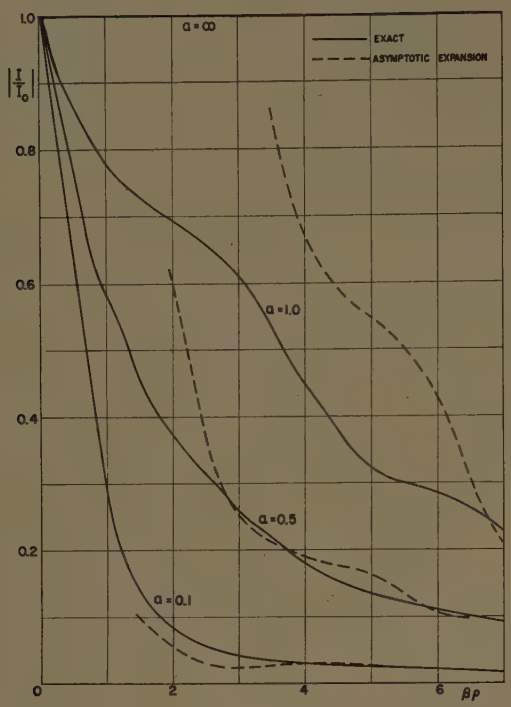

Fig. 8.

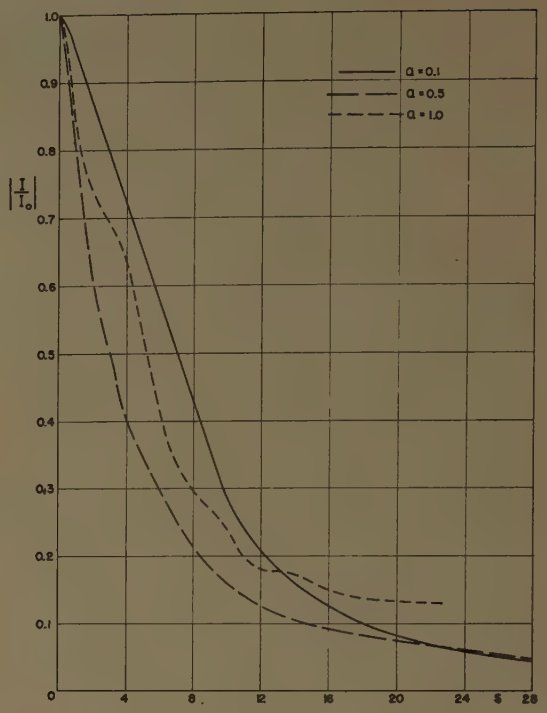

Fig. 10.

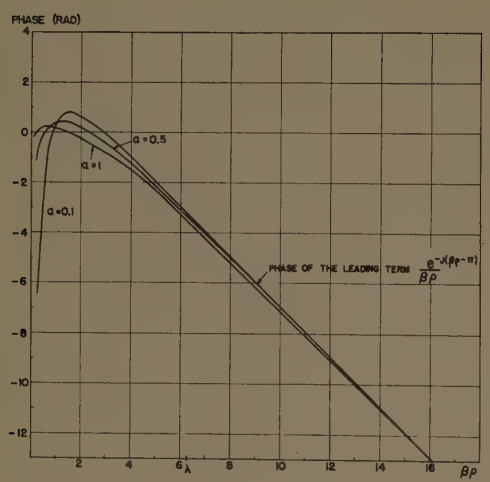

Fig. 9—Phase variation of current distribution as computed by numerical integration.

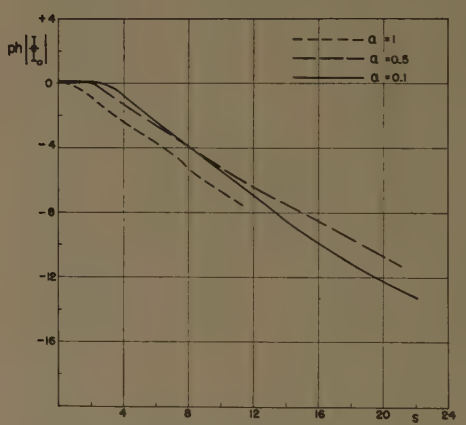

Fig. 11.

The Radiation Fields from a Circumferential Slot on a Metal Cylinder Coated with a Lossy Dielectric*

CHARLES M. KNOP†, MEMBER, IRE

Summary—The radiation fields produced by a sinusoidal distribution of axial-electric field along a thin circumferential slot, cut in a perfectly conducting infinite cylinder which is covered by a concentric dielectric coating, are found by applying the method of Wait[1] with two modifications. Initially, a structure consisting of a finite coated cylinder containing the slot and exciting a radial waveguide is considered. The fields in this waveguide are expressed in terms of derivatives of two axial Hertz vectors, and for a finite radial wall spacing are seen to consist of a double Fourier series. The radial walls are then allowed to become infinitely spaced; in this process, the Fourier-series representation for the axial dependence of the fields becomes a Fourier integral. The radiation fields are then found by asymptotically evaluating the Fourier integral by the method of stationary phase rather than by the saddle-point method.

Expressions for the radiation fields are then found, but are given explicitly for the equatorial plane only. Calculated radiation patterns in this plane, for a coating having a fixed dielectric constant with the thickness as a parameter, and for a fixed thickness with the dielectric constant as a parameter, are given for the case of a cylinder of size $\beta_0 a = 3$. Generalizations based on these calculations are suggested. The case of a specific plasma coating is briefly considered, and an approximate solution, readily obtained, which gives the same azimuthal form for the equatorial patterns, is also noted.

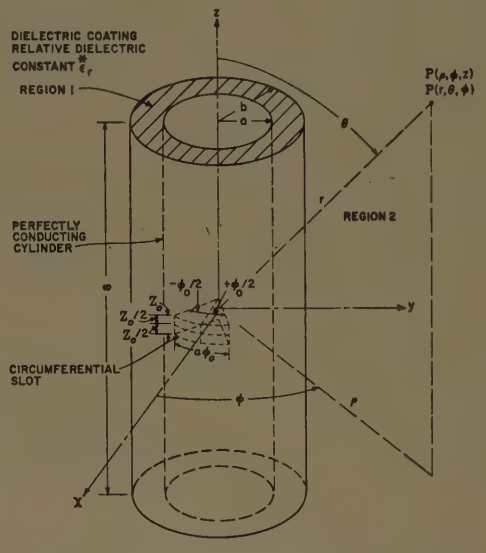

Fig. 1—Dielectric coated metal cylinder with a circumferential slot.

Introduction

THE radiating structure considered is an infinite, perfectly conducting cylinder of radius a, on which is cut a thin circumferential slot, of width $a\phi_0$, which is assumed to be excited with a sinusoidal, circumferential, varying, axial-electric field. The cylinder is covered by a nonmagnetic, concentric, dielectric coating of complex relative dielectric constant ϵ_r^* and of radius b. This structure is depicted in Fig. 1.

The electromagnetic fields produced by such a slot can be obtained by the method impeccably outlined by Wait.[1] His method will be used here with two slight modifications: 1) the use of Hertzian-vector potentials to initially derive the fields for a finite coated cylinder containing the slot and exciting a radial waveguide, as discussed below, and 2) the use of the method of stationary phase to evaluate the resulting integrals in the far field region. These modifications are substitutes for a direct expansion of the fields in an azimuthal Fourier series and an axial Fourier integral and the use of the saddle-point method to evaluate the same integrals, respectively. It is believed that this use of the Hertzian vector has more of a physical basis than the direct expansion of the fields as mentioned above, and that of the two methods of evaluating the asymptotic value of an integral, the method of stationary phase is the simplest.

Thus, in essence, the solution for the fields will be obtained by solving a two-region boundary value problem. The regions are defined by

$$\text{region 1:} \quad a \leq \rho \leq b$$

$$\text{region 2:} \quad b \leq \rho < \infty .$$

The boundary value problem is solved as follows: first, the fact that the $\boldsymbol{E}$ and $\boldsymbol{H}$ fields can be derived from two Hertzian-vector potentials $\boldsymbol{\Pi}$ and $\boldsymbol{\Pi}^*$, which have only axial components Π_z and Π_z^*, respectively, is utilized.[2] These Hertzian potentials are obtained for the structure considered as a limiting case of a radial waveguide whose walls are allowed to become infinitely spaced. By appropriate differentiation of Π_z and Π_z^*, the $\boldsymbol{E}$ and $\boldsymbol{H}$ fields in both regions are found. The resulting field expressions contain six unknown coefficients which can be evaluated by applying the six tangential boundary conditions at $\rho = a$ and $\rho = b$. To determine the fields in region 2, only two coefficients need be determined. This is done, and it is seen that the expressions for these coefficients are very lengthy. A partial check is then made by considering the special cases of a dielectric

* Received by the PGAP, June 21, 1961; revised manuscript received, July 31, 1961.

† Res. and Dev. Dept., The Hallicrafters Co., Chicago, Ill.; formerly with Chicago, Ill., Res. Lab. of the Bendix Systems Div. of Ann Arbor, Mich.

[1] J. R. Wait, "Electromagnetic Radiation from Cylindrical Structures," Pergamon Press, New York, N. Y., pp. 125–141; 1959.

[2] C. M. Knop, "The Radiation Fields from a Circumferential Slot on a Metal Cylinder Coated with a Lossy Dielectric," Bendix Systems Div., Ann Arbor, Mich., Res. Note 21, pp. I-1, I-3; October, 1960.

coating having an ϵ_r^* of unity or having a vanishing thickness. In both cases the resulting coefficients give, after integration by the method of stationary phase, the well-known radiation field expressions for a circumferential slot on a cylinder in free space (see Appendix I). Returning to the dielectric coating case, the method of stationary phase is applied to obtain the radiation fields, and it is then noted that the field expressions in the equatorial plane simplify considerably. Explicit expressions are then given for all the radiation field components in this plane, which, fortunately, is the plane of most interest. It is also noted that an approximate solution (see Appendix II) gives the same azimuthal dependence of the far fields in the equatorial plane, as obtained by the above exact method.

Formal Solution Procedure

A. Determination of Hertz Vectors

Consider the cylindrically excited, radial-waveguide arrangement depicted in Fig. 2. It is noted[3] that if L, the distance between the walls of the guide, extends to infinity, then the structure becomes identical to that depicted in Fig. 1.

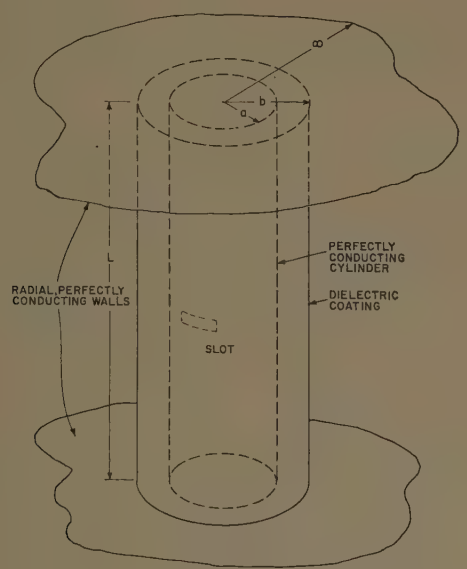

Fig. 2—Cylindrically excited radial waveguide.

In region 1, the Hertz potential Π_{z1} must satisfy the scalar wave equation[2]

$$\partial_\rho^2\Pi_{z1} + \frac{1}{\rho}\partial_\rho\Pi_{z1} + \frac{1}{\rho^2}\partial_\phi^2\Pi_{z1} + \partial_z^2\Pi_{z1} + \beta^2\Pi_{z1} = 0, \quad (1)$$

with an identical equation for Π_{z1}^*, where

$$\beta^2 \equiv \beta_0^2\epsilon_r^* \quad (2)$$

$$\beta_0^2 \equiv \omega^2\mu_0\epsilon_0. \quad (3)$$

[3] This technique of allowing a finite size guide to become infinite is adopted from G. I. Cohn and G. T. Flesher, "Theoretical radiation pattern and impedance of flush-mounted coaxial aperture," *Proc. Nat. Electronics Conf.*, Chicago, Ill., October, 1958, vol. 14, pp. 150–168; 1958.

The field components in region 1 are then[2]

$$\begin{cases} E_{\rho 1} = \partial_{z\rho}\Pi_{z1} - j\dfrac{\omega\mu_0}{\rho}\partial_\phi\Pi_{z1}^* \\ E_{\phi 1} = \dfrac{1}{\rho}\partial_{z\phi}\Pi_{z1} + j\omega\mu_0\partial_\rho\Pi_{z1}^* \\ E_{z1} = -\dfrac{1}{\rho}\partial_\rho(\rho\partial_\rho\Pi_{z1}) - \dfrac{1}{\rho^2}\partial_\phi^2\Pi_{z1} = \partial_z^2\Pi_{z1} + \beta^2\Pi_{z1}, \end{cases} \quad (4)$$

and

$$\begin{cases} H_{\rho 1} = \partial_{z\rho}\Pi_{z1}^* + j\dfrac{\omega\epsilon_0\epsilon_r^*}{\rho}\partial_\phi\Pi_{z1} \\ H_{\phi 1} = \dfrac{1}{\rho}\partial_{z\phi}\Pi_{z1}^* - j\omega\epsilon_0\epsilon_r^*\partial_\rho\Pi_{z1} \\ H_{z1} = -\dfrac{1}{\rho}\partial_\rho(\rho\partial_\rho\Pi_{z1}^*) - \dfrac{1}{\rho^2}\partial_\phi^2\Pi_{z1}^* = \partial_z^2\Pi_{z1}^* + \beta^2\Pi_{z1}^*. \end{cases} \quad (5)$$

Assuming a product solution to (1) then gives for region 1, where it is to be expected that both forward and backward traveling waves will exist in the radial direction due to the reflection at the dielectric-air interface at $\rho = b$

$$\Pi_{z1} = [EH_m^{(2)}(u\rho) + FJ_m(u\rho)][\zeta e^{-jm\phi} + \zeta' e^{+jm\phi}] \cdot [Ce^{-jhz} + De^{+jhz}], \quad (6)$$

where

$$u^2 \equiv \beta^2 - h^2, \quad (7)$$

with m being an integer, since the fields must be single valued, and where h is a constant to be determined.

Applying the boundary conditions at the upper and lower plates, which are assumed to be perfect conductors

$$E_{\rho}{}_{|z=\pm(L/2)} = 0 \quad (8)$$

gives, as seen from (4)

$$\partial_z\Pi_{z1}{}_{|z=\pm(L/2)} = \partial_\phi\Pi_{z1}^*{}_{|z=\pm(L/2)} = 0. \quad (9)$$

Applying the first of the conditions in (9) gives

$$-jhCe^{-jh(L/2)} + jhDe^{+jh(L/2)} = 0, \quad (10)$$

and

$$-jhCe^{+jh(L/2)} + jhDe^{-jh(L/2)} = 0. \quad (11)$$

Thus

$$C = D \quad (12)$$

and

$$\sin\frac{hL}{2} = 0, \quad (13)$$

therefore

$$h = \frac{2n\pi}{L}, \qquad n = 0, 1, 2, 3, \cdots. \quad (14)$$

Applying the latter condition of (9) gives

$$\Pi_{z1}^*{}_{z=\pm(L/2)} = 0, \tag{15}$$

which will be used later when obtaining the solution for Π_{z1}^*.

It is then seen from (4) and (5) that if (12), (14), and (15) hold, the tangential electric fields vanish ($E_\rho = E_\phi = 0$) and the normal magnetic field vanishes ($H_z = 0$) on the top and bottom walls of the radial waveguide. From (12) and (14), after redefining the coefficients, Π_{z1} then becomes

$$\Pi_{z1} = \sum_{m=-\infty}^{m=+\infty} \sum_{n=-\infty}^{n=+\infty} [a_{mn} H_m^{(2)}(u\rho) + A_{mn} J_m(u\rho)] \cdot e^{-jm\phi} e^{-j(2\pi n/L)z}. \tag{16}$$

It is seen that (16) is a double Fourier series in the ϕ and z variables. The Fourier coefficients are found in the usual way. Multiplying (16) by $e^{+jp\phi}d\phi$ and integrating from $-\pi$ to π, and then multiplying by $e^{+j(2\pi q/L)z}dz$ and integrating from $-L/2$ to $L/2$ gives

$$[a_{mn} H_m^{(2)}(\mu\rho) + A_{mn} J_m(\mu\rho)] = \frac{1}{2\pi L} \int_{-L/2}^{L/2} \int_{-\pi}^{\pi} \Pi_{z1}(\rho, \phi, z) e^{jm\phi} e^{j(2\pi n/L)z} d\phi dz. \tag{17}$$

Now, let

$$h \equiv \frac{2\pi n}{L}. \tag{18}$$

Therefore as n increases by one integer, h increases by an amount Δh of

$$\Delta h = 2(n+1)\frac{\pi}{L} - \frac{2\pi n}{L} = \frac{2\pi}{L}. \tag{19}$$

Then, rewriting (16) as

$$\Pi_{z1} = \sum_{m=-\infty}^{m=+\infty} \sum_{n=-\infty}^{n=+\infty} \left[\frac{a_{mn} H_m^{(2)}(u\rho) + A_{mn} J_m(u\rho)}{\Delta h}\right] \cdot e^{-jm\phi} e^{-jhz} \Delta h, \tag{20}$$

it is seen from (17) and (20) that as $L \to \infty$, $\Delta h \to 0$ and the quantity in the brackets becomes of the form zero over zero

$$\lim_{\substack{L\to\infty \\ \Delta h \to 0}} \left[\frac{a_{mn} H_m^{(2)}(u\rho) + A_{mn} J_m(u\rho)}{\Delta h}\right] = \frac{0}{0}, \tag{21}$$

and the quantity h becomes a continuous variable.

Since the integration over dz in (17) will still be bounded as the limits tend to infinity because Π_{z1} is to represent a physical field, the limit of (21) will be taken as finite, although, as yet unknown

$$\lim_{\substack{L\to\infty \\ \Delta h \to 0}} \left[\frac{a_{mn} H_m^{(2)}(u\rho) + A_{mn} J_m(u\rho)}{\Delta h}\right] \equiv [a_m(h) H_m^{(2)}(u\rho) + A_m(h) J_m(u\rho)]. \tag{22}$$

Thus

$$\Pi_{z1} = \sum_{m=-\infty}^{m=+\infty} \lim_{\Delta h \to 0} \sum_{n=-\infty}^{n=+\infty} \frac{[a_{mn} H_m^{(2)}(u\rho) + A_{mn} J_m(u\rho)]}{\Delta h} \cdot e^{-jm\phi} e^{-jhz} \Delta h. \tag{23}$$

The limit process in (23) converts the summation over n into an integral, thus[4]

$$\Pi_{z1} = \sum_{m=-\infty}^{m=+\infty} \left(\int_{-\infty}^{+\infty} [a_m(h) H_m^{(2)}(u\rho) + A_m(h) J_m(u\rho)] \cdot e^{-jhz} dh \right) e^{-jm\phi}, \tag{24}$$

where the coefficients $a_m(h)$ and $A_m(h)$ are as yet undetermined. By using (15) and following the above procedure, in an exactly similar way there results for Π_{z1}^*

$$\Pi_{z1}^* = \sum_{m=-\infty}^{m=+\infty} \left(\int_{-\infty}^{+\infty} [b_m(h) H_m^{(2)}(u\rho) + B_m(h) J_m(u\rho)] \cdot e^{-jhz} dh \right) e^{-jm\phi}. \tag{25}$$

Going through the same procedure for the Hertzian vectors in region 2, but noting that only an outgoing wave can exist in this region, gives

$$\Pi_{z2} = \sum_{m=-\infty}^{m=+\infty} \left(\int_{-\infty}^{+\infty} [c_m(h) H_m^{(2)}(u_0\rho)] e^{-jhz} dh \right) e^{-jm\phi} \tag{26}$$

and

$$\Pi_{z2}^* = \sum_{m=-\infty}^{m=+\infty} \left(\int_{-\infty}^{+\infty} d_m(h) H_m^{(2)}(u_0\rho) e^{-jhz} dh \right) e^{-jm\phi}, \tag{27}$$

where

$$u_0^2 \equiv \beta_0^2 - h^2. \tag{28}$$

Eqs. (24) through (27) constitute the solution of the Hertzian potentials of the problem. They contain the six unknown coefficients: $a_m(h)$, $A_m(h)$, $b_m(h)$, $B_m(h)$, $c_m(h)$, and $d_m(h)$ which must be evaluated by applying the remaining boundary conditions on the field components.

B. Determination of Field Components

Use of (4) and (5) will give the field components. This involves straightforward differentiation and gives, using the operator notation,

$$\Gamma f \equiv \sum_{m=-\infty}^{m=+\infty} \left(\int_{-\infty}^{+\infty} f e^{-jhz} dh \right) e^{-jm\phi} \tag{29}$$

for the field components, see Wait,[5] where $k \equiv \beta$, $k_0 = \beta_0$, and $i = j$, or also see Knop.[6]

[4] It should be noted here that the use of (12) and (13) gives rise to an expression for Π_{z1} which is an even function of z. However, if the equally valid choice of $C = -D$ and $\cos hL/2 = 0$ were made, Π_{z1} would be an odd function of z. Superimposing these solutions gives Π_{z1} in the form of (24) where Π_{z1} is an arbitrary function of z. See Knop, *op. cit.*, pp. IV-2–IV-4 for a thorough discussion.

[5] Wait, *op. cit.*, eqs. (336)–(347), pp. 126–127.

[6] Knop, *op. cit.*, pp. 9–10.

C. Evaluation of Coefficients

The coefficients are evaluated by insisting that the tangential boundary conditions are satisfied. These conditions are

$$\left.\begin{aligned} E_{z1} &= E_{z2} \\ E_{\phi 1} &= E_{\phi 2} \\ H_{z1} &= H_{z2} \\ H_{\phi 1} &= H_{\phi 2} \end{aligned}\right\} \text{ at } \rho = b \tag{30}$$

and

$$\left.\begin{aligned} E_{z1} &= E_{z \text{ specified}} \\ E_{\phi 1} &= 0 \end{aligned}\right\} \text{ at } \rho = a. \tag{31}$$

Here, the specified distribution of E_{z1} on the cylinder is zero everywhere except on the slot, where a sinusoidal distribution is taken, *i.e.*,

$$\begin{aligned} &E_{z \text{ specified}} \\ &\equiv E_0 \left\{ \sin \beta_0 a \left(\frac{\phi_0}{2} + \phi\right)\left[1\left(\phi + \frac{\phi_0}{2}\right) - 1(\phi)\right] \right. \\ &\quad \left. + \sin \beta_0 a \left(\frac{\phi_0}{2} - \phi\right)\left[1(\phi) - 1\left(\phi - \frac{\phi_0}{2}\right)\right]\right\} \\ &\quad \cdot \left[1\left(z + \frac{z_0}{2}\right) - 1\left(z - \frac{z_0}{2}\right)\right], \end{aligned} \tag{32}$$

where

$$1(x) \equiv \begin{cases} 1 & x > 0 \\ 0 & x < 0 \end{cases} \tag{33}$$

is the unit step function. Equating (32) and (336) of Wait[1] gives, after multiplying by $e^{jp\phi}d\phi$ and integrating from $-\pi$ to π,

$$\begin{aligned} &\int_{-\pi}^{\pi} E_{z \text{ specified}} e^{jm\phi} d\phi \\ &\quad = 2\pi \int_{-\infty}^{+\infty} u^2 [a_m H_m(ua) + A_m J_m(ua)] e^{-jhz} dh. \end{aligned} \tag{34}$$

Eq. (34) is then seen to be a representation of the L.H.S. by a Fourier integral. Thus

$$\begin{aligned} &u^2[a_m H_m(ua) + A_m J_m(ua)] \\ &= \frac{1}{(2\pi)^2} \int_{-\infty}^{+\infty} \left[\int_{-\pi}^{+\pi} E_{z \text{ specified}}(a, \phi, z) e^{jhz} e^{jm\phi} d\phi \right] dz \\ &\equiv Q_m(h). \end{aligned} \tag{35}$$

Use of the other five boundary conditions with (35) then gives a set of six equations of the form

$$\begin{aligned} &a_{mp}a_m + b_{mp}b_m + A_{mp}A_m + B_{mp}B_m + c_{mp}c_m \\ &\qquad + d_{mp}d_m = x_{mp}, \end{aligned} \tag{36}$$

where: $p = 1, 2, 3, 4, 5, 6$; and where the coefficients[7] a_{mp}, b_{mp}, etc., are tabulated by Wait,[8] and also appear in Wait and Mientka[7] and Knop.[9] If only the fields in region 2 are required, it suffices to find the coefficients c_m and d_m. These are found by using determinants, and are

$$\begin{aligned} \frac{c_m}{Q_m(h)} &= \frac{\mathfrak{L}u^4}{D}\left(\frac{u_0}{c'}\right)\left(j\frac{2}{\pi ub}\right)\left\{-\frac{m^2h^2}{ab}V_m\left[Fc'\left(\frac{u}{u_0} - \frac{u_0}{u}\right)\right]\right. \\ &\quad + \beta^2u^2\left[(A'E' - B'c')\left(F'c - \frac{u_0}{u}Fc'\right)\right. \\ &\quad \left.\left. - j\frac{2}{\pi ub}F'A'\right]\right\}, \end{aligned} \tag{37}$$

and

$$\begin{aligned} \frac{d_m}{Q_m(h)} &= -\frac{u^4\beta^2mhFu_0^2}{D}\left(j\frac{2}{\pi ub}\right) \\ &\quad \cdot \left\{\frac{1}{aE}\left[-\frac{V_m}{F}\left(E'F - \frac{\beta_0^2}{\beta^2}\frac{u}{u_0}F'E\right) + B\left(j\frac{2}{\pi ub}\right)\right]\right. \\ &\quad \left. + \frac{1}{b}(1 - u^2/u_0^2)(A'E - B'c)\right\}, \end{aligned} \tag{38}$$

where

$$U_m \equiv -(AE' - Bc') \tag{39}$$

and

$$V_m \equiv -(AE - Bc); \tag{40}$$

also

$$\begin{cases} A = H_m(ua) \\ A' = H_m'(ua) \\ B = J_m(ua) \\ B' = J_m'(ua) \\ c = H_m(ub) \\ c' = H_m'(ub) \end{cases} \tag{41}$$

$$\begin{cases} E = J_m(ub) \\ E' = J_m'(ub) \\ F = H_m(u_0b) \\ F' = H_m'(u_0b) \\ \mathfrak{L} = j\omega\mu_0 \\ D = \text{Determinant of } a_{mp}, b_{mp}, \text{ etc.} \end{cases} \tag{42}$$

(given explicitly in Knop[10]),

where the prime indicates differentiation with respect to the entire argument. Evaluation of the excitation factor $Q_m(h)$ gives, from (35) and (32)

$$Q_m(h) = \frac{E_0 z_0}{4\pi^2} I_m \frac{\sin\left(\frac{hz_0}{2}\right)}{\left(\frac{hz_0}{2}\right)}, \tag{43}$$

[7] It should be pointed out that in Wait[1] the coefficient a_{m5} is lacking a negative sign due to a misprint verified by consulting: J. R. Wait and W. Mientka, "Slotted-cylinder antenna with a dielectric coating," *J. Res. Natl. Bur. Standards*, vol. 58, pp. 287–296; June, 1957. See especially p. 291.

[8] Wait, *op. cit.*, Table I, p. 128.

[9] Knop, *op. cit.*, p. 12.

[10] Knop, *op. cit.*, p. 14.

where

$$I_m \equiv 2\int_0^{\phi_0/2} \sin\beta_0 a\left(\frac{\phi_0}{2}-\phi'\right)\cos m\phi' d\phi'$$

$$= \begin{cases} \dfrac{2\beta_0 a}{(\beta_0^2a^2-m^2)}\left[\cos\dfrac{m\phi_0}{2}-\cos\beta_0 a\dfrac{\phi_0}{2}\right], & m\neq\beta_0 a \\ \dfrac{\phi_0}{2}\sin\beta_0 a\dfrac{\phi_0}{2}, & m=\beta_0 a. \end{cases} \quad (44)$$

Insertion of (37), (38), and (43) into the field expressions for region 2 will then give explicit, but quite lengthy, expressions for these fields.

As a partial check on these expressions, the cases of an air dielectric coating ($\epsilon_r^*=1$) and a vanishing coating thickness ($b=a$) are considered in Appendix I. It is shown there that the resulting fields are identical to the well-known results for a circumferential slot on a cylinder in free space.

D. Evaluation of Far Fields

Use of Wait[11] gives

$$E_{z2} = \sum_{m=-\infty}^{m=+\infty} e^{-jm\phi}\int_{-\infty}^{+\infty} u_0^2 c_m(h)H_m(u_0\rho)e^{-jhz}dh. \quad (45)$$

Using the asymptotic expansion for the Hankel function, (69) gives for E_{z2} in the far field

$$E_{z2} = \sum_{m=-\infty}^{m=+\infty} e^{-jm\phi}e^{jm\pi/2}e^{j\pi/4}I, \quad (46)$$

where

$$I \equiv \int_{-\infty}^{+\infty} g(h)e^{+jrf(h)}dh \quad (47)$$

with

$$g(h) \equiv u_0^2 c_m(h)\left[\frac{2}{\pi u_0\rho}\right]^{1/2} \quad (48)$$

and

$$f(h) \equiv -[h\cos\theta + u_0\sin\theta], \quad (49)$$

since ρ and z are related to r and θ by (68) and (70), respectively. Integration of I by the method of stationary phase, as discussed in Appendix I, then gives for the radiation axial-electric field (dropping the subscript 2 for the radiation fields),

$$E_z = j2\beta_0^2\frac{e^{-j\beta_0 r}}{r}\sin^2\theta\sum_{m=-\infty}^{m=+\infty}(j)^m e^{-jm\phi}c_m(h_0), \quad (50)$$

where h_0 is the point where $f'(h)\equiv df/dh$ vanishes. This gives $h_0=\beta_0\cos\theta$. Now the expression for $c_m(h_0)$ is still very lengthy. However for the equatorial plane ($\theta=\pi/2$) it simplifies considerably

$$c_m(h_0)\big|_{\theta=\pi/2} = -j\frac{E_0 z_0 I_m}{(2b)(\beta_0\pi)^3\left[\dfrac{\beta}{\beta_0}FU_m - F'V_m\right]}, \quad (51)$$

where on this plane U_m and V_m reduce to

$$U_m = J_m(\beta a)H_m^{(2)\prime}(\beta b) - J_m'(\beta b)H_m^{(2)}(\beta a) \quad (52)$$

$$V_m = J_m(\beta a)H_m^{(2)}(\beta b) - J_m(\beta b)H_m^{(2)}(\beta a). \quad (53)$$

Now, noting that

$$I_{-m}=I_m,\ U_{-m}=U_m,\ V_{-m}=V_m,\ F_{-m}=(-1)^mF_m,$$
$$F'_{-m}=(-1)^mF',\ (j)^{-m}=(-1)^m j^m, \quad (54)$$

E_z on the equatorial plane becomes

$$E_z\big|_{\theta=\pi/2} = \frac{4V_0(a/b)}{\pi^3}\frac{e^{-j\beta_0 r}}{r} \cdot \sum_{m=0}^{\infty}\frac{(j)^m\cos\left[\dfrac{m\phi_0}{2}-\cos\beta_0 a\dfrac{\phi_0}{2}\right]\cos m\phi}{(\beta_0^2a^2-m^2)(1+\delta_0^m)\left[\dfrac{\beta}{\beta_0}FU_m - F'V_m\right]}, \quad (55)$$

where

$$V_0 \equiv E_0 z_0.$$

In particular, for a half-wavelength slot, $a\phi_0=\lambda_0/2$, and substituting for F and F'

$$E_z\big|_{\theta=\pi/2} = \frac{4V_0(a/b)}{\pi^3}\frac{e^{-j\beta_0 r}}{r}\times\sum_{m=0}^{\infty}\frac{j^m\cos\left[\dfrac{m\pi}{2\beta_0 a}\right]\cos m\phi}{(\beta_0^2a^2-m^2)(1+\delta_0^m)\left[\dfrac{\beta}{\beta_0}H_m^{(2)}(\beta_0 b)U_m - H_m^{(2)\prime}(\beta_0 b)V_m\right]} \equiv -V_0\frac{e^{-j\beta_0 r}}{r}f(\phi). \quad (56)$$

From the field expressions for region 2 it is seen that the E_ϕ, E_ρ, and H_z components vanish identically on the equatorial plane since they are directly proportional to h_0,

$$E_\phi = E_\rho = H_z = 0 \quad \text{for } \theta=\pi/2. \quad (57)$$

Further, inspection of the magnetic-field expressions reveals

$$H_\phi\big|_{\theta=\pi/2} = -E_z/\eta_0, \quad (58)$$

and that for $\theta=\pi/2$, $H_{\rho 2}$ is of order r^{-2}. As a partial check it is seen that if $b=a$ or $\epsilon_r^*=1$, (56) reduces to (84) as it should.

Thus, the complete radiation fields (*i.e.*, the fields of order $1/r$) in the equatorial plane for the case of a half-wavelength slot are given by (56) and (58). It is interesting to note (see Appendix II) that a relatively simple approximate solution gives the same azimuthal form for the radiation fields in the equatorial plane.

[11] Wait, *op. cit.* (342), p. 127.

Numerical Results

From (56), the effect of a dielectric coating of arbitary complex relative dielectric constant ϵ_r^* and of arbitary thickness $(b-a)$ on the equatorial-radiation fields produced by a half-wavelength circumferential slot on such a coated cylinder can be computed.

Computations were made for a cylinder of size $c \equiv \beta_0 a = 3.00$, having a coating of fixed thickness $w \equiv b/a = 1.50$, having various values of dielectric constant ($\epsilon_r^* = N^2$, $N = 0.70$, 1.00, 1.45, 2.10, 3.00, and 5.00) and for a coating of fixed dielectric constant ($N = 1.45$; $\epsilon_r^* = 2.10$), and of various values of thickness ($1 \leq w \leq 2.00$ in increments of 0.10).

The function $f(\phi)$ defined by (56) was computed for values of ϕ from 0 to 180° in increments of 5° from 0°–90° and in increments of 2° from 90°–180°. All the patterns are symmetrical with respect to ϕ. The on-axis values of the fields $f(\phi)\,|_{\phi=0}$ for all the cases computed are tabulated in Table I. These are the only tabulated results given here to save space, but all these calculations should be tabulated in a forthcoming company report. The table also shows the total number of terms taken in the summation. With the number of terms indicated, it is believed that at least five-significant-figure accuracy in both the amplitude and phase of $f(\phi)$ may be obtained. These computations were performed on the IBM 704 computer. Basically, the program for computation utilized the following methods: SHARE NU BES-3 and the technique of Goldstein and Thaler.[12] The technique employed in this electronic computation was to output the results after each sum, when a sum was formed for each value of ϕ used. Each sum was then examined, and when it was evident (as ascertained by inspection of future sums) that any more summing would not affect the seventh significant figure of $|f(\phi)|$, the process was stopped. The time required for the IBM 704 computer to process each case (*i.e.*, each radiation pattern $f(\phi)$ for $0° \leq \phi \leq 180°$) was approximately 20 seconds. Some cases were also manually calculated to serve as an initial check on the computer results. The manual calculations agreed within three significant figures with the computer calculations, since fewer terms were used in the manual summation. The time required for one manual calculation was 3 to 5 days and used tabulated values of Bessel functions.[13]

TABLE I

On Axis Field Strength Values

$c \equiv \beta_0 a = 3.00$, $\beta_0 = 2\pi/\lambda_0$, $N^2 = \epsilon_r^*$, $f(\phi) \equiv |f(\phi)|e^{j\vartheta_f}$, $V_0 = \text{constant}$

N	$w = b/a$	$\|f(\phi)\|_{\phi=0}$	$\vartheta_f\|_{\phi=0}$, Degrees	Number of Terms
1.45	1.00	0.32349	69.231	12
1.45	1.10	0.33927	68.667	12
1.45	1.20	0.38534	64.657	12
1.45	1.30	0.44561	53.867	12
1.45	1.40	0.46297	37.504	12
1.45	1.50	0.42209	24.517	12
1.45	1.60	0.37886	16.289	12
1.45	1.70	0.34384	15.505	12
1.45	1.80	0.37129	14.144	12
1.45	1.90	0.39942	7.642	12
1.45	2.00	0.44426	359.80	12
0.70	1.50	0.24535	85.351	15
1.00	1.50	0.32349	69.231	15
1.45	1.50	0.42209	24.517	15
2.10	1.50	0.32471	333.93	15
3.00	1.50	0.84238	278.79	15
5.00	1.50	0.88366	125.22	20

The variation of both the magnitude and phase of $f(\phi)$ from these computations (the cases of $N = 1.45$, $w = 1.10$, 1.70, and 1.90 are not shown for the sake of clarity) are shown plotted in Figs. 3, 4, 7 and 8. In addition, power plots in decibels

$$\left(\text{plots of } 20 \log_{10}\left[\frac{|f(\phi)|_{\phi=0}}{|f(\phi)|}\right]\right)$$

are shown in Figs. 5 and 6.

From these radiation patterns it is seen from Fig. 6 or Fig. 3 that for a fixed value of coating dielectric constant, if the coating thickness is small ($1.00 < w \simeq 1.30$) only a small deviation in the radiation pattern from the uncoated case results; as the thickness increases ($w = 1.40$, 1.50) more relative[14] radiation is concentrated in the back direction ($\phi = 180°$); a further increase ($w = 1.80$, 2.00) causes sharp lobes near the back direction and reduces the level of relative radiation in the back direction.

From Fig. 5 or Fig. 4 it is seen that for a fixed thickness, as the dielectric constant is increased ($N = 1.45$) from unity, the pattern becomes broader and also the relative radiation in the back direction increases; a further increase ($N = 2.10$) causes sharp lobes near the back direction, and a further increase ($N = 3.00$, 5.00) causes the pattern to become slightly sharper in the front direction than the uncoated case, with less relative radiation in the back direction.

From these results one may be tempted to form the generalization: for a given size cylinder with a coating of fixed real positive dielectric constant, there exists an optimum thickness for which the pattern is the broadest and the relative radiation in the back is maximum (close to $w = 1.50$ for Fig. 6); conversely for a fixed coating thickness there exists an optimum value of real positive dielectric constant for which this is also true (close to $N = 1.45$ for Fig. 5). For a cylinder of $\beta_0 a = 3.00$, it appears that a value of N near 1.45 and b/a near 1.50 will provide such an optimum coating. Stated in another way, the generalization would be: for a given sized metal cylinder, a coating having a real positive dielec-

[12] M. Goldstein and R. M. Thaler, "Recurrence techniques for the calculation of Bessel functions," in "Mathematical Tables and Other Aids to Computation," National Research Council, Washington, D. C., vol. 13, pp. 102–108; April, 1959.

[13] "Bessel functions part I and part II," in "British Association Mathematical Tables," Cambridge University Press, Cambridge, Eng., vols. 6 and 10; 1958 and 1952.

[14] Relative to the forward direction ($\phi = 0$) for the same coating.

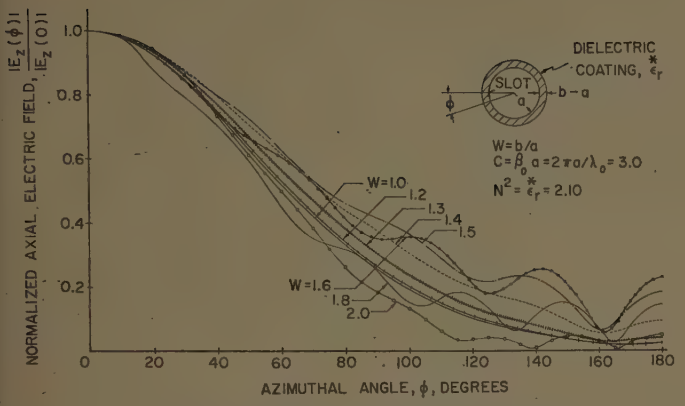

Fig. 3—Equatorial radiation patterns for coating of fixed dielectric constant and various values of thickness.

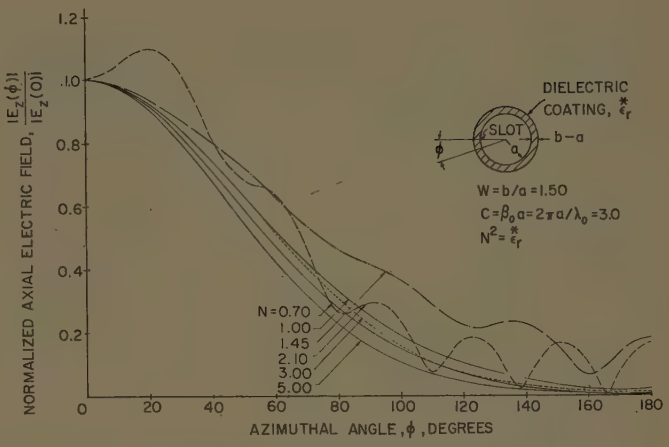

Fig. 4—Equatorial radiation patterns for coating of fixed thickness and various values of dielectric constant.

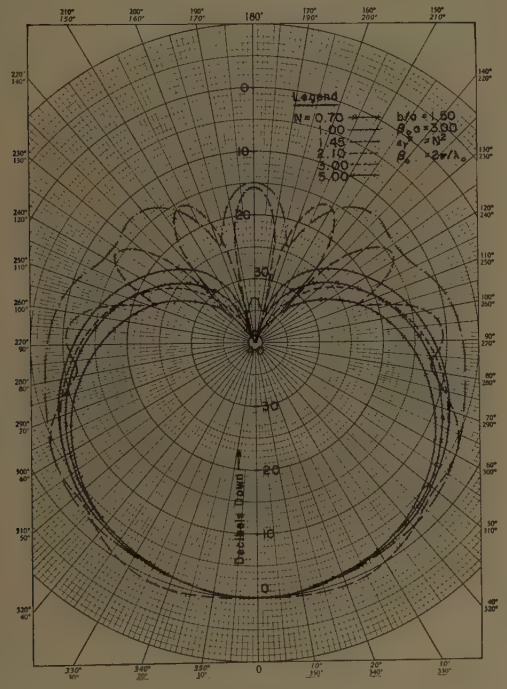

Fig. 5.

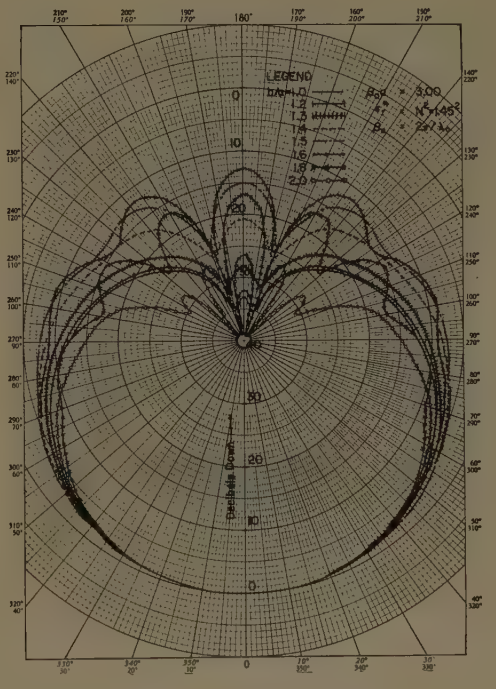

Fig. 6.

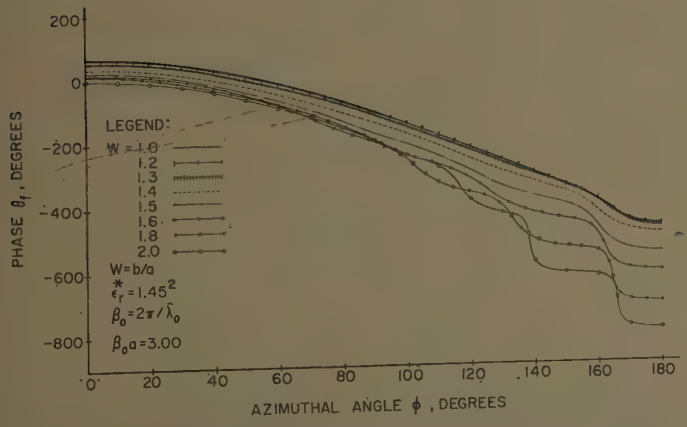

Fig. 7—Equatorial phase patterns for coating of fixed dielectric constant and various values of thickness.

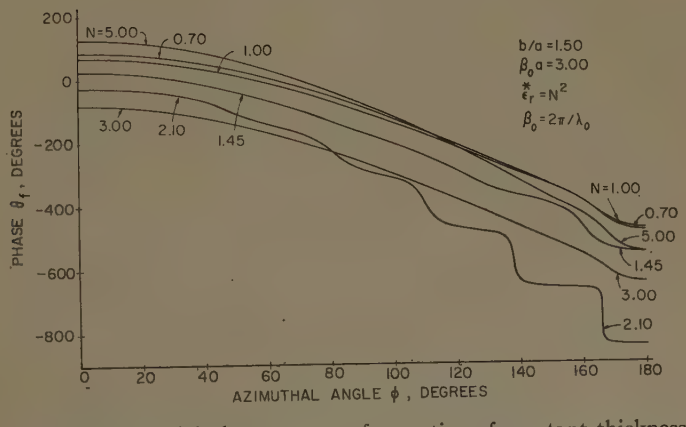

Fig. 8—Equatorial phase patterns for coating of constant thickness and various values of dielectric constant.

tric constant can serve to appreciably enhance the relative radiation in the back direction as well as broaden the pattern, if the coating is thick enough for a given dielectric constant or has a sufficiently high dielectric constant for a given thickness. However, these generalizations would have to be verified by further numerical work.

The radiation patterns for the specific case of a coating having a dielectric constant of $\epsilon_r^* = 0.49$, corresponding to $N = 0.70$, are also shown in Figs. 4 and 5. This value could represent a lossless plasma coating of thickness corresponding to $b/a = 1.50$. It is seen from Figs. 4 and 5 that a monotonically decreasing amplitude results, with less relative radiation in the back direction than for the uncoated case.

Conclusion

The radiation fields produced by a sinusoidal distribution of axial-electric field along a circumferential slot on a dielectric coated cylinder have been found by an application of the method of Wait, with two slight modifications. The field expressions are very lengthy except on the equatorial plane where they are given explicitly by (56) and (58) for the special case of a half-wavelength slot.

From these equations, calculations were made of the equatorial-plane radiation patterns for the case of a cylinder of fixed size having a fixed coating thickness with various values of dielectric constant, and for a coating of fixed dielectric constant with various values of thickness. These calculations reveal that the equatorial plane radiation pattern can be broadened, and that the radiation in the back direction (relative to the front direction for the same coating) can be appreciably enhanced by an appropriate choice of these two parameters.

List of Symbols

E = electric-field intensity, volts/meter.
H = magnetic-field intensity, amperes/meter.
D = electric-flux density, coulombs/meter^2.
B = magnetic-flux density, webers/meter^2.
μ_0 = permeability of free space $= 4\pi \cdot 10^{-7}$ henrys/meter.
ϵ_0 = permittivity of free space $= 1/36\pi \cdot 10^9$ farads/meter.
ϵ_r^* = complex relative dielectric constant of dielectric coating $= N^2$.
Π = Hertz-vector potential—electric type.
Π^* = Hertz-vector potential—magnetic type.
ρ, ϕ, z = radius, azimuthal angle, and axial distance, respectively, in circular cylindrical coordinates.
r, θ, ϕ = radius, elevation angle, and azimuthal angle, respectively, in spherical coordinates.
a = outer radius of perfectly conducting cylinder.
b = outer radius of dielectric coating.
β = propagation factor in dielectric coating.
β_0 = propagation factor in free space $= 2\pi/\lambda_0$.
λ_0 = free-space wavelength of wave-exciting slot.
$J_m(x)$ = Bessel function of first kind of order m and argument x.
$H_m^{(2)}(x)$ = Hankel function of second kind or order m and argument x.
$J_m'(x) = dJ_m(x)/dx$ = first derivative of $J_m(x)$ with respect to x.
$H_m^{(2)\prime}(x) = dH_m^{(2)}(x)/dx$ = first derivative of $H_m^{(2)}(x)$ with respect to x.
All other symbols are defined as they are introduced.

Appendix I

Radiation Fields from a Circumferential Slot on an Uncoated Cylinder

Consider the case for which the thickness of the coating vanishes, *i.e.*, $b = a$. Then

$$c = A, \quad c' = A', \quad B = E, \quad E' = B', \tag{59}$$

$$A'E' - B'c' = AE - Bc = 0, \tag{60}$$

$$V_m = 0, \tag{61}$$

$$U_m = -j\frac{2}{\pi ua}, \tag{62}$$

$$A'E - B'c = A'B - B'A = -j\frac{2}{\pi ua}. \tag{63}$$

Substitution of these results into (37) and (38) gives, respectively,

$$\left.\frac{c_m}{Q_m(h)}\right|_{b=a} = \frac{1}{u_0^2 H_m^{(2)}(u_0 a)}, \tag{64}$$

$$\left.\frac{d_m}{Q_m(h)}\right|_{b=a} = \frac{mh}{a\mathfrak{L}u_0^3 H_m^{(2)\prime}(u_0 a)}. \tag{65}$$

Next consider the case for which the dielectric constant of the coating is unity, $\epsilon_r^* = 1$. Then

$$u = u_0, \quad \beta = \beta_0, \quad F = c, \quad F' = c'. \tag{66}$$

Substitution of these results into (37) and (38) gives the same results as (64) and (65), respectively.

Thus, for the uncoated cylinder, the axial-electric field becomes, using (64) in (342) of Wait[1] and dropping the subscripts

$$E_z = \Gamma\left[\frac{H_m^{(2)}(u_0\rho)Q_m(h)}{H_m^{(2)}(u_0 a)}\right]. \tag{67}$$

Now,

$$\rho = r\sin\theta. \tag{68}$$

Therefore for large values of r, *and θ sufficiently far off the axis, i.e.*, $0 < \theta < \pi$, as $r \to \infty$, $\rho \to \infty$. Thus, using the asymptotic expansion of the Hankel function

$$H_m^{(2)}(x) \approx \sqrt{\frac{2}{\pi x}}\, e^{-jx} e^{j\pi/4} e^{jm\pi/2} \qquad (x \gg m^2), \tag{69}$$

and using

$$z = r\cos\theta, \tag{70}$$

gives

$$E_z = \sum_{m=-\infty}^{m=+\infty} e^{-jm\phi} e^{j\pi/4} e^{jm\pi/2} I, \tag{71}$$

where I is given by (47) and here

$$g(h) \equiv \sqrt{\frac{2}{\pi u_0 \rho}}\,\frac{Q_m(h)}{H_m^{(2)}(u_0 a)}, \tag{72}$$

and where $f(h)$ is given by (49), where

$$u_0^2 = \beta_0^2 - h^2. \tag{73}$$

It is now noted that since the fields must be bounded that the factor $e^{-jru_0\sin\theta}$ (which represents wave propagation in the ρ direction, which in region 2 can only be outward going) must be bounded. Therefore, since the time factor is $e^{j\omega t}$, to have an outward-going bounded wave we must choose u_0 to be

$$\begin{aligned} u_0 &= +\sqrt{\beta_0^2 - h^2} \qquad \text{for } |h_0| < \beta_0 \\ u_0 &= -j\sqrt{h^2 - \beta_0^2} \qquad \text{for } |h| > \beta_0, \end{aligned} \tag{74}$$

where h is a real variable varying from $-\infty$ to $+\infty$.

For large values of r, the integral I can be asymptotically evaluated by the method of stationary phase.[15] The result is [for $g(h)$ and $f(h)$ sufficiently regular and $f''(h_0) \neq 0$]

$$\begin{aligned} I &\equiv \int_{-\infty}^{+\infty} g(h) e^{jrf(h)} dh \\ &= e^{jrf(h_0)} g(h_0) \sqrt{\frac{2\pi j}{rf''(h_0)}} + O\left(\frac{1}{r}\right), \end{aligned} \tag{75}$$

where h_0 satisfies

$$f'(h)\big|_{h=h_0} = 0. \tag{76}$$

Therefore, here

$$h_0 = +\beta_0\cos\theta \tag{77}$$

$$\therefore\ f(h_0) = -\beta_0, \qquad f''(h_0) = \frac{1}{\beta_0 \sin^2\theta},$$

$$u_0\big|_{h=h_0} = \beta_0 \sin\theta. \tag{78}$$

Thus, using (43), and restricting our interest to the case where the height of the slot be small so that

$$\frac{\sin\left(\frac{h_0 z_0}{2}\right)}{\left(\frac{h_0 z_0}{2}\right)} = \frac{\sin\left(\frac{\beta_0 z_0}{2}\cos\theta\right)}{\left(\frac{\beta_0 z_0}{2}\cos\theta\right)} \approx 1. \tag{79}$$

This restriction is made so that the assumed field distribution over the slot can be more readily realized, and is used throughout this paper. This gives for I

$$I = \frac{e^{-j\beta_0 r}}{r}\,\frac{E_0 z_0 e^{j\pi/4} I_m}{2\pi^2 H_m^{(2)}(\beta_0 a \sin\theta)} + O\left(\frac{1}{r^n}\right), \quad n > 1. \tag{80}$$

Therefore, the axial-radiation field, the field of order $1/r$, is

$$E_z(r,\theta,\phi) = j\,\frac{E_0 z_0}{2\pi^2}\,\frac{e^{-j\beta_0 r}}{r} \sum_{m=-\infty}^{m=+\infty} \frac{e^{jm\pi/2} I_m e^{-jm\phi}}{H_m^{(2)}(\beta_0 a \sin\theta)}. \tag{81}$$

Now, noting that $I_{-m} = I_m$, $e^{-jm\pi/2} = (-1)^m e^{jm\pi/2}$, and $H_{-m}^{(2)}(x) = (-1)^m H_m^{(2)}(x)$, (81) can be written as

$$E_z(r,\theta,\phi) = j\,\frac{E_0 z_0}{\pi^2}\,\frac{e^{-j\beta_0 r}}{r} \sum_{m=0}^{\infty} \frac{I_m e^{jm\pi/2}\cos m\phi}{(1+\delta_0^m) H_m^{(2)}(\beta_0 a \sin\theta)}, \tag{82}$$

where

$$\delta_0^m \equiv \begin{cases} 1 & m = 0 \\ 0 & m \neq 0 \end{cases} = \text{Kronecker delta function.}$$

Considering the special case of a half-wavelength slot, *i.e.*,

$$a\phi_0 \equiv \frac{\lambda_0}{2}, \tag{83}$$

and using (44) then gives

$$\begin{aligned} E_z(r,\theta,\phi) &= j\,\frac{2V_0(\beta_0 a)}{\pi^2}\,\frac{e^{-j\beta_0 r}}{r} \\ &\cdot \sum_{m=0}^{\infty} \frac{(j)^m \cos\frac{m\pi}{2(\beta_0 a)}\cos m\phi}{(\beta_0^2 a^2 - m^2)(1+\delta_0^m) H_m^{(2)}(\beta_0 a \sin\theta)}, \end{aligned} \tag{84}$$

where $V_0 \equiv E_0 z_0 =$ voltage across the center of the slot and where, if $m = \beta_0 a$, then the ratio

$$\left.\frac{\cos\frac{m\pi}{2\beta_0 a}}{(\beta_0^2 a^2 - m^2)}\right|_{m=\beta_0 a} = \frac{\pi}{4(\beta_0 a)^2}.$$

In the far field, use of (342), (343) and (344) of Wait[1] then shows that the spherical radial components of the field are negligible compared with the θ and ϕ components, hence

$$E_\theta = \frac{-E_z}{\sin\theta}. \tag{85}$$

Therefore,

$$\begin{aligned} E_\theta &= \frac{-j2V_0(\beta_0 a)}{\pi^2 \sin\theta}\,\frac{e^{-j\beta_0 r}}{r} \\ &\cdot \sum_{m=0}^{\infty} \frac{(j)^m \cos\frac{m\pi}{2\beta_0 a}\cos m\phi}{(\beta_0^2 a^2 - m^2)(1+\delta_0^m) H_m^{(2)}(\beta_0 a \sin\theta)}. \end{aligned} \tag{86}$$

[15] G. Toraldo Di Francia, "Electromagnetic Waves," Interscience Publishers, Inc., New York, N. Y., pp. 36–38; 1955.

The E_ϕ component can be found by substituting (64) and (65) into (343) of Wait.[1] Then noting that in the far field

$$\left|\frac{1}{\rho H_m^{(2)}(u_0 a)}\right| \ll \left|\frac{1}{a H_m^{(2)\prime}(u_0 a)}\right|, \tag{87}$$

and performing a similar stationary phase integration, we derive for a half-wavelength slot, the circumferential-radiation field

$$E_\phi = \frac{-j2V_0 \cos\theta}{\pi^2 \sin^2\theta} \frac{e^{-j\beta_0 r}}{r} \cdot \sum_{m=0}^{\infty} \frac{m(j)^m \cos\frac{m\pi}{2\beta_0 a} \sin m\phi}{(\beta_0^2 a^2 - m^2) H_m^{(2)\prime}(\beta_0 a \sin\theta)}. \tag{88}$$

Inspection of the magnetic-field expressions then gives

$$H_\phi = \frac{E_\theta}{\eta_0}, \tag{89}$$

and

$$H_\theta = \frac{-E_\phi}{\eta_0}, \tag{90}$$

where

$$\eta_0 \equiv \sqrt{\mu_0/\epsilon_0}. \tag{91}$$

Eqs. (86)–(90) for the radiation fields of a noncoated cylinder agree identically with the well-known results.[16] Calculations of the radiation field patterns for this uncoated case for cylinders of various radii have been reported.[17,18]

Appendix II

Approximate Solution for the Radiation Fields from a Circumferential Slot on a Metal Cylinder Coated with a Lossy Dielectric

To obtain an approximate solution it will be assumed that no axial variation of the fields exists,

$$\partial_z = 0, \tag{92}$$

and that

$$H_{z1} = H_{z2} = 0. \tag{93}$$

Maxwell's curl equations

$$\nabla \times \boldsymbol{H}_1 = j\omega\epsilon_0\epsilon_r^* \boldsymbol{E}_1 \tag{94}$$

$$\nabla \times \boldsymbol{H}_2 = j\omega\epsilon_0 \boldsymbol{E}_2, \tag{95}$$

then give

$$E_{\rho 1} = E_{\rho 2} = E_{\phi 1} = E_{\phi 2} = 0 \tag{96}$$

$$j\omega\epsilon_0\epsilon_r^* E_{z1} = \frac{1}{\rho}[\partial_\rho(\rho H_{\phi 1}) - \partial_\phi H_{\rho 1}] \tag{97}$$

$$j\omega\epsilon_0 E_{z2} = \frac{1}{\rho}[\partial_\rho(\rho H_{\phi 2}) - \partial_\phi H_{\phi 2}], \tag{98}$$

and Maxwell's second curl equations

$$\nabla \times \boldsymbol{E}_1 = -j\omega\mu_0 \boldsymbol{H}_1 \tag{99}$$

$$\nabla \times \boldsymbol{E}_2 = -j\omega\mu_0 \boldsymbol{H}_2, \tag{100}$$

then give

$$H_{\rho 1} = -\frac{1}{j\omega\mu_0\rho}\partial_\phi E_{z1} \tag{101}$$

$$H_{\rho 2} = -\frac{1}{j\omega\mu_0\rho}\partial_\phi E_{z2} \tag{102}$$

$$H_{\phi 1} = \frac{1}{j\omega\mu_0}\partial_\rho E_{z1} \tag{103}$$

$$H_{\phi 2} = \frac{1}{j\omega\mu_0}\partial_\rho E_{z2}. \tag{104}$$

Using (101)–(104) in (97) and (98) gives

$$\partial_\rho^2 E_{z1} + \frac{1}{\rho}\partial_\rho E_{z1} + \frac{1}{\rho^2}\partial_\phi^2 E_{z1} + \beta^2 E_{z1} = 0 \tag{105}$$

and

$$\partial_\rho^2 E_{z2} + \frac{1}{\rho}\partial_\rho E_{z2} + \frac{1}{\rho^2}\partial_\phi^2 E_{z2} + \beta_0^2 E_{z2} = 0, \tag{106}$$

which have the respective solutions

$$E_{z1} = \sum_{m=0}^{\infty} A_m'[J_m(\beta\rho) + B_m' H_m^{(2)}(\beta\rho)] \cos m\phi, \tag{107}$$

and

$$E_{z2} = \sum_{m=0}^{\infty} c_m' H_m^{(2)}(\beta_0\rho) \cos m\phi. \tag{108}$$

Therefore,

$$H_{\phi 1} = \frac{\beta}{j\omega\mu_0}\sum_{m=0}^{\infty} A_m'[J_m'(\beta\rho) + B_m H_m^{(2)\prime}(\beta\rho)] \cos m\phi, \tag{109}$$

and

$$H_{\phi 2} = \frac{\beta_0}{j\omega\mu_0}\sum_{m=0}^{\infty} c_m' H_m^{(2)\prime}(\beta_0\rho) \cos m\phi. \tag{110}$$

Using the tangential boundary conditions

$$\left.\begin{aligned} E_{z1} &= E_{z2} \\ H_{\phi 1} &= H_{\phi 2} \end{aligned}\right\} \quad \text{at} \quad \rho = b, \tag{111}$$

[16] Wait, *op. cit.*, p. 44.
[17] *Ibid.*, p. 3.
[18] C. M. Knop and A. R. Battista, "Calculated equatorial plane radiation patterns produced by a circumferential slot on a cylinder," IRE Trans. on Antennas and Propagation (Communications), vol. AP-9, pp. 498–499; September, 1961.

the Hankel function, and substituting for I_m gives

$$E_{z2} = \frac{4V_0(a/b)}{\pi^3} G \frac{e^{-i\beta_0\rho}}{\rho} \sum_{m=0}^{\infty} \frac{j^m[\cos m\phi_0/2 - \cos \beta_0 a\phi_0/2] \cos m\phi}{(\beta_0{}^2a^2 - m^2)(1 + \delta_0{}^m)\left[\frac{\beta}{\beta_0} H_m{}^{(2)}(\beta_0 b)U_m - H_m{}^{(2)\prime}(\beta_0 b)V_m\right]}, \quad (115)$$

$$E_{z1} = E_{z \text{ specified}} = (32) \text{ of the text, at } \rho = a, \quad (112)$$

to evaluate c_m', B_m', A_m', gives, for c_m'

$$c_m' = \frac{-j\frac{E_0}{\pi^2}\frac{z_0}{L} I_m \frac{2}{(\beta_0 b)}}{\left[\frac{\beta}{\beta_0} H_m{}^{(2)}(\beta_0 b)U_m - H_m{}^{(2)\prime}(\beta_0 b)V_m\right](1 + \delta_0{}^m)}, \quad (113)$$

where I_m, U_m, and V_m are as defined in the text, and L is an arbitrary length, such that $L \geq z_0$. Therefore,

$$E_{z2} = -j\frac{E_0}{\pi^2}\left(\frac{z_0}{L}\right)\frac{2}{(\beta_0 b)} \cdot \sum_{m=0}^{\infty} \frac{I_m H_m{}^{(2)}(\beta_0\rho)\cos m\phi}{\left[\frac{\beta}{\beta_0} H_m{}^{(2)}(\beta_0 b)U_m - H_m{}^{(2)\prime}(\beta_0 b)V_m\right](1 + \delta_0{}^m)}. \quad (114)$$

It is noted that if no dielectric is present, *i.e.*, if $b = a$ or $\epsilon_r{}^* = 1$, (114) reduces to the known approximate solution[19] for the case of air surrounding the cylinder, if L is chosen equal to z_0. Using the asymptotic expansion for

[19] E. C. Jordan, "Electromagnetic Waves and Radiating Systems," Prentice-Hall, Inc., New York, N. Y., p. 598; 1950.

where

$$G \equiv \rho\frac{\pi}{L} e^{j\pi/4}\sqrt{\frac{2}{\pi(\beta_0\rho)}} = \frac{r\pi}{L} e^{j\pi/4}\sqrt{\frac{2}{\pi\beta_0 r}}, \quad (116)$$

since $\rho = r$ when $\theta = \pi/2$.

The exact solution, given by (55) and the above approximate solution are then related by

$$\frac{E_{z2}(r, \pi/2, \phi)_{\text{approximate}}}{E_z(r, \pi/2, \phi)_{\text{exact}}} = G, \quad (117)$$

where, for a given r, G is a constant.

Thus the form of (115) is seen to be the same, except for the constant factor G, as for the exact solution (55), as far as the dependence on ϕ is concerned. This would indicate that the far field dependence on z, and therefore on θ, when near the equatorial plane is very small.

Acknowledgment

The author would like to acknowledge the work of A. R. Battista of Bendix Systems Division (B.S.D.) who programmed the computational effort for the IBM 704 computer. The author would like to thank G. T. Flesher of B.S.D. for technical discussions and R. Murabayashi of B.S.D. for performing most of the manual calculations.

Radiation from a Radial Electric Dipole near a Long Finite Circular Cylinder*

HANS H. KUEHL†, MEMBER, IRE

Summary—**By use of the currents on the infinite cylinder excited by a radial dipole, approximate expressions for the two components of the far-zone electric field of a radial electric dipole near a perfectly conducting finite cylinder are derived. The validity of the approximation depends on the conditions, $kl_2 \gg 1$ and $kl_1 \gg 1$, *i.e.*, the cylinder must be long compared to a wavelength. The expressions are initially in integral form but it is shown that they may be evaluated approximately over most of the range of θ by use of the saddle point method. The theoretical results are compared to experimental results for a particular cylinder.**

I. Introduction

THE determination of the far-zone radiation from a radial electric dipole near a finite perfectly conducting cylinder is of interest from both a theoretical and a practical point of view. From a theoretical aspect, the problem presents a distinct mathematical difficulty; the surface of the perfectly conducting cylinder cannot be described by assigning a constant value to one of the coordinates. A rigorous solution to the problem is, therefore, very difficult since the boundary condition of zero tangential electric field must be imposed over parts of two different coordinate surfaces. However, if the cylinder is long compared to a wavelength an approximate solution to the problem can be obtained; the method of approximation is described in Section III.

The effect of a long finite cylinder near a radial dipole is of interest to the antenna designer because of the common occurrence of antenna systems in which a linear antenna is located near or supported by a conducting body. Examples are stub antennas on aircraft and linear antennas on space vehicles. In many cases the conducting body is more or less cylindrical so that the expressions for the finite cylinder can be employed for an approximate solution.

Closely related to the present problem is that of the radiation from a radial dipole near an infinite cylinder which has received the attention of various authors. Carter[1] derived expressions for the far-zone radiation from dipoles of various orientations near an infinite conducting cylinder using the principle of reciprocity. In a later paper, Lucke[2] obtained essentially the same results using the Green's function method. Moullin[3] has related results in his book and LePage, Harrington and Schlecht,[4,5] and Walsh[6] consider similar problems. A radial dipole in a cylindrical wedge region is considered by Wait[7] and theoretical and experimental radiation patterns in the principal plane are compared.

The configuration of interest here is an asymmetrical structure; the exciting dipole is not necessarily situated in the plane equidistant from the two ends of the cylinder. Therefore the radiation pattern is not necessarily symmetrical about the midplane of the system.

II. The Infinite Cylinder Excited by a Radial Dipole

It will be necessary in the approximate treatment of the long finite cylinder to have available the expressions for the currents on the infinite cylinder. The infinite cylinder of radius a excited by a radial dipole at radius b is shown in Fig. 1. Using a cylindrical coordinate system (Fig. 2) with the cylinder axis and the z-axis coincident and the dipole at $\rho = b$, $\phi = 0$, the magnetic field at the surface of the cylinder ($\rho = a$) can be shown to be

$$H_\phi(\rho = a) = \frac{M\omega}{4\pi^2} \sum_{m=0}^{\infty} \epsilon_m \left\{ \int_C \frac{\alpha}{\beta a} \left[\frac{H_m'(\beta b)}{H_m(\beta a)} - \frac{m^2}{\beta^2 ab} \frac{H_m(\beta b)}{H_m'(\beta a)} \right] e^{i\alpha z} d\alpha \right\} \cos m\phi \quad (1)$$

$$H_z(\rho = a) = \frac{iM\omega}{2\pi^2 b} \sum_{m=1}^{\infty} m \cdot \left\{ \int_C \frac{1}{\beta a} \frac{H_m(\beta b)}{H_m'(\beta a)} e^{i\alpha z} d\alpha \right\} \sin m\phi \quad (2)$$

where M is the dipole moment, the time dependence is taken to be $e^{-i\omega t}$, $k = \omega\sqrt{\mu\epsilon}$, $\beta = \sqrt{k^2 - \alpha^2}$, $\epsilon_m = 1$ for $m = 0$ and $\epsilon_m = 2$ for $m \neq 1$, and $H_m(x)$ is the Hankel function of the first kind of argument x. The contour of integration is shown in Fig. 3. The surface current densities on the cylinder are then

$$K_z = H_\phi(\rho = a) \qquad K_\phi = -H_z(\rho = a) \quad (3)$$

and the currents on the cylinder are completely determined.

* Received by the PGAP, February 9, 1961; revised manuscript received, July 22, 1961. The research reported in this article has been sponsored by the ONR, Electronic Branch, under contract Nonr 228(16), NR 372-561.

† Dept. of Elec. Engrg., University of Southern California, Los Angeles, Calif.

[1] P. S. Carter, "Antenna arrays around cylinders," PROC. IRE, vol. 31, pp. 671–693; December, 1943.

[2] W. S. Lucke, "Electric dipoles in the presence of elliptic and circular cylinders," *J. Appl. Phys.*, vol. 22, pp. 14–19; January, 1951.

[3] E. B. Moullin, "Radio Aerials," Oxford University Press, Oxford, Eng., ch. IV; 1949.

[4] W. R. LePage, R. F. Harrington, and R. F. Schlect, "A Study of Directional Antenna Systems for Radio D/F Purposes," Inst. of Industrial Res., Dept. of Elec. Engrg., Syracuse Univ., Syracuse, N. Y., September 15, 1949.

[5] R. F. Harrington and W. R. LePage, "Directional antenna arrays of elements circularly disposed about a cylindrical reflector," PROC. IRE, vol. 40, pp. 83–86; January, 1952.

[6] J. E. Walsh, "Radiation patterns of arrays on a reflecting cylinder," PROC. IRE, vol. 39, pp. 1074–1081; September, 1951.

[7] J. R. Wait, "Electromagnetic Radiation from Cylindrical Structures," Pergamon Press, New York, N. Y., pp. 76–87; 1959.

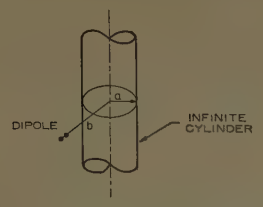

Fig. 1—Infinite cylinder with radial electric dipole.

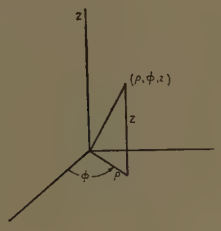

Fig. 2—Coordinate system.

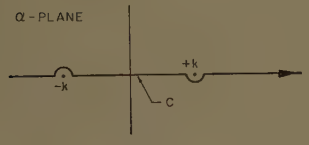

Fig. 3—Contour of integration in α-plane.

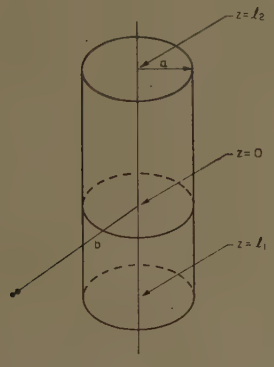

Fig. 4—Finite cylinder with radial electric dipole.

III. The Finite Cylinder Excited by a Radial Dipole; The Method of Approximation

The determination of the far-zone field of a finite cylinder, *i.e.*, a cylinder not of infinite extent in the $\pm z$ direction, when excited by a radial electric dipole presents greater difficulty than the case of the infinite cylinder. The case of the finite cylinder involves complicated boundary conditions in that the tangential electric field must vanish over parts of two different coordinate surfaces. As shown in Fig. 4, the tangential field must vanish at $\rho=a$ for $-l_1<z<l_2$ and also at $z=l_2$, $-l_1$ for $\rho<a$. These boundary conditions introduce considerable complications and usually the solutions to problems of this sort involve some method of approximation.

Frequently the far-zone field expressions for the infinite cylinder are used as an approximation to the case of a finite cylinder. However, this procedure yields poor results, especially near the axis of the cylinder where the expression for the θ-component of the electric field of the infinite cylinder actually diverges.[1] Also the minor lobes which are found to exist for the finite cylinder of small radius are not predicted in this approximation.

In order to carry out a more accurate approximate solution to this problem the current distribution on the finite cylinder will be taken identical to the distribution on the infinite cylinder. The procedure is as follows: First the current distribution on the infinite cylinder is determined. Then the portions of the infinite cylinder above $z=l_2$ and below $z=-l_1$ are removed with the assumption that the current on the remaining portion of the cylinder is unchanged. The far-zone field of this unchanged portion of the current between $-l_1$ and l_2 is then computed and added to the field of the dipole to obtain an expression for the total far-zone field of the configuration. A similar approximation has been used by Meixner[8] in treating the radiation from a slit in a finite plane.

This approximation neglects higher order current modes generated by the discontinuities at the ends of the cylinder and also the reflected waves from the ends. Since the cylinder is assumed to be long, the neglect of the higher order modes is not serious since these in general attenuate rapidly away from the cylinder ends and do not contribute appreciably to the radiation. It would seem that the neglect of the reflected current wave from either end of the cylinder is more serious. However, it can be shown by evaluating (1) and (2) by the saddle point method for large kz that the currents on the infinite cylinder attenuate with z at large distances from the origin. Specifically it can be shown that the following two proportionalities hold:

$$K_z \propto \frac{e^{ikz}}{\ln\left(\frac{kz}{k^2a^2}\right)} \tag{4}$$

$$K_\phi \propto \frac{\sin\phi e^{ikz}}{(kz)^2} \tag{5}$$

where K_z and K_ϕ are the z- and ϕ-components of the surface current densities on the cylinder. The amplitude of a current wave reflected from either end of the finite cylinder must be of the same order of magnitude as the amplitude of a wave which impinges on that end. Since the impinging waves are given by (4) and (5) it is evident that the reflected wave will be small as long as the ends of the cylinder lie at large kz. The major portion of the radiation will then be produced by the unperturbed current of the infinite cylinder in the region $-l_1\leq z\leq l_2$ and the preceding approximation is justified for the conditions $kl_2\gg 1$ and $kl_1\gg 1$.

[8] J. Meixner, "The radiation pattern and induced current in a circular antenna with an annular slit," IRE Trans. on Antennas and Propagation, vol. AP-4, pp. 408–411; July, 1956.

IV. The Finite Cylinder Excited by a Radial Dipole; The Approximate Solution

The far-zone radiation field of the radial dipole near a finite cylinder will now be derived using the approximation discussed in Section III. The physical configuration and coordinate systems are shown in Fig. 5. The field is to be calculated at an arbitrary point P. The field due to the current on the cylinder will first be

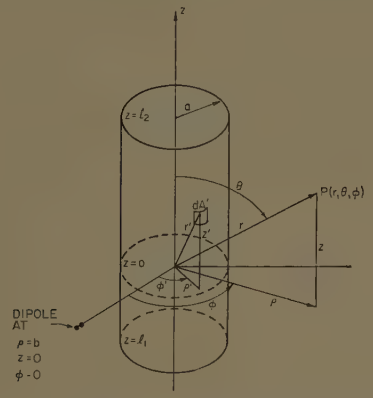

Fig. 5—Finite cylinder with dipole and coordinate systems.

derived and the dipole field will be added to give the total field. The far-zone ϕ-component of electric field due to a surface current density $\boldsymbol{K}$ flowing over an area A is[9]

$$E_\phi = \frac{i\omega\mu_0 e^{ikr}}{4\pi r}\int_A \boldsymbol{K}(\rho', \phi', z')\cdot \mathbf{e}_{\phi e}^{ik\mathbf{r}'\cdot\mathbf{e}_r} dA' \tag{6}$$

where $\mathbf{e}_\phi$ and $\mathbf{e}_r$ are unit vectors in the ϕ- and r-directions, respectively. For the cylinder of Fig. 5, (6) becomes

$$E_\phi = -\frac{i\omega\mu_0 a e^{ikr}}{4\pi r}\int_{-l_1}^{l_2}\int_0^{2\pi} H_z(\rho' = a)\cos(\phi' - \phi) \times e^{-ik[a\cos(\phi'-\phi)\sin\theta + z'\cos\theta]} d\phi' dz'. \tag{7}$$

Substituting (2) into (7), one obtains

$$E_\phi = \frac{M\omega^2\mu_0 a e^{ikr}}{8\pi^3 rb}\sum_{m=1}^{\infty} m\int_0^{2\pi}\sin m\phi'\cos(\phi' - \phi)\cdot e^{-ika\cos(\phi'-\phi)\sin\theta} d\phi' \times \int_{-l_1}^{l_2}\int_C \frac{H_m(\beta b)}{\beta a H_m'(\beta a)} e^{i\alpha z'} e^{-ikz'\cos\theta} d\alpha dz'. \tag{8}$$

It can be shown that the first integral in (8) is given by

$$\int_0^{2\pi}\sin m\phi'\cos(\phi' - \phi)e^{-ika\cos(\phi'-\phi)\sin\theta} d\phi' = 2\pi(-i)^{m-1}\sin m\phi J_m'(ka\sin\theta). \tag{9}$$

Thus (8) becomes

$$E_\phi = \frac{M\omega^2\mu_0 a e^{ikr}}{4\pi^2 rb}\sum_{m=1}^{\infty} m(-i)^{m-1}\sin m\phi J_m'(ka\sin\theta) \times \int_{-l_1}^{l_2}\int_C \frac{H_m(\beta b)}{\beta a H_m'(\beta a)} e^{i\alpha z'} e^{-ikz'\cos\theta} d\alpha dz'. \tag{10}$$

Performing the integration over z' in (10) and making the substitution $\alpha = kh$, one obtains

$$E_\phi = \frac{Mke^{ikr}}{4\pi^2\epsilon_0 rb}\sum_{m=1}^{\infty} m(-i)^m \sin m\phi J_m'(ka\sin\theta) \times \int_{C'} \frac{H_m(kb\sqrt{1-h^2})\left[e^{ikl_2(h-\cos\theta)} - e^{-ikl_1(h-\cos\theta)}\right]}{H_m'(ka\sqrt{1-h^2})\sqrt{1-h^2}(h-\cos\theta)} dh \tag{11}$$

where the contour C' is shown in Fig. 6. Adding the contribution to E_ϕ from the dipole alone, the total ϕ-

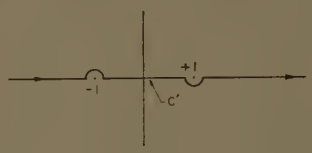

Fig. 6—Contour of integration in h-plane.

component of the far-zone field becomes

$$E_{\phi\text{tot}} = -\frac{Mke^{ikr}}{4\pi\epsilon_0 r}\left[k\sin\phi e^{-ikb\sin\theta\cos\phi} - \frac{1}{\pi b}\sum_{m=1}^{\infty} m(-i)^m \sin m\phi J_m'(ka\sin\theta)\Psi_m\right] \tag{12}$$

where

$$\Psi_m = \int_{C'} \frac{H_m(kb\sqrt{1-h^2})\left[e^{ikl_2(h-\cos\theta)} - e^{-ikl_1(h-\cos\theta)}\right]}{H_m'(ka\sqrt{1-h^2})\sqrt{1-h^2}(h-\cos\theta)} dh. \tag{13}$$

The far-zone θ-component of electric field due to a surface current density $\boldsymbol{K}$ is[9]

$$E_\theta = \frac{i\omega\mu_0 e^{ikr}}{4\pi r}\int_A \boldsymbol{K}\cdot\mathbf{e}_\theta e^{-ik\mathbf{r}'\cdot\mathbf{e}_r} dA' \tag{14}$$

where $\mathbf{e}_\theta$ and $\mathbf{e}_r$ are unit vectors in the θ- and r-directions, respectively. For the cylinder of Fig. 5, (14) becomes

$$E_\theta = -\frac{i\omega\mu_0 a e^{ikr}}{4\pi r}\int_{-l_1}^{l_2}\int_0^{2\pi} H_\phi(\rho' = a)\sin\theta \cdot e^{-ik[a\cos(\phi'-\phi)\sin\theta + z'\cos\theta]} d\phi' dz'. \tag{15}$$

Substituting (1) into (15), one obtains

$$E_\theta = -\frac{iM\omega^2\mu_0 a\sin\theta e^{ikr}}{16\pi^3 r}\sum_{m=0}^{\infty}\epsilon_m\int_0^{2\pi}\cos m\phi' \cdot e^{-ika\cos(\phi'-\phi)\sin\theta} d\phi' \times \int_{-l_1}^{l_2}\int_C \frac{\alpha}{\beta a}\left[\frac{H_m'(\beta b)}{H_m(\beta a)} - \frac{m^2}{\beta^2 ab}\frac{H_m(\beta b)}{H_m'(\beta a)}\right] \cdot e^{i\alpha z'} e^{-ikz'\cos\theta} d\alpha dz'. \tag{16}$$

[9] S. Silver, "Microwave Antenna Theory and Design," McGraw-Hill Book Co., Inc., New York, N. Y., pp. 87–90; 1949.

It can be shown that the first integral in (16) is given by

$$\int_0^{2\pi} \cos m\phi' e^{-ika\cos(\phi'-\phi)\sin\theta} d\phi' = 2\pi(-i)^m \cos m\phi J_m(ka\sin\theta). \quad (17)$$

Thus (16) becomes

$$E_\theta = -\frac{iM\omega^2\mu_0 a\sin\theta e^{ikr}}{8\pi^2 r}\sum_{m=0}^{\infty}\epsilon_m(-i)^m\cos m\phi J_m(ka\sin\theta) \times\int_{-l_1}^{l_2}\int_C \frac{\alpha}{\beta a}\left[\frac{H_m'(\beta b)}{H_m(\beta a)}-\frac{m^2}{\beta^2 ab}\frac{H_m(\beta b)}{H_m'(\beta a)}\right] \cdot e^{i\alpha z'}e^{-ikz'\cos\theta}\,d\alpha dz'. \quad (18)$$

Performing the integration over z' and letting $\alpha = kh$, one obtains

$$E_\theta = -\frac{Mk^2\sin\theta e^{ikr}}{8\pi^2\epsilon_0 r}\sum_{m=0}^{\infty}\epsilon_m(-i)^m\cos m\phi J_m(ka\sin\theta)\gamma_m \quad (19)$$

where

$$\gamma_m = \int_{C'}\frac{h}{\sqrt{1-h^2}}\left[\frac{H_m'(kb\sqrt{1-h^2})}{H_m(ka\sqrt{1-h^2})}-\frac{m^2}{k^2ab(1-h^2)}\frac{H_m(kb\sqrt{1-h^2})}{H_m'(ka\sqrt{1-h^2})}\right] \times\frac{\left[e^{ikl_2(h-\cos\theta)}-e^{-ikl_1(h-\cos\theta)}\right]}{(h-\cos\theta)}\,dh. \quad (20)$$

Adding the contribution to E_θ due to the dipole alone, the total θ-component of the far-zone electric field becomes

$$E_{\theta\text{tot}} = \frac{Mk^2e^{ikr}}{4\pi\epsilon_0 r}\left[\cos\theta\cos\phi e^{-ikb\sin\theta\cos\phi} - \frac{\sin\theta}{2\pi}\sum_{m=0}^{\infty}\epsilon_m(-i)^m\cos m\phi J_m(ka\sin\theta)\gamma_m\right]. \quad (21)$$

It should be noted that in deriving (12) and (21), fields due to currents which flow on the end plates of the cylinder have been neglected. This is a good approximation for long cylinders because the currents which flow on the end plates are of the same order of magnitude as the currents which flow near the ends of the cylinder on the cylindrical surface itself. These currents were shown to be small so that the neglect of radiation from the end plates is justified.

Eqs. (12) and (21) are the desired expressions for the two components of the far-zone field. They are, however, not simple to evaluate because of the integrals, Ψ_m and γ_m, appearing in each expression. If results exact to the order of the approximation of Section III are desired, an electronic computer can be used to evaluate Ψ_m and γ_m. On the other hand, since kl_1 and kl_2 are large, the saddle point method can be applied; this method of attack is followed in the next sections.

V. Evaluation of γ_0

In many cases of interest the quantity ka is small enough so that only the first term in the series of (12) and (21) is significant. This will be assumed to be true throughout the remainder of this paper. Thus (21) becomes

$$E_{\theta\text{tot}} = \frac{Mk^2e^{ikr}}{4\pi\epsilon_0 r}\left[\cos\theta\cos\phi e^{-ikb\sin\theta\cos\phi} - \frac{\sin\theta J_0(ka\sin\theta)\gamma_0}{2\pi}\right]. \quad (22)$$

It will also be assumed that kb is small, *i.e.*, the dipole is near the cylinder. From (20), γ_0 is given by

$$\gamma_0 = \int_{C'}\frac{h}{\sqrt{1-h^2}}\frac{H_0'(kb\sqrt{1-h^2})}{H_0(ka\sqrt{1-h^2})} \cdot\frac{\left[e^{ikl_2(h-\cos\theta)}-e^{-ikl_1(h-\cos\theta)}\right]}{(h-\cos\theta)}\,dh \quad (23)$$

where the contour C' is shown in Fig. 6. Eq. (23) may be divided into two parts:

$$\gamma_0 = \gamma_{01} + \gamma_{02} \quad (24)$$

where

$$\gamma_{01} = \int_{C'}\frac{h}{\sqrt{1-h^2}}\frac{H_0'(kb\sqrt{1-h^2})e^{ikl_2(h-\cos\theta)}}{H_0(ka\sqrt{1-h^2})(h-\cos\theta)}\,dh \quad (25)$$

and

$$\gamma_{02} = -\int_{C'}\frac{h}{\sqrt{1-h^2}}\frac{H_0'(kb\sqrt{1-h^2})e^{-ikl_1(h-\cos\theta)}}{H_0(ka\sqrt{1-h^2})(h-\cos\theta)}\,dh. \quad (26)$$

It must be noted that although the integrand of (23) has no pole at $h=\cos\theta$, the integrands of (25) and (26) do because of the separation of the original integral γ_0. For this reason it is necessary to use the same contour, passing either above or below the point $h=\cos\theta$, in the evaluation of γ_{01} and γ_{02} although this was not essential in evaluating γ_0. The contour passing below $h=\cos\theta$ will be used; γ_{01} will be considered first.

Since the exponential factor in the integrand of (25) vanishes on a circle of large radius in the first and second quadrants of the h-plane, the contour C' may be deformed into the contours C_1 and C_2 as shown in Fig. 7 if the point $h=\cos\theta$ does not coincide with the branch point $h=+1$. Branch cuts extend from the points

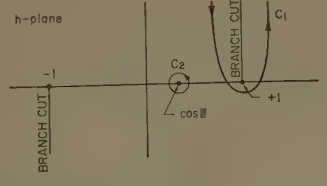

Fig. 7—Deformation of C' into C_1 and C_2.

$h=\pm 1$ so that, as shown in Fig. 7, the integral along C' may be considered as an integral around the pole at $h=\cos\theta$ and along both sides of one of the branch cuts. The contribution from C_2 may be evaluated at once from the theory of residues to yield

$$\gamma_{01}=\frac{2\pi i\cos\theta}{\sin\theta}\frac{H_0'(kb\sin\theta)}{H_0(ka\sin\theta)}+\int_{C_1}\frac{h}{\sqrt{1-h^2}}\frac{H_0'(kb\sqrt{1-h^2})e^{ikl_2(h-\cos\theta)}}{H_0(ka\sqrt{1-h^2})(h-\cos\theta)}dh. \quad (27)$$

In order to evaluate the integral along C_1 by the saddle point method, the integral of (27) is written

$$\int_{C_1}\frac{H_0'(kb\sqrt{1-h^2})e^{kl_2f(h)}}{H_0(ka\sqrt{1-h^2})}dh \quad (28)$$

where

$$f(h)=ih-i\cos\theta+\frac{1}{kl_2}[\ln h-\tfrac{1}{2}\ln(1-h^2)-\ln(h-\cos\theta)]. \quad (29)$$

The condition for a saddle point is

$$f'(h_0)=i+\frac{1}{kl_2}\left[\frac{1}{h_0}+\frac{1}{2(1-h_0)}-\frac{1}{2(1+h_0)}-\frac{1}{(h_0-\cos\theta)}\right]=0 \quad (30)$$

where h_0 is the location of a saddle point. Eq. (30) may be written

$$h_0(1-h_0^2)(h_0-\cos\theta)=-\frac{(h_0^3-\cos\theta)}{ikl_2}. \quad (31)$$

Eq. (31) is a quartic and is difficult to solve in general. However, since kl_2 is large, (31) exhibits that the roots lie near $h=0$, ± 1 and $\cos\theta$. The only saddle points which could possibly be crossed by the contour C_1 are those near $h=+1$ and $h=\cos\theta$. Near these points (30) simplifies, since the terms $1/h_0$ and $1/2(1+h_0)$ are much smaller than $1/2(1-h_0)$ and $1/(h_0-\cos\theta)$ so that in solving for these saddle points, (30) becomes

$$\frac{1}{ikl_2}\left[\frac{1}{2(1-h_0)}-\frac{1}{(h_0-\cos\theta)}\right]+1=0. \quad (32)$$

Solving (32), one obtains

$$h_0=\frac{1}{2}\left[1+\cos\theta+\frac{3}{2ikl_2}\pm\sqrt{(1-\cos\theta)^2-\frac{1}{ikl_2}(1-\cos\theta)-\frac{9}{4(kl_2)^2}}\right]. \quad (33)$$

In the region in which $\cos\theta$ is not near $+1$, the inequality

$$(1-\cos\theta)^2\gg\frac{(1-\cos\theta)}{kl_2} \quad (34)$$

holds so that the binomial expansion of the radical in (33) may be employed to yield

$$h_0\approx 1+\frac{1}{2ikl_2},\qquad \cos\theta+\frac{1}{ikl_2} \quad (35)$$

where the first two terms of the expansion have been retained. The saddle point at $h_0\approx\cos\theta+1/ikl_2$ does not lie in the path of integration so that the only contribution to the integral over C_1 comes from the saddle point $h_0\approx 1+1/2ikl_2$. The general formula for a saddle point integration is[10]

$$\int_C\phi(h)e^{\alpha f(h)}dh=\phi(h_0)e^{\alpha f(h_0)}\sqrt{\frac{2\pi}{\alpha e^{i\pi}f''(h_0)}} \quad (36)$$

where α is a large quantity, h_0 is the location of the saddle point, $f''(h)$ is the second derivative of $f(h)$ and $\phi(h)$ is a slowly varying function near the saddle point. From (28), $\phi(h)$ is slowly varying for the assumed condition of small ka and kb. From (30)

$$f''(h)=\frac{1}{kl_2}\left[-\frac{1}{h^2}+\frac{1}{2(1-h)^2}+\frac{1}{2(1+h)^2}+\frac{1}{(h-\cos\theta)^2}\right]. \quad (37)$$

Using (37) and (34), neglecting higher-order terms, one obtains $f''(h_0)\approx -2kl_2$ so that (36) yields for the integral (28)

$$\int_{C_1}\frac{H_0'(kb\sqrt{1-h^2})}{H_0(ka\sqrt{1-h^2})}e^{kl_2f(h)}dh=\frac{H_0'\left(kb\sqrt{\frac{i}{kl_2}}\right)e^{ikl_2(1-\cos\theta)}\sqrt{e\pi}}{H_0\left(ka\sqrt{\frac{i}{kl_2}}\right)(1-\cos\theta)\sqrt{\frac{i}{kl_2}}\,kl_2} \quad (38)$$

where higher-order terms in $f(h_0)$ and $\sqrt{1-h_0^2}$ have been neglected. Since kl_2 is large the arguments of the Hankel functions in (38) are small so that the small argument approximation,

$$\frac{H_0'\left(kb\sqrt{\frac{i}{kl_2}}\right)}{H_0\left(ka\sqrt{\frac{i}{kl_2}}\right)}\approx\frac{1}{kb\sqrt{\frac{i}{kl_2}}\left[\ln\left(\frac{\gamma}{2}ka\sqrt{\frac{i}{kl_2}}\right)-\frac{i\pi}{2}\right]} \quad (39)$$

[10] P. M. Morse and H. Feshbach, "Methods of Theoretical Physics," McGraw-Hill Book Co., Inc., New York, N. Y., p. 441; 1953.

can be used where $\gamma = 1.781$. Using (39), (38) becomes

$$\int_{C_4} \frac{H_0'(kb\sqrt{1-h^2})}{H_0(ka\sqrt{1-h^2})} e^{kl_2 f(h)}\, dh = \frac{i\sqrt{e\pi}\, e^{ikl_2(1-\cos\theta)}}{kb(1-\cos\theta)\left[\ln\left(\frac{ka}{2}\sqrt{\frac{i}{kl_2}}\right) - \frac{i\pi}{2}\right]} = \frac{2i\sqrt{e\pi}\, e^{ikl_2(1-\cos\theta)}}{kb(1-\cos\theta)\left[\ln\left(\frac{4kl_2}{\gamma^2k^2a^2}\right) + \frac{i\pi}{2}\right]}. \quad (40)$$

Substituting this expression into (27), one obtains

$$\gamma_{01} = \frac{2\pi i \cos\theta H_0'(kb\sin\theta)}{\sin\theta H_0(ka\sin\theta)} + \frac{2i\sqrt{e\pi}\, e^{ikl_2(1-\cos\theta)}}{kb(1-\cos\theta)\left[\ln\left(\frac{4kl_2}{\gamma^2k^2a^2}\right) + \frac{i\pi}{2}\right]}. \quad (41)$$

In order to evaluate γ_{02}, it is observed that the contour C' can be deformed into the contour C_3 (Fig. 8) since the exponential term in the integrand disappears on a circle of large radius in the third and fourth quadrants. Again, the saddle point method is applied and it is found that for the condition

$$(1+\cos\theta)^2 \gg \frac{(1+\cos\theta)}{kl_1}, \quad (42)$$

the only contributing saddle point lies at

$$h_0 = -1 - \frac{1}{2ikl_1}. \quad (43)$$

Using (36) to evaluate γ_{02}, one obtains

$$\gamma_{02} = -\frac{2i\sqrt{e\pi}\, e^{ikl_1(1+\cos\theta)}}{kb(1+\cos\theta)\left[\ln\left(\frac{4kl_1}{\gamma^2k^2a^2}\right) + \frac{i\pi}{2}\right]}. \quad (44)$$

Adding (41) and (44) yields

$$\gamma_0 = \gamma_{01} + \gamma_{02} = \frac{2\pi i \cos\theta H_0'(kb\sin\theta)}{\sin\theta H_0(ka\sin\theta)} + \frac{2i\sqrt{e\pi}\, e^{ikl_2(1-\cos\theta)}}{kb(1-\cos\theta)\left[\ln\left(\frac{4kl_2}{\gamma^2k^2a^2}\right) + \frac{i\pi}{2}\right]} - \frac{2i\sqrt{e\pi}\, e^{ikl_1(1+\cos\theta)}}{kb(1+\cos\theta)\left[\ln\left(\frac{4kl_1}{\gamma^2k^2a^2}\right) + \frac{i\pi}{2}\right]}. \quad (45)$$

This expression is valid in the region expressed by the inequalities (34) and (42) which are the mathematical statements of the conditions that $\cos\theta$ not be near ± 1.

The region designated by (34) and (42) takes in the greatest portion of the range of $\cos\theta$ if kl_1 and kl_2 are large. In addition, there are two other regions in which γ_0 may be evaluated. One occurs when $\cos\theta$ is near unity for which

$$\frac{9}{4(kl_2)^2} \gg \left|(1-\cos\theta)^2 - \frac{(1-\cos\theta)}{ikl_2}\right| \quad (46)$$

since under this condition the radical of (33) can again be approximated by the first two terms of the binomial expansion to yield

$$h_0 \approx \frac{2+\cos\theta}{3}, \qquad \frac{1+2\cos\theta}{3} + \frac{3}{2ikl_2}. \quad (47)$$

One of the saddle points now lies on the real axis between the two poles at $h = \cos\theta$, 1 and the other lies approximately below it as shown in Fig. 9. The correct

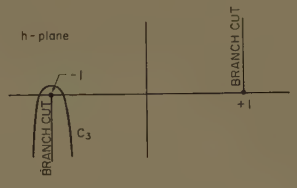

Fig. 8—Deformation of C' into C_3.

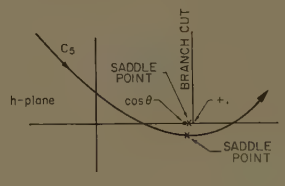

Fig. 9—Contour for $\cos\theta$ near unity.

direction of traversal of the second saddle point proves to be parallel to the real axis so it is clear that for the condition (46) the correct contour in evaluating γ_{01} is C_5; only one saddle point is crossed when $\cos\theta$ is very near unity. Since $\cos\theta \approx 1$, the saddle point under consideration is given by

$$h_0 \approx 1 + \frac{3}{2ikl_2}. \quad (48)$$

Computing the saddle point contribution with $f''(h_0) \approx -2kl_2/3$, one obtains

$$\gamma_{01} = \frac{e^{3/2}\sqrt{\pi}\, 2i}{\sqrt{3}\sqrt{\frac{-3}{ikl_2}}} \frac{H_0'\left(kb\sqrt{\frac{-3}{ikl_2}}\right)}{H_0\left(ka\sqrt{\frac{-3}{ikl_2}}\right)}. \quad (49)$$

Using the small argument approximation for the Hankel functions, one obtains

$$\gamma_{01} = \frac{-4e^{3/2}\sqrt{\pi}\, kl_2}{3\sqrt{3}\, kb\left[\ln\left(\frac{4kl_2}{3\gamma^2k^2a^2}\right) + \frac{i\pi}{2}\right]}. \quad (50)$$

Eq. (44) for γ_{02} is still valid in this region but will be neglected since it is an order of magnitude smaller than γ_{01}. Thus

$$\gamma_0 = \frac{-4e^{3/2}\sqrt{\pi}\, kl_2}{3\sqrt{3}\, kb\left[\ln\left(\frac{4kl_2}{3\gamma^2k^2a^2}\right)+\frac{i\pi}{2}\right]} \tag{51}$$

in the region given by (46). Similarly in the region in which

$$\frac{9}{4(kl_1)^2} \gg \left|(1+\cos\theta)^2 - \frac{(1+\cos\theta)}{ikl_1}\right| \tag{52}$$

γ_0 is given by

$$\gamma_0 = \frac{4e^{3/2}\sqrt{\pi}\, kl_1}{3\sqrt{3}\, kb\left[\ln\left(\frac{4kl_1}{3\gamma^2k^2a^2}\right)+\frac{i\pi}{2}\right]}. \tag{53}$$

Thus the integral γ_0 has been evaluated in three separate regions comprising most of the range of $\cos\theta$. $E_{\theta\,\mathrm{tot}}$ is obtained by substituting the value of γ_0 appropriate to the value of $\cos\theta$ into (22).

VI. Evaluation of Ψ_1

For the case of small ka, (12) for the ϕ-component of the electric field becomes

$$E_{\phi\,\mathrm{tot}} = -\frac{Mke^{ikr}}{4\pi\epsilon_0 r}\left[k\sin\phi e^{-ikb\sin\theta\cos\phi} + \frac{i\sin\phi J_1'(ka\sin\theta)\Psi_1}{\pi b}\right] \tag{54}$$

where

$$\Psi_1 = \int_{C'} \frac{H_1(kb\sqrt{1-h^2})\left[e^{ikl_2(h-\cos\theta)} - e^{-ikl_1(h-\cos\theta)}\right]}{H_1'(ka\sqrt{1-h^2})\sqrt{1-h^2}\,(h-\cos\theta)}\,dh. \tag{55}$$

This integral can be evaluated in the same manner as was used to evaluate γ_0. The integral is again split into two parts

$$\Psi_1 = \Psi_{11} + \Psi_{12} \tag{56}$$

where

$$\Psi_{11} = \int_{C'} \frac{H_1(kb\sqrt{1-h^2})e^{ikl_2(h-\cos\theta)}}{H_1'(ka\sqrt{1-h^2})\sqrt{1-h^2}(h-\cos\theta)}\,dh \tag{57}$$

$$\Psi_{12} = -\int_{C'} \frac{H_1(kb\sqrt{1-h^2})e^{-ikl_1(h-\cos\theta)}}{H_1'(ka\sqrt{1-h^2})\sqrt{1-h^2}(h-\cos\theta)}\,dh. \tag{58}$$

In the region defined by (34) and (42), Ψ_{11} is composed of an integration around the pole at $h=\cos\theta$ and an integration along both sides of a branch cut as in Fig. 7. The integration around the pole can be evaluated by the theory of residues so that

$$\Psi_{11} = \frac{2\pi i H_1(kb\sin\theta)}{H_1'(ka\sin\theta)\sin\theta} + \int_{C_1} \frac{H_1(kb\sqrt{1-h^2})e^{ikl_2(h-\cos\theta)}}{H_1'(ka\sqrt{1-h^2})\sqrt{1-h^2}(h-\cos\theta)}\,dh. \tag{59}$$

The integral of (59) can be evaluated by the saddle point method. However, it will be neglected since upon evaluation it proves to contain the factor $1/kl_2$ and is therefore an order of magnitude smaller than the first term on the right of (59). Similarly, Ψ_{12} is negligible so that

$$\Psi_1 = \frac{2\pi i H_1(kb\sin\theta)}{H_1'(ka\sin\theta)\sin\theta} \tag{60}$$

in the region defined by (34) and (42).

In the regions defined by (46) and (52), the saddle point method yields the result

$$\Psi_1 = -\frac{(ka)^2 ie\sqrt{2\pi}}{kb}. \tag{61}$$

Thus, to this order of approximation, Ψ_1 is independent of kl_1 and kl_2. $E_{\phi\,\mathrm{tot}}$ is obtained by substituting the value of Ψ_1 appropriate to the value of $\cos\theta$ into (54). In the range defined by (34) and (42) it can be shown that the expression for $E_{\phi\,\mathrm{tot}}$ is identical to that of the infinite cylinder.

VII. Comparison with Experiment

For the case of the dipole contiguous to the cylinder, $ka=kb$, measurements of $E_{\theta\,\mathrm{tot}}$ and $E_{\phi\,\mathrm{tot}}$ can be easily made since the radiating system is then closely approximated by a short radial stub antenna on a cylinder. In comparing such measurements to the theory presented here, the quantities kl_1 and kl_2 must be known very accurately because of the exponential manner in which they appear in the expression for γ_0 [see (45)].

The experimental configuration used is shown in Fig. 10, in which the exciting dipole is simulated by an extension of the inner conductor of a coaxial line. This is a good approximation to the theoretically analyzed problem if the radius of the outer conductor of the coaxial line and the length of the stub are small compared to a wavelength. These conditions were satisfied since the diameter of the coaxial line was approximately $\lambda/100$ and the length of the stub was approximately $0.12\,\lambda$.

The measurements were carried out on a cylinder which had $kl_1=5.236$, $kl_2=10.472$ and $ka=0.6317$. Even though the conditions $kl_1 \gg 1$ and $kl_2 \gg 1$ are not well satisfied, the experimental and theoretical radiation patterns agree sufficiently to warrant comparison.

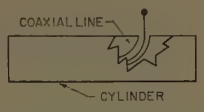

Fig. 10—Experimental simulation of dipole near cylinder.

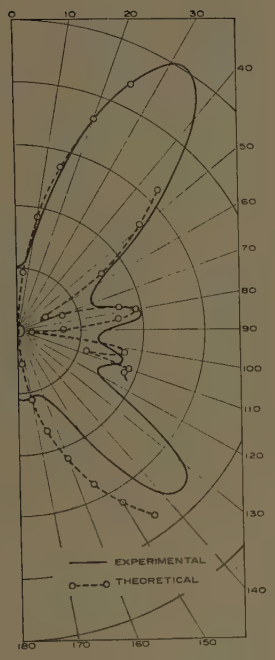

Fig. 11—$E_{\theta\,\mathrm{tot}}$ vs θ for $\phi=90°$, $kl_1=5.236$, $kl_2=10.472$, $ka=0.6317$.

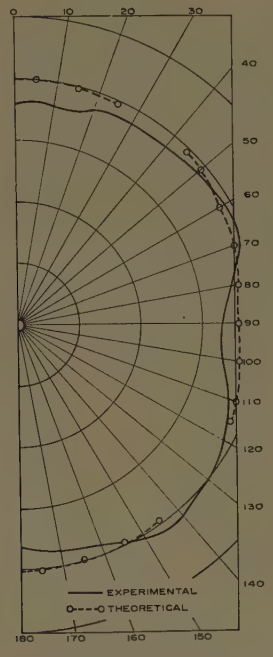

Fig. 12—$E_{\phi\,\mathrm{tot}}$ vs θ for $\phi=90°$, $kl_1=5.236$, $kl_2=10.472$, $ka=0.6317$.

Theoretical and experimental patterns of $E_{\theta\,\mathrm{tot}}$ for $\phi=90°$ are shown in Fig. 11. The theoretical results are shown in the regions given by (34), (42), (46) and (52) which in this case were taken to be $0°\leq\theta\leq25°$, $45°\leq\theta\leq115°$, $144°\leq\theta\leq180°$. For angles not contained in these regions, the expressions derived previously do not apply although they may be used there as an approximation. Since kl_2 is twice kl_1, it is expected that (45) will be most accurate in the region where the term containing kl_1 is least in magnitude since the condition $kl_2\gg1$ is better satisfied than $kl_1\gg1$. Similarly, (51) is expected to yield more accurate results than (53) for this case. Since the term involving kl_1 is least in the range $0°\leq\theta\leq90°$, this portion of the radiation pattern is expected to be the most accurate. Accordingly, since only the relative amplitude of $E_{\theta\,\mathrm{tot}}$ was measured, it was adjusted to give the best agreement with the theoretical pattern in the range $0°\leq\theta\leq90°$. It is seen from Fig. 11 that the agreement is quite good in this range except near the minima. This is probably due to the fact that the higher-order terms in the series of (21) have been neglected and also because the radiation from the end plates of the cylinder has not been included. The agreement in the region $90°\leq\theta\leq180°$ is not as good and is attributed to the fact that $E_{\theta\,\mathrm{tot}}$ is more dependent on kl_1 through (45) and (53). It is expected that the agreement would improve for larger kl_1.

The general characteristics of the $E_{\theta\,\mathrm{tot}}$ pattern at $\phi=90°$ for other cylinder lengths are quite similar to those of Fig. 11. In general, there are two large lobes near the axis of the cylinder which grow larger and lie closer to the axis as the cylinder length increases. In addition, there are a number of smaller lobes which are produced by the second and third term of (45). The magnitudes of these minor lobes decrease and their number increases as the cylinder length increases.

The theoretical and experimental patterns of $E_{\phi\,\mathrm{tot}}$ are shown in Fig. 12. The experimental amplitude was adjusted for a good fit and it is seen to agree quite well throughout the whole region.

VIII. Conclusions

An approximate expression for the far-zone field of a radial dipole near a finite cylinder has been derived. The results can be used to predict the radiation from such a configuration under the condition $kl_2\gg1$ and $kl_1\gg1$. In the case of small ka and kb, the expressions for the field components are evaluated in three regions of the variable θ, and assume different forms in each.

IX. Acknowledgment

The author wishes to express his appreciation to Prof. C. H. Papas for many helpful discussions and C. Yeh for assistance in the experimental portion of this investigation.

ELF Waves in the Presence of Exponential Ionospheric Conductivity Profiles*

JANIS GALEJS†, MEMBER, IRE

Summary—Based on the theory of Nicolet and Aikin, the profile of ionospheric conductivity exhibits a nearly exponential variation with altitude through the *D* layer and the lower edge of the *E* layer. Propagation of ELF waves below this exponential layer is considered after calculating the surface impedance Z_s at an altitude h where the local refractive index n does not necessarily satisfy $|n|\gg 1$. The propagation constant is determined by an iteration process. This model of an isotropic nonhomogeneous ionosphere is a closer approximation of the propagation geometry than are earlier models, where Z_s was defined at h where $|n|\gg 1$. The present model accounts simultaneously for ELF attenuation rates as measured by Jean, and earth-ionosphere cavity resonances as observed by Balser and Wagner.

I. Introduction

A MODEL of a sharply-bounded homogeneous ionosphere is simplest to analyze and is commonly used in investigations of VLF and ELF propagation.[1–3] However, this model does not account for measured attenuation characteristics. The ionospheric model of exponentially increasing conductivity has been introduced in mode theory by Shmoys[4] in an analysis that is based on the differential equations for horizontally-polarized waves. An ionosphere which consists of several homogeneous layers has been described by Wait.[5–7] It has been possible to construct two-layer models that provide reasonable agreement with measured attenuation rates over a limited frequency range.[8] The exponential model of Wait,[5–7,9] where the refractive index n changes exponentially after a sudden transition from $n=1$ in the atmosphere to $n\gg 1$ at the lower ionosphere edge, accounted for measured attenuation rates[10] only by using more gradual changes of the refractive index than those obtained from ionospheric profile data.[11] In an alternate approach,[12] the attenuation rates calculated with a homogeneous ionosphere may be brought into agreement with measured data[10] by defining a frequency-dependent ionosphere altitude, which is tailored to fit measured attenuation rates.

For frequencies below 100 cps, the attenuation of the ELF waves is low, and it has been possible to observe earth-ionosphere cavity resonances.[13,14] The frequencies of resonance which are calculated with neglected cavity losses[6,15] are higher than the measured ones. The use of a model of a homogeneous sharply-bounded ionosphere having a frequency-dependent height and conductivity may give the correct resonant frequencies.[16] However, the losses introduced by this model are so high that the calculated cavity Q is approximately 2.5 times lower than the measured one.[17]

In this paper, an attempt will be made to incorporate an ionospheric model in the mode analysis which is based on established ionosphere characteristics and which provides a reasonable agreement with measured attenuation rates of ELF signals[8,10] and with ELF resonance measurements.[13,14]

An examination of ionospheric profiles (Section II) indicates that the exponential model provides a good representation of the conductivity σ through the lower edge of the D and E regions. As long as the ELF signals do not penetrate beyond the E region (this does not take into consideration possible whistler-mode signals) the exponential increase of σ that is assumed in this

* Received by the PGAP, May 1, 1961; revised manuscript received, June 26, 1961. This research has been supported by the Office of Naval Research.

† Applied Research Lab., Sylvania Electronic Systems Div., Sylvania Electric Products, Inc., Waltham, Mass.

[1] K. G. Budden, "The propagation of very low frequency radio waves to great distances," *Phil. Mag.*, vol. 44, pp. 504–513; May, 1953.

[2] W. O. Schumann, "Über die Ausbreitung sehr langer elektrischer Wellen und der Blitzentladung um die Erde," *Z. angew. Phys.*, vol. 4, pp. 474–480; December, 1952.

[3] J. R. Wait, "The mode theory of VLF ionosphere propagation for finite ground conductivity," PROC. IRE, vol. 45, pp. 760–767; June, 1957.

[4] J. Shmoys, "Long-range propagation of low-frequency radio waves between the earth and ionosphere," PROC. IRE, vol. 44, pp. 163–170; February, 1956.

[5] J. R. Wait, "Extension to mode theory of VLF propagation," *J. Geophys. Res.*, vol. 63, pp. 125–135; March, 1958.

[6] J. R. Wait, "Terrestrial propagation of VLF radio waves—a theoretical investigation," *J. Res. NBS*, vol. 64D, pp. 153–203; March–April, 1960.

[7] J. R. Wait, "Mode theory and the propagation of ELF radio waves," *J. Res. NBS*, vol. 64D, pp. 387–404; July–August, 1960.

[8] A. G. Jean, Jr., A. C. Murphy, J. R. Wait, and D. F. Wasmundt, "Propagation attenuation rates at ELF," *J. Res. NBS*, vol. 65D; September–October, 1961.

[9] J. R. Wait, "On the propagation of ELF radio waves and the influence of a nonhomogeneous ionosphere," *J. Geophys. Res.*, vol. 65, pp. 597–600; February, 1960.

[10] F. W. Chapman and R. C. Macario, "Propagation of audio frequency radio waves to great distances," *Nature*, vol. 177, pp. 930–933; May, 1956.

[11] Wait[7,9] shows that an ionosphere where the refractive index n increases by $e=2.72$ in $\Delta h\approx 30$ km gives measured nighttime attenuation rates.[10] However, it will be shown later that measured D- and E-region profiles exhibit $\Delta h\approx 4$ to 6.5 km which would result in too low an attenuation when applying Wait's theory.

[12] E. T. Pierce, "The propagation of radio waves of frequency less than 1 kc," PROC. IRE, vol. 48, pp. 329–331; March, 1960.

[13] M. Balser and C. A. Wagner, "Observations of earth-ionosphere cavity resonances," *Nature*, vol. 188, pp. 638–641; November, 1960.

[14] M. Balser and C. A. Wagner, "Measurements of the spectrum of radio noise from 50 to 100 cycles per second," *J. Res. NBS*, vol. 64D, pp. 415–418; July–August, 1960.

[15] W. O. Schumann, "Elektrische Eigenschwingungen des Hohlraumes Erde-Luft-Ionosphäre," *Z. angew. Phys.*, vol. 9, pp. 373–378; August, 1957.

[16] H. R. Raemer, "On the extremely low frequency spectrum of earth-ionosphere cavity response to electric storms," *J. Geophys. Res.*, vol. 66, pp. 1580–1583; May, 1961.

[17] This follows from the ionosphere parameters used by Raemer[16] and from the Q_i expression listed in Section VI of this paper.

model above the E layer would not affect the propagation below the ionosphere. The exponential variation of σ continues well below the height h where the refractive index $|n| = |\sqrt{1+\sigma/(i\omega\epsilon_0)}| \gg 1$. The solutions of the differential equations that characterize propagation in the ionosphere and that are discussed in Section III should be valid also for values of n which do not satisfy the above inequality. The effects of the ionosphere on the propagation below it are considered by a surface impedance at a height where the conduction currents may be smaller than the displacement currents ($\sigma < \omega\epsilon$). This surface impedance depends on the propagation constant of the waves below the ionosphere. The roots of the modal equation and the attenuation constant are obtained by an iteration procedure as shown in Section IV. The atmospheric conductivity due to cosmic-ray ionization exhibits an exponential profile between the ground and the lower edge of the ionosphere, which was also shown in Section II. The additional attenuation due to these losses is calculated as in waveguide filled with slightly lossy dielectric (Section V). The earth-ionosphere cavity resonance frequencies and Q factors are discussed in Section VI.

The effects of the earth's magnetic field have not been considered in this paper. The presence of the magnetic field tends to increase the attenuation of the fields in particular if the longitudinal component of the gyrofrequency is large as compared with the collision frequency of electrons at the reflecting layer of the ionosphere.[7] This may affect the accuracy of the calculated nighttime data.

II. Ionospheric Model

Ionospheric conductivity,

$$\sigma_i = \frac{\epsilon_0 \omega_p^2}{\nu} = 2.83 \times 10^{-2} \frac{N_e}{\nu}, \qquad (1)$$

(ω_p = plasma frequency, ν = collision frequency, N_e = number of electrons per cm^3) may be computed based on collision-frequency data of Nicolet[18] and Moler,[19] daytime electron density by Nicolet and Aikin[20] and Waynick[21] and nighttime electron density of the ARDC standard ionosphere,[22] as indicated in Table I. According to the theory of Phelps, the ionospheric conductivity figures should be approximately 30 per cent lower than those indicated by (1) for low frequencies.[23] In the presence of the earth's magnetic field the conductivity becomes anisotropic.[24] Calculations of the refractive index n which consider electrons or electrons plus ions and ignore the collision effects show that the presence of ions tends to make the refractive index n more isotropic, particularly at frequencies below 1 kc.[25] The same conclusion applies when collision effects are taken into account, and the refractive index n, which is computed for altitudes $h < 70$ km, differs insignificantly from the refractive index n which is based on electrons in the absence of the earth's magnetic field.[26] Eq. (1) will be used in the present conductivity calculations, although it may be subject later to modifications. The conductivity of the atmosphere due to cosmic-ray ionization has been calculated and experimentally verified.[27] The resulting conductivity figures have been depicted by the solid curves in Fig. 1. The conductivity profiles may be approximated by

$$\sigma = \sigma_0 \exp[\beta(z - z_0)]. \qquad (2)$$

For daytime, $\sigma_0 = 10^{-6}$ mho/m, $z_0 = 70$ km, $\beta^{-1} = 3.25$ km, which gives the line indicated by dots and dashes in Fig. 1. For nighttime, $\sigma_0 = 10^{-6}$ mho/m, $z_0 = 95.5$ km, $\beta^{-1} = 2$ km, which gives the dashed line of Fig. 1. The cosmic-ray ionization curve is approximated by letting $\sigma_0 = 10^{-10}$ mho/m, $z_0 = 50$ km, $\beta^{-1} = 7.25$ km in (2).

The refractive index $n = \sqrt{1+\sigma/(i\omega\epsilon_0)}$ will exhibit an

TABLE I

Calculation of Ionospheric Conductivity

h km	ν sec^{-1}	Day		Night	
		N_e cm^{-3}	σ_i mho/m	N_e cm^{-3}	σ_i mho/m
50	1.4(8)	1.1(1)	2.1(−9)		
55	7.6(7)	5(1)	1.8(−8)		
60	4.2(7)	1(2)	6.4(−8)		
65	2.2(7)	2(2)	2.5(−7)		
70	1.1(7)	3.5(2)	8.9(−7)		
75	4.9(6)	9.1(2)	5.1(−6)		
80	2.2(6)	1.5(3)	1.9(−5)		
85	1.2(6)	2(3)	4.7(−5)		
90	5(5)	1(4)	5.6(−4)	1	5.6(−8)
95	2.5(5)	4(4)	5.1(−3)		
100	7.9(4)	1(5)	2.8(−2)	3(1)	1.1(−5)
110	2(4)	1.6(5)	2.3(−1)	2(3)	2.8(−3)
120	5(3)			6.5(3)	3.7(−2)
130				1(4)	

$a(n) = a \times 10^n$ $\qquad \sigma_i = 2.83 \times 10^{-2} N_e/\nu$

[18] M. Nicolet, "The collision frequency of electrons in the terrestrial atmosphere," *Phys. of Fluids*, vol. 2, pp. 95–99; March–April, 1959.

[19] W. F. Moler, "VLF propagation effects of a D-region layer produced by cosmic rays," *J. Geophys. Res.*, vol. 65, pp. 1459–1468; May, 1960.

[20] M. Nicolet and A. C. Aikin, "The formation of the D-region of the ionosphere," *J. Geophys. Res.*, vol. 65, Fig. 4, pp. 1469–1483; May, 1960.

[21] A. H. Waynick, "Present state of knowledge concerning the lower ionosphere," Proc. IRE, pp. 741–749; June, 1957.

[22] USAF, "Handbook of Geophysics," Air Res. and Dev. Command, AF Cambridge Res. Ctr., Macmillan Co., New York, N. Y.; 1960.

[23] A. V. Phelps, "Propagation constants for electromagnetic waves in weakly ionized dry air," *J. Appl. Phys.*, vol. 31, pp. 1723–1729; October, 1960.

[24] J. A. Ratcliffe, "Physics of the upper atmosphere," Academic Press, New York, N. Y., sect. 9.3, pp. 392–397; 1960.

[25] C. O. Hines, "Heavy-ion effects in audio-frequency radio propagation," *J. Atmos. Terr. Phys.*, vol. 11, no. 1, pp. 36–42; 1957. See Fig. 1.

[26] Private Communication by Dr. R. Row, Appl. Res. Lab., Sylvania Electronic Systems, Waltham, Mass.

[27] R. E. Bourdeau, E. C. Whipple, Jr., and J. F. Clark, "Analytic and experimental conductivity between the stratosphere and the ionosphere," *J. Geophys. Res.*, vol. 64, pp. 1363–1370; October, 1959.

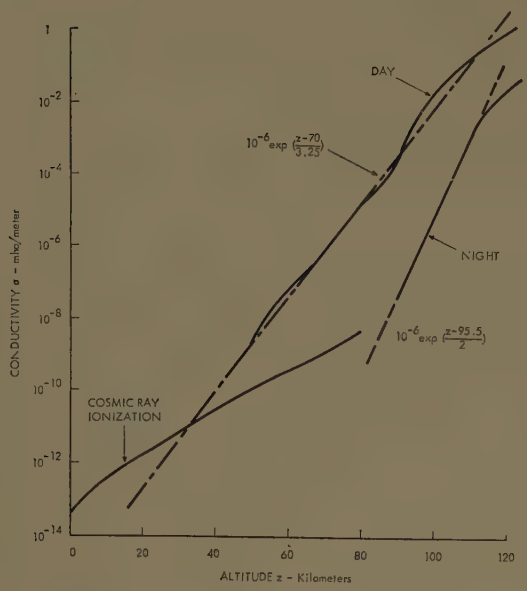

Fig. 1—Conductivity profiles and their exponential approximations.

exponential variation for $|n| \gg 1$ with half the slope of the σ curves. Excluding the cosmic-ray ionization of Fig. 1 from consideration, n will increase by a factor of e in a vertical increment $\Delta h = 4$ to 6.5 km as was indicated.[11] Similar Δh figures are also obtained from other D-layer profiles.[28]

III. Surface Impedance of the Ionosphere

It follows from Maxwell's equations and from the equation of continuity that the vertical electric-field component E_z in a vertically-stratified lossy medium of complex dielectric constant

$$\epsilon = \epsilon_0 + \frac{\sigma}{i\omega} \tag{3}$$

is of the form

$$E_z = Z(z)e^{-ik_0 x + i\omega t}, \tag{4}$$

where x is the direction of propagation of the vertically-polarized fields below the dielectric medium. $Z(z)$ satisfies the differential equation

$$Z'' + \frac{\epsilon'}{\epsilon} Z' + \left[\mu_0 \epsilon \omega^2 + \frac{\epsilon''}{\epsilon} - \left(\frac{\epsilon'}{\epsilon}\right)^2 - k_0^2\right] Z = 0. \tag{5}$$

With E_z determined, the field components E_x and H_y follow from Maxwell's equations as

$$E_x = \frac{1}{ik_0\epsilon} \frac{\partial}{\partial z} (\epsilon E_z) \tag{6}$$

and

$$H_y = -\frac{\omega\epsilon}{k_0} E_z. \tag{7}$$

The field components (4), (6), and (7) will be examined, first, for an exponentially increasing refractive index $n = \sqrt{\epsilon/\epsilon_0}$, and second, for exponentially increasing conductivity σ.

For exponential variation of the refractive index n, the variable in (5) is changed from z to

$$u = n^2 = \frac{\epsilon}{\epsilon_0} = -iBe^{\beta z}. \tag{8}$$

This results in

$$Z''(u) + \frac{2}{u} Z'(u) + \frac{k^2 u - k_0^2}{u^2 \beta^2} Z(u) = 0, \tag{9}$$

where

$$k = \omega\sqrt{\mu_0\epsilon_0}. \tag{10}$$

A solution of (9) is[29,30]

$$Z(u) = An^{-1}K_\nu(iw) \tag{11}$$

where K_ν is the modified Bessel function of the second kind of order

$$\nu = \sqrt{1 + 4\frac{k_0^2}{\beta^2}}, \tag{12}$$

and where

$$w = 2kn/\beta. \tag{13}$$

For $|w| \ll 1$ the first-order approximation of the K_ν function shows that

$$E_z \sim n^{-2}. \tag{14}$$

Substitution of (11) in (4) and in (6) and (7) results in

$$\frac{E_x}{H_y} = \sqrt{\frac{\mu_0}{\epsilon_0}} \frac{1}{n} \frac{K_{\nu-1}(iw)}{K_\nu(iw)} - \frac{\beta}{2i\omega\epsilon_0} \frac{1-\nu}{n^2}. \tag{15}$$

For $w \ll 1$ (15) may be approximated by

$$\frac{E_x}{H_y} = \sqrt{\frac{\mu_0}{\epsilon_0}} \frac{k}{\beta}\left[2i\left(0.116 - \ln\frac{2k|n|}{\beta}\right) + \frac{\pi}{2} + \frac{k_0^2}{ik^2n^2}\right]. \tag{16}$$

[28] J. A. Fejer, "The interaction of pulsed radio waves in the ionosphere," *J. Atmos. Terr. Phys.*, vol. 7, no. 6, pp. 322–332; 1955. See Fig. 4.

[29] E. Jahnke and F. Emde, "Tables of Functions," Dover Publications, New York, N. Y., p. 146; 1945.

[30] E. Kamke, "Differential Gleichungen," Chelsea Publishing Co., New York, N. Y., p. 440; 1948.

The ratio (15) or (16) which represents the surface impedance of the exponential ionosphere differs from (13.15) of Wait[6] by the last term, which becomes small for $|n|^2$ large.

For an exponential variation of the ionospheric conductivity σ the variable in (5) is changed from z to

$$v = \frac{\sigma}{\omega\epsilon_0} = Be^{\beta z}. \tag{17}$$

This results in

$$Z''(v) + F(v)Z'(v) + G(v)Z(v) = H(v)Z(v), \tag{18}$$

where

$$F(v) = \frac{1}{v} + \frac{1}{i+v} \tag{19}$$

$$G(v) = \frac{1}{v^2}\left[\frac{v}{i+v} - \left(\frac{v}{i+v}\right)^2\right] \tag{20}$$

$$H(v) = \frac{k_0^2 - k^2(1-iv)}{\beta^2 v^2}. \tag{21}$$

The solution of the homogeneous equation ($H(v)=0$) will be considered first. Its power-series solution may be summed into

$$\phi_1 = \frac{i}{i+v}, \tag{22}$$

which satisfies the homogeneous equation for any value of v. For $|H(v)| \ll |G(v)|$, ϕ_1 represents an approximate solution of the nonhomogeneous equation. This inequality is satisfied for

$$\frac{|k_0^2 - k^2|}{\beta^2} < \frac{k^2}{\beta^2} \ll v \ll \frac{\beta}{k} \tag{23}$$

A second solution of the homogeneous equation is obtained as[31]

$$\phi_2 = \phi_1 \int \phi_1^{-2} \exp\left[-\int F(v)dv\right]dv$$

$$= \frac{\ln v - iv}{i+v}. \tag{24}$$

The solution of the nonhomogeneous equation is given by[31]

$$Z(v) = A\left[\phi_1 + \phi_2 \int \frac{\phi_1 HZ}{W}dv - \phi_1 \int \frac{\phi_2 HZ}{W}dv\right], \tag{25}$$

where

$$W = \phi_1\phi_2' - \phi_1'\phi_2. \tag{26}$$

[31] *Ibid.*, p. 117.

As long as ϕ_1 represents an approximate solution of the nonhomogeneous equation, it may be used for Z under the integral signs. This results in

$$Z(v) = \frac{A}{i+v}\left\{-\frac{k_0^2}{\beta^2}[(i+v)\ln(i+v) + iI]\right.$$

$$-\frac{k^2 - k_0^2}{\beta^2}\left[\frac{i}{2}(\ln v)^2 + v\ln v\right]$$

$$\left.+\frac{k^2}{\beta^2}(i+v) + k(\ln v - iv) + i(1-L)\right\}, \tag{27}$$

where

$$I = \int \frac{\ln(i+v)}{v}dv, \tag{28}$$

and where K and L are arbitrary constants. Substitution of (27) in (6) and (7) shows that

$$\frac{E_x}{H_y} = \sqrt{\frac{\mu_0}{\epsilon_0}}\frac{k}{\beta}\left\{-i\ln v\right.$$

$$\left.-i\frac{k_0^2}{k^2}[\ln(i+v) - \ln v] + \frac{K\beta}{k^2}\right\}. \tag{29}$$

The models of exponential refractive index n and conductivity σ differ insignificantly for $|n| \gg 1$. Hence, the constant K of (29) may be determined by equating (15) and (29) for $|n| \gg 1$. With

$$\ln(i+v) - \ln v = -\sum_{m=1}^{\infty}\frac{(iv)^{-m}}{m} \approx \frac{i}{v}, \tag{30}$$

this results in

$$\frac{K\beta}{k^2} = i\ln v + \frac{\beta}{k\sqrt{v}}\frac{\sqrt{i}\,K_{v-1}(iw)}{K_v(iw)}. \tag{31}$$

With $|w| = 2k|n|/\beta \ll 1$, an expansion of the Bessel functions gives

$$\frac{K\beta}{k^2} = 2i\left(0.116 - \ln\frac{2k}{\beta}\right) + \frac{\pi}{2}.$$

For $|w| > 1$, K of (31) is not constant and the solution (27) of the differential equation (18) becomes inaccurate. The function ϕ_1 of (22) is no longer an approximate solution of the nonhomogeneous equation. A solution more accurate for $|w| > 1$ may be obtained by substituting Z of (11) in the integrals of (25). These calculations will not be carried out since the present development emphasizes the case of $|w| = 2k/\beta(1+v^2)^{1/4} \ll 1$. For $v < 1$

$$\ln(i+v) = \frac{i\pi}{2} - \sum_{m=1}^{\infty}\frac{(iv)^m}{m}. \tag{33}$$

Substitution of (32) and (33) in (29) gives

$$\frac{E_x}{H_y} = \sqrt{\frac{\mu_0}{\epsilon_0}}\,\frac{k}{\beta}\left[2i\left(0.116 - \ln\frac{2k}{\beta}\right) + \frac{\pi}{2}\,\frac{k^2 + {k_0}^2}{k^2} + i\,\frac{{k_0}^2 - k^2}{k^2}\ln v + i\,\frac{{k_0}^2}{k^2}\sum_{m=1}^{\infty}\frac{(iv)^m}{m}\right]. \quad (34)$$

The validity of (29) and (32) are restricted by the inequality (23). For $\beta = 1/3.25$ km^{-1} and $f = 1000$ cps, v should satisfy $0.46 \times 10^{-2} \ll v \ll 15$.

IV. Propagation in a Lossless Atmosphere

The propagation constant in the space between earth and ionosphere is

$$\gamma_0 = ik_0 = ikS = \alpha + i\beta. \quad (35)$$

For a homogeneous ionosphere of refractive index n_i that is much smaller than the refractive index of the ground n_g, the first-order perturbation solution of the modal equation gives for the zero-order mode,[32]

$$S = \sqrt{1 - \frac{i}{khn_i}\sqrt{1 - \left(\frac{S}{n_i}\right)^2}}, \quad (36)$$

where h is the height of the ionosphere. In the presence of a nonhomogeneous ionosphere, one may define an equivalent homogeneous ionosphere of refractive index n_i^e which exhibits the same surface impedance Z_i as the nonhomogeneous ionosphere. It follows from the discussion of the Appendix that for $n_i^e \gg 1$,

$$(n_i^e)^2 \approx \frac{\mu_0}{\epsilon_0 {Z_i}^2} - S^2. \quad (37)$$

Examination of (29) and (34) shows that Z_i is also dependent on $S = k_0/k$. In order to adapt an iteration procedure for solving (36), it is rewritten as

$$S_n = \sqrt{1 - \frac{i}{khn_i^e(S_{n-1})}\sqrt{1 - \left[\frac{S_{n-1}}{n_i^e(S_{n-1})}\right]^2}}. \quad (38)$$

The subscripts of S designate the successive iterations and the procedure may be started with $S_0 = 1$ in the right-hand side of (38).

The attenuation constants α_i are calculated from (29), (34), (35), (37), and (38), and are shown in Figs. 2 and 3 for an ionosphere which is sharply bounded at an altitude h where $v = \sigma(h)/(\omega\epsilon_0) = \text{const}$. The curves in Fig. 2 show that significant contributions to α are made by ionospheric layers where $v < 1$. The curve indicated by dots and dashes is obtained using (15) and (16) for the surface impedance with $n^2 = 10/i$. It differs from the $v = 10$ curve at the higher frequencies where the inequality (23) is not satisfied strictly.

[32] This can be verified by substituting $R_g = 1$ and $R_i \approx \exp(-2Z_i/\eta)$ in (54) where Z_i is given by (58).

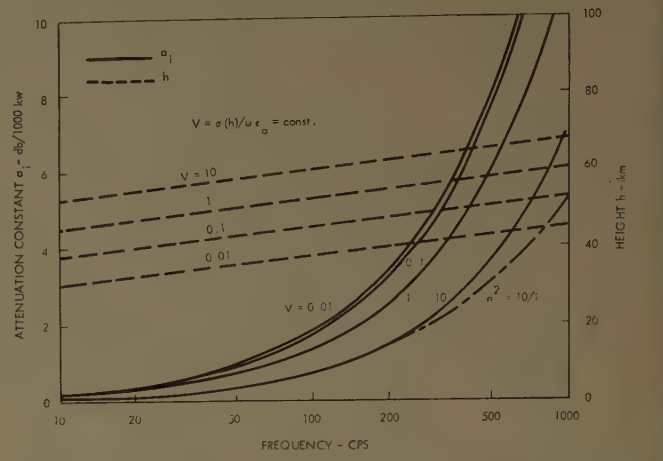

Fig. 2—Daytime attenuation constants for an ionosphere of exponential conductivity profile which is sharply bounded at h where $V = \sigma(h)/\omega\epsilon_0 = \text{const}$.

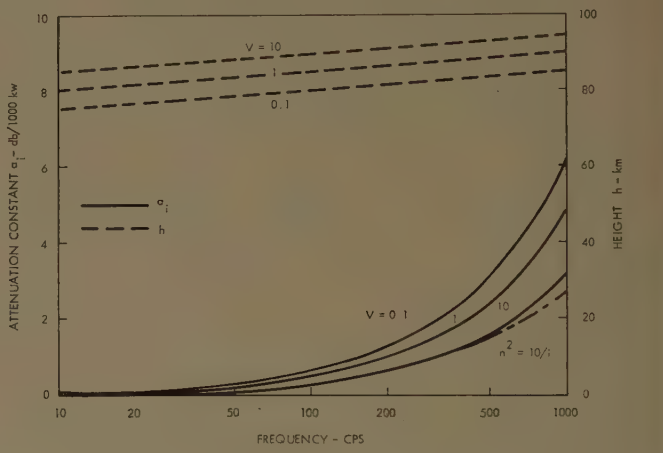

Fig. 3—Nighttime attenuation constants for an ionosphere of exponential conductivity profile which is sharply bounded at h where $V = \sigma(h)/\omega\epsilon_0 = \text{const}$.

The roots of the modal equation S and the attenuation constant α_i are shown in Figs. 4 and 5 for an ionosphere which is sharply bounded at $h = \text{const}$. According to Fig. 1, the heights h may be selected as $h_{\text{day}} \approx 50$ km and $h_{\text{night}} = 90$ km.

V. Losses Due to Cosmic-Ray Ionization

The cosmic-ray ionization[27] will also contribute to the attenuation of ELF radio waves. The atmospheric conductivity that is due to cosmic-ray ionization can be approximated by an exponential curve of a gradient which is smaller than that for ionospheric conductivity. The over-all conductivity profile in Fig. 1 can be represented by two exponential curves, which suggests a two-region problem for a proper analysis of wave propagation. Provided that the atmospheric losses are small, the ionospheric fields can be assumed to be locally unperturbed by the former losses. The additional attenuation of the fields due to atmospheric losses (attenuation constant α_a) can be calculated as in a waveguide filled with a lossy dielectric. Such calculations will result in a correction of the attenuation constant $\alpha = -k\ \text{Im}\ S$,

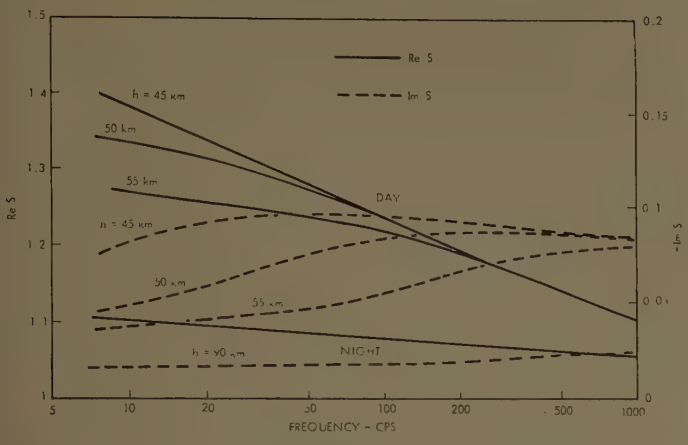

Fig. 4—Roots of the modal equation S for an ionosphere of exponential conductivity profile which is sharply bounded at h= const.

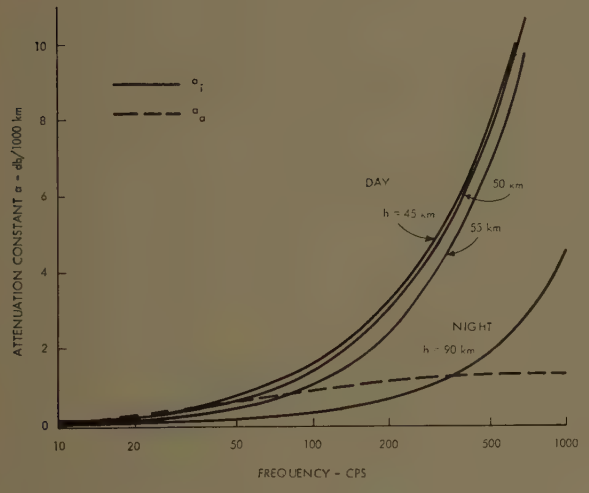

Fig. 5—Attenuation constants for ionosphere of exponential conductivity profile which is sharply bounded at h-const.

but will not change the phase constant $\beta = k$ Re S. This limitation of the approximate procedure will become noticeable under conditions where the atmospheric losses α_a are comparable to the ionospheric losses α_i computed from Sections III and IV. It follows from waveguide considerations that

$$\alpha_a = \frac{\int_a^{a+h} \sigma \boldsymbol{E}\cdot\boldsymbol{E}^* dr}{2\,\mathrm{Re}\int_a^{a+h} (\boldsymbol{E}\times\boldsymbol{H}^*)\cdot 1_\theta dr} \approx \frac{\int_a^{a+h} \sigma \left| E_r \right|^2 dr}{-2\,\mathrm{Re}\int_a^{a+h} E_r H_\phi^* dr} \tag{39}$$

for $E_\theta \ll E_r$. The variation of E_r with altitude may be determined from

$$(\sigma + i\omega\epsilon_0)E_r = \text{const.} \tag{40}$$

H_ϕ is related to $\boldsymbol{E}$ by

$$H_\phi = \frac{1}{i\omega\mu r}\left[\frac{\partial E_r}{\partial\theta} - \frac{\partial(rE_\theta)}{\partial r}\right] \approx \frac{1}{i\omega\mu a}\frac{\partial E_r}{\partial\theta}. \tag{41}$$

As long as the atmospheric losses do not affect the θ dependence of E_r,

$$E_r \sim (\sin\theta)^{-0.5}\exp(-i\omega a\theta S/c),$$

where S is determined for a lossless atmosphere. For $c\cot\nu/(2i\omega aS) \ll 1$, this gives

$$\frac{H_\phi}{E_r} \approx -S\sqrt{\frac{\epsilon_0}{\mu_0}}, \tag{42}$$

which can be also obtained from (13) and (15) of Wait.[7] Substituting (40) and (42) in (39) and evaluating the integrals after changing the variable of integration from r to σ gives

$$\alpha_a = \frac{\omega}{2c}\frac{1}{\mathrm{Re}\,S}\frac{\tan^{-1}\left[\dfrac{\sigma(h)}{\omega\epsilon_0}\right]}{\ln\dfrac{\sigma(h)}{\sigma(0)} - \dfrac{1}{2}\ln\left\{1+\left[\dfrac{\sigma(h)}{\omega\epsilon_0}\right]^2\right\}}, \tag{43}$$

where $\sigma(z) = \sigma\big|_{r=a+z}$ and where $\sigma(0)/(\omega\epsilon_0) \ll 1$. For $\sigma(h)/(\omega\epsilon_0) \ll 1$, (43) simplifies to

$$\alpha_a \approx \frac{\sigma(h)}{2\,\mathrm{Re}\,S}\sqrt{\frac{\mu_0}{\epsilon_0}}\left[\ln\frac{\sigma(h)}{\sigma(0)}\right]^{-1}, \tag{44}$$

which also may be obtained by substituting E_r = const. instead of (40) in (39). For $\sigma(h)/(\omega\epsilon_0) \gg 1$, (43) is approximated by

$$\alpha_a \approx \frac{\pi\omega}{4c\,\mathrm{Re}\,S}\left[-\ln\frac{\sigma(0)}{\omega\epsilon_0}\right]^{-1}. \tag{45}$$

When it is assumed that H_ϕ and E_r are related by

$$\frac{H_\phi}{E_r} = \sqrt{\frac{\sigma + i\omega\epsilon_0}{i\omega\mu_0}}, \tag{46}$$

the evaluation of (39) shows α_a to be the same as in (44) and (45), but with Re $S = 1$. For intermediate values of $\sigma(h)$ there are insignificant numerical differences between the α_a figures based on (42) or (46), provided Re $S = 1$.

In daytime, $\sigma(50) \approx 10^{-10}$ mho/m and $\alpha_a < 0.025$ db/1000 km. The calculated nighttime α_a figures are shown in Fig. 5 for $\sigma(90) \approx 10^{-8}$ mho/m. The attenuation constant $\alpha_a < 1.4$ db for $f < 1000$ cps, but $\alpha_a > \alpha_i$ at the lower frequencies. The roots of the modal equation S, which have been determined with $\alpha_i = 0$ and have been used in α_a calculations, are inaccurate for $\alpha_a > \alpha_i$. The nighttime atmospheric losses appear to be comparable with ionospheric losses for $f < 400$ cps and a more exact treatment of the propagation problem may be desirable for these frequencies.

VI. Earth-Ionospheric Cavity Resonances

The frequencies of the earth-ionosphere cavity resonances may be calculated for a uniform cavity from[6,15]

$$|\, n(n+1) - (kaS)^2 \,| = \min, \tag{47}$$

where a is the earth radius. The roots of the modal equation S which have been computed for a lossless atmosphere in Section IV should be corrected for the atmospheric losses discussed in Section V. With S different during daytime and nighttime, one may use the average value of S in (47). As pointed out in Section V, the calculated nighttime S figures are inaccurate; hence, a more exact determination of the day and night effects will not be made at present. The resonance frequencies calculated from (47) using daytime S and the average of day and night S figures are summarized in Table II.

TABLE II

Resonance Frequencies of the Spherical Shell between the Earth and Ionosphere

Resonance Frequency f_n in cps	n	1	2	3	4	5
	Lossless cavity[6,15]	10.6	18.3	25.9	33.5	41.1
	Daytime with $h=50$ km	8.3	14.2	20	25.8	31.7
	Average data of day with $h=50$ km and of night with $h=90$ km	9.1	15.5	22	28.1	34.5
	Daytime with $\sigma(h)/\omega\epsilon_0=1$ =const.	8	13.8	19.5	25.4	31.3
	Measurements[13]	8	14.1	20.3	26.4	32.5

The ionospheric and atmospheric losses are accounted for by defining separate Q factors in analogy with microwave cavities.[33] The Q factor due to ionospheric losses is

$$\frac{1}{Q_i} = \frac{c}{\omega} \frac{\left.\dfrac{\operatorname{Re} n_i}{|n_i|^2}\right|_{\text{day}} + \left.\dfrac{\operatorname{Re} n_i}{|n_i|^2}\right|_{\text{night}}}{h_{\text{day}} + h_{\text{night}}}. \tag{48}$$

This factor considers only the losses due to the fundamental cavity modes. The losses due to the higher modes which are excited by the height discontinuity between day and night hemispheres can be shown to be negligible.[34] The Q factor due to atmospheric losses is

$$\frac{1}{Q_a} = \frac{2\int \sigma \boldsymbol{E}\cdot\boldsymbol{E}^* d\tau}{\omega\epsilon_0 \int \boldsymbol{E}\cdot\boldsymbol{E}^* d\tau + \omega\mu_0 \int \boldsymbol{H}\cdot\boldsymbol{H}^* d\tau}. \tag{49}$$

[33] J. C. Slater, "Microwave Electronics," D. Van Nostrand, Co., Inc., New York, N. Y.; 1950.

[34] J. Galejs, "Resonator Type Oscillations Between the Earth and Ionosphere and Effects of Ionosphere Height and Conductivity Changes Between Day and Night Hemispheres," Appl. Res. Lab., Sylvania Electronic Systems, Waltham, Mass., Internal. Mem.; July 5, 1960.

Evaluating the integrals, using the same approximations as in Section V, gives

$$\frac{1}{Q_a} = 2\left\{\tan^{-1}\frac{\sigma(h)}{\omega\epsilon_0}\bigg|_{\text{day}} + \tan^{-1}\frac{\sigma(h)}{\omega\epsilon_0}\bigg|_{\text{night}}\right\} \Bigg/ \left\{(1+SS^*)\left[\ln\frac{\sigma(h)}{\sigma(0)} - \frac{1}{2}\ln\left(1+\frac{\sigma^2(h)}{(\omega\epsilon_0)^2}\right)\right]_{\text{day}} + (1+SS^*)\left[\ln\frac{\sigma(h)}{\sigma(0)} - \frac{1}{2}\ln\left(1+\frac{\sigma^2(h)}{(\omega\epsilon_0)^2}\right)\right]_{\text{night}}\right\}. \tag{50}$$

Numerical values for the combined Q factor

$$\frac{1}{Q} = \frac{1}{Q_a} + \frac{1}{Q_i} \tag{51}$$

are shown in Table III for daytime and combined daytime and nighttime data.

TABLE III

Q Factors of Earth-Ionosphere Cavity Resonances

Q—Factors	f in cps	10	30	100
	Day with $h=50$ km, night with $h=90$ km +cosmic-ray ionization.	6.2	6.3	7.1
	Daytime only with $h=50$ km.	7.6	5.8	5.1
	Day with $h=45$ km, night with $h=90$ km +cosmic-ray ionization.	5.3	5.7	6.6
	Daytime only with $h=45$ km.	4.3	4	4.3
	Day and night with $\sigma(h)/\omega\epsilon_0=1=$const. +cosmic-ray ionization.	5.3	6.7	8.6
	Daytime only with $\sigma(h)/\omega\epsilon_0=1=$const.	3.8	4.8	5.7
	Measurements[13,14]	4	6	

VII. Discussion

A. The Conductivity Profiles

The conductivity profiles calculated in Section II and depicted in Fig. 1 have been based on the set of electron-density and collision-frequency data shown in Table I without considering effects of ions and of the earth's magnetic field. Although the data are believed to represent average daytime conditions, it may be desirable to consider the variation of electron density with geomagnetic latitude and solar zenith angle and to construct the daytime conductivity profile with a suitable averaging process. There are indications that the gradual taper of the electron density through the lower edge of the D layer continues below the height $h=50$ km, indicated in Fig. 1, down to approximately 45 km (see Fig. 5 of Moler[19]). The daytime data for $h=45$ km in Figs. 4 and 5 are included to show the effect of such an extension of the D layer. The nighttime electron density of Table I is based on a single curve.[22] More detailed data are desirable in particular for heights below $h=90$ km. The cosmic-ray ionization[27] appears to provide a continuation of the nighttime ionosphere. The exact shape of the

nighttime conductivity curve below $h=90$ km is important for frequencies below 400 cps, where a significant part of the attenuation is due to losses in the lower layers according to Section V.

B. The Attenuation Rates

The attenuation constants α are plotted in Figs. 2 and 3 for an ionosphere which is sharply bounded at a hypothetical frequency-dependent altitude h, where $v=\sigma(h)/\omega\epsilon_0=$const. The increments in α, between the plotted curves, characterize the amounts of losses introduced by various ionosphere layers. It is seen that layers where $v<1$ give significant contributions to the attenuation constant and must be considered if they appear in the ionospheric model. It is not permissible to neglect ionospheric layers of refractive index $|n^2|<|n_0^2|\gg 1$.

The attenuation constants α_i for an ionosphere which is sharply bounded at a height $h=$const. are shown in Fig. 5. The daytime ionosphere of the conductivity profile, shown in Fig. 1, is assumed to be bounded at $h=45$, 50 or 55 km. The difference of the attenuation rates between the curves is, in per cent, higher at the lower frequencies. This indicates that the ionosphere model of exponential conductivity is particularly sensitive to changes in the ionosphere height (or to changes in the conductivity at the lower ionosphere edge) at the lowest frequencies. The nighttime ionospheric attenuation constant α_i is smaller for $f<350$ cps than the atmospheric attenuation constant α_a, which considers ionized layers of $h<90$ km. The procedure used for calculating α_a in Section VI is not accurate for $\alpha_a>\alpha_i$. The sum of α_a and α_i gives only a qualitative indication of nighttime attenuation rates.

A comparison between calculated and measured attenuation rates is shown in Fig. 6. The experimental data of Jean[8] are approximated by daytime α_a curves of $h=$const., where 50 km $<h<$ 55 km. The measurements of Jean[8] provide lower attenuation constants than do early Chapman and Macario[10] data, obtained by less accurate techniques. The nighttime $\alpha=\alpha_a+\alpha_i$ curve for $h=90$ km provides a fair agreement with Chapman and Macario[10] data.

C. Earth-Ionosphere Cavity Resonances

The resonance frequencies computed from the exponential ionosphere model are compared with the measured frequencies[13] in Table II. Using only daytime data with either $h=50$ km$=$const. or $\sigma(h)/\omega\epsilon_0=1=$const., the calculated resonances differ by 1 cps or less from measurements. Combined daytime and nighttime data provide a less accurate agreement. It follows from (47) that the shifts of the resonance frequencies are determined principally by the real parts of the modal equation roots S, which are inversely proportional to phase velocity. A significant part of the nighttime losses are due to layers of $h<90$ km. The procedure used for calculating these losses in Section V does not provide

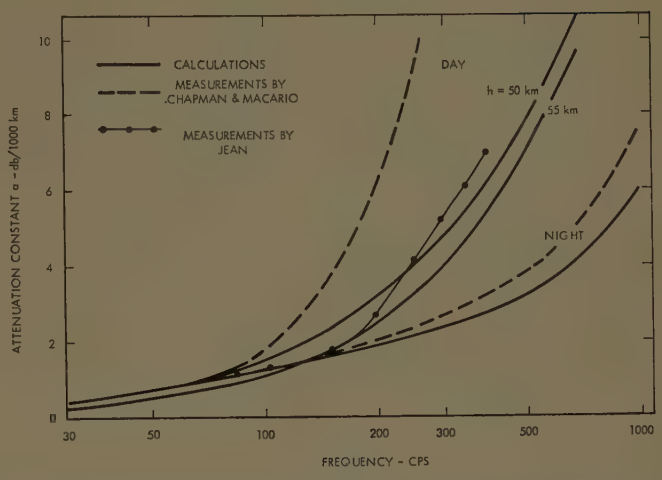

Fig. 6—Comparison of theoretical and experimental attenuation constants. Ionosphere of an exponential conductivity profile. Daytime $h=50$ and 55 km, nighttime $h=90$ km.

corrections for Re S. This causes increased discrepancies between measured and calculated resonance frequencies if one attempts to use the combined day and night data.

The calculated and measured Q factors of individual cavity resonances have been listed in Table III. The best agreement with the measurements is provided by a daytime ionosphere of $\sigma(h)/\omega\epsilon_0=1=$const. Combined day and night data result in Q figures that are too high at the lower frequencies. Daytime data for $h=$const. exhibit Q figures that decrease with frequency contrary to observations.[13]

In view of the deficient nighttime data, the best model for representing the earth-ionosphere cavity effects is the daytime ionosphere which is sharply bounded at a frequency-dependent height h where $\sigma(h)/\omega\epsilon_0=1=$const.

The above ionosphere model is useful for calculating the terrestrial extra-low-frequency noise spectrum. The results of these calculations, which follow the general pattern of Raemer's analysis,[16] will be reported elsewhere.[35]

D. Limitations of the Present Analysis

The observed daytime and nighttime attenuation rates have been satisfactorily explained with the model of the exponential ionosphere which is bounded at $h=$const. The approximate method which was used for calculating the nighttime losses due to cosmic-ray ionization below h did not account for expected changes in phase velocity or in the real part of the modal equation root S, which caused difficulties in computing the earth-ionosphere cavity resonance effects. The approximation of the nighttime conductivity profile by two exponentials along the lines suggested in Section V and the solution of the resultant two-region problem are required for refining the ionosphere model proposed in this paper.

[35] J. Galejs, "Terrestrial extremely-low frequency noise spectrum in the presence of exponential ionospheric conductivity profiles," *J. Geophys. Res.*, vol. 66; September, 1961.

The propagation constant of the fields is dependent on the structure of the lowest ionized layers, in particular at the lowest frequencies. Further studies of the ionospheric day and night conductivity profiles may necessitate some changes of the proposed model. Such studies should consider also the effects of ions and of the earth's magnetic field.

The exponential ionosphere model was used for frequencies below 1000 cps, but it should be applicable also to frequencies in the VLF range. The VLF analysis will be more involved if the first-order perturbation solution of the modal equation is considered inaccurate, and if higher-order approximations are used for the radial-field distribution.

Appendix

Equivalent Refractive Index of a Nonhomogeneous Boundary Medium

The mode characteristics in the space between earth and ionosphere may be calculated after determining the surface impedance at the two boundaries. If E_ρ and H_ϕ designate the tangential components of the electric and magnetic fields at the boundary $z=$const., the surface impedance in a cylindrical coordinate system is simply

$$Z_s = \frac{E_\rho}{H_\phi}. \tag{52}$$

When a homogeneous medium is on one or both sides of the boundary, the surface impedance Z_s is related to the components of the Hertz vector Π_z of a *homogeneous* medium by (3.1) of Wait[6] as

$$Z_s = \frac{i\omega\mu}{k^2}\frac{\frac{\partial}{\partial z}\Pi_z}{\Pi_z}, \tag{53}$$

with $k^2=\omega^2\mu\epsilon-i\omega\mu\sigma$. Using (53), it is possible to relate the amplitudes of the upgoing and downgoing waves in the space between earth and ionosphere in (3.5) of Wait[6] to the surface impedances at the two boundaries. A development that follows the pattern of Wait's[6] Section 3 results in the modal equation

$$1 - R_g R_i \exp(-2ikCh) = 0, \tag{54}$$

where

$$R_g = \frac{C\eta + Z_g}{C\eta - Z_g} \tag{55}$$

$$R_i = \frac{C\eta - Z_i}{C\eta + Z_i}. \tag{56}$$

C is a root of the modal equation, the impedance $\eta=\sqrt{\mu_0/\epsilon_0}$ and where Z_g and Z_i are the surface impedances of ground and ionosphere, respectively. Note that (54)–(56) apply both to homogeneous and to nonhomogeneous media beyond the boundaries. For homogeneous ground and ionosphere a substitution of (3.6) to (3.8) of Wait[6] in (53) results in

$$Z_g = -\frac{\eta}{n_g}\sqrt{1-\left(\frac{S}{n_g}\right)^2} \tag{57}$$

$$Z_i = \frac{\eta}{n_i}\sqrt{1-\left(\frac{S}{n_i}\right)^2}, \tag{58}$$

where $S^2=1-C^2$ and $n_k^2=(i\omega\epsilon_k+\sigma_k)/(i\omega\epsilon_0)$. A substitution of (57) and (58) in (55) and (56) gives the conventional expressions of reflection coefficient as in (3.11) and (3.12) of Wait.[6]

The solutions of the modal equation (54) depend on the surface impedance of the boundaries. If a surface impedance Z_s of a nonhomogeneous medium is known, one may define by (58) an equivalent refractive index n^e of a homogeneous medium which gives the same surface impedance Z_s. Considering a nonhomogeneous ionosphere,

$$(n_i^e)^2 = \left(\frac{\eta}{Z_i}\right)^2\left[\frac{1}{2}+\sqrt{\frac{1}{4}-\frac{S^2Z_i^2}{\eta^2}}\right]. \tag{59}$$

For $\eta/Z_i \gg 1$, (59) may be approximated by

$$(n_i^e)^2 = \left(\frac{\eta}{Z_i}\right)^2 - S^2 \approx \left(\frac{\eta}{Z_i}\right)^2. \tag{60}$$

The simplified expression (60) applies for $|n_i^e| \gg 1$. There are no simple relations between the local refractive index n_i and the equivalent refractive index n_i^e for a nonhomogeneous ionosphere. The relation (60) may apply also to geometries where n_i does not satisfy $|n_i| \gg 1$.

Some Remarks on Green's Dyadic for Infinite Space*

J. VAN BLADEL†, SENIOR MEMBER, IRE

Summary—**The validity of the often used dyadic**

$$-\left(\mathfrak{I}+\frac{1}{k^2}\nabla\nabla\right)\frac{e^{-ikR}}{4\pi R}$$

to compute the electric field *inside* a current-carrying region is investigated. It is found that care must be exercised in the definition of the integrals, which should be taken as principal values around the field point.

I. Introduction

THE electric field outside a current-carrying volume is often expressed in terms of a Green's dyadic as

$$\bar{E}(\bar{r}_0) = \iiint_V j\omega\mu_0 \bar{J}(\bar{r})\cdot\mathfrak{G}(\bar{r}\,|\,\bar{r}_0)\,dV \qquad (1)$$

where

$$\mathfrak{G}(\bar{r}\,|\,\bar{r}_0) = -\frac{1}{4\pi}\left(\mathfrak{I}+\frac{1}{k^2}\,\mathrm{grad}\,\mathrm{grad}\right)\frac{e^{-jk|\bar{r}-\bar{r}_0|}}{|\bar{r}-\bar{r}_0|},$$

and $\mathfrak{I}$ is the identity dyadic. One is normally interested in points outside volume V (Fig. 1), particularly when computing the radiation pattern of the current distribution. It is not without practical interest, however, to inquire whether (1) is still valid when $\bar{r}_0$ is *inside* V. Clearly, Green's dyadic becomes infinite when $\bar{r}$ approaches $\bar{r}_0$, so that the integral appearing in (1) is an improper one. It is our purpose to investigate the character of this improper integral. The divergent character of certain integrals where derivatives of e^{-ikR}/R appear is well known to the mathematician, and has been prominently mentioned in relation with the surface integral equations of diffraction theory.[1,2] The remarks which follow are consequently not directed to the mathematician and his desire for rigor, but rather to the practicing engineer who might want to apply (1) in the middle of an electron beam, for instance.

II. The Electric Field Inside a Simple Current Distribution

Consider a column of current occupying the circular cylindrical volume shown in Fig. 2. The current density $\bar{J}$ is uniform, and is represented by the phasor

$$\bar{J} = J\bar{u}_z$$

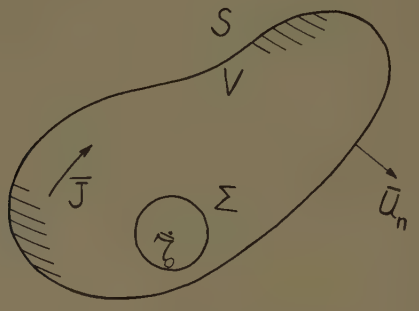

Fig. 1—Current-carrying region.

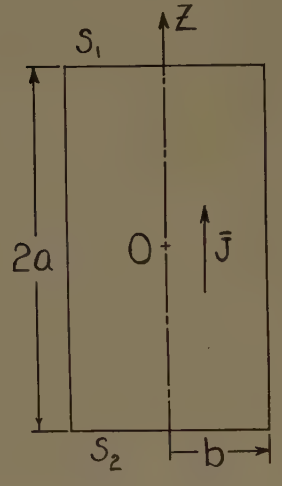

Fig. 2—Cylindrical current beam.

where $\bar{u}_z$ is the unit vector in the z direction. We notice, without raising questions as to how such a current distribution might be realized in practice, that its form is perfectly correct from a mathematical point of view, and is quite suitable for use in (1). We wish to find the electric field at the center O of the current-carrying column. The method of retarded potentials, which we take to be correct and choose to be our starting point, provides the answer immediately:

$$\bar{E}(\bar{r}_0) = -\,\mathrm{grad}_0\frac{1}{4\pi\epsilon_0}\left[\iiint_{V'}\rho(\bar{r})\phi\,dV + \iint_S \eta(\bar{r})\phi\,dS\right] - \frac{j\omega\mu_0}{4\pi}\iiint_{V'}\bar{J}(\bar{r})\phi\,dV \qquad (2)$$

where ϕ stands for $e^{-jk|\bar{r}-\bar{r}_0|}/|\bar{r}-\bar{r}_0|$, ρ for the volume-charge density $-1/j\omega$ div $\bar{J}$, and η for the surface-charge density $1/j\omega(\bar{J}\cdot\bar{u}_n)$. The volume integrals appearing in (2) are extended over volume V' obtained by

* Received by the PGAP, May 15, 1961; revised manuscript received, June 19, 1961.

† Elec. Engrg. Dept., University of Wisconsin, Madison, Wis.

[1] A. W. Maue, "Zur Formulierung eines allgemeinen Beugungsproblems durch eine Integralgleichung," *Z. Physik.*, vol. 126, nos. 7–9, pp. 601–618; 1949.

[2] C. J. Bouwkamp, "Diffraction theory," *Reports on Progress in Physics*, vol. 17, pp. 35–100; 1954.

excluding from V a small volume v (a sphere, for instance), centered at $\bar{r}_0$, and of vanishing linear dimensions. These integrals are, in fact, the limit obtained when these dimensions approach zero, and potential theory[3] shows that this limit exists and is independent of the shape of v. In our configuration, $\rho=0$, $\eta=\pm J/j\omega$ for $z=\pm a$, and $\bar{J}$ is constant. This simplifies calculations, and we find that $\bar{E}$ is in the z direction, and equal to

$$E_z(0) = \underbrace{+\frac{Ja}{j\omega\epsilon_0}\left[-\frac{e^{-jka}}{a}+\frac{e^{-jk\sqrt{a^2+b^2}}}{\sqrt{a^2+b^2}}\right]}$$

contribution from the scalar potential,

$$\underbrace{+\sqrt{\frac{\mu_0}{\epsilon_0}}\,J\int_0^a e^{-jk\sqrt{b^2+z^2}}\,dz+\frac{J}{j\omega\epsilon_0}\left[e^{-jka}-1\right]}, \quad (3)$$

contribution from the vector potential.

Let us now try to evaluate (1). With the present value of $\bar{J}$, the integral yields

$$-\frac{j\omega\mu_0}{4\pi}\iiint\frac{\bar{J}(\bar{r})e^{-jk|\bar{r}-\bar{r}_0|}}{|\bar{r}-\bar{r}_0|}\,dV$$
$$-\frac{j\omega\mu_0}{4\pi k^2}J\iiint\frac{\partial}{\partial z}\left[\operatorname{grad}\frac{e^{-jk|\bar{r}-\bar{r}_0|}}{|\bar{r}-\bar{r}_0|}\right]dV. \quad (4)$$

The first term does not give any trouble; it is a convergent integral, identical with that contributed by the vector potential in (2) and (3). It is the second term which is interesting. It will, by reason of symmetry, yield a vector oriented along the z axis when $\bar{r}_0$ is equal to zero. This means that we should investigate

$$\iiint\frac{\partial^2}{\partial z^2}\left(\frac{e^{-jkR}}{R}\right)dV$$

where R is the distance to the origin. The integrand clearly becomes infinite at $R=0$. To give a meaning to the integral, we should exclude the origin by a small volume v, and extend the integration over $V'=V-v$. The difficulty, however, is that the resulting integral does not converge. The reason is that the limit depends on the shape of the excluded volume, as can be seen by considering a circular cylinder of radius η and height $2h$ (Fig. 3). For this shape, the integral takes the form

$$I = 2\pi\iint_{\text{I+II+III}}\frac{\partial^2}{\partial z^2}\left[\frac{e^{-jk\sqrt{r^2+z^2}}}{\sqrt{r^2+z^2}}\right]rdrdz$$

which, after a few trivial steps, is found to be equal to

$$I = 4\pi\left[1-e^{-jka}+\frac{a}{\sqrt{a^2+b^2}}e^{-jk\sqrt{a^2+b^2}}-\frac{1}{\sqrt{1+\frac{\eta^2}{h^2}}}\right].$$

[3] O. D. Kellogg, "Foundations of Potential Theory," Springer-Verlag, Berlin, Germany; 1929.

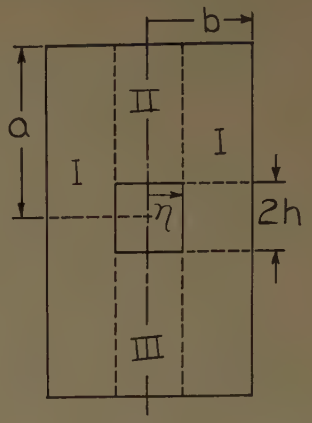

Fig. 3—Current volume with small cylindrical volume excluded.

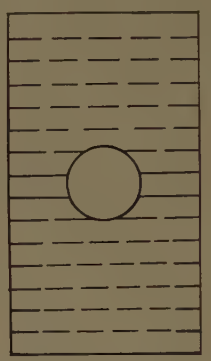

Fig. 4—Current volume with small spherical volume excluded.

The limit obviously depends on the aspect ratio η/h of the cylinder. Let us now surround the origin by a small sphere of radius η (Fig. 4), and inquire about the behavior of integral I as η approaches zero. A few more simple steps now lead to the value

$$I = 4\pi\left[\frac{a}{\sqrt{a^2+b^2}}e^{-jk\sqrt{a^2+b^2}}-e^{-jka}+\frac{1}{3}\right].$$

Clearly, I is now well defined as the limit obtained when the radius of the sphere approaches zero. We shall call this limit the "principal value" of the integral. Upon substitution in (4) and comparison with (3), the meaning of the right-hand member of (1) becomes clear. In our particular geometry

$$\text{P.V.}\iiint_V j\omega\mu_0\bar{J}(\bar{r})\cdot\mathcal{G}(\bar{r}\,|\,\bar{r}_0)dV = \bar{E}(\bar{r}_0)+\frac{\bar{J}}{3j\omega\epsilon_0}. \quad (5)$$

Now we wish to show that this formula is correct for an arbitrary current distribution, provided that the "principal value" is defined as in the preceding example.

III. General Formula for the Electric Field Inside a Current Distribution

We start from (2) where V' is now the volume obtained by excluding a small sphere around $\bar{r}_0$. Let us first concentrate on the scalar-potential term. As in potential theory, and because ϕ has the same kind of dis-

continuity as $1/|\bar{r}-\bar{r}_0|$, we bring the gradient operator inside the integral and obtain

$$-\frac{1}{j\omega 4\pi\epsilon_0}\iiint_{V'} \operatorname{div}\bar{J}\,\operatorname{grad}\phi\,dV + \frac{1}{j\omega 4\pi\epsilon_0}\iint_S (\bar{u}_n\cdot\bar{J})\,\operatorname{grad}\phi\,dS.$$

The first integral can be transformed by utilizing the following formulas of dyadic analysis:

$$\operatorname{div}(\bar{a}\,\bar{b}) = (\operatorname{div}\bar{a})\bar{b} + \bar{a}\cdot\operatorname{grad}\bar{b}$$

$$\iiint_V \operatorname{div}(\bar{a}\,\bar{b})dV = \iint_S (\bar{u}_n\cdot\bar{a})\bar{b}\,dS.$$

Combining with the second integral we find[4]

$$\frac{1}{j\omega 4\pi\epsilon_0}\iiint_{V'} \bar{J}\cdot\operatorname{grad}\operatorname{grad}\phi\,dV + \frac{1}{j\omega 4\pi\epsilon_0}\iint_\Sigma (\bar{u}_R\cdot\bar{J})\,\operatorname{grad}\phi\,d\Sigma.$$

The surface integral is easy to evaluate. For small radii η, $\operatorname{grad}\phi = -\bar{u}_R/\eta^2$. Introducing spherical coordinates centered at $\bar{r}_0$, with the polar axis in the direction of $\bar{J}$, we obtain, after a few trivial steps, the value

$$-\frac{1}{3}\frac{\bar{J}(\bar{r}_0)}{j\omega\epsilon_0}$$

for the surface integral. Eq. (5) then follows immediately.

It is worthwhile deriving (5) in an alternate way. One easily checks that $\mathcal{G}$ satisfies Helmholtz equation (when $\bar{r}\neq\bar{r}_0$) and the radiation condition at infinity. Starting from equations

$$\begin{aligned} &-\operatorname{curl}\operatorname{curl}\bar{E} + k^2\bar{E} = j\omega\mu_0\bar{J} \\ &-\operatorname{curl}\operatorname{curl}\mathcal{G} + k^2\mathcal{G} = 0, \end{aligned} \tag{6}$$

and using the following formula for dyadic analysis,

$$\iiint_V [-\operatorname{curl}\operatorname{curl}\bar{a}\cdot\mathfrak{A} + \bar{a}\cdot\operatorname{curl}\operatorname{curl}\mathfrak{A}]dV = \iint_S [\bar{a}\cdot(\bar{u}_n\times\operatorname{curl}\mathfrak{A}) - (\bar{u}_n\times\operatorname{curl}\bar{a})\cdot\mathfrak{A}]dS$$

as applied to the volume bounded by $\sum$ and the sphere at infinity, and where $\bar{a}$ is a vector and $\mathfrak{A}$ a dyadic, one finds

$$-\iint_\Sigma \bar{E}\cdot(\bar{u}_R\times\operatorname{curl}\mathcal{G})dS + \iint_\Sigma \operatorname{curl}\bar{E}\cdot(\bar{u}_R\times\mathcal{G})dS = \iiint_{V'} j\omega\mu_0\bar{J}\cdot\mathcal{G}(\bar{r}\,|\,\bar{r}_0)dV \tag{7}$$

after noticing that the contribution from the sphere at infinity vanishes because of the radiation condition. Interest focuses on the evaluation of the left-hand member. This task has been performed in an excellent paper by Wilcox.[5] The following method appears to be more concise. For small radii η,

$$\bar{u}_R\times\mathcal{G} = \frac{1}{4\pi k^2\eta^3}(\bar{u}_\phi\bar{u}_\theta - \bar{u}_\theta\bar{u}_\phi) = \frac{1}{4\pi k^2\eta^3}(\bar{u}_R\times\mathfrak{I})$$

$$\bar{u}_R\times\operatorname{curl}\mathcal{G} = -\frac{1}{4\pi\eta^2}(\bar{u}_\theta\bar{u}_\theta + \bar{u}_\phi\bar{u}_\phi).$$

The first surface integral of (7) can be rewritten as

$$\frac{1}{4\pi}\iint_\Sigma \frac{E_\theta\bar{u}_\theta + E_\phi\bar{u}_\phi}{\eta^2}\eta^2 d\Omega = \bar{E}(\bar{r}_0) - \frac{1}{4\pi}\iint_\Sigma (\bar{E}\cdot\bar{u}_R)\bar{u}_R d\Omega.$$

Again introducing spherical coordinates centered at $\bar{r}_0$ with the polar axis in the direction of $\bar{E}$, we find that the second term is equal to $\frac{1}{3}\bar{E}(\bar{r}_0)$. Consequently, the first surface integral of (7) is equal to $\frac{2}{3}\bar{E}(\bar{r}_0)$. The second surface integral can be transformed as follows:

$$\begin{aligned} -\iint_\Sigma \operatorname{curl}\bar{E}\cdot\frac{(\bar{u}_R\times\mathfrak{I})}{4\pi k^2\eta^3}dS &= \frac{1}{4\pi k^2\eta^3}\iint_\Sigma (\bar{u}_R\times\operatorname{curl}\bar{E})dS \\ &= \frac{1}{4\pi k^2\eta^3}\iiint_{V''}\operatorname{curl}\operatorname{curl}\bar{E}dV \\ &= \frac{1}{3k^2}\operatorname{curl}_0\operatorname{curl}_0\bar{E}(\bar{r}_0) \end{aligned}$$

where V'' is the volume of the small sphere surrounding P. Finally,

$$\frac{2}{3}\bar{E}(\bar{r}_0) + \frac{1}{3k^2}\operatorname{curl}_0\operatorname{curl}_0\bar{E}(\bar{r}_0) = \iiint_{V'} j\omega\mu_0\bar{J}\cdot\mathcal{G}(\bar{r}_0\,|\,\bar{r})dV \tag{8}$$

which is the desired relation (5) if (6) is taken into account. Eqs. (5) and (8) are now in a form which explicitly details the computations which should be performed to evaluate $\bar{E}(\bar{r}_0)$.

[4] It is worth mentioning, as suggested by a reviewer, that we could have started from (2) to find

$$\bar{E}(\bar{r}_0) = \frac{-j\omega\mu_0}{4\pi}\iiint_V \bar{J}(\bar{r})\phi dV - \frac{1}{j\omega\epsilon_0 4\pi}\operatorname{grad}_0\iiint_V \bar{J}(\bar{r})\cdot\operatorname{grad}\phi dV.$$

This can be represented operationally by (1) with a Green's dyadic obtained from $\mathcal{G}$ by changing the term grad grad into $-\operatorname{grad}_0\operatorname{grad}$, a form which evidences the symmetry with respect to the $\bar{r}$ and $\bar{r}_0$ coordinates. The present note is concerned with the grad grad representation which is often used in textbooks, and rather carelessly introduced behind the integral sign.

[5] C. H. Wilcox, "Debye potentials," *J. Math. and Mech.*, vol. 6, pp. 167–202; March, 1957. Dr. Wilcox was kind enough to read the present paper, and to point out that the need for the use of principal values was already recognized by him in an unpublished note, "The Diffraction of Radiation by Inhomogeneous Lenses," Lockheed Aircraft Co., Sunnyvale, Calif., Rept. No. LMSD-5126; 1958.

Appendix

Although the establishment of (5) and (8) represents the main purpose of the present note, it is perhaps not superfluous to add a few comments on the way to represent the singularity of the $\mathcal{G}$ dyadic with the help of δ-functions.

It is customary to write the differential equation satisfied by $\mathcal{G}$ in the following form:

$$-\text{curl curl } \mathcal{G} + k^2\mathcal{G} = \delta(\bar{r} - \bar{r}_0)\mathfrak{I}. \tag{9}$$

Eq. (9) can be used, by means of a few simple steps which are not reproduced here,[6] to establish (1), regardless of whether $\bar{r}_0$ is inside or outside the current-carrying region. Eq. (1) is valid, however, only for $\bar{r}_0$ outside this region. It will be necessary, therefore, to replace (9) by an equation which gives more meaningful results in terms of distribution theory. Let us review the basic concepts of that theory.[7] Let ϕ be a function (called testing function) which has continuous derivatives of all orders, and vanishes outside a finite volume. A distribution T is, by definition, a linear continuous functional of ϕ. It associates a number $T(\phi)$ with each testing function. A well-known example is the Dirac distribution $D_{\bar{r}_0}$ which associates the value of ϕ at $\bar{r}_0$ with each testing function ϕ.

Another example is

$$\text{P.V.} \int_{-\infty}^{+\infty} \frac{\phi(x)dx}{x} = \lim_{\epsilon \to 0} \left[\int_{-\infty}^{-\epsilon} \frac{\phi(x)dx}{x} + \int_{\epsilon}^{+\infty} \frac{\phi(x)dx}{x} \right]. \tag{10}$$

Some distributions can be written in the form

$$T(\phi) = \int t(\bar{r})\phi(\bar{r})dV \tag{11}$$

where t is a summable function. For other distributions, no such function can be found (a famous example is the Dirac distribution), but one still writes (11) in a symbolic way, and associates the (symbolic) function t with the distribution T. In the Dirac case,

$$T_{\bar{r}_0}(\phi) = \phi(\bar{r}_0) = \int \delta(\bar{r} - \bar{r}_0)\phi(\bar{r})dV.$$

For the distribution defined by (10), one takes P.V. $1/x$ to be the "generating" function t.

The nth derivative of a distribution T is, by definition, a new distribution which associates the value $T[(-1)^n(\partial^n\phi/\partial x^n)]$ with each testing function ϕ. The "generating" function of this new distribution is $\partial^n t/\partial x^n$. This reduces to the usual derivative when function t has one, but it can serve to define the derivative when the latter is not a usual function. For example, the first derivative of the δ-function is now defined by the property

$$D_{\bar{r}_0}\left(-\frac{\partial\phi}{\partial x}\right) = -\left(\frac{\partial\phi}{\partial x}\right)_{\bar{r}=\bar{r}_0} = \int \frac{\partial\delta(\bar{r} - \bar{r}_0)}{\partial x}\phi(\bar{r})dV.$$

These various notions can be applied immediately to our particular problem. Now it is necessary to work with vectors, however, and distributions will now associate a vector with each testing vector $\bar{\phi}(\phi_x, \phi_y, \phi_z)$. Each distribution will be written as

$$T(\bar{\phi}) = \int \bar{\phi}(\bar{r}) \cdot \mathfrak{F}(\bar{r})dV$$

where $\mathfrak{F}$ is the generating tensor. The Dirac distribution $\bar{D}_{\bar{r}_0}$ associates $\bar{\phi}(\bar{r}_0)$ with $\bar{\phi}$, and will be written as

$$\bar{D}_{\bar{r}_0}(\bar{\phi}) = \bar{\phi}(\bar{r}_0) = \int \bar{\phi}(\bar{r}) \cdot \mathfrak{I}\delta(\bar{r} - \bar{r}_0)dV.$$

The distribution S which yields

$$\left[\frac{2}{3}\bar{\phi} + \frac{1}{3k^2}\text{curl curl } \bar{\phi}\right]_{\bar{r}=\bar{r}_0} = \left[\bar{\phi} + \frac{1}{3k^2}(\text{curl curl } \bar{\phi} - k^2\bar{\phi})\right]_{\bar{r}=\bar{r}_0}$$

is, according to the definition of the derivative of a distribution,

$$\bar{S} = \frac{2}{3}\bar{D}_{\bar{r}_0} + \frac{1}{3k^2}\text{curl curl } \bar{D}_{\bar{r}_0}.$$

This distribution was also shown to be

$$\bar{S} = \text{P.V.} \iiint [-\text{curl curl } \bar{\phi} + k^2\bar{\phi}] \cdot \mathcal{G}(\bar{r} \mid \bar{r}_0)dV.$$

Equating "generating tensors" of both forms finally gives us the symbolic equation we were looking for:

$$-\text{curl curl (P.V. } \mathcal{G}) + k^2(\text{P.V. } \mathcal{G}) = \frac{2}{3}\mathfrak{I}\delta(\bar{r} - \bar{r}_0) + \frac{1}{3k^2}\text{curl curl } [\mathfrak{I}\delta(\bar{r} - \bar{r}_0)]$$

$$= \mathfrak{I}\delta(\bar{r} - \bar{r}_0) - \frac{1}{3k^2}(-\text{curl curl} + k^2)\mathfrak{I}\delta(\bar{r} - \bar{r}_0).$$

It is interesting to notice that the tensor

$$\mathcal{G}' = \text{P.V. } \mathcal{G} + \frac{\mathfrak{I}}{3k^2}\delta(\bar{r} - \bar{r}_0)$$

satisfies (9), and could be taken as our fundamental Green's tensor. We do not need distribution theory to establish the fact. Eq. (8) can, indeed, always be rewritten as

$$\bar{E}(\bar{r}_0) = \text{P.V.} \iiint j\omega\mu_0\bar{J}(\bar{r}) \cdot \mathcal{G}(\bar{r} \mid \bar{r}_0)dV + \frac{1}{3k^2}\iiint j\omega\mu_0\bar{J}(\bar{r}) \cdot \mathfrak{I}\delta(\bar{r} - \bar{r}_0)dV.$$

This form is valid whether $\bar{r}_0$ is outside the current-carrying volume or not. It clearly indicates that $\mathcal{G}'$ is the tensor we should use in (1).

[6] F. E. Borgnis and C. H. Papas, "Randwertprobleme der Mikrowellen Physik," Springer-Verlag, Berlin, Germany; 1955.

[7] L. Schwartz, "Methodes Mathematiques de la Physique," Centre de Documentation Universitaire, Paris, France. This account presents the theory in a relatively simple form.

Apparent Temperatures of Smooth and Rough Terrain*

S. N. C. CHEN†, MEMBER, IRE, AND W. H. PEAKE†, MEMBER, IRE

Summary—**The apparent temperatures of smooth and rough terrain surfaces are calculated for frequencies between 1 and 75 kMc, for angles of incidence between 5° and 80°, and for observation altitudes between 2 km and 32 km. The attenuation and thermal radiation caused by the atmosphere are accounted for by an experimental model atmosphere, and the surface emissivities are based on measured complex dielectric constants (for the smooth surfaces) and measured radar return (for the rough surfaces). It is found that perpendicular polarization provides the greatest temperature contrast between rough and smooth surfaces, and that the contrast decreases as the altitude of observation increases; at $f=75$ kMc (approximately the resonant frequency of the oxygen molecule), there is likely to be little, if any, contrast between rough and smooth surfaces.**

I. Introduction

THE concept of the apparent temperature [1], [2] of natural surfaces, such as various types of earth surfaces, has been used commonly in predicting the performance of radio telescopes and radiometers. It is impossible to consider all types of natural surfaces for all frequencies; there are, however, two interesting limiting cases, the "rough" or diffusely scattering surface and the "smooth" or specularly scattering surface, for which analytical results can be derived. Whether a given surface is to be considered smooth or rough is, in general, determined by the frequency at which the surface is viewed (see Section III-B).

The present work attempts to show how the apparent surface temperatures of both smooth and rough surfaces vary as a function of the observation angle from which the surface is viewed, using the frequency, the height of observation, the polarization, and the scattering behavior of the surface as parameters. The effect of water vapor and oxygen resonance upon the apparent surface temperature observed at a certain height above the surface is demonstrated also through the calculated results. These calculations are useful in estimating the performance of airborne mapping radiometers and have also been used to calculate antenna temperature [3].

II. Equations for Predicting Apparent Surface Temperature

The blackbody radiation $i_o(T, \lambda)$ of a given polarization state within a frequency interval Δf and traveling in a specific direction can be approximated by the well-known Rayleigh-Jeans relationship for sufficiently high temperature and long wavelengths [4], that is,

$$i_o(T, \lambda) = \frac{kT\Delta f}{\lambda^2} \text{ watts-meter}^{-2}\text{-steradian}^{-1},$$

in which k is Boltzmann's constant 1.37×10^{-23} joule/°K, T is the radiation temperature in °K, and λ is the wavelength of radiation in meters. The apparent temperature of arbitrary thermal radiation is generally defined to be equal to the temperature of the blackbody radiation having the same power density per unit solid angle in the small frequency interval of interest. Thus, the apparent temperature of a surface, when viewed from a specific direction, is the apparent temperature of the radiation issuing from the surface in a given polarization state and direction.

A. Smooth Surface

A surface is considered smooth, or only slightly rough, if its scattering property is predominantly specular at a given frequency. For a smooth surface, the reflecting properties can be adequately accounted for by the well-known Fresnel coefficient for both parallel and perpendicular polarizations. If a detector with an ideal, narrow-beam antenna is placed at a height h above the earth's surface and views the surface at an angle θ_o with respect to the surface normal, then the apparent surface temperatures [1] T_{ah} or T_{av} for the cases of perpendicular and parallel polarizations, observed at the height h and the angle θ_o, are

$$T_{ah} = T_g(1 - |R_h|^2)[t(h)] + T_c|R_h|^2 t(h_c)t(h) + T_{\text{air}}[1 - t(h_c)][t(h)]|R_h|^2 + T_{\text{air}}[1 - t(h)] \quad (1)$$

or

$$T_{av} = T_g(1 - |R_v|^2)[t(h)] + T_c|R_v|^2 t(h_c)t(h) + T_{\text{air}}[1 - t(h_c)][t(h)]|R_v|^2 + T_{\text{air}}[1 - t(h)], \quad (2)$$

in which the subscript h refers to perpendicular polarization (often called "horizontal" polarization in the engineering literature) and the subscript v refers to parallel polarization (often called "vertical" polarization). The quantities contained in (1) and (2) are defined in the following manner:

T_g = actual, or thermometer, temperature of the ground (assumed, in the calculations which follow, to be 300°K).

T_{air} = actual, or thermometer, temperature of the atmosphere (assumed, in the calculations which follow, to be 300°K and independent of altitude).

T_c = thermal radiation temperature of the cosmic noise sources.

R_h, R_v = Fresnel reflection coefficients for waves of perpendicular and parallel polarizations.

$t(h)$ = transmission coefficient for the layer of atmosphere between the antenna and the ground.

* Received by the PGAP, May 22, 1961. The work described in this article was sponsored in part by a contract from Aeronautical Systems Div., USAF Systems Command, Wright-Patterson AFB, Ohio.

† The Antenna Lab., Dept. of Elec. Engrg., The Ohio State University, Columbus, Ohio.

$t(h_c)$ = transmission coefficient for the layer of atmosphere between the ground and the location of cosmic noise sources.

If the atmospheric density is assumed to decay exponentially as the height above above the earth's surface increases, then the transmission coefficients $t(h)$ and $t(h_c)$ can be expressed explicitly as

$$t(h) = \exp(-0.2303\alpha h_e \sec\theta_0) \tag{3a}$$

$$t(h_c) = \exp(-0.2303\alpha H \sec\theta_0). \tag{3b}$$

For the above equations, α is the ground-level attenuation of the atmosphere in db/km; h_e is the effective height of the atmosphere, defined as

$$h_e = H[1 - \exp(-h/H)], \tag{4}$$

where H is the so-called scale height of the atmosphere, taken to be 8 km. The values of α at ground level can be found from various published works [5], and for convenience, the values of α used later are shown also in Table I.

TABLE I

f(kMc)	α* (db/km)	γ_o† (rough surface)
1	0.0037	
4	0.0058	
10.3	0.0089	0.032
15.2	0.019	0.063
23.5	0.085	0.160
27	0.045	
34.9	0.038	
75	0.38	0.32

* The values of α are for an atmosphere with moderate water vapor content.

† The values of γ_o are typical of experimental values for rough surfaces [6].

The four terms of the right side of (1) and (2) represent four different sources of radiation temperature. The first term is the radiation temperature of the surface. The second term is the radiation temperature of cosmic noise sources reflected by the surface. The third term is the radiation temperature of the atmosphere reflected by the surface. The fourth term is the radiation temperature of the atmosphere between the surface and the point of observation. An expression of the form given in (1) and (2) has been shown to be in reasonably good agreement with experimental values [7]. The contribution to the apparent surface temperature by the cosmic noise sources for the range of frequencies under consideration here is usually small in comparison with other sources of radiation temperature and will not be considered explicitly. The effect of the sun reflected by a smooth surface into the main-lobe or principal sidelobes of an antenna may be more serious, and has been treated elsewhere [3].

B. Rough Surface

A surface is classified as rough when its scattering behavior is predominantly diffuse. The equation for calculating the apparent surface temperature can be derived by taking advantage of the bistatic scattering coefficient of the surfaces and the reciprocity relations [1]. The equation can be expressed as

$$\begin{aligned} T_a(\theta_o) &= T_g[t(h)]\left\{1-\left(\frac{1}{4\pi}\right)\int[\gamma_{hh}(o,s)+\gamma_{hv}(o,s)]d\Omega_s\right\} \\ &+ T_{\text{air}}[t(h)]\left\{(1/4\pi)\int[1-\exp(-0.2303\alpha H\sec\theta_s)]\right. \\ &\left.\cdot[\gamma_{hh}(o,s)+\gamma_{hv}(o,s)]d\Omega_s\right\} \\ &+ T_{\text{air}}[1-t(h)], \end{aligned} \tag{5}$$

in which the $\gamma(o, s)$ is the bistatic scattering coefficient, and its variables o and s symbolize θ_o, ϕ_o (the direction from which radiation impinges on the surface) and θ_s, ϕ_s (the direction into which radiation is scattered), respectively. The subscripts hv of the scattering coefficient mean that the incident wave has perpendicular polarization whereas the scattered wave has parallel polarization, and on the basis of this explanation, the meaning of the subscripts hh follows immediately. In (5), the integration is performed over a hemisphere above the surface. For the rough surfaces under consideration, the scattering coefficients tend to be approximately independent of polarization; consequently, the apparent surface temperature of rough surfaces, given by (5), is assumed to be the same for both states of polarization. In (5) the contribution of the sun to the apparent surface temperature of rough surfaces is not included since it is usually less than 0.1°K at microwave frequencies.

In order to evaluate the integrals in (5), it is necessary to express the complete bistatic scattering pattern of the surface, namely, the quantity $\gamma(o, s) = \gamma_{hh}(o, s) + \gamma_{hv}(o, s)$ in a mathematical form. The simplest choice [1] for $\gamma(o, s)$, which is consistent with the reciprocity principle and is in moderately good agreement with experimental observations [6], can be written as

$$\gamma(o, s) = (\gamma_o/2)(\cos\theta_o + \cos\theta_s)/(\cos\theta_o) \tag{6}$$

where γ_o is a constant that can be estimated from the back-scattering data of the surface. Thus, (5) becomes

$$\begin{aligned} T_a(\theta_o) &= T_g[t(h)][1 - \gamma_o/4 - \gamma_o/(8\cos\theta_0)] \\ &+ T_{\text{air}}[t(h)][\gamma_o F_1(\chi)/4 + \gamma_o F_2(\chi)/(8\cos\theta_o)] \\ &+ T_{\text{air}}[1 - t(h)], \end{aligned} \tag{7}$$

in which

$$\begin{aligned} F_1(\chi) &= \int_0^{\pi/2}(1-\chi^{\sec\theta_s})\sin\theta_s d\theta_s \\ &= 1 - \chi + (\ln\chi)Ei(\ln\chi), \end{aligned} \tag{8}$$

$$\begin{aligned} F_2(\chi) &= 2\int_0^{\pi/2}(1-\chi^{\sec\theta_s})\cos\theta_s\sin\theta_s d\theta_s \\ &= 1 - \chi - \chi\ln\chi + (\ln\chi)^2 Ei(\ln\chi), \end{aligned} \tag{9}$$

where $\chi = \exp(-0.2303\alpha H)$ and the values of the function $Ei(\ln\chi)$ are tabulated functions [8].

III. Discussions of Calculated Results

A. Smooth Surface

Figs. 1, 2, and 3 contain a group of apparent surface-temperature curves for both parallel and perpendicular polarizations computed from (1) and (2). They are plotted as a function of the incidence angle (or the observation angle) θ_o using the relative dielectric constant ϵ_r, the frequency f, and the height h as parameters with $T_{air}=300°K$ and the values of α given in Table I. Upon

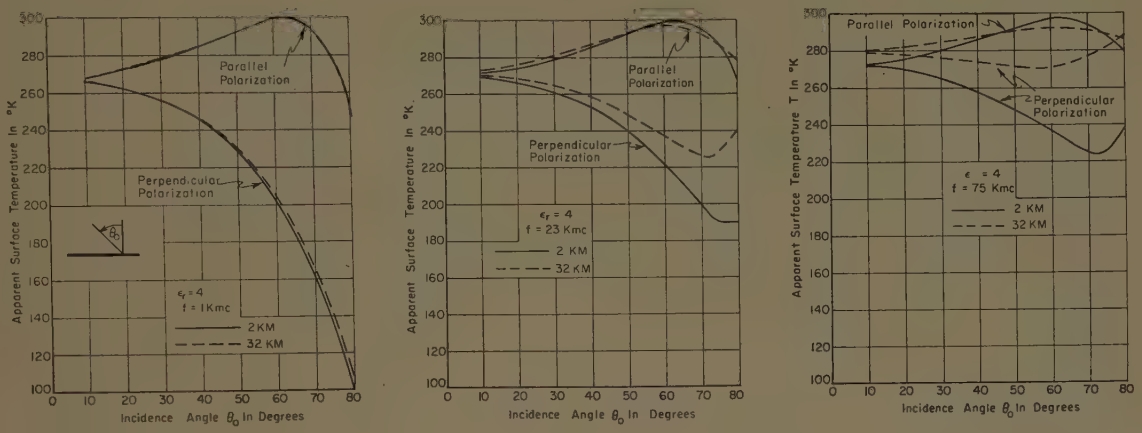

Fig. 1—Apparent surface temperature vs angle of incidence for a smooth surface with dielectric constant $\epsilon_r=4$, as seen from altitudes of 2 km and 32 km.

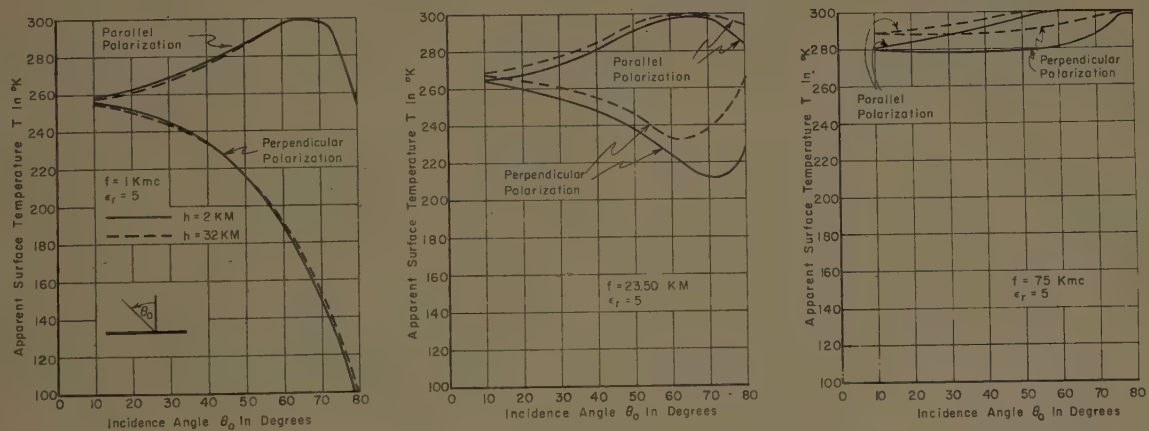

Fig. 2—Apparent surface temperature vs angle of incidence for a smooth surface with dielectric constant $\epsilon_r=5$, as seen from altitudes of 2 km and 32 km.

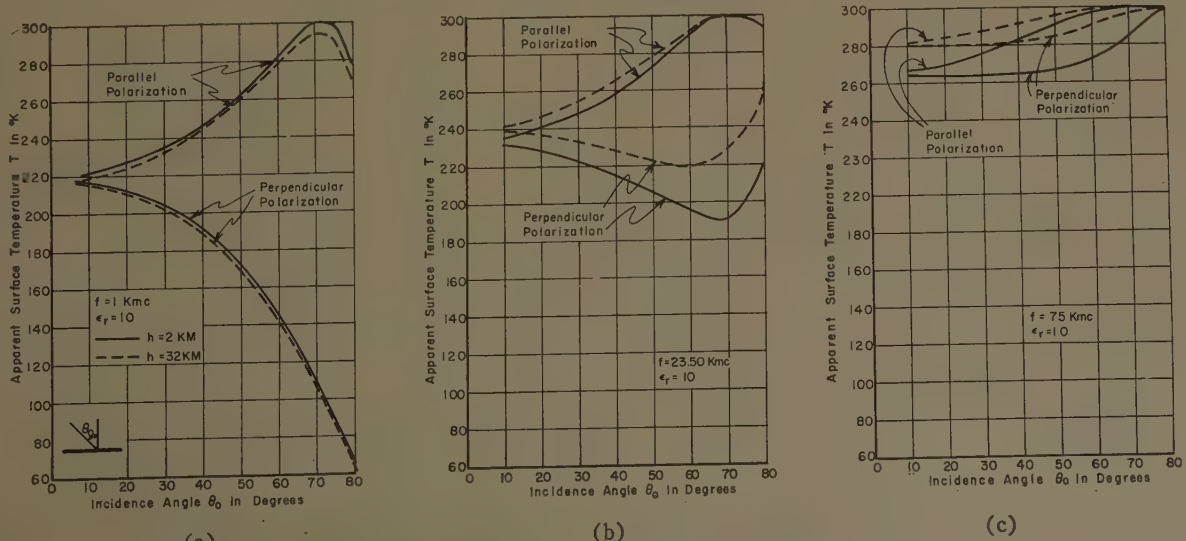

Fig. 3—Apparent surface temperature vs angle of incidence for a smooth surface with dielectric constant $\epsilon_r=10$, as seen from altitudes of 2 km and 32 km.

studying these curves, few qualitative conclusions can be drawn. In general, for a given ϵ_r the apparent surface temperature for the case of parallel polarization is quite insensitive to variations of height and changes slightly as frequency varies. However, at $f=75$ kMc (approximately the resonant frequency of the oxygen molecule), the apparent surface temperature of two different heights, 2 km and 32 km, show some noticeable differences. In addition, the apparent surface temperature for the case of parallel polarization attains its maximum value, equal to the assumed ground temperature, at the incidence angle corresponding to the Brewster angle where the reflection coefficient is zero. For lossy surfaces, where the reflection coefficient never reaches zero, the apparent temperature will be a maximum near the pseudo-Brewster angle, but will not attain the ground temperature.

For the case of perpendicular polarization, the variations of the apparent surface temperature show different features from those for the case of parallel polarization. Below the frequency $f=23.5$ kMc (approximately the resonant frequency of water vapor), the variation of the apparent surface temperature for a given ϵ_r as a function of height is not very noticeable. Above $f=23.5$ kMc, an up-turn of the apparent surface temperature curve can be seen for an incidence angle higher than 70°, approximately; this up-turn is primarily a consequence of increased attenuation in the atmosphere at higher frequencies.

To obtain an over-all view of the variation of the apparent surface temperature as a function of frequency, such calculated variations for both polarizations using ϵ_r as a parameter are shown in Fig. 4. Generally speaking, the apparent surface temperature is always higher at greater height and larger ϵ_r than at lower height and smaller ϵ_r for both polarizations at a given frequency. It is to be noticed that the calculations are limited to the incidence angle range from 10° to 80°. For $\theta_o<10°$, the apparent surface temperatures can be extrapolated by extending the curves. For $\theta_o>80°$, the observation is made at a grazing angle, and the uncertainty in the atmospheric absorption and the scattering of the surface will affect grossly the accuracies of the calculated results.

B. Rough Surface

Fig. 5 shows the calculated results of the difference between actual temperature and apparent surface temperature as a function of the grazing angle, $90°-\theta_o$, at ground level, using frequency as a parameter; the constant γ_o contained in the scattering coefficient is a function of frequency and is usually obtainable from experimental investigations of the bistatic scattering behavior of a rough surface [6]. For present calculations, γ_o's based on experimental values are used for convenience; the values used are shown in Table I.

Fig. 6 shows a group of calculated results of the temperature difference as a function of grazing angle for a

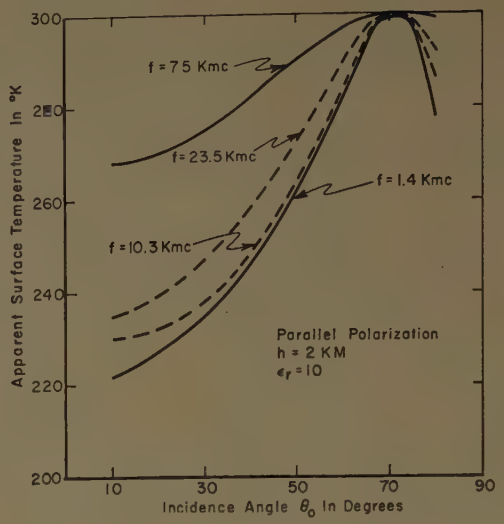

(a)

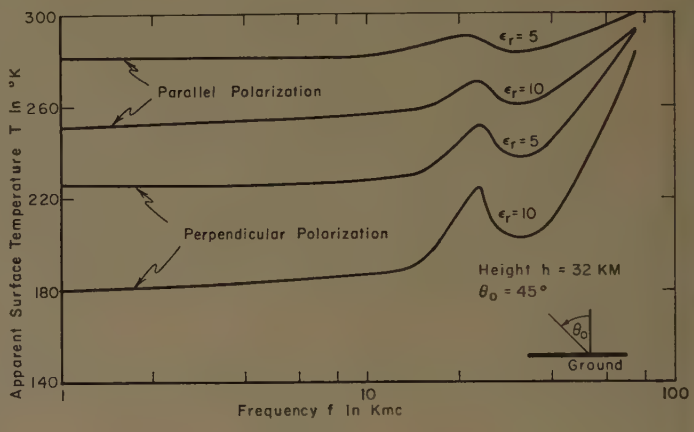

(b)

Fig. 4—(a) Comparison of apparent surface temperatures of a smooth surface for parallel polarization and various frequencies ($\epsilon_r=10$). (b) Comparison of apparent surface temperature of a smooth surface as a function of frequency for various dielectric constants ($h=32$ km, $\theta_o=45°$).

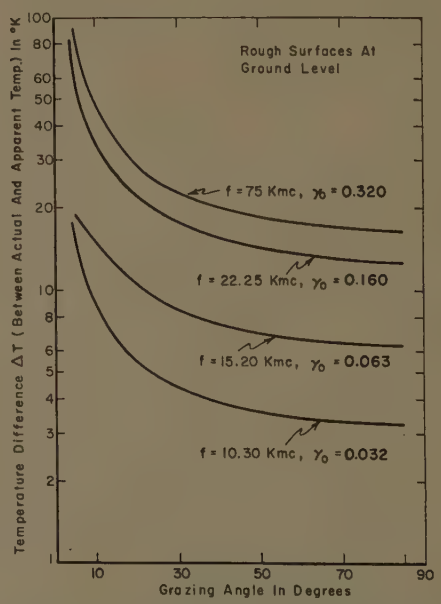

Fig. 5—Apparent temperatures of rough surfaces at various wavelengths and incidence angles, $h=0$ ft.

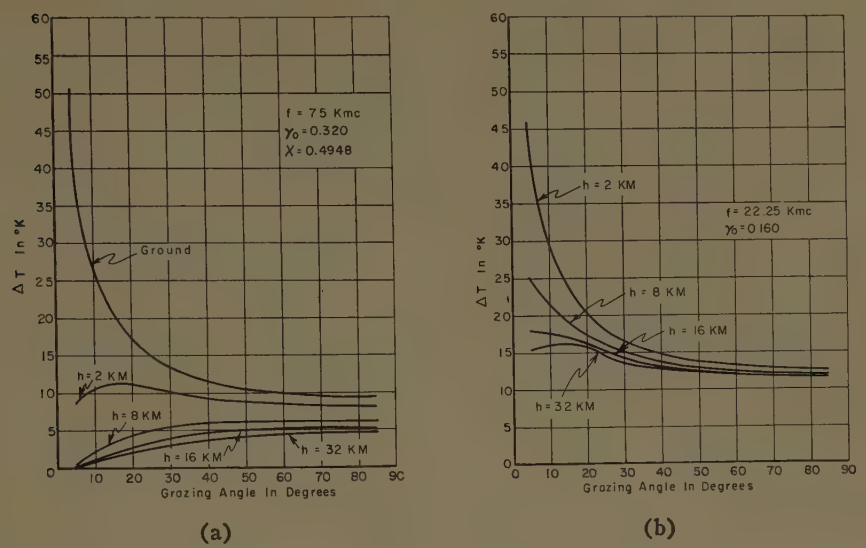

(a) (b)

Fig. 6—Temperature differences (between actual and apparent temperature) of a rough surface for various altitudes.

given frequency using the height as a parameter. It is seen that at approximately the resonant frequencies of water vapor and oxygen molecules, the temperature difference at greater height diminishes as the grazing angle approaches zero. As in the case of the smooth surface, it is generally true that the apparent surface temperature at a given frequency increases as the height increases.

The emissivity[1] of the surface is an often-used parameter that can be obtained directly from the scattering properties [1],

$$e = 1 - (1/4\pi) \int [\gamma_{hh}(o, s) + \gamma_{hv}(o, s)] d\Omega_s. \quad (10)$$

For the particular surface represented by (6), this becomes

$$e = 1 - \gamma_0[1/4 + (1/8) \sec \theta_0]. \quad (11)$$

Fig. 7 shows the calculated emissivity of a rough surface, whose back-scattering behavior satisfied (6), as a function of frequency; the coefficient γ_0 has again been taken from Taylor [6]. Thus, Fig. 7 represents the dependence of emissivity on frequency for typical vegetation covered surface. However, the type of vegetation for which the model is valid is itself dependent on frequency. At 1 kMc, for example, it would require extremely tall vegetation, such as a dense wood or forest, to provide a surface which is rough in terms of a wavelength and is sufficiently deep so that little of the incident radiation can be reflected from the underlying ground. For further illustrations, at 10 kMc shrubbery would appear as a rough surface and at 35 kMc grass would appear quite rough. In Fig. 7, it is seen that the

[1] The emissivity is defined here as the ratio of the power emitted by the surface to that emitted by a black body at the same temperature per unit area per unit solid angle per unit frequency interval.

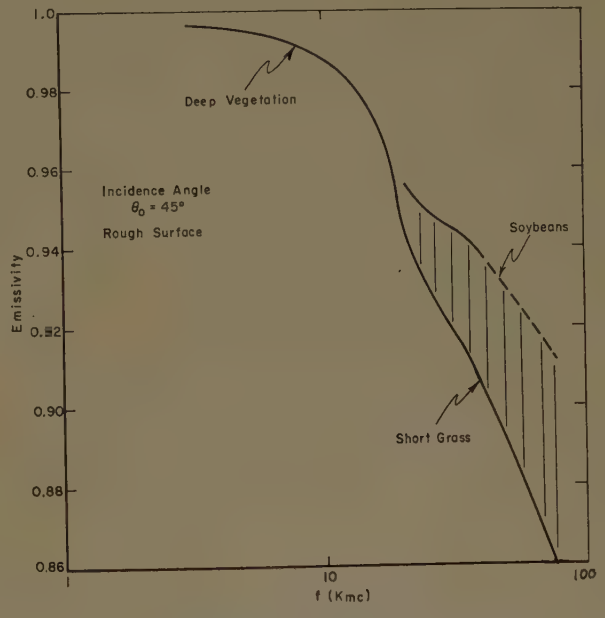

Fig. 7—Emissivities of a rough surface as a function of frequency.

emissivity decreases with frequency. This decrease is caused primarily by an increase in the ratio of the physical size of the scattering elements (which, being leaves, etc., are more or less fixed) to the wavelength, as frequency increases. Thus, at lower frequency, there is less scattering but more absorption by the rough surface; consequently the emissivity is higher.

In Fig. 8, the temperature contrast between rough and smooth surfaces is plotted, for altitudes of 2 and 32 km, as a function of the incidence angle. It is clear from these figures that perpendicular polarization always provides the greatest temperature contrast, and that at the higher altitude, especially for $f = 75$ kMc, there is likely to be little, if any, contrast between rough and smooth surfaces.

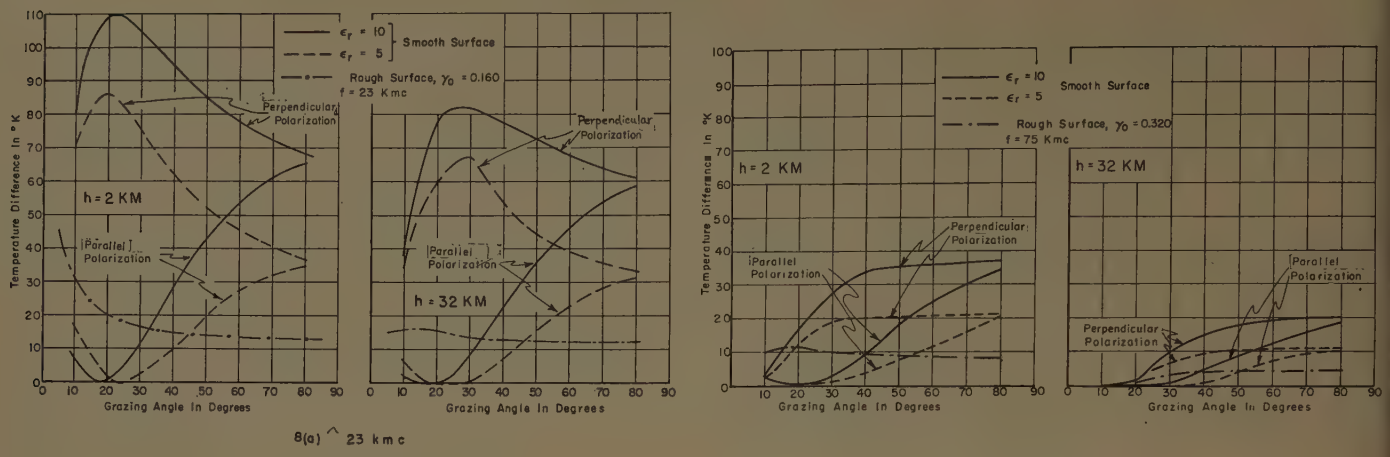

Fig. 8—Difference between actual temperature and apparent temperature of rough and smooth surfaces at 10.3 kMc as a function of grazing angle. (Altitude of observation: 2 km or 32 km.)

IV. Conclusions

It has been shown that the Fresnel coefficient can be used to predict the apparent surface temperature of a smooth surface for both parallel and perpendicular polarizations, and that the bistatic scattering coefficient can be used to predict the apparent surface temperature of a rough surface.

For a smooth surface, the apparent surface temperatures for the case of parallel polarization is higher than that for the case of perpendicular polarization. It is generally true that the apparent surface temperature for both polarizations at a given frequency is higher at greater height and larger ϵ_r than at smaller values of these parameters.

For a rough surface, as in the case of a smooth surface, it is generally true that the apparent surface temperature at a given frequency increases as the height increases. At approximately the resonant frequencies of water vapor and oxygen molecules, the difference between actual temperature and apparent surface temperature at a given height diminishes as the grazing angle approaches zero. Atmospheric absorption caused by oxygen and water vapor resonances decreases the contrast between rough and smooth surfaces.

References

[1] W. H. Peake, "Interaction of electromagnetic waves with some natural surfaces," IRE Trans. on Antennas and Propagation, vol. AP-7, pp. S324–S329; December, 1959.
[2] E. Weger, "Apparent thermal noise temperatures in the microwave region," IRE Trans. on Antennas and Propagation, vol. AP-8, pp. 213–217; March, 1960.
[3] R. Caldecott and W. H. Peake, "Designing low-noise antenna," *Electronics*, vol. 34, pp. 60–63; January 20, 1961.
[4] J. L. Pawsey and R. N. Bracewell, "Radio Astronomy," Oxford University Press, Oxford, Eng.; 1955.
[5] D. C. Hogg, "Effective antenna temperature due to oxygen and water vapor in the atmosphere," *J. Appl. Phys.*, vol. 30, pp. 1417–1419; September, 1959.
[6] R. C. Taylor, "Terrain return measurements, at X, Ku, and Ka band," 1959 IRE National Convention Record, pt. 1, pp. 19–26.
[7] A. W. Straiton, C. W. Tolbert, and C. O. Britt, "Apparent temperature distribution of some terrestrial materials and the sun at 4.3 mm wavelength," *J. Appl. Phys.*, vol. 29, pp. 776–782; May, 1958.
[8] E. Jahnke and F. Emde, "Tables of Functions," Dover Publications, Inc., New York, N. Y.; 1948.

Diffraction of a Plane Wave by a Perfectly Conducting Sphere with a Concentric Shell*

MARTIN A. PLONUS†, MEMBER, IRE

Summary—**A general solution to the problem of diffraction from a perfectly conducting sphere with a concentric shell spaced any distance from the surface of the sphere is presented. If the shell consists of a dielectric material the solution simplifies by using asymptotic expressions for the spherical Bessel function. Another simplification results when the shell is assumed to be thin.**

THE THEORY of diffraction of plane-electromagnetic waves from a sphere was formulated by Mie.[1] This theory and the relevant method of Hansen are concisely presented by Stratton.[2] Aden and Kerker[3] gave the exact solution for scattering of an incident plane wave by a sphere of arbitrary material, with a surface layer of arbitrary material imbedded in an arbitrary medium. Scharfman[4] specialized these results for a perfectly conducting sphere with a dielectric coating.

The opinion was held by some people that the scattering cross section of a perfectly conducting sphere with a shell spaced a resonant distance from the sphere could be increased markedly above that of a sphere alone. To obtain some insight, the easier analogous two-dimensional problem of a perfectly conducting cylinder with two surrounding layers was done first.[5] Calculations were performed which showed that the scattering return over a reasonable bandwidth was not changed significantly. These calculations did show, however, the existence of sharp, narrow peaks and dips as the shell spacing was varied. Having shown the negative conclusions for the cylinder, it was found desirable to analyze the sphere.

This paper gives a general solution to the problem of electromagnetic diffraction from a perfectly conducting sphere with a concentric surrounding shell spaced any distance from the surface of the sphere. The shell is of arbitrary thickness and of material characterized by a propagation constant β. The space between the shell and the sphere is characterized by the propagation constant k, which is also the propagation constant of the medium in which this whole structure is inserted. Fig. 1 shows the notation and cross section of the spherical structure and the orientation of the incident plane wave. The perfectly conducting sphere has a radius a, the shell is spaced a distance b from the sphere, and the thickness of the shell is $c-b$. The symbol δ will be used later for the shell thickness. The different regions are denoted by Roman numerals and their respective propagation constants. The only restriction on the different media is that the permeability be the same in all regions, *i.e.*,

$$\mu_{\mathrm{I}} = \mu_{\mathrm{II}}.$$

Different permeabilities could be included, but this would lengthen the algebra somewhat.

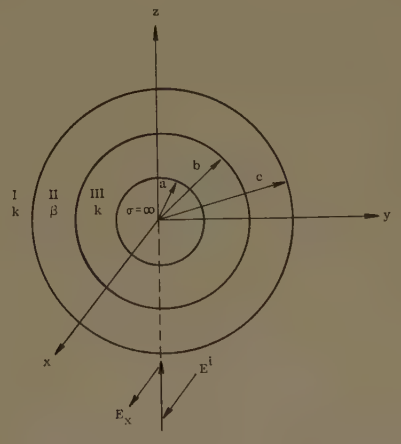

Fig. 1—Notation and cross section of the spherical structure.

The incident plane wave propagates in the positive z direction, its electric vector is linearly polarized in the x direction, and time dependence of $e^{-i\omega t}$ is implied. With these restrictions the expressions for the incident plane wave have the form given by Stratton[2]

$$E_i^{\mathrm{I}} = E_0 \sum_{n=1}^{\infty} i^n \frac{2n+1}{n(n+1)} \left[m_{o1n}^{(1)} - i n_{e1n}^{(1)} \right]$$

$$H_i^{\mathrm{I}} = \frac{-kE_0}{\omega\mu} \sum_{n=1}^{\infty} i^n \frac{2n+1}{n(n+1)} \left[m_{e1n}^{(1)} + i n_{o1n}^{(1)} \right].$$

* Received by the PGAP, July 7, 1961. The research reported in this paper was supported by the AF Cambridge Res. Labs., under contract AF 19(604)6655.

† Dept. of Elec. Engrg., Northwestern University, Evanston, Ill.

[1] G. Mie, "Beiträge zur Optik trüber Medien," *Ann. der Phys.*, vol. 25, pp. 377–445; 1908.

[2] J. A. Stratton, "Electromagnetic Theory," McGraw-Hill Book Co., Inc., New York, N. Y., pp. 563–573; 1941.

[3] A. L. Aden and M. Kerker, "Scattering of electromagnetic waves from two concentric spheres," *J. Appl. Phys.*, vol. 22, pp. 1242–1246; October, 1951.

[4] H. Scharfman, "Scattering from dielectric coated spheres in the region of the first resonance," *J. Appl. Phys.*, vol. 25, pp. 1352–1356; November, 1954.

[5] M. A. Plonus, "Backscattering from a conducting cylinder with a surrounding shell," *Canad. J. Phys.*, vol. 38, pp. 1665–1676; December, 1960.

The diffracted fields are written as expansions similar to those for the incident wave, but with unknown amplitude coefficients a_n and b_n, thus

$$E_s^{\mathrm{I}} = E_0 \sum_{n=1}^{\infty} i^n \frac{2n+1}{n(n+1)} [a_n m_{o1n}^{(3)} - i b_n n_{e1n}^{(3)}]$$

$$H_s^{\mathrm{I}} = \frac{-kE_0}{\omega\mu} \sum_{n=1}^{\infty} i^n \frac{2n+1}{n(n+1)} [b_n m_{e1n}^{(3)} + i a_n n_{o1n}^{(3)}].$$

In region II the electromagnetic field can be written

$$E^{\mathrm{II}} = E_0 \sum_{n=1}^{\infty} i^n \frac{2n+1}{n(n+1)} [c_n m_{o1n}^{(1)} - i d_n n_{e1n}^{(1)} + e_n m_{o1n}^{(3)} - i f_n n_{e1n}^{(3)}]$$

$$H^{\mathrm{II}} = \frac{-\beta E_0}{\omega\mu} \sum_{n=1}^{\infty} i^n \frac{2n+1}{n(n+1)} [d_n m_{e1n}^{(1)} + i c_n n_{o1n}^{(1)} + f_n m_{e1n}^{(3)} + i e_n n_{o1n}^{(3)}],$$

where the unknown coefficients are c_n, d_n, e_n, and f_n. In region III the electromagnetic field can be written similarly

$$E^{\mathrm{III}} = E_0 \sum_{n=1}^{\infty} i^n \frac{2n+1}{n(n+1)} [g_n m_{o1n}^{(1)} - i h_n n_{e1n}^{(1)} + 1_n m_{o1n}^{(3)} - i p_n n_{e1n}^{(3)}]$$

$$H^{\mathrm{III}} = \frac{-kE_0}{\omega\mu} \sum_{n=1}^{\infty} i^n \frac{2n+1}{n(n+1)} [h_n m_{e1n}^{(1)} + i g_n n_{o1n}^{(1)} + p_n m_{e1n}^{(3)} + i l_n n_{o1n}^{(3)}],$$

with unknown coefficient g_n, h_n, l_n, and p_n. To solve for these ten coefficients we apply the boundary conditions

$$\hat{\imath}_1 \times E^{\mathrm{III}}(kb) = \hat{\imath}_1 \times E^{\mathrm{II}}(\beta b)$$
$$\hat{\imath}_1 \times H^{\mathrm{III}}(kb) = \hat{\imath}_1 \times H^{\mathrm{II}}(\beta b)$$
$$\hat{\imath}_1 \times E^{\mathrm{II}}(\beta c) = \hat{\imath}_1 \times E^{\mathrm{I}}(kc)$$
$$\hat{\imath}_1 \times H^{\mathrm{II}}(\beta c) = \hat{\imath}_1 \times H^{\mathrm{I}}(kc)$$
$$\hat{\imath}_1 \times E^{\mathrm{III}}(ka) = 0,$$

where $\hat{\imath}_1$ is a unit vector in the radial direction.

These conditions lead to two sets of simultaneous equations involving five unknowns each. However, since we are interested only in the diffracted field we solve only for coefficients a_n and b_n explicitly. The total cross section is

$$Q_s = \frac{2\pi}{|k|^2} \sum_{n=1}^{\infty} (2n+1)(|a_n|^2 + |b_n|^2)$$

and the backscattering cross section is

$$\sigma = \pi \left| \frac{1}{k} \sum_{n=1}^{\infty} (-1)^n (2n+1)(a_n - b_n) \right|^2.$$

In the subsequent solution for the scattering coefficients the notation has been simplified by deleting all subscripts $_n$ on the spherical Bessel functions, *i.e.*,

$$j(ka) = j_n(ka) = \sqrt{\frac{\pi}{2ka}}\, J_{n+\frac{1}{2}}(ka)$$

$$[\beta b h(\beta b)]' = \frac{\partial}{\partial \beta b} [\beta b h_n^{(1)}(\beta b)] = \frac{\partial}{\partial \beta} \sqrt{\frac{\pi \beta b}{2}}\, H_{n+\frac{1}{2}}^{(1)}(\beta b).$$

After solving these sets of equations the first scattering coefficient a_n is

$$a_n = -\frac{[kcj(kc)]'A + j(kc)B}{[kch(kc)]'A + h(kc)B},$$

where A is given by

$$\begin{aligned} A = {} & j(ka)\{j(\beta c)(h(\beta b)[kbh(kb)]' - h(kb)[\beta b h(\beta b)]') \\ & - h(\beta c)(j(\beta b)[kbh(kb)]' - h(kb)[\beta b j(\beta b)]')\} \\ & - h(ka)\{j(\beta c)(h(\beta b)[kbj(kb)]' - j(kb)[\beta b h(\beta b)]') \\ & - h(\beta c)(j(\beta b)[kbj(kb)]' - j(kb)[\beta b j(\beta b)]')\} \end{aligned}$$

and B is given by

$$\begin{aligned} B = {} & [\beta c j(\beta c)]'\{h(ka)(h(\beta b)[kbj(kb)]' - j(kb)[\beta b h(\beta b)]') \\ & - j(ka)(h(\beta b)[kbh(kb)]' - h(kb)[\beta b h(\beta b)]')\} \\ & - [\beta c h(\beta c)]'\{h(ka)(j(\beta b)[kbj(kb)]' - j(kb)[\beta b j(\beta b)]') \\ & - j(ka)(j(\beta b)[kbh(kb)]' - h(kb)[\beta b j(\beta b)]')\}. \end{aligned}$$

The second scattering coefficient b_n is given by

$$b_n = -\frac{kj_n(kc)C + \frac{1}{kc}[kcj_n(kc)]'D}{kh_n^{(1)}(kc)C + \frac{1}{kc}[kch_n^{(1)}(kc)]'D}$$

where C is given by

$$\begin{aligned} C = {} & [kaj(ka)]'\left\{\frac{1}{\beta c}[\beta c j(\beta c)]'\left(kh(kb)\frac{1}{\beta b}[\beta b h(\beta b)]' - \beta h(\beta b)\frac{1}{kb}[kbh(kb)]'\right)\right. \\ & - \frac{1}{\beta c}[\beta c h(\beta c)]'\left(kh(kb)\frac{1}{\beta b}[\beta b j(\beta b)]' - \beta j(\beta b)\frac{1}{kb}[kbh(kb)]'\right) \\ & - [kah(ka)]'\left\{\frac{1}{\beta c}[\beta c j(\beta c)]'\left(kj(kb)\frac{1}{\beta b}[\beta b h(\beta b)]' - \beta h(\beta b)\frac{1}{kb}[kbj(kb)]'\right)\right. \\ & \left. \left. - \frac{1}{\beta c}[\beta c h(\beta c)]'\left(kj(kb)\frac{1}{\beta b}[\beta b j(\beta b)]' - \beta j(\beta b)\frac{1}{kb}[kbj(kb)]'\right)\right\} \end{aligned}$$

and D is given by

$$D = \beta j(\beta c)\left\{[kah(ka)]'\left(kj(kb)\frac{1}{\beta b}[\beta bh(\beta b)]' - \beta h(\beta b)\frac{1}{kb}[kbj(kb)]'\right)\right\}$$
$$- [kaj(ka)]'\left(kh(kb)\frac{1}{\beta b}[\beta bh(\beta b)]' - \beta h(\beta b)\frac{1}{kb}[kbh(kb)]'\right)\Bigg\}$$
$$- \beta h(\beta c)\left\{[kah(ka)]'\left(kj(kb)\frac{1}{\beta b}[\beta bj(\beta b)]' - \beta j(\beta b)\frac{1}{kb}[kbj(kb)]'\right)\right.$$
$$\left. - [kaj(ka)]'\left(kh(kb)\frac{1}{\beta b}[\beta bj(\beta b)]' - \beta j(\beta b)\frac{1}{kb}[kbh(kb)]'\right)\right\}.$$

A check on these expressions can be made by letting $\beta = k$. When this is done, the above coefficients become the coefficients for a perfectly conducting sphere of radius ka.[2]

If the shell is a dielectric with $\beta > k$ and if $\beta b > 1$, asymptotic expressions for the spherical Bessel and Hankel functions can be used, which are

$$j(\beta c) \cong \frac{1}{\beta c}\cos\left(\beta c - \frac{n+1}{2}\pi\right)$$
$$h(\beta b) \cong \frac{1}{\beta b}e^{i(\beta b-(n+1)/2\pi)}$$
$$[\beta bj(\beta b)]' \cong -\sin\left(\beta b - \frac{n+1}{2}\pi\right)$$
$$[\beta ch(\beta c)]' \cong ie^{i(\beta c-(n+1)/2\pi)}.$$

When these are substituted in the above expressions for the coefficients a_n and b_n and the value for the Wronskian, which is

$$j(kb)h'(kb) - h(kb)j'(kb) = \frac{i}{(kb)^2},$$

is used to simplify the results, the following expressions for the coefficients are derived:

$$a_n = -\frac{\beta cj(kc)(\alpha\cos\beta\delta - \beta b\rho\sin\beta\delta) - [kcj(kc)]'(\alpha\sin\beta\delta \times \beta b\rho\cos\beta\delta)}{\beta ch(kc)(\alpha\cos\beta\delta - \beta b\rho\sin\beta\delta) - [kch(kc)]'(\alpha\sin\beta\delta + \beta b\rho\cos\beta\delta)}$$
$$b_n = -\frac{\beta cj(kc)(\xi\cos\beta\delta - \beta b\gamma\sin\beta\delta) - (\beta/k)^2[kcj(kc)]'(\xi\sin\beta\delta + \beta b\gamma\cos\beta\delta)}{\beta ch(kc)(\xi\cos\beta\delta - \beta b\gamma\sin\beta\delta) - (\beta/k)^2[kch(kc)]'(\xi\sin\beta\delta + \beta b\gamma\cos\beta\delta)},$$

where

$$\delta = c - b$$
$$\rho = h(ka)j(kb) - j(ka)h(kb)$$
$$\alpha = h(ka)[kbj(kb)]' - j(ka)[kbh(kb)]'$$
$$\gamma = j(kb)[kah(ka)]' - h(kb)[kaj(ka)]'$$
$$\xi = ([kah(ka)]'[kbj(kb)]' - [kaj(ka)]'[kbh(kb)]')(\beta/k)^2.$$

These scattering coefficients can be checked by letting $b = c = a$ or $\delta \to 0$. When this is done the coefficients for a perfectly conducting cylinder of radius a should be obtained.[2] This is indeed the case, since the above expressions under these substitutions become

$$a_n = -\frac{j(ka)}{h(ka)}$$
$$b_n = -\frac{[kaj(ka)]'}{[kah(ka)]'}.$$

Similarly, letting $\beta \to \infty$ the shell becomes perfectly reflecting and the scattering coefficients are identical to those of a perfectly conducting cylinder of radius c.

A further simplification results in the expression for the coefficients becoming more manageable if the shell is assumed also to be thin, *i.e.*,

$$\beta\delta < 1.$$

When this is the case all terms containing kc and βc can be expanded in a Taylor series about kb and βb, respectively. Thus,

$$j(kc) = j(kb) + k\delta j'(kb) + \cdots$$
$$[kch(kc)]' = [kbj(kb)]' + k\delta[kbj(kb)]'' + \cdots$$
$$\sin\beta\delta = \beta\delta + \cdots$$
$$\cos\beta\delta = 1 + \cdots.$$

Keeping only terms of order $k\delta$ and $\beta\delta$ in the above expansions and making use of the conditions $\beta > k$ and $\beta b > 1$, the last expressions for the coefficients simplify to

$$a_n = -\frac{i(\beta/k)j(ka) + \beta\delta\rho j(kb)((\beta b)^2 - (kb)^2 + n(n+1))}{i(\beta/k)h(ka) + \beta\delta\rho h(kb)((\beta b)^2 - (kb)^2 + n(n+1))}$$
$$b_n = \frac{i(\beta/k)^3[kaj(ka)]' - \beta\delta[\xi(kbj(kb)]'(1 - (\beta/k)^2) - \gamma j(kb)((\beta b)^2 - (\beta/k)^2((kb)^2 - n(n+1)))]}{i(\beta/k)^3[kah(ka)]' - \beta\delta[\xi[kbh(kb)]'(1 - (\beta/k)^2) - \gamma h(kb)((\beta b)^2 - (\beta/k)^2((kb)^2 - n(n+1)))]}.$$

For further simplification, the denominator of each expression can be expanded and, again neglecting terms of order higher than $\beta\delta$, the scattering coefficients are expressed in a convenient form that exhibits the scattering coefficients of the perfectly conducting cylinder and a perturbation term due to the shell, *i.e.*,

$$a_n = -\frac{j(ka)}{h(ka)}\left(1 - ik\delta\frac{\rho^2((\beta b)^2 - (kb)^2 + n(n+1))}{j(ka)h(ka)}\right)$$

$$b_n = -\frac{[kaj(ka)]'}{[kah(ka)]'}\Bigg)1 - ik\delta\frac{k}{b}$$

$$\cdot\frac{\xi^2(k/\beta)^2(1-(k/\beta)^2) + \gamma^2 n(n+1)}{[kaj(ka)]'[kah(ka)]'}\Bigg).$$

The form of these coefficients is similar to that obtained for a perfectly conducting cylinder, with a surrounding thin shell.[5] It is believed, therefore, that the scattering properties of a perfectly conducting sphere with a concentric thin shell should not differ markedly from those of a cylinder with a thin shell. Calculations for a cylinder with a thin shell showed that the scattering cross section is not significantly increased or decreased over a reasonable bandwidth.

ACKNOWLEDGMENT

The author wishes to thank Prof. K. M. Siegel, Dr. R. F. Goodrich and Dr. T. B. A. Senior for some valuable discussions. Their assistance is gratefully acknowledged.

CORRECTION

Roger F. Harrington, author of "Sidelobe Reduction by Nonuniform Element Spacing," which appeared on pages 187–192 of the March, 1961, issue of these TRANSACTIONS, has called the following to the attention of the *Editor*.

Define Neumann's number as

$$\beta_n = \begin{cases} 1 & n = 0 \\ 2 & n > 0. \end{cases}$$

Replace $\sum_n$ by $\sum_n \beta_n$ in (4) and (7) to (10). Delete the number 2 from the right-hand sides of (11), (13) and (16). These corrections make no changes in the calculations because the amplitudes of the ϵ_n were adjusted by a trial procedure.

communications

Aperture Fields*

Several recent reports[1,2] utilize an expression for the field radiated by an aperture source as given by Silver,[3] but they fail to recognize the limitation of this formula. Specifically, use is made of (8a)[4] which is

$$U_p \approx \frac{j}{2\lambda R}(1+\cos\theta)e^{-jkR}\int_A F(\xi,\eta) \cdot e^{jk\sin\theta(\xi\cos\phi+\eta\sin\phi)}d\xi d\eta.$$

In this equation, U_p is the scalar field component in the same direction as the uniformly polarized aperture field, while $F(\xi,\eta)$ is the aperture field distribution; the polar axis is taken normal to the aperture.[5]

If the details of the derivation of the above equation are considered, then the following assumptions are required:

1) field point is in the far zone,
2) the aperture field is uniformly polarized,
3) a uniform aperture phase distribution,
4) polar angle θ is small.

Condition 4) is the one which is violated in Adams, *et al.*,[1] and Blumberg,[1,2] and the behavior for $30°<\theta<90°$ is incorrectly predicted. Actually, the above equation may be derived in a somewhat different way whereupon no restriction on θ is imposed, and where condition 3) does not appear.

If, for example, the aperture electric field is $F(\xi,\eta)$ in the η direction, then the aperture may be closed by a perfect conductor on which a magnetic surface current

$$nxE = -Fa_\xi$$

is placed. Assuming the aperture to lie in a conducting screen of infinite extent, the effect of this screen may be accounted for by image theory. The result is a doubling of the magnetic current which now is assumed to be in free space. The magnetic vector potential π of the magnetic current $-2Fa_\xi$ is simply

$$\pi = \frac{1}{2\pi}\int \frac{nxFa_\eta}{r}e^{-jkr}dS.$$

This produces an electric field given by $\nabla x\pi$ so that for the assumed geometry, and subject to the usual far-zone approximation,

$$E = (a_\eta\cos\theta - a_z\sin\theta\sin\phi)\frac{je^{-jkR}}{\lambda R}\int_A F(\xi,\eta) \cdot e^{jk\sin\theta(\xi\cos\phi+\eta\sin\phi)}d\xi d\eta.$$

This shows the correct dependence of the electric field, in both direction and magnitude, on the polar angle θ and azimuth angle ϕ (measured from the ξ axis). For $\theta\approx 0$, this result reduces to the earlier form.

R. Plonsey
Case Inst. Tech.
Cleveland, Ohio

* Received by the PGAP, June 9, 1961.

[1] W. B. Adams, *et al.*, "Synthetic Aperture Antenna Investiation," General Electric Co., Syracuse, N. Y., Tech. Note No. 1; September, 1960.
[2] M. Blumberg, "The Effect on the Antenna Pattern of Symmetrical Phase Shifts in a One-Dimensional Aperture," Electronic Defense Labs., Mountain View, Calif.; December, 1959.
[3] S. Silver, "Microwave Antenna Theory and Design," McGraw-Hill Book Co., Inc., New York, N. Y.; 1949.
[4] *Ibid.*, p. 173.
[5] *Ibid.*, see Fig. 6.1, p. 170.

Feed System for Clockwise and Counterclockwise Circular Polarization*

For certain radioastronomical applications (for instance, investigating the "atmosphere" of planets), the use of antennas which permit the simultaneous reception of clockwise and counterclockwise circularly-polarized signals is necessary. Recently, a novel feed system of this kind for an 85-feet paraboloid antenna was developed.

* Received by the PGAP, June 12, 1961. This work was carried out for the Jet Propulsion Lab., Pasadena, Calif., as part of Contract No. P.1.104499.

Description of the Feed System

The feed system consists of four main parts (Fig. 1):

1) Combiner
2) 45° Transformer
3) 90° Phase Shifter
4) Finloaded Horn.

The function of these components will be descrbed below.

1) *Combiner:* The combiner is the heart of the feed system. It combines two signals, linearly polarized but perpendicularly oriented to each other, into a common output and vice versa. The combiner has two rectangular standard inputs (Fig. 2). These inputs are connected to a square waveguide section via quarter-wave transformers. The

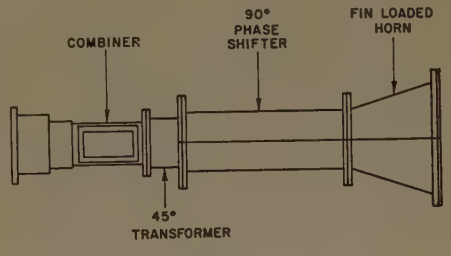

Fig. 1.

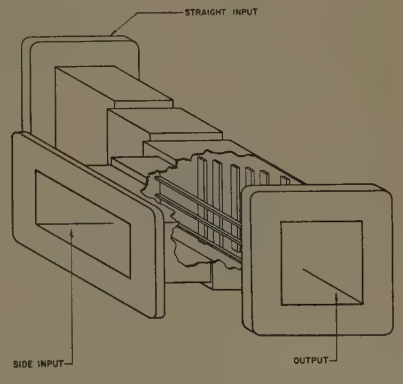

Fig. 2.

size of the square waveguide section is chosen so that both polarizations can be supported ($\lambda > 2a$) where a is the dimension of the side of the square. In the square section there are thin and narrow metal strips, perpendicular to the electric field of the straight input arm, which operate similar to a 90° miter elbow for the waves coming from the side arm. At the same time, the orientation of these strips ensures that they have practically no effect on the waves coming from the straight input arm.

At the joint of the side arm and the square section there are similar strips, which act as waveguides below cutoff for the signal from the straight arm. Thus, they prevent this signal from entering the side arm, and from causing a direct cross-coupling. As the strips are perpendicular to the E vector in the side arm, they have no effect on the waves coming from there.

The combiner's output is square, where eventually both polarizations appear.

2) *45° Transformer:* The combiner is followed by a quarter-wave long circular guide. Its output flange is rotated 45° relative to the input. This section breaks any linearly-polarized wave coming from the input into two perpendicular and equal-amplitude components at the output.

3) *90° Phase Shifter:*[1] If the relative phase of one of the two perpendicular components is shifted by 90° relative to the other, the result will be a circularly polarized wave.[2] The 90° Phase Shifter shifts the phase of the components in this manner. The phase shift is obtained with five pairs of fins located along the two opposite sides of the phase shifter (with square cross section). The fins are capacitive and inductive irises, respectively, for the two polarizations, causing a differential phase shift between the two components.[3] The average phase shift per fin is $\pm 10°$, but according to a Tchebycheff distribution, the middle ones are causing more phase shift than the two end ones.

4) *Finloaded Horn:* The radiating element of the feed system is a specially designed Finloaded Horn.[4] The finloaded horn differs from the conventional pyramidal horn in that it has thin metal fins perpendicular to all four sides (Fig. 3). The fins modify the field in the horn, and, therefore, this new horn has several advantages over the simple pyramidal horn, such as:

a) By proper selection of the fin size the E- and H-plane patterns can be made equal at any arbitrary power level of the main lobe.
b) With the proper number of fins, the first sidelobes can be made equal in both planes.

[1] The 90° Phase Shifter is similar to the one designed by the Rantec Corp. and reported in "Final Report, Design & Test of Primary Feeds for Goldstone Transmitting Antenna," Rantec Project No. P576/621.
[2] J. D. Kraus, "Antennas," McGraw-Hill Book Co., Inc., New York, N. Y., p. 465; 1950.
[3] A. J. Simmons, "Phase shift by periodic loading of waveguide and its application to broad-band circular polarization," IRE TRANS. ON MICROWAVE THEORY AND TECHNIQUES, vol. MTT-3, pp. 18–21; December, 1955.
[4] P. Foldes, "The Finloaded Horn," to be published.

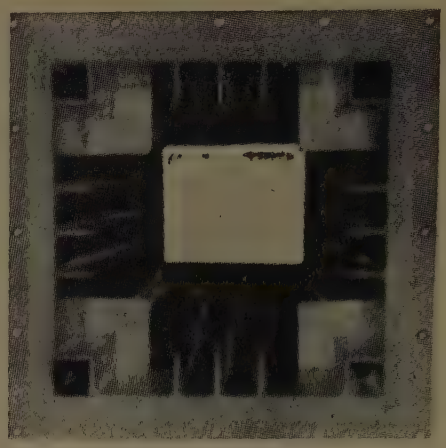

Fig. 3—Finloaded horn.

c) The square shaped horn retains its two symmetry planes, therefore behaves identically for the two perpendicular polarizations.

Over-All System Characteristics and Measuring Methods

The requirements called for a very narrow-band system; therefore, there was no attempt made of broadbanding any of the components of the feed system. A better than 32-db VSWR figure was obtained for all the individual components, over a 1 per cent relative bandwidth.

Table I shows the measured data of the completely-assembled feed system (measured at the design frequency), and Fig. 4 shows the same in diagrams.

TABLE I

	Straight	Input	Side
Reflection (Γ)	1.4 per cent (37 db)		0.7 per cent (43 db)
Cross-coupling (c_{12})		0.28 (51 db)	
Ellipticity (e)	0.2 db		0.2 db

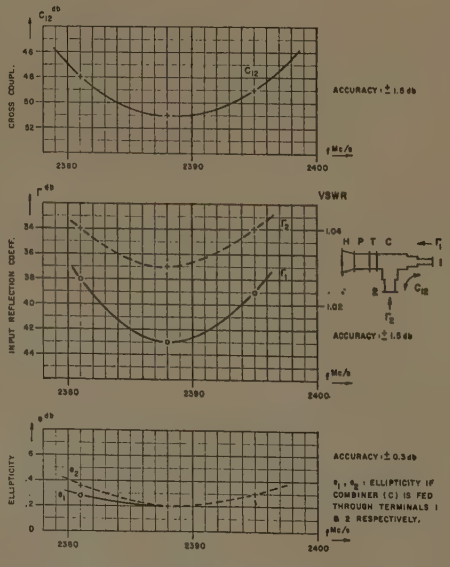

Fig. 4—Electrical characteristics of dual (clockwise and counterclockwise) polarized feed system (measured on 14-db taper horn).

When measuring the ellipticity and cross-coupling, extreme care was taken in avoiding all reflections between the horn and nearby objects because they would cause considerable measuring error. The linearly-polarized antenna for the ellipticity measurement was a piece of waveguide with a slot radiator at its end. It is worthwhile to note the extremely low cross-coupling and ellipticity figures. This low value of ellipticity is practically maintained along the total aperture of the paraboloid because of the high degree of axial symmetry in the feed pattern.

S. G. Komlos
P. Foldes
K. Jasinski
Technical Products Div.
RCA Victor Co., Ltd.
Montreal, Quebec, Canada

Basic Laws of Ionospheric Propagation for Topside Sounding*

In attempting to determine power relations for a topside ionospheric sounder satellite experiment, the author noted that certain well-established relations of ionospheric propagation, such as Breit-Tuve's Theorem and the Secant Law, do not hold in the simple form in which they were originally presented. These results were given in part by Gross.[1] Although these relations may no longer be of great significance in studies of the physics of the ionosphere, they are of importance in power calculations when pulsing the ionosphere from above and for an HF communication link between satellites, if this is conceivable.

It is comparatively easy to understand the physical basis for the modifications when the finite electron density at satellite altitude is considered. Based upon the simplifying assumptions of no magnetic field, negligible collision frequency, variation of electron density with height only, and a flat earth, the basic relationships are revised as proved below.

Fig. 1 illustrates a wave radiated downward at an oblique angle θ_0 from a satellite at point S. This wave is refracted by the ionosphere and returned via an upward-

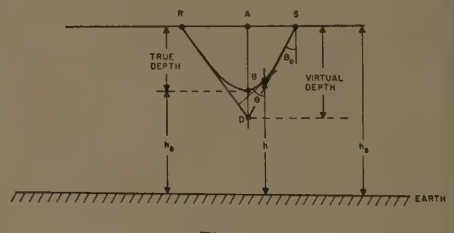

Fig. 1.

* Received by the PGAP, June 12, 1961; revised manuscript received, June 28, 1961.
[1] S. H. Gross, "Ionospheric Characteristics for Topside Sounding," Commission III, presented at the URSI Winter Meeting, Boulder Colo.; December 13, 1960.

traveling ray that crosses the satellite altitude at R.

In the practical example of an ionospheric sounder experiment, the satellite will move from S to R in the time of transmission, and θ_0 will be nearly vertical. However, for the purpose of illustrating relationships, θ_0 will assume all possible values.

The illustration specifies that the virtual depth is the distance $\overline{AD}$, where D is the intersection of the tangents to the curved path $\overset{\frown}{SBR}$ at S and R. This definition conforms to the bottomside meaning of virtual height, rather than an arbitrary convention for vertical incidence, such as $\frac{1}{2}c\tau$, where τ is the time delay between transmitted and received pulses.

$$\text{Virtual depth} = d' = \overline{AD} = \overline{SD}\cos\theta_0 = \overline{SA}/\tan\theta_0. \quad (1)$$

$$\overline{SA} = -\int_{h_s}^{h_B} \tan\theta\, dh$$

$$\overline{SD} = \frac{\overline{SA}}{\sin\theta_0} = -\int_{h_s}^{h_B} \frac{\tan\theta\, dh}{\sin\theta_0}, \quad (2)$$

where

h = altitude
h_s = satellite altitude
h_B = altitude at bottom of path.

The time delay between S and R is

$$\tau = -2\int_{h_s}^{h_B} \frac{dh}{v_g\cos\theta}, \quad (3)$$

where

$$v_g = c\mu = c\sqrt{\left(1 - \frac{Ne^2}{\pi m f_{ob}^2}\right)}$$

= group velocity at any point along $\overset{\frown}{SB}$ (4)

c = velocity of light in a vacuum
μ = index of refraction at frequency f_{ob}
N = electron density
e and m = the electronic charge and mass.

Therefore,

$$\tau = -2\int_{h_s}^{h_B} \frac{dh}{c\mu\cos\theta}. \quad (5)$$

From (2) and Snell's Law, which is

$$\mu\sin\theta = \mu_0\sin\theta_0, \quad (6)$$

where μ_0 = index of refraction of f_{ob} at the satellite altitude,

$$\overline{SD} = -\int_{h_s}^{h_B} \frac{\sin\theta\, dh}{\sin\theta_0\cos\theta}$$

$$= -\mu_0\int_{h_s}^{h_B} \frac{dh}{\mu\cos\theta} \quad (7)$$

$$= \tfrac{1}{2}c\mu_0\tau = \tfrac{1}{2}v_{g_0}\tau \quad (8)$$

or

$$\tau = \frac{2\overline{SD}}{v_{g_0}} = \frac{\overline{SDR}}{v_{g_0}} \neq \frac{\overline{SDR}}{c}, \quad (9)$$

where v_{g_0} = group velocity at the satellite altitude.

Thus, from (9) Breit-Tuve's Theorem is restated as follows: The time taken to traverse the actual curved path $\overset{\frown}{SBR}$ at the group velocity is equal to the time to traverse the triangular path $\overline{SDR}$ at the group speed of the point of emission.

In the limit of zero electron density, as at the earth's surface, $v_{g_0} = c$, and the commonly accepted form of the theorem applies.

If we radiate obliquely at a frequency f_{ob} and reach the same depth $\overline{AB}$ as a vertically downward radiation at frequency f_v, the modified Secant Law is derivable as follows: The oblique ray makes an angle of 90° to the vertical at B where the plasma frequency must be f_v; therefore,

$$\mu_B(f_{ob}) = \mu_s(f_{ob})\sin\theta_0 \quad (10)$$

where $\mu_B(f_{ob})$ and $\mu_S(f_{ob})$ are the indexes of refraction at B and S for frequency f_{ob}. Using f_0 as the local plasma frequency at the satellite altitude,

$$\mu_B^2(f_{ob}) = 1 - \frac{f_v^2}{f_{ob}^2} \quad (11)$$

$$\mu_s^2(f_{ob}) = 1 - \frac{f_0^2}{f_{ob}^2} \quad (12)$$

and, from (10)–(12),

$$f_{ob} = \sqrt{f_v^2 - f_0^2\sin^2\theta_0}\sec\theta_0. \quad (13)$$

Eq. (13) is the modified form of the Secant Law, which for zero electron density, as at the earth's surface, becomes the commonly used form.

Since the Breit-Tuve and Secant relations are modified, what about Martyn's Theorem?

Let μ_{ob} and μ_v be the indexes of refraction at the same height but at oblique and vertical incidence frequencies, respectively. Then, using $\mu_s(f_{ob})$ and $\mu_s(f_v)$ for the conditions at satellite altitude, we have, from Snell's Law [(6) and (13)], the relationship

$$\mu_{ob}\cos\theta = \frac{\mu_v\cos\theta_0}{\sqrt{1 - \frac{f_0^2}{f_v^2}\sin^2\theta_0}}. \quad (14)$$

This applies all along $\overline{SB}$ and is equally applicable to $\overline{S}$, for which we have

$$\mu_s(f_{ob})\cos\theta_0 = \frac{\mu_s(f_v)\cos\theta_0}{\sqrt{1 - \frac{f_0^2}{f_v^2}\sin^2\theta_0}}. \quad (15)$$

Using (7) for vertical incidence ($\cos\theta = 1$), the vertical incidence virtual depth is

$$d'_{v.i.} = -\mu_s(f_v)\int_{h_s}^{h_B} \frac{dh}{\mu_v}. \quad (16)$$

From (1) and (7) for oblique incidence

$$d'_{ob.i.} = -\mu_s(f_{ob})\cos\theta_0\int_{h_s}^{h_B} \frac{dh}{\mu_{ob}\cos\theta}. \quad (17)$$

From (14) and (15),

$$\frac{\mu_s(f_{ob})\cos\theta_0}{\mu_{ob}\cos\theta} = \frac{\mu_s(f_v)}{\mu_v}. \quad (18)$$

Using (18) in (17) and (16),

$$d'_{ob.i.} = -\mu_s(f_v)\int_{h_s}^{h_B} \frac{dh}{\mu_v} = d'_{v.i.}. \quad (19)$$

Thus, though the Breit-Tuve Theorem and the Secant Law required modification, Martyn's Theorem holds in its original form, namely (using depths instead of heights):

The virtual depth of an oblique radiation at frequency f_{ob}, which turns at the same depth as a vertical incidence of frequency f_v, is equal to the virtual depth of the vertical incidence.

Of additional interest, using (1) and (8), virtual depth is

$$d'_{ob.i.} = \tfrac{1}{2}v_{g_0}\tau\cos\theta_0 \quad (20)$$

which for vertical incidence becomes

$$d'_{v.i.} = \tfrac{1}{2}v_{g_0}\tau \quad (21)$$

instead of $\frac{1}{2}c\tau$, the bottomside relation. Similar to bottomside propagation, the time delays for oblique and vertical incidence are related by

$$\tau_{v.i.} = \tau_{ob.i.}\cos\theta_0. \quad (22)$$

S. H. Gross
Airborne Instruments Lab.
Deer Park, N. Y.

Reflector Antennas for Radio and Radar Astronomy*

The number of reflector antennas that have been developed during the past three years and that are being contemplated today for radio astronomy has increased substantially. In some areas of research, higher-resolution radio telescopes with improved sensitivity are still in demand; elsewhere, existing instruments appear adequate to provide reliable data. The trend has been toward larger apertures, physical and synthetic, to provide the needed resolution and sensitivity throughout the radio spectrum.

It is the purpose of a recently completed report[1] to present the results of a comprehensive survey of electromechanical data on reflector-type radio telescopes that were known and anticipated as of April, 1961. The results are tabulated for each antenna, grouped by sponsoring countries. The list of 150 reflector entries includes 70 radio observatories in 20 countries.

The tabulation does not cover reflectors that are used exclusively either to determine properties of the earth's ionosphere or to track meteors and space vehicles. Moreover, the physical size of antennas in the survey is no smaller than 10 square meters. Consequently, the author has not included the abundance of small reflectors to be found in solar radio astronomy.

The tabulated information includes the following:

1) The name of the operating observatory and its sponsors.
2) The location of the reflector.

* Received by the PGAP, June 24, 1961.

[1] A. R. Giddis, "Reflector Antennas for Radio and Radar Astronomy," Western Dev. Labs., Philco Corp., Palo Alto, Calif., Rept. No. WDL-TR-1500; April, 1961.

3) The type and dimensions of the reflector.
4) Some of the antenna's mechanical characteristics.
5) The frequency range of operation.
6) Data on the radiation parameters.
7) Use of the reflector in an interferometer.
8) The status of the antenna system.
9) Current and planned uses for the antenna in radio astronomy.
10) Sources of information on each antenna.

The radio observatories are listed alphabetically according to countries, and their associated antennas are tabulated in order of increasing, physical, cross-sectional area above 10 square meters. Data are recorded in both metric and English units.

An extensive list of references consulted during the survey is included.

In order that this report of electromechanical data on the world's radio telescope reflectors will continue to be a useful working document, the author welcomes comments from the reader and will appreciate receiving on a nonconfidential basis for possible future publications, information on new developments and plans for radio telescopes.

ALBERT R. GIDDIS
Communications Sciences Dept.
Western Dev. Labs.
Philco Corp.
Palo Alto, Calif.

Some Comments on the Transmission of Power by the Use of Microwave Beams*

A number of studies and experiments directed toward investigating the feasibility of transmitting power by means of focused microwave beams have been carried out in Raytheon Laboratories during recent years. It is not the purpose of this note to review the entire scope of that activity; however, certain results will be discussed. Representative programs under contract include the fabrication and test of superpower Amplitron tubes,[1] design study and demonstration of a microwave heat exchanger for incorporation into a gas turbine engine,[2] and studies of high-altitude platform design.[3] A number of oral presentations of various aspects of this program have been made;[4] however, data have been published only in reports which receive limited circulation.

We have discussed numerous potential applications of beamed microwave power. Perhaps the most widely known is the Raytheon Airborne Microwave Platform (RAMP) system. Power beamed from a ground antenna is collected at high altitude by an array mounted beneath a rotary-wing platform. Microwave energy is guided to a heat exchanger in which it is converted to heat. The heat exchanger, in turn, provides power to drive a closed-cycle gas turbine engine. A large compressor, turned by the engine shaft, pumps ambient air through blade ducts and out of tip-jets to turn the rotor.

Systems of focused beams have been more widely applied in optical problems than in the microwave field.[5] However, the normal microwave parabolic reflector relies on focusing to transfer the energy from the reflector to the feed device, and numerous antenna systems have been studied which use focusing principles to approximate the far-zone pattern at a convenient site in the near zone.[6,7] A brief discussion of focused antennas for certain power transfer applications has also been published.[8] Thus, the optical principles applicable to quite efficient focused antenna systems have been established in detail.

Under the physical conditions envisioned for the RAMP system, a very large fraction of the energy emitted by the transmitting aperture appears at the focal plane within the focal spot (Airy disk). In an optically perfect, uniformly illuminated, system, nearly 84 per cent of the radiated energy falls within this spot; however, aberrations as well as distortions introduced by the atmosphere tend to degrade the system. By tapering the illumination of the transmitting reflector in a manner which reduces the minor-lobe radiation, as much as 98 per cent of the energy radiated can be confined to the focal spot. Such tapered illumination results in a larger focal spot for a given transmitting antenna. However, if for a given pair of antennas, the coupling is such that uniform illumination would result in more than about 78 per cent of the radiated energy being intercepted by the receiving aperture, the use of apertures with the same diameters would result in a greater interception of energy for the case of tapered illumination. This improvement is a result of the increase in the major lobe energy content due to sidelobe reduction and to the change in the distribution of energy across the focal spot resulting from tapering. The diameter of the focal spot D_A produced in the focal plane at a distance R from an antenna of diameter D_T radiating at wavelength λ is well approximated by

$$D_A = K\lambda R/D_T,$$

where

$K=2.00$ for uniformly illuminated rectangular apertures,
$K=2.44$ for uniformly illuminated circular apertures,
$K=3.26$ for a $(1-\rho^2)$ illumination function.

A typical set of antenna parameters for the RAMP application would be: transmitting aperture 350 ft in diameter, altitude of platform 65,000 ft, and wavelength 1/6 ft. The diameter of the resulting focal spot would be 75 ft. An optimization procedure (weight, power, cost) for the entire system has led to fixing the receiving aperture diameter at 50 ft. This aperture, if centered on the axis of the 350-ft transmitting antenna, would intercept 75 per cent of the transmitted energy (89 per cent of the focal-spot energy). This figure is not to be taken as the efficiency of the antenna system. A realistic over-all figure, estimating both transmitting and receiving apertures to have an efficiency of 65 per cent, is 32 per cent. Although the actual antenna design proposed for the RAMP system was more sophisticated than the simple uniformly illuminated reflector considered in this example, the aperture areas and fraction of radiated power intercepted were similar to the values found above.

In a recent unclassified report, given rather wide circulation and reprinted essentially in full in these TRANSACTIONS,[9] it was asserted that the maximum altitude (R_0) at which the RAMP vehicle could hover with the desired path efficiency is determined by the expression:

$$R_0 \leq (1/\lambda)(AA'/\eta)^{1/2},$$

in which the aperture areas are denoted by A and A' and η is the path efficiency. That author provides a graphical means of estimating the path efficiency as a function of the system parameters.[10] The present authors, scaling from this published graph, determined a path efficiency of 66 per cent for a system using 350-ft diameter and 50-ft antennas. Using this efficiency, the proposed RAMP wavelength of 1/6 ft and aperture areas based on the above diameters yield an altitude of 102,000 ft.

Another parameter of great interest is the depth of focus of the RAMP transmission system. This can be estimated readily from classical theory. At a distance of approximately 10,000 ft above and below the image plane, the 50-ft-diameter receiving aperture could intercept 85 per cent of the

* Received by the PGAP, July 3, 1961.

[1] Rome Air Dev. Ctr., Contract No. AF 30(602)-2205.

[2] Wright Air Dev. Div., Contract No. AF 33(616)-6716.

[3] Army Rocket and Guided Missile Agency, Contract No. DA-19-020-ORD-4944.

[4] For example: W. Brown, NEREM, 1959; H. M. Hart, NEREM, 1959; H. Letaw, Jr., NEREM, 1960.

[5] An excellent discussion is available in M. Born and E. Wolf, "Principles of Optics," Pergamon Press, New York, N. Y.; 1959.

[6] R. W. Bickmore, "Fraunhofer pattern measurement in the Fresnel region," *Can. J. Phys.*, vol. 35, pp. 1299–1308; November, 1957.

[7] G. W. Farnell, "Measured phase distribution in the image space of a microwave lens," *Can. J. Phys.*, vol. 36, pp. 935–943; July, 1958.

[8] R. W. Bickmore, "Power transmission via radio waves," PROC. IRE (Correspondence), vol. 48, pp. 366–367; March, 1960.

[9] A. F. Kay, "Near-field gain of aperture antennas," IRE TRANS. ON ANTENNAS AND PROPAGATION, vol. AP-8, pp. 586–593; November, 1960.

[10] Reference 9 included a computation of the maximum hovering altitude of the RAMP vehicle. Unfortunately, erroneous RAMP system parameters based on a brief discussion of the RAMP system reported in a popular magazine were used. The figures used for antenna aperture sizes were equivalent to a 50-ft-radius airborne antenna and an 11-ft-radius (400 square ft) ground antenna. A wavelength of 0.327 ft was assumed, rather than the value 0.167 ft actually proposed. The ground antenna size was suspected by the author to be erroneous and in a footnote to his example, he surmised that the printed figure, "400 sq ft," might have been a misprint for "400 ft square." Unfortunately, that author computed in his example two inapplicable values for R_0 of 9640 ft and 5040 ft.

maximum focal spot energy. Confirmation of the theoretical depth of focus values for microwave frequencies can be found in the literature.[11]

H. Letaw, Jr.
G. Hamm
Surface Radar and
Navigation Operation, Equipment Div.,
Raytheon Co.
Wayland, Mass.
R. W. Slocum
Systems Requirement Dept., Equipment Div.,
Raytheon Co.
Waltham, Mass.

[11] See for example: C. W. Morrow, P. E. Taylor, and H. T. Ward, "Phase and amplitude measurements in the near field of microwave lenses," 1958 IRE National Convention Record, pt. 1, pp. 166–176.

The Use of the Statistical Matrix and the Stokes Vector in Formulating the Effective Aperture of Antennas*

In a recent communication, Tai[1] has proposed a revised definition for the effective aperture of an antenna which has a broader coverage than the definition given in the "IRE Standards on Antennas." According to the "IRE Standards on Antennas,"[2] the effective aperture (or the aperture area) of an antenna is defined as $\lambda^2 D/4\pi$ where D is the directive gain of the antenna and λ is the wavelength. In many textbooks on antennas, the effective aperture A_e is defined as

$$A_e = \frac{W_{av}}{P_i} = \frac{\text{available power from antenna}}{\text{incident power density}}. \quad (1)$$

Let us consider a monochromatic plane wave $\boldsymbol{E}_i$ incident on an antenna. When the value of W_{av}/P_i as contained in (1) is evaluated, one obtains[1,3]

$$A_e(\theta, \Phi) = p\frac{\lambda^2 D(\theta, \Phi)}{4\pi} \quad (2)$$

where

$$p = \text{polarization factor} = \frac{|\boldsymbol{h}\cdot\boldsymbol{E}_i|^2}{|\boldsymbol{h}|^2|\boldsymbol{E}_i|^2}$$

$\boldsymbol{h}$ = complex vector effective height of the antenna

$\boldsymbol{E}_i$ = incident electric field.

Both $\boldsymbol{h}$ and $\boldsymbol{E}_i$ are complex vectors, representing complete (*i.e.*, elliptical) polarizations. When the polarizations are matched, $p=1$; (2) reduces to the IRE definition. Thus, Tai has suggested the use of (2) as the definition of the effective aperture, which becomes consistent with the physical interpretation of the effective aperture as given by (1).

The formulation as shown in (2) may be further improved in two respects. First, (2) contains a polarization factor p which depends on the polarization state of the incident electric field. It is more satisfactory to formulate the effective aperture only in terms of the parameters associated with the antenna proper. Second, the use of (2) is limited to an incident wave which is completely polarized (*i.e.*, elliptically polarized). An elliptically polarized radio wave is a limiting case of a more general type of wave, that is, a partially polarized wave. Thus, it is desirable to formulate the effective aperture in a form which is applicable to partially polarized waves. The use of antennas for the reception of partially polarized radio waves occurs in radio astronomy, passive radar mapping, microwave plasma diagnostics, etc.

The purpose of this communication is to present two alternative formulations for the effective aperture of the antenna, one based on the statistical matrix and the other based on the Stokes vector. The statistical matrix and the Stokes vector are both used in optics[4] and in the quantum mechanical treatment of the polarization of photons and elementary particles.[5,6] The statistical matrix is sometimes referred to as a density matrix or coherency matrix. The author has recently applied this formalism to the theory of radio antennas.[7]

Let $\boldsymbol{E}_i$ represent the electric field of a quasi-monochromatic wave incident upon a receiving antenna and $\boldsymbol{E}_t$ represent the distant monochromatic electric field produced by the antenna when it is used for transmitting. We may write

$$\boldsymbol{E}_i = \sqrt{\langle \boldsymbol{E}_i\cdot\boldsymbol{E}_i^*\rangle}\,\boldsymbol{n}_i = \sqrt{\langle \boldsymbol{E}_i\cdot\boldsymbol{E}_i^*\rangle}\,(i_\theta n_\theta + i_\Phi n_\Phi) \quad (3)$$

$$\boldsymbol{E}_t = \sqrt{\langle \boldsymbol{E}_t\cdot\boldsymbol{E}_t^*\rangle}\,\boldsymbol{m}_t = \sqrt{\langle \boldsymbol{E}_t\cdot\boldsymbol{E}_t^*\rangle}\,(i_\theta m_\theta + i_\Phi m_\Phi), \quad (4)$$

where $\boldsymbol{n}_i$ and $\boldsymbol{m}_t$ are unit polarization vectors (*i.e.*, $\langle \boldsymbol{n}_i\cdot\boldsymbol{n}_i^*\rangle = 1$ and $\langle \boldsymbol{m}_t\cdot\boldsymbol{m}_t^*\rangle = 1$), $n_\theta = a_1(t)\exp j[\omega t + kr - \alpha_1(t)]$, $n_\Phi = a_2(t)\exp j[\omega t + kr - \alpha_2(t)]$; $m_\theta = b_1 \exp j(\omega t - kr - \beta_1)$, $m_\Phi = b_2 \exp j(\omega t - kr - \beta_2)$. a_1, a_2, α_1 and α_2 vary with time since the incident wave is assumed to be a partially polarized wave. b_1, b_2, β_1 and β_2 are constants. The asterisk represents complex conjugate, and the angular brackets represent the time averages.

We shall define a statistical matrix for the antenna[7] by

$$A_e[\rho_{ij}'] = A_e\begin{bmatrix}\langle m_\theta m_\theta^*\rangle & \langle m_\theta^* m_\Phi\rangle \\ \langle m_\theta m_\Phi^*\rangle & \langle m_\Phi m_\Phi^*\rangle\end{bmatrix}. \quad (5)$$

Similarly, we define a statistical matrix for the incident wave by

$$P[\rho_{ij}] = P\begin{bmatrix}\langle n_\theta n_\theta^*\rangle & \langle n_\theta n_\Phi^*\rangle \\ \langle n_\theta^* n_\Phi\rangle & \langle n_\Phi n_\Phi^*\rangle\end{bmatrix}, \quad (6)$$

where P represents the total power flux of the incident wave. Thus, $P = \frac{1}{2}\langle \boldsymbol{E}_i\cdot\boldsymbol{E}_i^*\rangle/Z_0$ where Z_0 is the intrinsic impedance of the medium

It can be shown[7] that the power available from the antenna due to the incident wave is given by

$$W = \text{Trace}\,\{A_e[\rho_{ij}'] \times P[\rho_{ij}]\}. \quad (7)$$

An alternative formulation for the effective aperture may be made by the use of the Stokes parameters or the Stokes vector. It has been pointed out by Deschamps[8] that the available power from a receiving antenna due to a completely polarized (*i.e.*, elliptically polarized) incident wave may be formulated in terms of the Stokes parameters for the incident wave and for the antenna. It has been shown[7] that the formulation based on the Stokes vector is also valid for an incident wave which is partially polarized. This is due to the fact that the Stokes parameters for a mixture of independent radio waves are the sum of the respective Stokes parameters of the separate waves.

A partially polarized wave may be considered as a mixture of a randomly polarized wave and an elliptically polarized wave independent of the former. Let d represent the degree of polarization which is the ratio of the power flux of the polarized part to the total power flux P. We can then write the Stokes vector for the partially polarized incident wave as

$$P[s_i] = P\begin{bmatrix}s_0\\ s_1\\ s_2\\ s_3\end{bmatrix} = (1-d)P\begin{bmatrix}1\\ 0\\ 0\\ 0\end{bmatrix} + P\begin{bmatrix}d\\ \langle a_1^2\rangle - \langle a_2^2\rangle\\ \langle 2a_1a_2\cos(\alpha_2-\alpha_1)\rangle\\ \langle 2a_1a_2\sin(\alpha_2-\alpha_1)\rangle\end{bmatrix}. \quad (8)$$

The Stokes vector for the antenna may be defined by

$$A_e[s_i'] = A_e\begin{bmatrix}1\\ (b_1^2 - b_2^2)\\ 2b_1b_2\cos(\beta_1-\beta_2)\\ 2b_1b_2\sin(\beta_1-\beta_2)\end{bmatrix}. \quad (9)$$

* Received by the PGAP, June 3, 1961. This work was supported in part by the AF Cambridge Res. Labs. under Contract No. AF 19(604)-4079 through the Ohio State University Res. Foundation.

[1] C. T. Tai, "On the definition of the effective aperture of antennas," IRE Trans. on Antennas and Propagation (Communications), vol. AP-9, pp. 224–225; March, 1961.

[2] "IRE Standards on Antennas, Modulation Systems, and Transmitters," (48 IRE 2, 11, 15.S1) (Separate Report).

[3] E. Roubine, "Les propriétés directives des antennes de réception," *L'Onde Électrique*, vol. 30, pp. 259–266; June, 1950.

[4] M. Born and E. Wolf, "Principles of Optics," Pergamon Press, New York, N. Y.; 1959.

[5] U. Fano, "Remarks on the classical and quantum-mechanical treatment of partial polarization," *J. Opt. Soc. Am.*, vol. 39, pp. 859–863; 1949. Also "Description of states in quantum mechanics by density matrix and operator techniques," *Rev. Mod. Phys.*, vol. 29, pp. 74–93; January, 1957.

[6] J. M. Jauch and F. Rohrlich, "Theory of Photons and Electrons," Addision Wesley Publishing Co., Inc., Reading, Mass.; 1955.

[7] H. C. Ko, "Theoretical techniques for handling partially polarized radio waves with special reference to antennas," Proc. IRE (Correspondence), vol. 49, pp. 1446–1447; September, 1961.

[8] G. A. Deschamps, "Geometrical representation of the polarization of a plane electromagnetic wave," Proc. IRE, vol. 39, pp. 540–544; May, 1951.

It can be shown[7] that

$$W = \tfrac{1}{2}A_e P[\widetilde{s_i'}][s_i] = \tfrac{1}{2}A_e P \sum_{i=0}^{3} s_i' s_i, \quad (10)$$

where $[\widetilde{s_i'}]$ is the transpose of the matrix $[s_i']$.

Thus, either (5) or (9) may be used as a concise definition of the antenna effective aperture. The use of the statistical matrix and the Stokes vector for the antenna also fits in very well with the formalism of the modern theory of optics[4,9] and the quantum theoretical treatment of the polarization of photons and electrons.[5,6]

The author wishes to thank Prof. C. T. Tai for stimulating discussions.

H. C. Ko
Radio Observatory
Dept. of Elec. Engrg.
The Ohio State University
Columbus, Ohio

[9] G. B. Parrent and P. Roman, "On the matrix formulation of the theory of partial polarization in terms of observables," *Nuovo Cimento*, vol. 15, ser. 10, pp. 370–380; February 1, 1960.

Backward-Wave Radiation from an Equiangular Spiral Antenna*

In a recent article, Mayes, *et al.*,[1] suggested the concept of backward waves as an explanation of log periodic antenna behavior. This note applies this concept to Dyson's[2,3] equiangular spiral antennas and shows that it does indeed offer an explanation that agrees with reported experimental results.

First consider the bidirectional equiangular spiral antenna[2] with equal beams radiated from the front and back of the plane structure. The spiral is a periodic structure which supports space harmonics of phase constant

$$\beta_n = \beta_0 + \frac{2n\pi}{a}, \quad (1)$$

where β_0 represents the fundamental wave and a the period of the structure measured in the radial direction. Let the fundamental wave travel along the spiral arms in a regular transmission-line mode with a phase velocity v.

If the first backward wave ($n=-1$) is to propagate in directions perpendicular to the spiral plane, then its relative phase shift along the periodic structure must be zero. That is

$$\beta_{-1} = 0, \quad (2)$$

thus

$$0 = \beta_0 - \frac{2\pi}{a},$$

or

$$\beta_0 a = 2\pi. \quad (3)$$

This means that the fundamental wave changes phase by 2π radians in going one period along the structure. But one period is also one turn, hence, for the first backward wave to radiate broadside, the spiral arm should be about one wavelength long. In this radiation region the backward wave radiates, resulting in a large attenuation in the fundamental wave. Dyson[2] found the low-frequency cutoff to occur when the arm length was in the neighborhood of one wavelength. Thus it appears that radiation could be indeed from the first backward wave. The spirals used by Dyson were less than two turns, producing a very rapid change of the structure per unit wavelength. For these spirals the active radiation region is probably small and not too symmetrical, producing the variation in pattern as a function of the polar angle as recorded by Dyson. He also stated that tighter-spiraled antennas have more uniform patterns. This is to be expected since the tighter spiral reduces the rate of change of the periodic structure and thus increases the active radiation region.

The unidirectional spiral antenna[3] offers an even more interesting comparison. Again let the fundamental wave travel along the conical spiral with a relative phase velocity v. For regular end fire propagation in a direction toward the cone apex, the backward wave must have a relative phase shift along the periodic structure just equal to that of a free-space wave, that is

$$|\beta_{-1}| = |k|.$$

The phase constants of the fundamental and first backward-wave are related as follows:

$$\beta_0 a - 2\pi = \beta_{-1} a = -ka \quad (4)$$

where the minus sign merely indicates that the backward-wave phase constant is negative compared to a positive value for the fundamental wave. Reference to Fig. 1 shows that

$$\beta_0 a = \beta L, \quad (5)$$

where

$\beta = k(c/v)$ phase constant along the wire,
L = length of 1 turn
$a = L\cos\alpha$ = periodic spacing,
$\pi D = L\sin\alpha$ = average circumference.

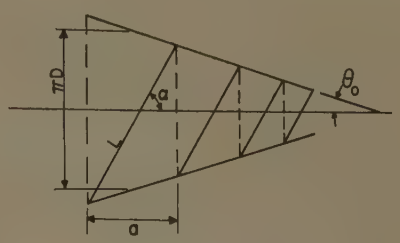

Fig. 1—Conical antenna.

Substitution of (5) into (4) shows that radiation occurs when

$$\lambda = \frac{\pi D}{\sin\alpha}\left[\frac{c}{v} + \cos\alpha\right]. \quad (6)$$

As an example, let $c/v = 1.0$ and $\alpha = 73°$, then (6) gives $D \approx 0.24\ \lambda$. Thus, for a given frequency, the fundamental wave travels from the feed point away from the apex until the cone diameter reaches 0.24 λ. At this point the backward wave radiates and thus extracts energy from the fundamental wave. On a triangular-tooth log periodic antenna[4] the fundamental wave is attenuated some 20 db in a distance, measured along the axis, of 0.3 to 0.4 of a wavelength. For the examples given by Dyson,[3] the active region appears to be about the same length. The active region starts when $D \approx 0.25\ \lambda$ and terminates when D reaches 0.3 to 0.35 λ. Thus, as the frequency is decreased, this active region moves away from the apex toward the base. When the base diameter approaches 0.3 to 0.35 λ, the lowest cutoff frequency is reached. In a similar manner, an apex diameter of about 0.24 λ represents the upper cutoff frequency.

R. A. Hessemer, Jr.
University of Arizona
Tucson, Ariz.

[4] R. L. Bell, *et al.*, "Near-field measurements on a logarithmically periodic antenna," IRE Trans. on Antennas and Propagation, vol. AP-8, pp. 559–567; November, 1960.

Reflection of a TE Wave from an Inverse Parabolic Ionization Density*

The presence of shock-induced ionization of the atmosphere in the vicinity of high-speed bodies has motivated the solution of Maxwell's equations for the propagation of a plane wave in media in which the complex index of refraction varies with the depth. (Such solutions are also of interest in ionospheric propagation studies.) For most purposes, the quantity of primary interest is the complex reflection coefficient R. In the present note, we shall determine the reflection coefficient for an electron density which varies as z^{-2}. This variation is intended to represent in the right half plane an electron density which increases monotonically from zero at some positive z, rising to a large (but finite) value at $z=0$, and terminated in a metallic wall at the origin.

We consider an electrically neutral medium in which the electron density varies as z^{-2}. The index of refraction in the medium is taken to be

$$n = [1 - \gamma z^{-2}]^{1/2}, \quad (1)$$

* Received by the PGAP, July 8, 1961.
[1] P. E. Mayes, *et al.*, "Backward-wave radiation from periodic structures and application to the design of frequency independent antennas," Proc. IRE (Correspondence), vol. 49, pp. 962–963; May, 1961.
[2] J. D. Dyson, "The equiangular spiral antenna," IRE Trans. on Antennas and Propagation, vol. AP-7, pp. 181–187; April, 1959.
[3] J. D. Dyson, "The unidirectional equiangular spiral antenna," IRE Trans. on Antennas and Propagation, vol. AP-7, pp. 329–334; October, 1959.

* Received by the PGAP, July 29, 1961. This work was supported by Air Force Contract 30(602)-1968.

where

$$\gamma = [1 - iv_c/\omega]^{-1}. \quad (2)$$

Here ω is the frequency of the incident electromagnetic wave and v_c is the effective electron-collision frequency. The negative sign appears in (2) by virtue of the choice of the positive exponential for the time dependence of the field. Eq. (1) may be considered to be the result of choosing a coordinate scale such that the critical density level is reached at $z=1$. Assuming a TE wave incident from $+\infty$ in the yz-plane, it may be shown from Maxwell's equations[1] that

$$E_x(y, z, t) = u(z) \exp [i(k_0 \sin\theta_i \cdot y + \omega t)], \quad (3)$$

where $k_0 = w/c$ and

$$\frac{d^2u}{dz^2} + k_0^2[n^2(z) - \sin^2\theta_i]u = 0. \quad (4)$$

In these expressions, θ_i is the angle of incidence. Eq. (3) is the result of a separation of variables; the form of the y-dependence is an expression of the generalized Snell's Law, $k \sin\theta = \text{const}$. Combining (1) and (4) we obtain

$$\frac{d^2u}{dz^2} + (\beta^2 - k_0^2\gamma z^{-2})u = 0, \quad (5)$$

where

$$\beta = k_0 \cos\theta_i. \quad (6)$$

It is convenient to define

$$P^2 = k_0^2\gamma + \tfrac{1}{4}. \quad (7)$$

Then (5) may be written as

$$\frac{d^2u}{dz^2} + \left(\beta^2 - \frac{4P^2 - 1}{4z^2}\right)u = 0. \quad (8)$$

Eq. (8) reduces to a standard form of the Bessel equation when $z^{1/2}v(z)$ is substituted for the dependent variable. Thus

$$u = Az^{1/2}J_P(\beta z) + Bz^{1/2}J_{-P}(\beta z), \quad (9)$$

where P is taken as the positive root of (7), and is complex. Despite the novelty of the complex order, the usual expansions[2] for the Bessel functions are still valid. Therefore,

$$J_{-P}(\beta z) = \sum_{r=0}^{\infty} \frac{(-1)^r(\beta z/2)^{2r-P}}{r!\Gamma(r + 1 - P)}. \quad (10)$$

As z approaches zero,

$$z^{1/2}J_{-P}(\beta z) \sim z^{1/2-P}. \quad (11)$$

Since from (7) Re $\{P\} > \frac{1}{2}$, the magnitude of this term diverges as z approaches zero and we must take $B=0$ in (9). Thus

$$u = Az^{1/2}J_P(\beta z). \quad (12)$$

The asymptotic expansions of the Bessel functions are valid for complex orders, so that at large z the wave function may be written as

$$u \sim A(2/\pi\beta)^{1/2} \cos [\beta z - \pi P/2 - \pi/4]. \quad (13)$$

Expanding,

$$u \sim A(2/\pi\beta)^{1/2}[\cos (P\pi/2 + \pi/4) \sin\beta z + \sin (P\pi/2 + \pi/4) \cos\beta z]. \quad (14)$$

However, for large z, the wave function consists of a unit wave to the left plus a reflected wave to the right:

$$u \sim e^{i\beta z} + \text{Re}^{-i\beta z} = (1 + R) \cos\beta z + i(1 - R) \sin\beta z. \quad (15)$$

Equating coefficients and eliminating A, we find

$$R = [1 + i \tan (P\pi/2 + \pi/4)] / [1 - i \tan (P\pi/2 + \pi/4)]. \quad (16)$$

Whence

$$|R| = [1 - \tanh\psi]/[1 + \tanh\psi], \quad (17)$$

where

$$\psi = (\pi/2) \text{ Im } \{[k_0^2\gamma + \tfrac{1}{4}]^{1/2}\}. \quad (18)$$

In Fig. 1 we plot the magnitude of the power reflection coefficient vs ψ.

In general, computation of the field amplitude requires knowledge of the Bessel functions of complex order, but in the lossless case P is real, and we find (neglecting the phase factor) the formula

$$u(z) = (2\pi z \cos\theta_i)^{1/2}(P^2 - \tfrac{1}{4})^{1/4} \cdot J_P\{[P^2 - \tfrac{1}{4}]^{1/2} z \cos\theta_i\}. \quad (19)$$

In Fig. 2, we plot this function, which represents the (half) envelope of the standing-wave pattern for various P and normal incidence. We observe that the amplitude is not zero at $z=1$ (contrary to a common supposition that the critical density level acts as a perfect reflector), and that the amplitudes actually increase slightly as $z=1$ is approached. This last may be understood upon recalling that as the electron density increases, the index of refraction and the dielectric constant decrease. As a result, the impedance of the medium increases with a consequent increase in wave amplitude in a lossless medium.

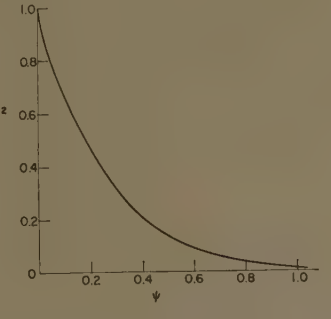

Fig. 1—Power reflection coefficient.

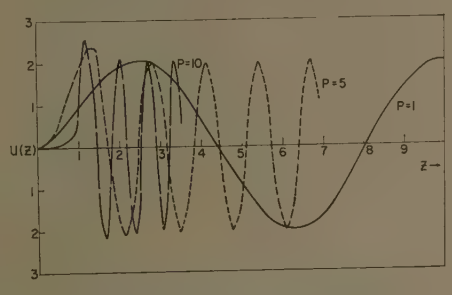

Fig. 2—Wave pattern half-envelopes.

It appears that severe mathematical difficulties prevent a general extension of the method used here. The source of this difficulty is that even though the appropriate asymptotic forms for $u(z)$ may be simply obtained for densities proportional to z^{-N}, $N>1$ at large z, there is no general procedure to determine the "circuit relations" between these solutions and the asymptotic solutions at small z. They are known only in certain special cases (such as the one considered here).

Leonard S. Taylor
Sciences Lab.
General Electric Co.
Valley Forge, Pa.

Dual Operation with the Two-Wire Spiral Antenna*

Two circuits consisting of identical components—a single two-wire Archimedean spiral antenna connected by two equal lengths of coaxial cable to a ring network—are described, which permit simultaneous operation with two independent signals from a single antenna structure. The two circuits differ only in the spiral configuration. The first circuit allows selection of either the first or second mode of radiation, and the second circuit allows selection of either sense of circular polarization in the first mode.

It has been shown[1] that when the input terminals of a two-wire Archimedean spiral antenna are excited anti-phase, currents on adjacent filaments become in-phase at the one-wavelength circumference, where radiation occurs most strongly. This has been defined as the first mode of radiation. Similarly, when the input terminals are excited in-phase, currents on adjacent filaments become anti-phase at the one-wavelength circumference but in-phase again at the two-wavelength circumference, where radiation is maximum. The latter case has been defined as the second mode of radiation.

A spiral-antenna mode-selector circuit which allows selection of either mode of radition is shown in an exploded view in Fig. 1. The center conductors of two coaxial lines connect the input terminals of the spiral antenna to terminals 2 and 4 of the ring network. The outer conductors of the coaxial cable connect the microstrip ground plane (metal plate) to the ground plane of the ring network. The size of the microstrip ground plane sets the high-frequency limit of operation. Minimum outer circumference of the spiral is two wavelengths at the lowest frequency, *i.e.*, diameter $\geq 2\lambda/\pi$. For equal lengths of coaxial cable, terminal 1 of the ring network excites anti-phase currents at

[1] M. Born and E. Wolf, "The Principles of Optics," Pergamon Press, Inc., New York, N. Y., pp. 50–54; 1959.
[2] G. N. Watson, "Theory of Bessel Functions," Cambridge University Press, Cambridge, Eng., 2nd ed., p. 199; 1952.

* Received by the PGAP, August 1, 1961.
[1] J. A. Kaiser, "The Archimedean two-wire spiral antenna," IRE Trans. on Antennas and Propagation, vol. AP-8, pp. 312–323; May, 1960.

the spiral input, giving rise to radiation in the first mode. On the other hand, terminal 3 of the ring network excites in-phase currents at the spiral input, resulting in radiation in the second mode. Donnellan[2] has shown radiation patterns for the second mode. The two modes of radiation are inherently isolated from each other due to the current phase relationships. This isolation generally exceeds 20 db in practice.

The second circuit allows generation of either sense of circular polarization from a single spiral antenna. It differs from the previously described circuit only in that the spiral diameter is approximately $\frac{3}{8}\lambda$, and the over-all filament lengths differ by $\lambda/4$. This is accomplished by removing a quarter wavelength of one filament at its outer extremity. (See Fig. 2.) Currents excited at the input terminals in-phase reach the end terminals of the spiral practically undiminished in amplitude since they pass through the one-wavelength region in an anti-phase condition. Because the filament lengths differ by $\lambda/4$, the reflected current on one filament travels a distance of $\lambda/2$ less (two-way travel) than the reflected current on the other filament. The reflected currents reach the one-wavelenth circumference of the spiral in-phase, whence radiation occurs. The sense of this radiation is opposite to that obtained when exciting the input terminals with anti-phase currents. Thus one sense of circular polarization is generated when exciting the input terminals anti-phase, and the opposite sense of circular polarization is obtained when exciting the input terminals in-phase. Radiation of both senses of circular polarization occurs from the same region of the spiral, which indicates that the radiation patterns should be identical except for the sense of rotation. Frequency range of the polarization sense-selector circuit is limited by the $\lambda/4$ filament length difference.

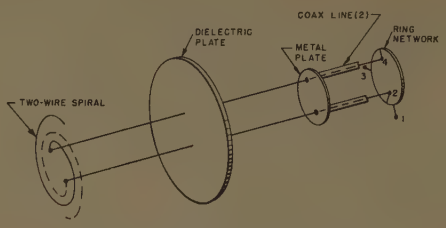

Fig. 1—Spiral mode-selector circuit (exploded view).

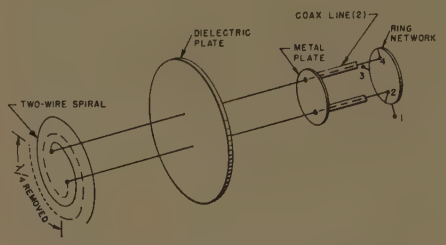

Fig. 2—Spiral sense-selector circuit (exploded view).

A 12-turn spiral of a 5-in diameter printed on one side of a $\frac{1}{32}$-in thick teflon-fiberglass dielectric was tested over the frequency range of 850 Mc to 1200 Mc. A $2\frac{1}{4}$-in diameter copper plate to serve as a microstrip ground plane was centered on the opposite side of the dielectric plate. The inner four turns of the spiral and approximately $2\frac{5}{8}$ in of one filament at its outer extremity were removed. Two equal lengths of RG-223/U coaxial cable connected the spiral inner terminals to a ring network designed for 1 Gc. The antenna was placed $3\frac{1}{4}$ in over a 30 in $\times$ 30 in ground plane for measurement.

The VSWR looking into either terminal 1 or 3 of the ring network was below 2.0 over the measured frequency band from 850 Mc to 1200 Mc. Isolation between terminals 1 and 3 was 12 db or greater, reaching a maximum of 30 db at 1000 Mc. The axial ratio for both senses of circular polarization was generally below 2.5 db. With a linearly-polarized transmitting antenna, the difference in signal level between terminals 1 and 3 was 3 db or lower at frequencies up to 1175 Mc, with the signal from terminal 1 always greater than that from terminal 3.

J. A. KAISER
Diamond Ordnance Fuze Lab.
Washington, D. C.

[2] J. R. Donnellan, "Second-mode operation of the spiral antenna," IRE TRANS. ON ANTENNAS AND PROPAGATION (Communication), vol. AP-8, p. 637; November, 1960.

Contributors

Sinclair N. C. Chen (S'54–M'60) was born in Shanghai, China, on June 8, 1930. He received the B.S.E.E. degree from Stanford University, Stanford, Calif., in 1952; the M.S. degree from Syracuse University, Syracuse, N. Y., in 1954; and the Ph.D. degree from The Ohio State University, Columbus, in 1960.

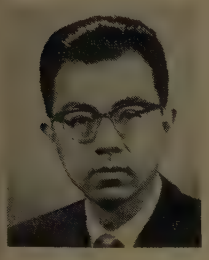

S. N. C. CHEN

From 1952 to 1953, he was associated with the Standard Coil Products Company in Los Angeles, Calif. Since 1954, he has been with the Antenna Laboratory of the Department of Electrical Engineering of The Ohio State University as a Research Assistant and presently as a Research Associate. His main interest in research is in the area of electromagnetic wave theory.

Dr. Chen is a member of Sigma Xi.

❖

B. Ru-Shao Cheo (S'59–M'61) was born in Nanking China, on May 29, 1930. He received the B.Sc. degree in electrical engineering from Taiwan College of Engineering, Taiwan, China, in 1954. He came to the U.S.A. in 1954 where he received the M.S.E.E. degree from the University of Notre Dame, Notre Dame, Ind., in 1956, and the Ph.D. degree in electrical engineering from the University of California at Berkeley in 1961.

B. R.-S. CHEO

Since 1960, he has been employed by the Bell Telephone Laboratories, Murray Hill, N. J., where he is a member of the Technical Staff engaged in microwave research and development in the millimeter wave transmission system and the communication satellite.

Dr. Cheo is a member of Sigma Xi.

❖

Janis Galejs (A'52–M'57) was born in Riga, Latvia, on July 21, 1923. He received the Engineering Diploma in electrical engineering from the Technical University, Brunswick, Germany in 1950, and the M.S. and Ph.D. degrees in electrical engineering from the Illinois Institute of Technology, Chicago, in 1953 and 1957, respectively,

J. GALEJS

While attending I.I.T., he worked for the Cook Research Laboratory on fire control problems, radar, and communications systems. He joined the Applied Research Laboratory of Sylvania Electric Products, Inc., in Waltham, Mass., in 1957. He has been engaged in studies of radar systems and in statistical analysis of radar and communication problems. More recently he has been concerned with propagation in dispersive media and in the ionosphere.

Dr. Galejs is a member of Sigma Xi and Tau Beta Pi.

❖

Akira Ishimaru (M'58) was born in Fukuoka, Japan, on March 16, 1928. He received the B.S. degree in 1951, from Tokyo University, Tokyo, Japan, and the Ph.D. degree in electrical engineering in 1958, from the University of Washington, Seattle.

A. ISHIMARU

From 1951 to 1952, he worked with the Electrotechnical Laboratories, Tokyo. He came to the United States in 1952 as a graduate student. He was an Instructor at the University of Washington from 1954–1958, where he was appointed Assistant Professor in 1958. During the summer of 1956, he was employed by the Bell Telephone Laboratories, Holmdel, N. J., where he worked on antenna problems. He did research on antenna pattern synthesis, propagation, and diffraction and scattering. Currently, he is Associate Professor of electrical engineering at the University of Washington, and Consultant in microwave antennas and propagation to the Boeing Company, Seattle.

Dr. Ishimaru is a member of Sigma Xi.

❖

Richard Kieburtz (S'53–M'61) was born in Spokane, Wash., on November 28, 1933. He received the degrees of B.S.E.E. in 1955, M.S.E.E. in 1957, and Ph.D. in 1961, from the University of Washington, Seattle.

R. KIEBURTZ

From January, 1957 until December, 1960 he held the position of Acting Instructor in the Department of Electrical Engineering at the University of Washington. He did research on antennas and electromagnetic diffraction and scattering in the Microwave Antenna Laboratory there. In February, 1961 he joined the faculty of New York University, New York, N. Y., where he is now Assistant Professor of electrical engineering.

Dr. Kieburtz is a member of Tau Beta Pi and Sigma Xi.

❖

Charles M. Knop (M'60) was born in Chicago, Ill. on February 18, 1931. He received the B.S.E.E. and M.S.E.E. degrees from the Illinois Institute of Technology, Chicago, Ill., in 1954 and 1960, respectively. He is presently completing the requirements for the Ph.D.E.E. degree at the Institute.

C. M. KNOP

He was with the Hughes Research and Development Laboratories of Culver City, Calif., from 1954 to 1955. From 1955 to 1956 he was a Research Assistant at Princeton University, Princeton, N. J. From 1956 to 1960 he was with the Armour Research Foundation of Chicago, Ill. From 1960 to 1961 he was with the Bendix Systems Division Research Laboratory of Chicago, Ill. In May, 1961 he joined the Research and Development Department of The Hallicrafters Company, also in Chicago. His main work has been research and development in the fields of microwaves, antennas, and electro magnetic wave propagation.

Mr. Knop is a member of Sigma Xi, Tau Beta Pi, and Eta Kappa Nu.

❖

Hans H. Kuehl (M'60) was born in Detroit, Mich., on March 16, 1933. He received the B.S.E. degree in electrical engineering in 1955 from Princeton University, Princeton, N. J., and the M.S. and Ph.D. degrees in electrical engineering from the California Institute of Technology, Pasadena, in 1956 and 1959, respectively.

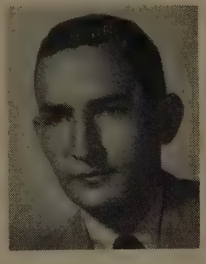

H. H. KUEHL

He was a member of the technical staff of the Research Laboratories of the Hughes Aircraft Company, Culver City, Calif., from 1958 to 1959. From 1959 to 1960, he was a research fellow at the California Institute of Technology, where he was engaged in the study of radiation in anisotropic plasma. In September, 1960, he

joined the faculty of the University of Southern California, Los Angeles, where he is now an Assistant Professor of electrical engineering.

Dr. Kuehl is a member of Eta Kappa Nu, Phi Beta Kappa, Sigma Xi, Tau Beta Pi, and the American Physical Society.

❖

William H. Peake (M'57) was born in Binghamton, N. Y., on June 10, 1926. He received the B.S. degree from the Massachusetts Institute of Technology, Cambridge, in 1946, and the Ph.D. degree in physics from The Ohio State University, Columbus, in 1959.

W. H. PEAKE

After service in the U. S. Air Force, he was employed as Research Assistant at the Ordnance Research Laboratory of the Pennsylvania State University, University Park, and from 1951 to 1952, he was a physicist at the Naval Ordnance Laboratory, Silver Spring, Md. In 1952, he joined the Antenna Laboratory of The Ohio State University, as a Research Assistant, where he was engaged in studies of the effects of turbulence on antenna design and the scattering properties on nonuniform surfaces; in 1959, he became Assistant Professor of electrical engineering at that university.

Dr. Peake is a member of Sigma Xi.

❖

Martin A. Plonus (M'55) was born in Trumpininken, Lithuania, on December 21, 1933. He holds three degrees in electrical engineering; he received the B.S. and M.S. degrees from the University of Illinois, Urbana, in 1956 and 1957, respectively, and the Ph.D. degree from the University of Michigan, Ann Arbor, in 1961. From 1957 to 1961, Dr. Plonus was an Assistant Research Engineer at the Radiation Laboratory of the University of Michigan. He joined the faculty of Northwestern University, Evanston, Ill., this fall as an Assistant Professor. His principal research interests are in diffraction and antenna theory.

M. A. PLONUS

Dr. Plonus is a member of Sigma Xi, Sigma Tau and Eta Kappa Nu.

❖

J. H. Richmond (S'49–M'56–SM'59), for a photograph and a biography please see page 420 of the July, 1961, issue of these TRANSACTIONS.

❖

V. H. Rumsey (SM'50–F'60), for a photograph and biography, please see page 504 of the September, 1961, issue of these TRANSACTIONS.

❖

William M. Sherrill (M'60) was born in San Antonio, Tex., on February 23, 1936. He received the B.A. degree in mathematics and the B.S. degree in physics from the University of Texas, Austin, in 1957, and the M.A. degree in physics from Rice Institute, Houston, Tex., in 1959.

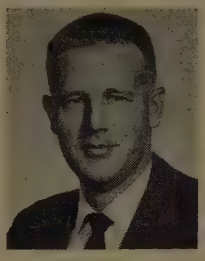

W. M. SHERRILL

Since 1959, he has been employed as Research Engineer in the department of electronics and electrical engineering at Southwest Research Institute, San Antonio, Tex., where he has been engaged in radio direction finding research.

Mr. Sherrill is a member of Phi Beta Kappa.

❖

Douglas N. Travers (A'52–M'57) was born in San Antonio, Tex., on June 27, 1928. He received the B.E. degree in electrical engineering from The Johns Hopkins University, Baltimore, Md., in 1951.

D. N. TRAVERS

Since 1956, he has been a Senior Research Engineer in the department of electronics and electrical engineering at Southwest Research Institute, San Antonio, Tex., where he has been actively engaged in research on radio direction finding systems. He has devoted special attention to the application of multiloop antennas to radio direction findings.

Mr. Travers is a member of the Scientific Research Society of America.

❖

Jean G. Van Bladel (M'54-SM'56) was born in Antwerp, Belgium on July 24, 1922. He holds the degree of Electrical Engineer from Brussels University, Belgium, which he received in 1947. He obtained the Ph.D. degree in electrical engineering at the University of Wisconsin, Madison, in 1950.

J. G. VAN BLADEL

He was Head of the Radar Department at the M.B.L.E. Factories, Brussels from 1950 to 1954 and he was Associate Professor of electrical engineering at Washington University, St. Louis, Mo., from 1954 to 1956. Since 1956, he has been at the University of Wisconsin where he is now Professor of electrical engineering. He is also a consultant with the M.U.R.A. Accelerator Project in Madison.

Mr. Van Bladel is a member of Sigma Xi and Eta Kappa Nu.

❖

William J. Welch (S'56–M'57) was born in West Chester, Pa., on January 17, 1934. He attended Oberlin College, Oberlin, Ohio, and received the B.S. degree in physics from Stanford University, Stanford, Calif., in 1955, and the Ph.D. degree in engineering science from the University of California, Berkeley, in 1960.

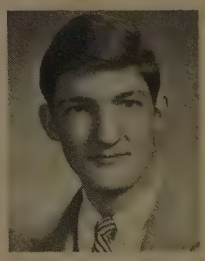

W. J. WELCH

He is currently Assistant Professor of electrical engineering at the University of California, Berkeley, and is presently associated with a milimeter-wave radio-astronomy project. His interests include antennas, electromagnetic theory and radio astronomy.

Dr. Welch is a member of Sigma Xi.

IRE Transactions on Antennas and Propagation

Index to Volume AP-9, 1961

Contents

Volume AP-9, Number 4, July, 1961

Volume AP-9, Number 5, September, 1961

Volume AP-9, Number 6, November, 1961

Index to Authors

Index to Subjects

PAPERS TO BE PUBLISHED IN FUTURE ISSUES

Scattering and Guided Waves at an Interface Between Air and a Compressible Plasma ..... *A. Hessel, N. Marcuvitz and J. Shmoys*

The Influence of Complex Waves on the Radiation Field of a Slot-Excited Plasma Layer ..... *T. Tamir and A. A. Oliner*

Particle and Photon Transport in Plasmas ..... *R. K. Osborn*

Transconductance Properties of Plasma ..... *J. E. Drummond*

The Relations between the Transport and the Orbit Models for a Plasma ..... *S. Frankenthal and W. P. Allis*

A Coaxial Low-Density Plasma Experiment ..... *A. Olte, J. S. King and E. K. Miller*

Interaction of a High Intensity EM Field Field with a Low Density Plasma ..... *K-M. Chen*

Non-Linear Electrical Conductivity of a Fully Ionized Gas ..... *K-M. Chen*

The Radiation Pattern of a Microwave Horn and a Plasma Layer ..... *W. L. Flock and R. S. Elliott*

Anisotropic Plasma-Covered Magnetic Line Source ..... *R. Shore and G. Meltz*

Radiation from Linear Electric or Magnetic Antennas Surrounded by a Spherical Plasma Shell .... *H. R. Raemer*

Plasma Simulation by Artificial Dielectrics and Parallel-Plate Media ..... *W. Rotman*

Array Factors with Non-Uniform Spacing Parameter ..... *A. L. Maffett*

Linear Arrays with Variable Interelement Spacings ..... *M. G. Andreasen*

On the Mapping of Extended Sources with Non-Linear Correlation Antennas .. *C. J. Drane and G. B. Parrent, Jr.*

Antennas and Data Processing ..... *R. N. Bracewell*

Electromagnetic Radiation from a Cyclindrically Capped Bi-Wedge ..... *M. A. Plonus*

Closed Form Analysis for the Radiation Pattern of the Modulated Antenna ..... *A. Ishimaru and G. D. Bernard*

Digital Computation of the Mutual Impedance Between Thin Dipoles ..... *H. C. Baker and A. H. LaGrone*

Sandwich-Wire Antenna ..... *K-M. Chen*

Frequency Scanning Antennas ..... *A. Ishimaru and H-S. Tuan*

Multiple Target Response of Data Processing Antennas ..... *M. E. Pedinoff and A. A. Ksienski*

Effect of Obstacle Profile on Knife-Edge Diffraction ..... *M. P. Bachynski and M. G. Kingsmill*

Elliptically Polarized Leaky-Wave Array ..... *W. J. Getsinger*

An Analysis of Polarization Variation and Its Application to Circularly-Polarized Radiators ..... *T-S. Chu and R. G. Kouyoumjian*

An Antenna Array of Longitudinally-Slotted Dielectric-Loaded Waveguides .... *E. D. Sharp and E. M. T. Jones*

INSTITUTIONAL LISTINGS

The IRE Professional Group on Antennas and Propagation is grateful for the assistance given by the firms listed below, and invites application for Institutional Listing from other firms interested in the field of Antennas and Propagation.

AERO GEO ASTRO CORP., 1200 Duke St., Alexandria, Va.
Space Instrumentation; Antennas; Transponders; Command Receivers; Augmenters; Telemetry; Radar

ANDREW CORPORATION, P.O. Box 807, Chicago 42, Ill.
Antennas, Antenna Systems, Transmission Lines, Development and Production

THE BOEING COMPANY, Antenna Dept., P. O. Box 3976, Seattle 24, Wash.
Development, Fabrication & Installation; Precision Airborne & Ground Antennas & Systems

DECO ELECTRONICS, INC., Leesburg, Va.; Boston, Mass.; Boulder, Colo.; Malibu, Calif.; Washington, D C.
Antenna Research, Design, Evaluation; Propagation Studies; Communications Systems Engineering

DORNE & MARGOLIN, INC., 29 New York Ave., Westbury, L. I., N. Y.
Research, Development and Manufacture—Antenna and Microwave Technology

FXR, Inc., 25–26 50th St., Woodside 77, N. Y.
Precision Microwave Test Equip., High Power Microwave Electronics, Microwave Components & Instrumentation

JANSKY & BAILEY, A Div. of Atlantic Research Corp., Shirley Highway & Edsall Rd., Alexandria, Va.
Complete Engineering Services for Antennas and Propagation Programs

SCIENTIFIC-ATLANTA, INC., 2162 Piedmont Rd., N.E., Atlanta 9, Ga.
Antenna Pattern Ranges, R & D, RF Components, Telemetry Tracking Systems, Fourier Computer & Computation

TECHNICAL APPLIANCE CORP., 1 Taco St., Sherburne, N. Y.
Des., Dev., & Mfg.: Antennas & Antenna Systems for Communications, Telemetry, & Tracking

WHEELER LABORATORIES, INC., Great Neck, N. Y.; Antenna Lab., Smithtown, N. Y.
Consulting Services, Research and Development, Microwave Antennas and Waveguide Components

WEINSCHEL ENGINEERING COMPANY, INC., Kensington, Md.
Antenna Pattern Receivers; Bolometer Amplifiers; Microwave Sources; Insertion Loss Measuring Systems

The charge for Institutional Listing is $50 for one issue or $200 for six consecutive issues (one year). Application may be made to the Professional Groups Secretary, The Institute of Radio Engineers, Inc., 1 East 79 Street, New York 21, N. Y.